

I. CATALYTIC ASYMMETRIC BROMO-SPIROLACTONIZATION
II. DESIGN AND DEVELOPMENT OF ORGANIC DYES FOR TRANSPARENT
LUMINESCENT SOLAR CONCENTRATOR (TLSC)
III. DISCOVERY OF A NOVEL CYANINE DEGRADATION PATHWAY

By

Mehdi Moemeni

A DISSERTATION

Submitted to
Michigan State University
in partial fulfillment of the requirements
for the degree of

Chemistry—Doctor of Philosophy

2022

ABSTRACT

In Chapter I, a novel enantioselective method has been developed that leads to the formation of a variety of substituted spirolactones. This process furnishes the desired spirolactones in excellent yields and high enantioselectivities. Different categories of acidic and basic chiral catalysts were screened and the lead hit for achieving minimal enantioselectivity was obtained with a cinchona alkaloid derivatized at its C9-OH as a carbamate. With these results, we pursued the synthesis of a library of new catalyst families, in particular urea, thio-urea, carbamate and thio-carbamate systems and investigated them as asymmetric catalysts for the bromo spirolactonization reaction of oxo-alkenyl carboxylic acid substrates.

In Chapter II, a variety of near-infrared dyes with high quantum yield and large Stokes shift were synthesized for fabrication of transparent luminescent solar concentrators (TLSC) devices, leading to high power conversion efficiencies. Based on a combined experimental and computational study, a simple strategy for optimizing the Stokes shift in fluorescing cyanines was proposed. As a result, a significant Stokes shift enhancement in cyanine dyes was achieved as a result of C4'-substitution with amines.

In Chapter III, we discovered a non-photoactivated, oxygen-free, thermal degradation of cyanine dyes. Reaction optimization led to the developing of a new method for converting cyanines to truncated symmetric and asymmetric derivatives with high efficiency. We later used deuterium label tracing studies and deuterium exchange studies in addition to other supporting experiments to propose a mechanism for these transformations.

Dedicated to my parents, my family and Rahele for their endless love and support

ACKNOWLEDGMENTS

First, I would like to express my sincere gratitude and appreciation to my Ph.D. advisor, professor Babak Borhan for his understanding, endless support, motivation and kind guidance. I am really grateful to him for welcoming me to his research group and helping me through my projects while giving me the freedom to come up with new ideas and enjoy my chemistry. He is an amazing friend and accepted his students as his family and invited us for Thanksgiving, Christmas and New Year. We had great times in summer group camping, soccer games, fireworks on the 4th of July, and birthday cakes parties for everyone. Thanks for advising me both in my research and as well as on my career.

I am greatly thankful to my committee member, Professor James Jackson, Professor Xuefei Huang and Professor James Geiger, for their time, patience, support and guidance during my PhD program.

I would like to thank all my lab members, for their amazing friendship, help and support. I especially want to express my appreciation and gratitude to Dr. Chrysoula Vasileiou, for her endless help. The past members of Borhan group, especially Dr. Wei Sheng, Dr. Hadi Gholami, Dr. Bardia Soltanzadeh, Dr. Jun Zhang, Dr. Setare Tahmasebi Nick, Dr. Daniel Steigerwald and Dr. Debarshi Chakraborty for teaching me their skills and sharing their valuable knowledge and experience. I am very grateful to the current and former members of Borhan group that I have had the chance to work with them, especially Aria Vahdani, for working with me and helping me with multiple projects.

I would also like to thank my amazing collaborators: Professor Richard Lunt, Professor Gary Blanchard, Professor James Jackson, Professor Marcos Dantus,

Professor Benjamin Levine, Professor Piotr Piecuch, Dr. Chenchen Yang, Dr. Jurick Lahiri, Dr. Briana Capistran, Dr. Ilias Magoulas, Dr. Stephen Yuwono, Dr. Matthew Bates, Chris Herrera, Fangchun Liang and Andrew Wendel. I would like to extend my sincere gratitude to the MSU facility's leads, Dr. Daniel Holmes (NMR), Dr. Richard Staples (Crystallography) and Dr. Tony Schillmiller (Mass Spectrometry).

I want to deeply thank my family, especially my parents for their endless love, patience, support and encouragement. They spent countless times helping me during my education, and I will be forever grateful.

Finally, I want to thank the most important person in my life, Rahele my beloved wife. It is impossible to use words to describe how thankful I am to her. During these years in graduate school, I had many ups and downs, and she always was there to support me and cheer me up. She has been my driving force to wake up every morning from the first day I met her, and I couldn't want anything more than to work with her in the same lab and share all moments together. I definitely would not be standing here if it was not because of her love and encouragement. I dedicate this milestone to my best friend, Rahele.

TABLE OF CONTENTS

LIST OF TABLES	vii
LIST OF FIGURES	ix
LIST OF SYMBOLS AND ABBREVIATIONS	xiv
Chapter I: Catalytic Asymmetric Bromo-Spirolactonization	1
I-1 Introduction; structural features of the spiro lactone moiety.....	2
I-2 Chemical synthesis of spiro lactones (previous approaches)	3
I-3 Development of halenium initiated spiro lactonization	5
I-4 Development of asymmetric bromospiro lactonization.....	12
I-5 Future work	34
I-6 Experimental section.....	39
REFERENCES.....	95
Chapter II: Design and Development of Organic Dyes for Transparent Luminescent Solar Concentrators (TLSCs)	100
II-1 Introduction of transparent luminescent solar concentrators (TLSCs)	101
II-2 Important parameters for investigating TLSC devices	102
II-3 Development of organic dyes for use with TLSC devices.....	104
II-4 Future work	137
II-5 Experimental section.....	140
REFERENCES.....	194
Chapter III: Discovery of a Novel Cyanine Degradation Pathway	199
III-1 Introduction to cyanine fluorescent dyes.....	200
III-2 Photo-degradation pathways of cyanine dyes	201
III-3 Discovery and development of a non-photoactivated, oxygen-free degradation of cyanine dyes.	205
III-4 Experimental section.....	231
REFERENCES.....	251

LIST OF TABLES

Table I-1. Reaction optimization for improving the diastereoselectivity of spiro lactonization.....	14
Table I-2. Asymmetric bromospirolactonization with basic catalysts	18
Table I-3. Reaction optimization for cat. I-51 ; temperature, solvent and Br source were altered	19
Table I-4. Study of the effects of different carbonyl linkers on asymmetric bromospirolactonization	22
Table I-5. Reaction optimization for cat. I-54 ; temperature, solvent and Br source were altered	23
Table I-6. Catalyst optimization; study of electronic effect on the carbamate aryl group	25
Table I-7. Catalyst optimization; electronic and steric effect on aryl carbamate and quinoline	26
Table I-8. Study of thiourea, urea and carbamate catalysts	28
Table I-9. Grubbs cross metathesis results	31
Table I-10. Substrate scope study of uncatalyzed bromospirolactonizations	32
Table I-11. Substrate scope study of catalytic asymmetric bromospirolactonizations ...	34
Table II-1. Strategy toward large Stokes shift cyanine dyes	107
Table II-2. Spectroscopic data of amine substituted heptamethine cyanines	111
Table II-3. Spectroscopic data of dye II-13 in different solvents	113
Table II-4. Spectroscopic data of amine substituted ICG based cyanine dyes	115
Table II-5. Structure and spectroscopic data of amine substituted benzothiazole based cyanines	116
Table II-6. Important geometric parameters that determine the electronic character (bipolar vs. cyanine-like) of the five structures in the parallel conformation ^a	123
Table II-7. Spectroscopic properties and TLSC photovoltaic parameters of CO₈DFIC	131

Table II-8. Spectroscopic properties and TLSC photovoltaic parameters of CO₂DFIC	136
Table II- 9. Absolute energies of optimized geometries on the DFT level of theory. (CAM-B3LYP/6-31G*)	168
Table II-10. Important geometric parameters for CAM-B3LYP/6-31G* structures ^a	169
Table III-1. Reaction optimization with secondary amine.....	209
Table III-2. Reaction optimization with tertiary amine	211

LIST OF FIGURES

Figure I-1. Spirolactone moiety embedded in the structure of natural products	2
Figure I-2. Spirolactonization via photo-oxidation of hydroxyalkyl furans	3
Figure I-3. Spirolactonization via palladium catalized CO insertion	4
Figure I-4. Rodriguez's approach to access the enantioselective spirolactones	5
Figure I-5. Yeung's approach to access the enantioselective spirolactones	5
Figure I-6. Glossary of our published enantioselective chlorocyclization methodologies	6
Figure I-7. Two possible TS (classic vs NAAA) for chlorolactonizations	7
Figure I-8. Strategies towards diastereoselective bromospiroketalization.....	8
Figure I-9. Bromocyclization of I-38 yields the macrocyclic bromoether as the major product	9
Figure I-10. Substrate I-40 -THP furnished the desired bromospiroketal I-37 as a single isomer.....	10
Figure I-11. Diastereoselective dibromospiroketalization	11
Figure I-12. Enantioselective bromo spiroketalization with vaulted biaryl catalysts	12
Figure I-13. Strategy towards diastereoselective bromospirolactonization	13
Figure I-14. Bromospirolactonization results; X-ray crystal structure of I-46a and I-46b	13
Figure I-15. Diastereoselectivity study in the presence of acid	15
Figure I-16. Asymmetric bromospirolactonization with acidic catalysts; TS in dashed box.....	16
Figure I-17. Generalized structures for basic catalysts based on the cinchona alkaloid structure.....	19
Figure I-18. General synthesis of basic catalysts	21
Figure I-19. Synthetic methods for making substrates	30
Figure I-20. X-ray crystal structure of I-99a	33

Figure I-21. Development of di-bromo and di-halospirrolactonization	35
Figure I-22. Proposed total syntheses of obtusallenes VI	37
Figure I-23. X-ray structure of I-46a (different views)	81
Figure I-24. X-ray structure of I-46b (different views)	85
Figure I-25. X-ray structure of I-100 (different views)	89
Figure I-26. X-ray structure of I-99a (different views)	94
Figure II-1. A. TLSC model that both UV and NIR light could absorb while visible light passing through. B. Spectra of chromophore; <i>S</i> stand for Stokes shift, <i>W</i> is the width of emission peak (Permission to reproduce this figure is kindly provided by Prof. Lunt and Dr. Yang)	101
Figure II-2 A. Examples of <i>J-V</i> curves for two different solar cells. B. External quantum efficiency spectra of a silicon and GaAs PV cells (Permission to reproduce this figure is kindly provided by Prof. Lunt and Dr. Yang).....	104
Figure II-3. LSC system as a function of calculated Stokes shift (Permission to reproduce this figure is kindly provided by Prof. Lunt and Dr. Yang)	105
Figure II-4. Correlation of Stokes shift and self-quenching.....	106
Figure II-5. Bis-dipole structure of substituted cyanines.....	108
Figure II-6. Synthesis of heptamethine cyanine dyes.....	109
Figure II-7. Synthesis of first series of amine substituted heptamethine cyanine dyes.....	110
Figure II-8. Normalized absorption and fluorescence emission spectra (measured in DCM) for dyes II-10 (top left) and II-12 (top right), and dyes II-14 (bottom left) and II-15 (bottom right).	112
Figure II-9. Structure of second series of amine substituted heptamethine cyanine dyes.....	114
Figure II-10. Generalized cyanine-like and bis-dipolar structures of cyanine dyes	118
Figure II-11. Scatter plot of the experimental spectral energy maxima as a function of the DFT-computed theoretical excitation energies. Absorption and emission energies are shown by blue and red dots, respectively. The lowest energy conformer is chosen for II-9 – II-14 and II-16 , while for II-15 , both the parallel (II-15) and perpendicular (II-15_⊥) conformers are shown.....	120

Figure II-12. Scatter plot of the experimental spectral energy maxima as a function of the DFT-optimized bond length alternation coordinate (in angstrom). Absorption and emission energies are shown by blue and red dots, respectively.	121
Figure II-13. Broad absorbing spectra leads to harvesting higher photon numbers	125
Figure II-14. Structures of D-A-D dyes; DRCN7T and CO8DFIC	127
Figure II-15. Synthesis steps of CO8DFIC	128
Figure II-16. Data for CO8DFIC ; a. Normalized absorption and emission spectra of in chlorobenzene solution, b. Normalized absorption and emission spectra of in polymer matrix, c. Current density versus voltage ($J-V$) characteristics of TLSCs with different concentrations, d. Average $EQ_{ELSC}(\lambda)$ spectra of TLSCs with different concentrations, e. Photographs of all the TLSC devices. (Permission to utilize the Spartan helmet logo is kindly provided by MSU.)	130
Figure II-17. Schematic of the working principle of the dual-band selective harvesting TLSC.	133
Figure II-18. Molecular structure, normalized absorption and emission spectra of $Cs_2Mo_6I_8(CF_3CF_2COO)_6$ nanocluster	134
Figure II-19. Molecular structure, normalized absorption and emission spectra of BODIPY	135
Figure II-20. a. $J-V$ characteristics of TLSCs, b. Average $EQ_{ELSC}(\lambda)$ spectra of TLSCs.....	135
Figure II-21. a. Amine C2-substituted cyanines, b. asymmetric cyclized aminated cyanine	137
Figure II-22. Proposed head groups to redshift the Cy5 core and, proposed new Cy5 structures.....	138
Figure II-23. General structure of D–A–D NIR I/II fluorophores.....	139
Figure II-24. Scatter plot of the experimental spectral energy maxima as a function of the DFT-optimized bond length alternation coordinate (in angstrom). Absorption and emission energies are shown by blue and red dots, respectively.	167
Figure III-1. Structure of famous cyanine dyes.....	200
Figure III-2. Cyanine photolysis products	201
Figure III-3. Mechanism and degradation products of cyanine photooxidation	202

Figure III-4. Photoblueing results from two carbon truncation	203
Figure III-5. Photodegradation mechanism (by Schnermann and co-workers)	204
Figure III-6. Photodegradation mechanism (by Lee and co-workers).....	205
Figure III-7. A. Amination at C4' for tuning the Stokes shift, B. Amination at C3' resulted in corresponding Cy5 and As-Cy5 derivatives	206
Figure III-8. General synthesis of heptamethine cyanines	207
Figure III-9. Study the conversions on Cy7 to investigate the generality of this reaction.....	208
Figure III-10. Identified compounds from cyanine truncation with secondary amine ...	210
Figure III-11. Conversion of Cy7.5 in the presence of tertiary amine (DIPEA)	213
Figure III-12. Conversion of di-substituted cyanine	213
Figure III-13. Normalized absorption and emission of all cyanine's degradation fragments.....	214
Figure III-14. A. Synthesis of Cy7-D₅ , B. Conversion of deuterated Cy7 with secondary amine.....	218
Figure III-15. A. Deuterium exchange in D ₂ O, B. Deuterium exchange in D ₂ O and DIPEA.....	219
Figure III-16. Proposed mechanism of cyanine conversion with secondary amines ...	221
Figure III-17. Conversion of deuterated Cy7 with tertiary amine (DIPEA)	221
Figure III-18. Recombinative chain shortening	222
Figure III-19. Proposed mechanism of cyanine conversion with tertiary amines.....	224
Figure III-20. Proposed mechanism of Cy7 conversion to Cy3	225
Figure III-21. Cy7 reaction with; A. neutralized head group, B. charged head group	225
Figure III-22. Cy5 conversion reactions failed in different conditions	226
Figure III-23. Optimized cyanine conversion reactions.....	227
Figure III-24. <i>top</i> : Normalized absorptions (in DCM), <i>bottom</i> : Normalized emissions (in DCM)	228

Figure III-25. Cyanine structures for stability study229

LIST OF SYMBOLS AND ABBREVIATIONS

λ_{em}	emission wavelength
λ_{max}	absorption wavelength
<	less than
>	larger than
Å	angstrom
ACN	acetonitrile
Ar	aryl
As-Cy	asymmetric cyanine
AVT	average visible transmittance
Bn	benzyl
BODIPY	boron-dipyrromethene
CaH ₂	calcium hydride
CDCl ₃	deuterated chloroform
CHCl ₃	chloroform
cm ⁻¹	wavenumber
Cy	cyanine
d	doublet
DBDMH	1,3-dibromo-5,5-dimethylhydantoin
DCDMH	1,3-dichloro-5,5-dimethylhydantoin
DCM	dichloromethane
DFT	density functional theory

DIBAL-H	diisobutylaluminium hydride
DMF	dimethylformamide
DMSO	dimethyl sulfoxide
<i>ee</i>	enantiomeric excess
<i>EQE</i> (λ)	external quantum efficiency spectrum
equiv.	equivalent
<i>er</i>	diastereomeric ratio
ESI	electrospray ionization
Et ₃ N	triethylamine
EtOH	ethanol
<i>FF</i>	fill factor of a solar cell
g	gram
h	hour
Hal A	halenium affinity
HCl	hydrochloric acid
HPLC	high pressure liquid chromatography
HRMS	high resolution mass spectrometry
Hz	hertz
<i>i</i> -Pr	isopropyl
<i>IQE</i>	internal quantum efficiency
IR	infrared
<i>I</i> _{sc}	short-circuit current

<i>J</i>	current density
<i>J</i>	NMR coupling constant
<i>J-V</i>	current density-voltage characteristic
KOH	potassium hydroxide
M	molar
m	multiple
MeOH	methanol
mg	milligram
MgSO ₄	magnesium sulfate
min	minute
mmol	millimole
N.R.	No Reaction
Na ₂ SO ₄	sodium sulfate
NAAA	nucleophile assisted alkene activation
NaH	sodium hydride
NaOH	sodium hydroxide
NBS	N-bromosuccinimide
<i>n</i> BuLi	<i>n</i> -butyllithium
NC	nanocluster
NCS	N-chlorosuccinimide
NIR	near-infrared
nm	nanometer

NMR	nuclear magnetic resonance
<i>PCE</i>	power conversion efficiency
PV	photovoltaic
q	quartet
<i>QY</i>	quantum yield
r.t.	room temperature
SS	Stokes shift
t	triplet
TFA	trifluoroacetic acid
THF	tetrahydrofuran
TLC	thin layer chromatography
TLSC	transparent luminescent solar concentrator
UV	ultraviolet
UV-Vis	ultraviolet-visible
δ	chemical shift
ε	molar absorption coefficient

Chapter I: Catalytic Asymmetric Bromo-Spirolactonization

I-1 Introduction; structural features of the spiro lactone moiety

The spiro lactone moiety is a key skeletal unit of a number of biologically active natural products. Examples vary from the simple Massarinolin A and its analogs¹ with antibacterial activity against drug-resistant strains to the structurally complex compounds Lancifodilactone G² and Phainanoid F³ that show anti-HIV and immunosuppressive activity, respectively. Most spiro lactone motifs found in natural products contain [5,5], [5,6], [6,5] and [6,6] rings with different biological properties (Figure I-1). The spiro lactones considered here are a subset of the spiroketal family with an ester functional group in one of the spiro rings.

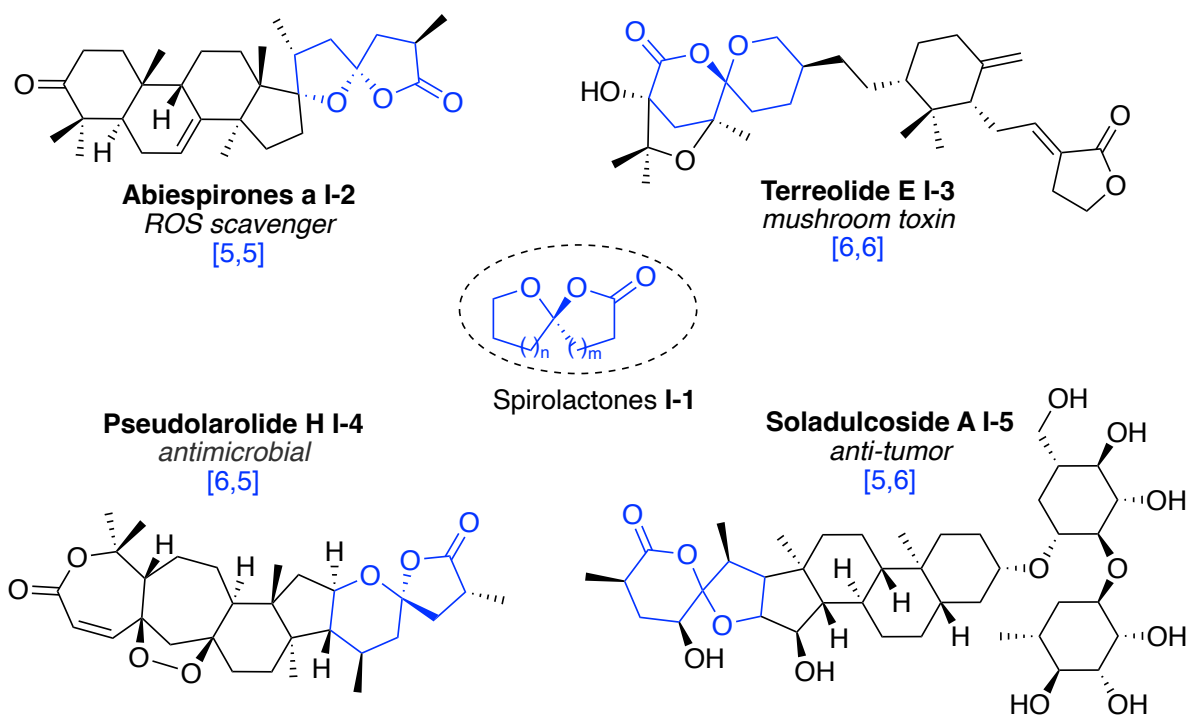


Figure I-1. Spirolactone moiety embedded in the structure of natural products

Spirolactones' biological applications and structural designs have attracted a large number of synthetic discoveries over the past few decades. In this vein, several approaches for the synthesis of racemic spiro lactones have been reported.⁴⁻⁹ However,

stereoselective approaches for the synthesis of these motifs is still under development. Inspired by our success in asymmetric halofunctionalization of olefins, we aimed to develop a novel catalytic asymmetric method to furnish enantioselectively halogenated spirolactones.

I-2 Chemical synthesis of spirolactones (previous approaches)

Oxaspirolactones were synthesized for the first time in 1979 by Mitsunobu and co-workers.¹⁰ The photo-oxidation of hydroxyalkyl furans by Rose Bengal and oxygen, followed by attack with hydroxyl, resulted in the formation of the corresponding spirolactone. (Figure I-2).

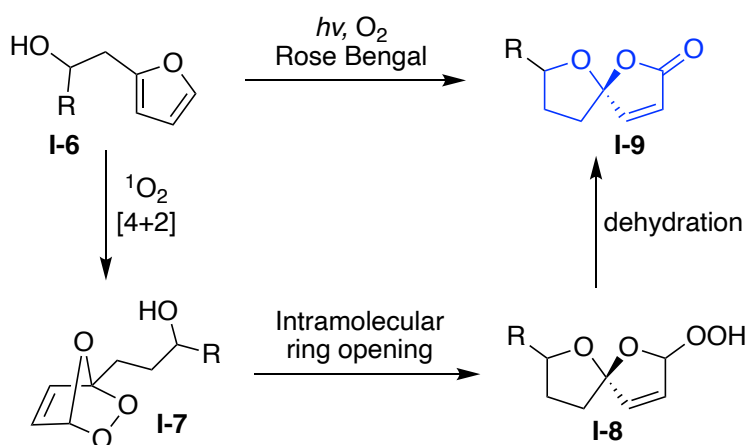


Figure I-2. Spirolactonization via photo-oxidation of hydroxyalkyl furans

Since then, different groups have reported the racemic reactions for synthesis of oxaspirolactone through different mechanisms such as retro-aldol rearrangement, Wittig olefination, acid catalyzed spirolactonization, etc.^{4, 7, 9, 11, 12} One of the most recent approaches to access these motifs is the palladium-catalyzed cascade carbonylative cyclization, which was reported by Dai and co-workers.⁵ The mechanism goes through a

palladium C-C cleavage, followed by ketal formation and CO insertion which finally undergoes the lactonization to form the oxaspirolactone structure (Figure I-3).

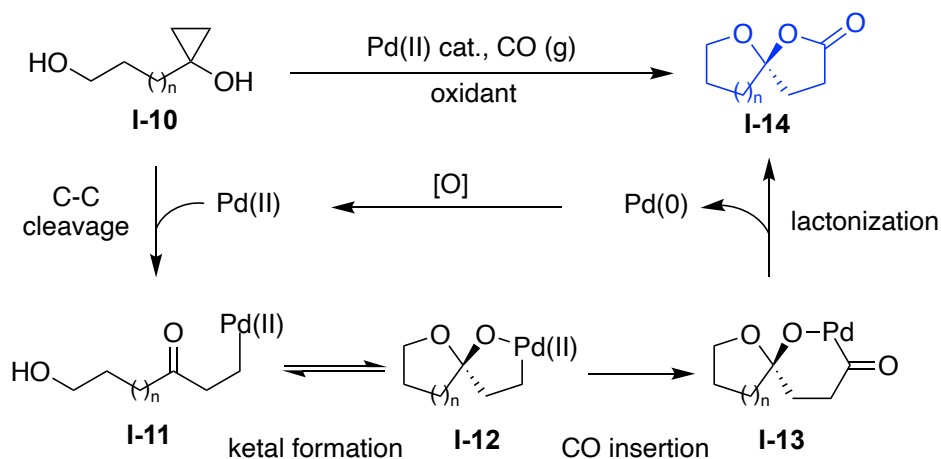


Figure I-3. Spirolactonization via palladium catalyzed CO insertion

In terms of enantioselective approaches, there are only two examples, both of which have significant substrate bias. The first one was reported in 2013 by Rodriguez and co-workers. There an aminated spirolactone was formed by an asymmetric [3+2] reaction in the presence of BINOL-based chiral phosphoric acid and gold catalysts¹³ (Figure I-4). Primary aryl amines are obligatory starting material for this reaction. The second approach, published in 2020 by Yeung and co-workers, synthesized a phenyl substituted spirolactone through an asymmetric domino halocyclization of olefinic keto-acids. An electron-rich amino-thiourea catalyzed this transformation with high enantioselectivity¹⁴ (Figure I-5). All of the substrates studied in this work have the (vinylbenzoyl)benzoic acid core, which would result only in 5,5- bis-phenyl substituted spirolactones.

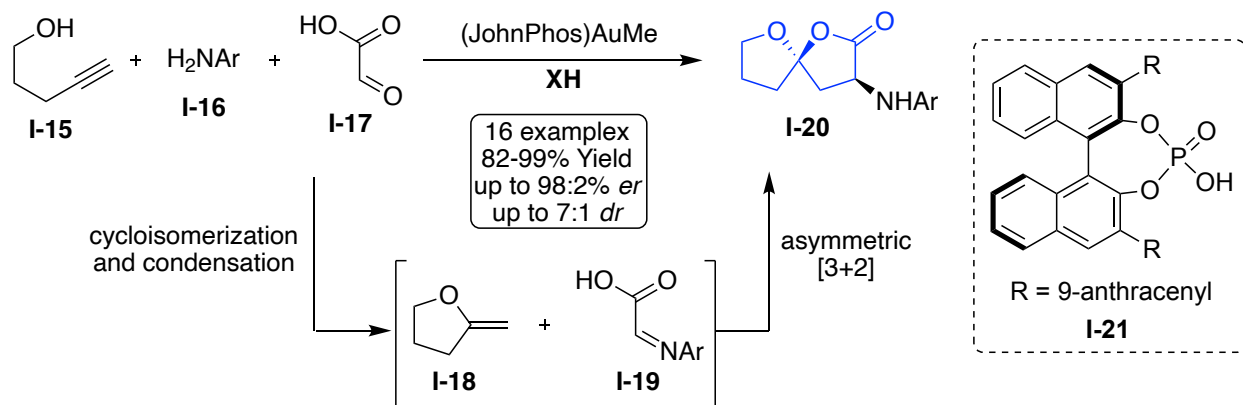


Figure I-4. Rodriguez's approach to access the enantioselective spiro lactones

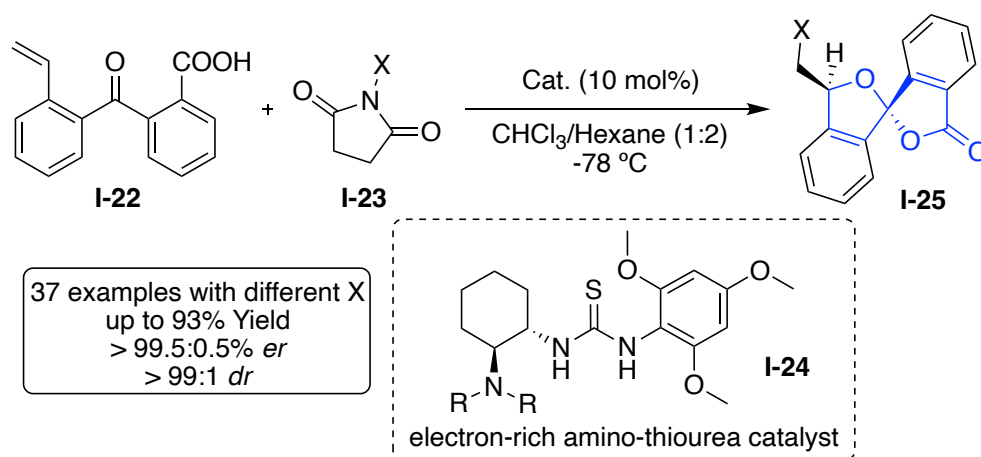


Figure I-5. Yeung's approach to access the enantioselective spiro lactones

I-3 Development of halenium initiated spiro lactonization

Our strategy toward the synthesis of spiro lactones originated from our group's efforts towards the halofunctionalization of olefins. A summary of our asymmetric halofunctionalization methods is shown in Figure I-6. In 2010, our group reported the first asymmetric chlorofunctionalization of olefins¹⁵. The Sharpless ligand $(\text{DHQD})_2\text{PHAL}$ was discovered to be the preferred catalyst for the enantioselective chlorocyclization of 4-aryl-4-pentenoic acids in the presence of 1,3-dichloro-5,5-diphenylhydantoin (DCDPH) as the terminal chlorenium source. The generality of this condition to promote enantioselective

halocyclization of other substrates was then evaluated. This effort showed that unsaturated amides could be chlorocyclized using similar reaction conditions to give access to chiral halogenated oxazoline products.¹⁶ Intriguingly, implementation of an unsaturated carbamate led to the development of a solvent-dependent enantiodivergent reaction whereby either enantiomer of the product could be accessed using the same catalyst by simply changing the reaction solvent.¹⁷

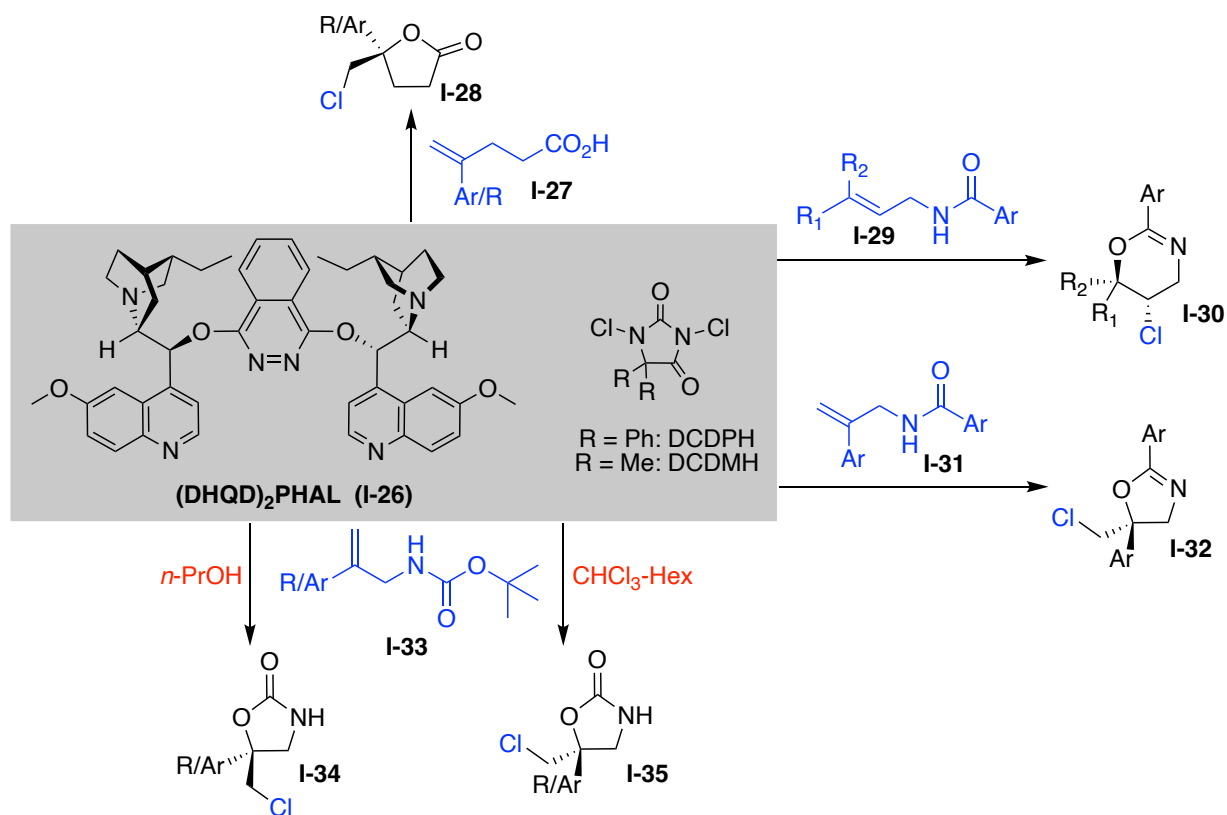


Figure I-6. Glossary of our published enantioselective chlorocyclization methodologies

The study of the mechanism of chlorolactonizations of olefins prompted the development of new concepts to be able define the transition state structures for this chemistry. The halonium affinity scale (HaIA) was developed to introduce a thermodynamic measure that quantifies the donor/acceptor interaction with the halonium

that is being transferred.¹⁸ The HalA values of numerous molecules were reported, and their patterns were experimentally verified through NMR studies, supporting the concept of HalA-guided predictive reactivity. Examination of the HalA of olefins and halogenation species showed that the classical stepwise reaction mechanism of electrophilic addition to alkenes would not lead to formation of the observed products. This resulted in the discovery of the role of nucleophiles in halofunctionalization reactions. We found a direct and strong correlation between the strength of the nucleophile and rate of halofunctionalization, which led to the proposal of the Nucleophile Assisted Alkene Activation (NAAA) concept.¹⁹

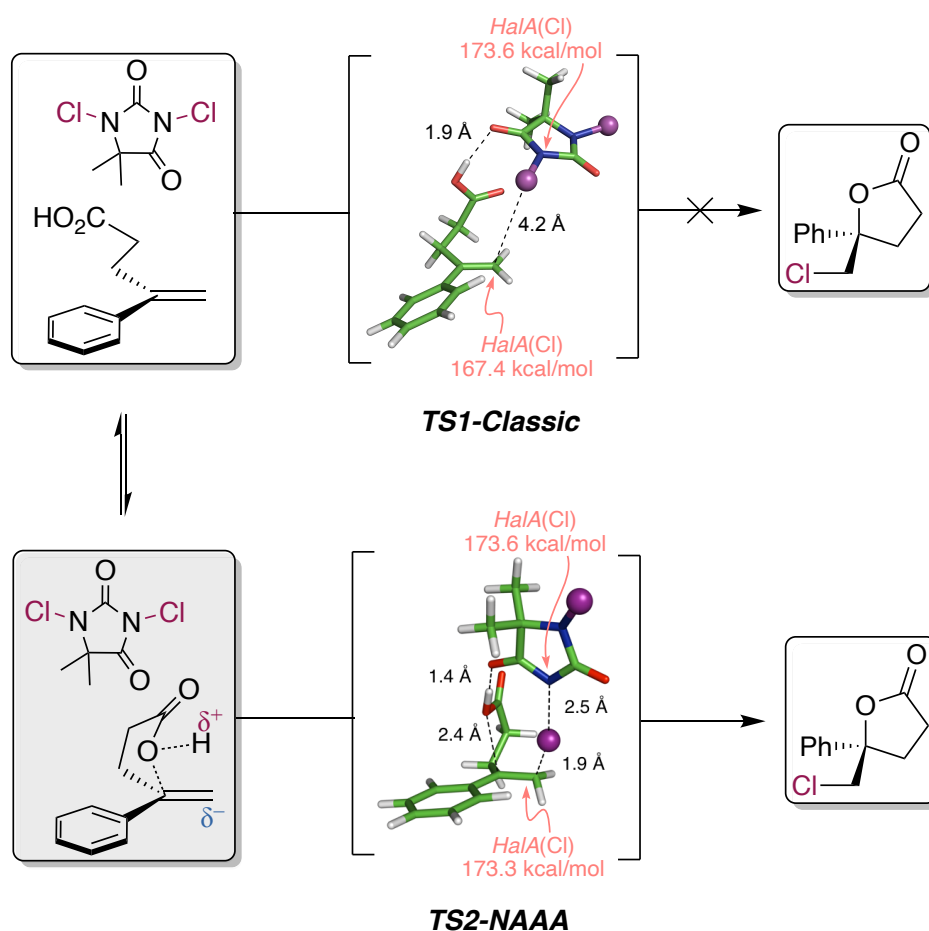


Figure I-7. Two possible TS (classic vs NAAA) for chlorolactonizations

As shown in Figure I-7, the calculation of the transition state does not lead to a Cl^+ transfer in the classical transition state picture (TS1) since the HalA of the double bond is 167.4 kcal/mol: around 6 kcal/mol less than that of our halogen donor DCDMH. The HalA values indicate that the halogen would prefer to remain on DCDMH, rather than to transfer to the nucleophile. However, in the NAAA figure, the carboxylic acid adds in a concerted manner with the halonium to the olefin, leading to an increase of the olefin's HalA , enabling it to compete with the halogen donor (TS2). The interaction of the carboxylic acid group leads to an increase of HalA (173.3 kcal/mol), approaching the HalA of DCDMH anion (173.6 kcal/mol).

The NAAA concept has guided us in reaction design and more recently we reported, a diastereoselective halonium initiated bromo- and dibromospiroketalization method²⁰. A plethora of structurally diverse bioactive natural products reveals the spiroketal moiety. Not surprisingly, their biochemical properties have attracted a great deal of synthetic exploration over the past few decades. In this vein, several elegant strategies towards stereoselective construction of spiroketal cores have been reported. In contrast to approaches that focus on controlling the stereoselectivity in the ketalization

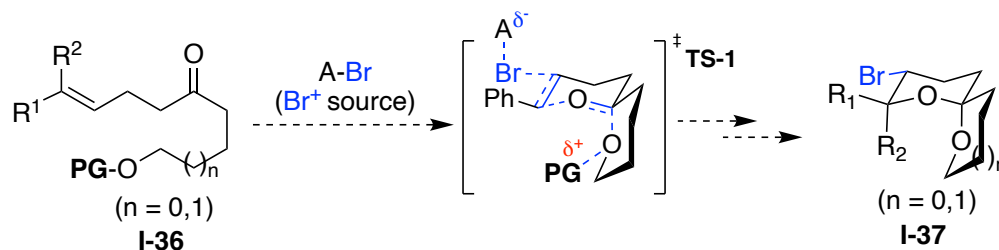


Figure I-8. Strategies towards diastereoselective bromospiroketalization

event²¹⁻²³ our work was based on exploiting the thermodynamics associated with the transition state (TS) in halofunctionalization of olefin **I-36** (see TS-1, Figure I-8). Owing to

the weak nucleophilicity of the templated ketone, interception of the halenium atom by the activated olefin in **I-36** will transpire putatively via a late transition state. In the proposed asynchronous concerted addition (Ade3), it is anticipated that stereospecificity will be defined by the templating group (-OPG), engaged in enhancing the nucleophilic character of the ketone in the incipient oxocarbenium. Initial HalA(Br) guided optimizations revealed 3-bromo-1-chloro-5,5-dimethylhydantoin (BCDMH) as an ideal bromenium source generated in situ by combining equimolar amounts of DBDMH and DCDMH.

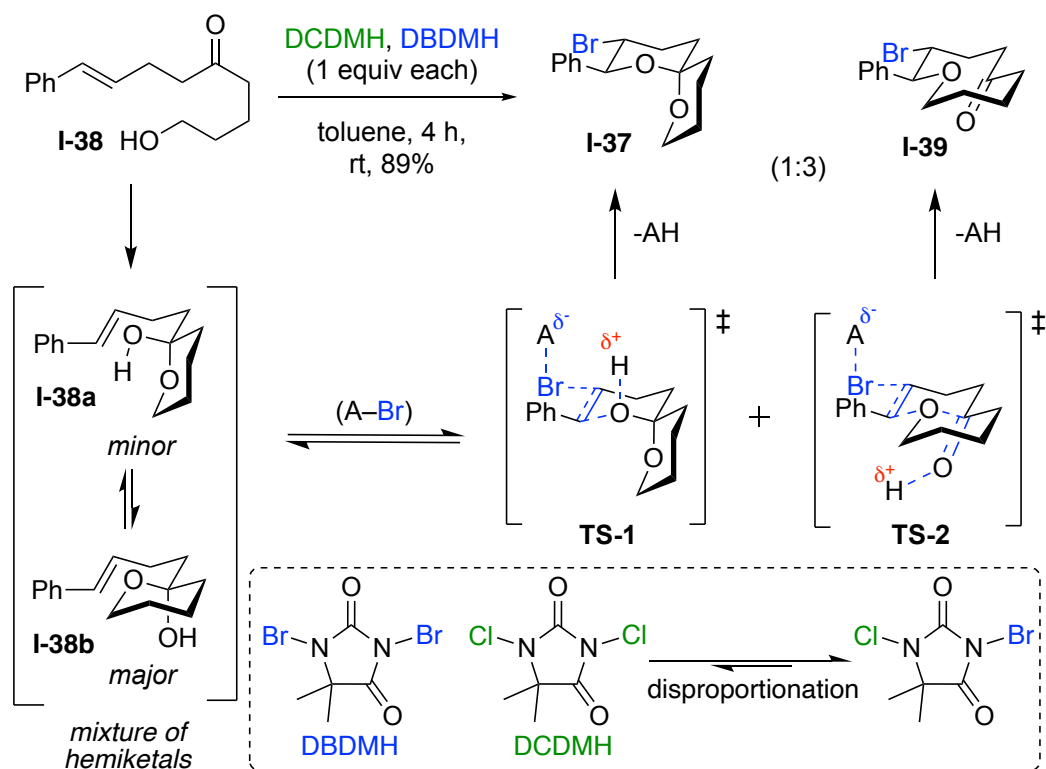


Figure I-9. Bromocyclization of **I-38** yields the macrocyclic bromoether as the major product

Substrate **I-38**, which exists in equilibrium with the corresponding hemiketals, reveals either an alkene proximal ether moiety in **I-38a** or the hydroxyl moiety in **I-38b**, poised for pre-polarization of the alkene (Figure I-9). Surprisingly, bromofunctionalization

of **I-38** furnished the macrocyclic bromoether **I-39** as a major product (>98:2 *dr*), indicating a conformational preference of the hemiketal intermediate, kinetically biased towards **I-38a**.

As anticipated from the HalA(Br) values, substrate **I-40**-THP furnished the desired bromospiroketal **I-37** as a single isomer (Figure I-10). The generality of this transformation was evaluated with a variety of substrates, and good to excellent yields and *drs* were obtained.

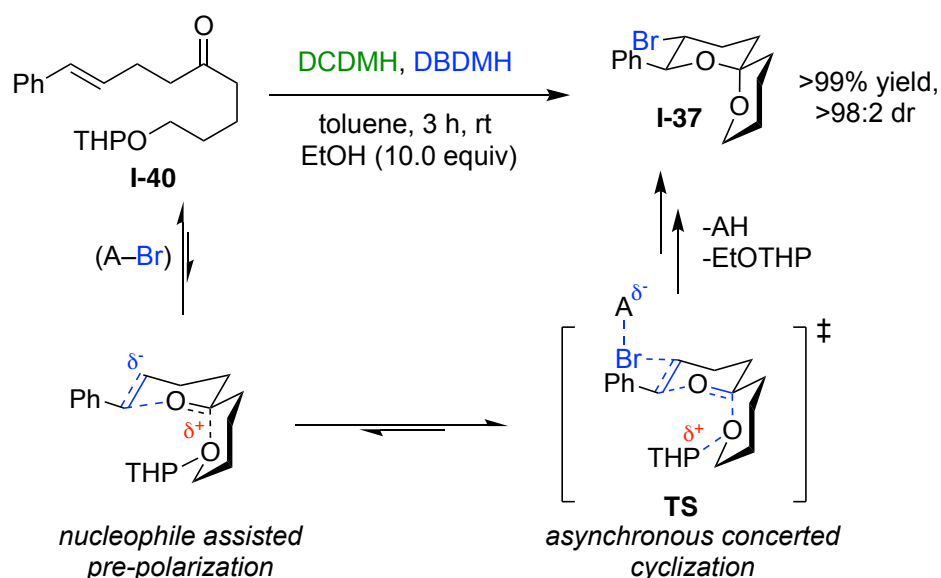


Figure I-10. Substrate **I-40**-THP furnished the desired bromospiroketal **I-37** as a single isomer

To access the dibromo- spiroketal scaffold of natural products, we initially exploited the stereoelectronics associated with the six- membered oxocarbenium ion, using a variety of keto- alkenols. As it shown in Figure **I-11**, when ethanol was omitted from the reaction mixture to avoid the early trans-ketalization of tetrahydropyranyl from intermediate-(I), the templated oxocarbenium underwent rapid conversion to enol ether (II) via deprotonation at the β -carbon (C3). A pseudo- axial capture of another bromonium

ion by the nucleophilic olefin in (II) did eventually yield the dibromo-spiroketal. Unexpectedly, inclusion of water from conc. HCl facilitates the removal of THP group. HCl was necessary to effect the desired transformation. With the oxocarbenium intermediate embedded in a six- membered ring, dibromospiroketal were obtained in good yields and diastereoselectivities.

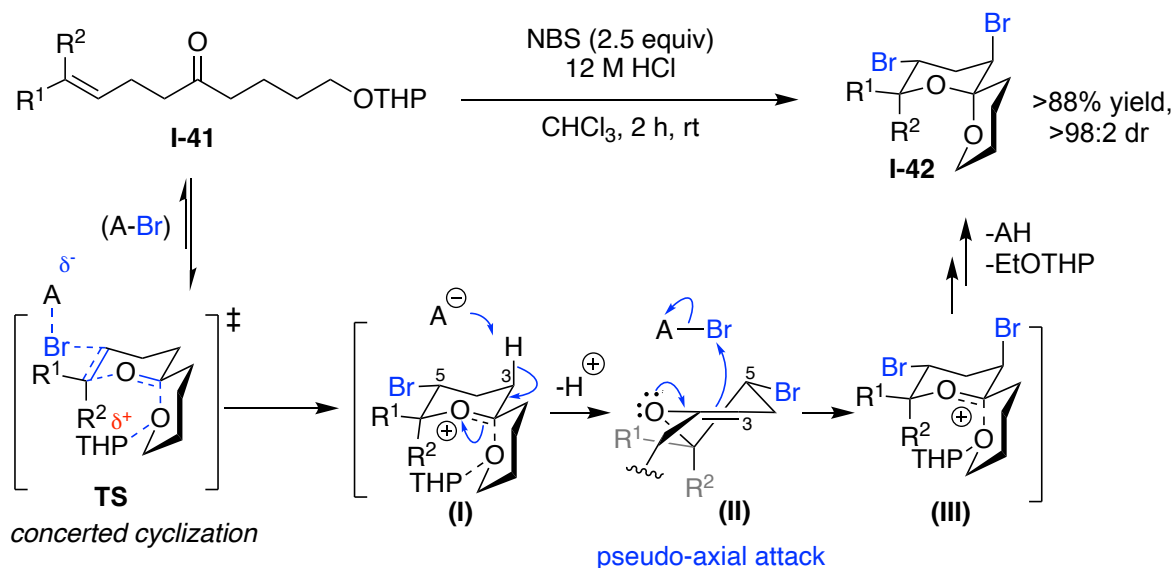


Figure I-11. Diastereoselective dibromospiroketalization

Our group's attempts to develop an enantioselective version of the bromospiroketalization failed with (DHQD)₂PHAL (cinchona alkaloid dimers). This motivated us to evaluate a new Brønsted acid/Lewis base catalytic system. To this aim, we investigated the Vanol- Imidodiphosphoramidate type catalysts. The initial data showed the dihedral angle (the angle between the substituents at the 7,7'-positions on each VANOL ligands of the catalyst), plays a critical role in enantioinduction (dashed box in Figure I-12). This angle depends on the nature of the 7,7'-substituents, and further studies indicated that an adamantyl group at these positions induced the highest enantioselectivity in the asymmetric bromospiroketalization reaction (Figure I-12). In this

recent work, the generality of this enantioselective transformation was evaluated for different substrates, and good to excellent yields and enantiomeric ratios (*er*) were obtained.

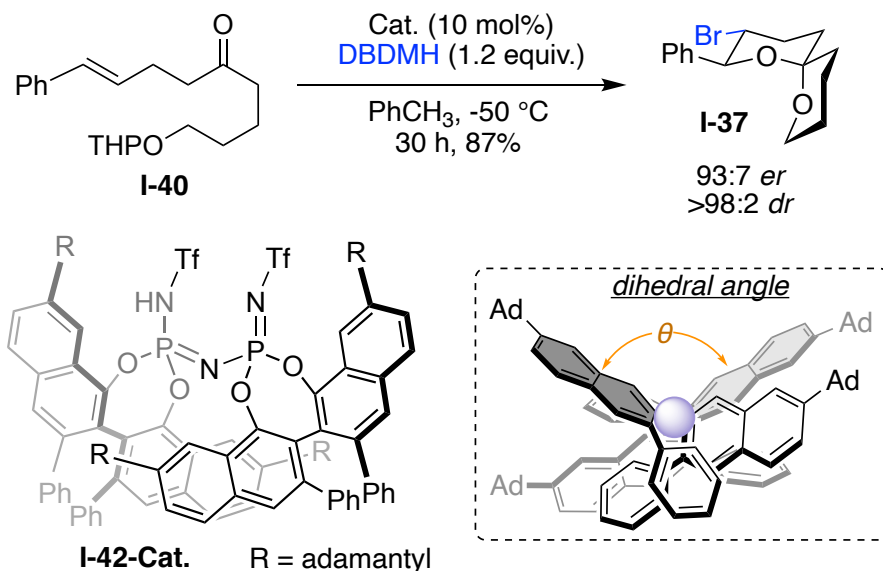


Figure I-12. Enantioselective bromo spiroketalization with vaulted biaryl catalysts

I-4 Development of asymmetric bromospirolactonization

We sought to further extend our methodology by replacing THP protected alcohols with carboxylic acids. We planned to take advantage of halofunctionalization of olefins, with the intention of generating the valuable spiro lactone moiety which, as previously mentioned, is a key skeletal moiety found in a number of biologically active natural products. Based on our previous studies, we envisioned that unsaturated substrate **I-48** would undergo bromofunctionalization followed by nucleophilic attack of the ketone, resulting in the formation of the oxacarbenium. Upon generation of the oxacarbenium, subsequent trapping by the carboxylic acid would furnish the spiro lactone (Figure I-13).

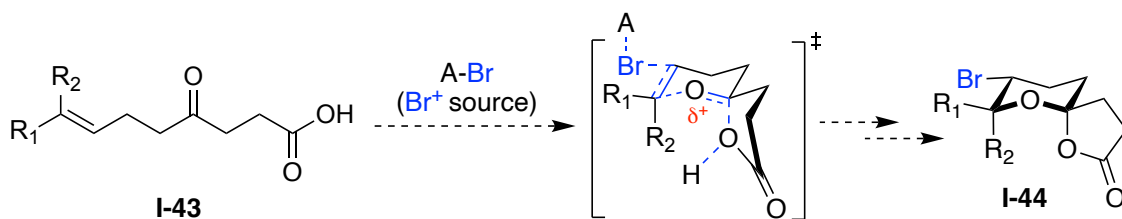


Figure I-13. Strategy towards diastereoselective bromspirolactonization

As illustrated in Figure I-14, our initial study for the uncatalyzed reaction exhibited excellent yields (up to 92%) and moderate diastereoselectivity (2.5:1) for 6,5-bromo spirolactones.

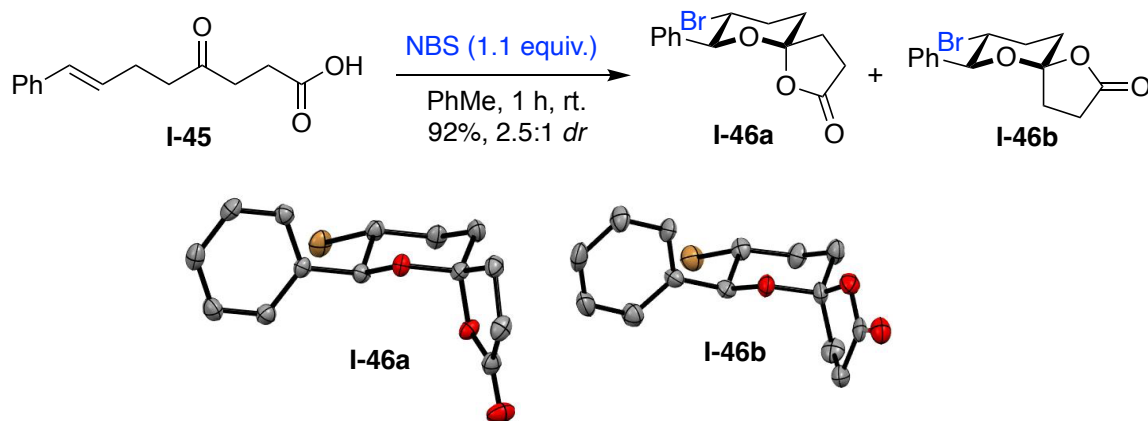
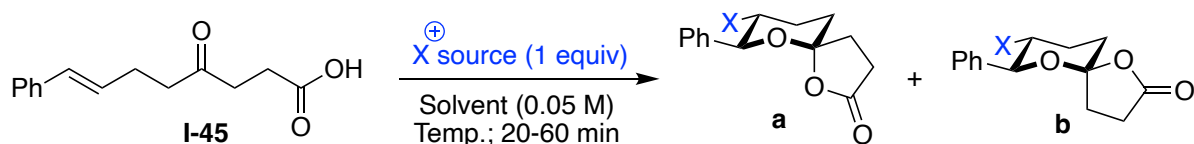


Figure I-14. Bromspirolactonization results; X-ray crystal structure of **I-46a** and **I-46b**

The reaction showed similar results with different bromine sources (NBS, DBDMH, DBDPH, and BCDMH). The relative stereochemistry of halogenated spirolactone products was established by X-ray crystal structure. The directed diastereoselectivity stems from the direction of attacking acid relative to the ketone. Attempts toward improving the diastereoselectivity are listed in Table I-1. The effects of temperature, solvent and various halogen sources were examined.

Table I-1. Reaction optimization for improving the diastereoselectivity of spirocyclization



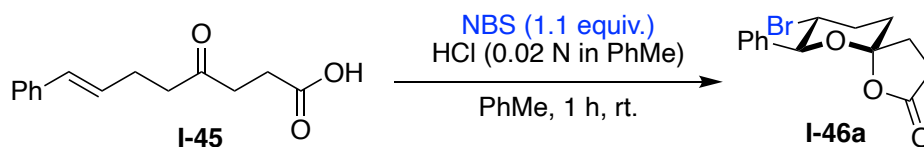
Entry	Halenium Source	Solvent	Temperature	<i>dr</i> ^a (a:b)
1 ^b	BCDMH	Toluene	r.t.	1.5:1
2 ^b	BCDMH	Toluene	0 °C	1.6:1
3	NBS	Toluene	r.t.	2.5:1
4 ^c	NBS	Toluene	0 °C	1.3:1
5	NBS	Toluene	50 °C	4:1
6	NBS	EtOH	r.t.	1.2:1
7	NBS	CHCl ₃	r.t.	1:1.2
8	NBS	CHCl ₃ /EtOH	r.t.	1.8:1
9 ^c	DCDMH	Toluene	r.t.	1:1
10 ^c	DCDMH	CHCl ₃	r.t.	1.6:1

[a] *drs* were estimated by ¹H NMR (500 MHz) analysis. [b] BCDMH generated in situ by combining 1 equivalent of each DBDMH and DCDMH, [c] reaction did not complete in 1 hour.

The results indicate that the halonium source does not affect the *dr* ratio, while higher temperatures (50 °C), increase the diastereoselectivity to 4:1 (entry 5). We then focused on the reversible ring opening of the oxaspirolactone motif under acidic conditions. As shown in Figure I-15a, running the bromospirolactonization reaction under the same conditions with a catalytic amount of HCl (12N), led to complete

diastereoselective conversion. We envisioned that acid would play a role after the formation of products, and to confirm our hypothesis, a 1:1 mixture of the two diastereomers were treated with a catalytic amount of acid in toluene. After one hour, the ^1H NMR showed a single diastereomer (**a**) in the reaction, which reaffirmed the complete conversion of **b** to **a** under acidic condition (Figure I-15). In the presence of acid, the oxygen atom opens the lactone ring, resulting in the oxacarbonium intermediate. Subsequently, the nucleophilic carboxylic acid could then attack from either axial or equatorial direction, with the axial product favored as anticipated due to the anomeric stabilization. (Figure I-15b).

a. acid mediated bromospirolactonization



b. proposed mechanism

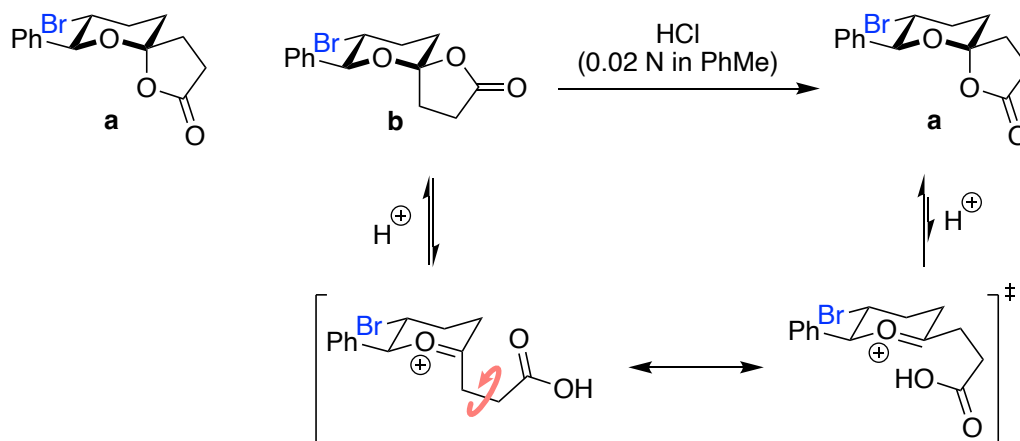


Figure I-15. Diastereoselectivity study in the presence of acid

We started our investigation of the stereoselective bromospirolactonization reaction with acidic catalysts, since they were previously shown to induce excellent

enantioselectivity in the case of bromospiroketalization. The reactions carried out with different acid catalysts, are shown in Figure I-16. The reaction with aryl-substituted (*S*)-VANOL phosphoric acid catalyst **I-47**, showed no enantiomeric excess (50:50% *er*) and a 2.5:1 diastereomeric ratio. Studying the reaction with the adamantyl substituted vaulted biaryl catalyst **I-42**, previously shown to be successful for the enantioselective bromospiroketalization reaction, led to improvement of the diastereoselectivity to >10:1, but no enantiomeric excess was observed in this reaction. Also, the rate of the reaction for phosphoric acid catalysts did not differ compared to the uncatalyzed reaction, while the vaulted biaryl catalyst provided a slight improvement in the reaction rate.

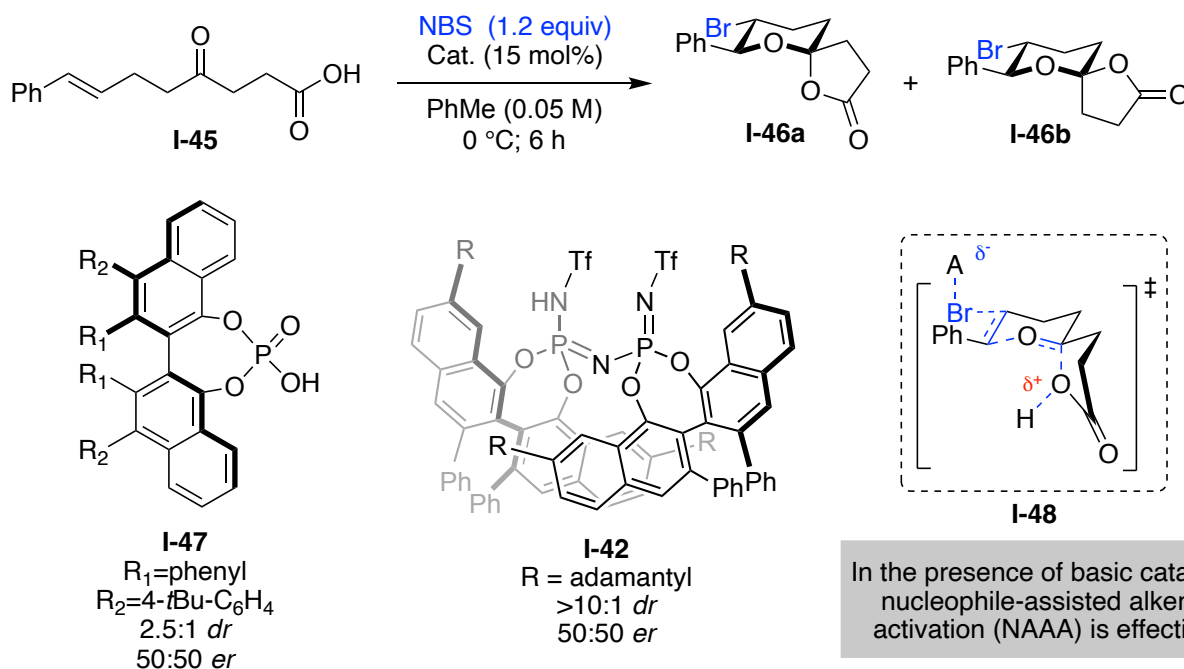
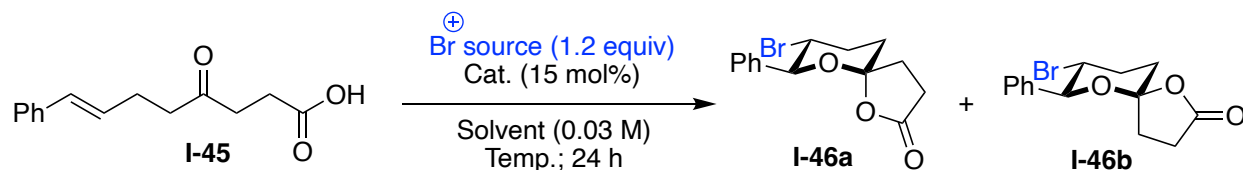


Figure I-16. Asymmetric bromospirolactonization with acidic catalysts; TS in dashed box

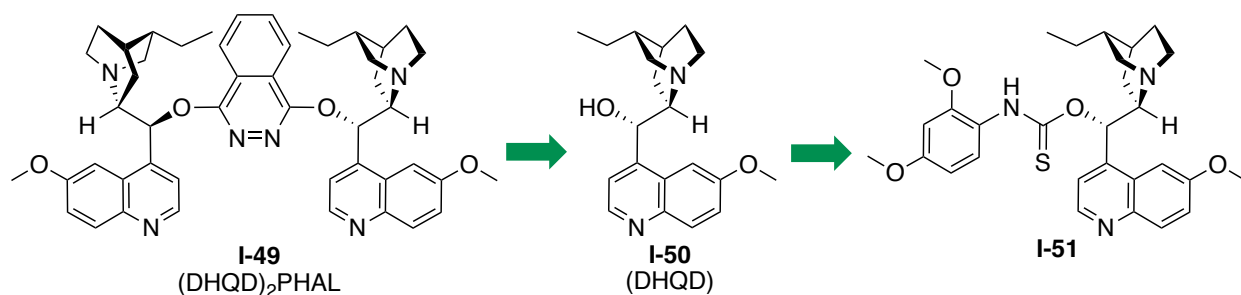
Perhaps, the weak nucleophilicity of the carboxylic acid group, especially under acidic conditions, does not promote the formation of the proposed intermediate (see **I-48**, Figure I-16). NAAA activation of the olefin would seemingly be more effective in the

presence of basic catalyst. Based on these results, we began to investigate a series of basic catalysts. From this investigation we found an interesting result from our previous cinchona alkaloid dimers. As shown in Table I-2, the studies were performed at $-40\text{ }^{\circ}\text{C}$, since background reactions are effectively suppressed at this temperature. Although (DHQD)₂PHAL did not induce chirality in the reaction, it did highly accelerate the rate of the reaction relative to the uncatalyzed version. It led to good yield (82%) with 2:1 diastereomeric ratio and 55:45 enantiomeric ratio. Optimization of the reaction with (DHQD)₂PHAL with different temperatures and a variety of solvents resulted in good yield (73-84%) and almost analogous *dr* (2:1), but no significant improvement in *er* was observed. To narrow down which component of (DHQD)₂PHAL is catalyzing the reaction we truncated the structure it into its constituent components, and ran the reaction with only DHQD as the catalyst. The reaction proceeded with comparable rate and yield. At this point, we realized the need to introduce a handle to our catalyst to induce facial selectivity. Inspired by previous halolactonizations,²⁴ we designed and synthesized a thiocarbamate cinchona derivative catalyst I-51. Applying this catalyst in the same conditions led to 69:31 *er*, providing a promising start for further structural optimizations (see Table I-2, entry 4).

Table I-2. Asymmetric bromospirolatonization with basic catalysts

Entry	Cat.	Br Source	Solvent	Temp.	Yield (%)	<i>dr</i> ^a (a:b)	<i>er</i> ^b (%)
1	-	NBS	PhMe:CHCl ₃ (2:1)	-40 °C	N.R.	-	-
2	I-49	NBS	PhMe:CHCl ₃ (2:1)	-40 °C	82	2:1	55:45
3	I-50	NBS	PhMe:CHCl ₃ (2:1)	-40 °C	70	1.2:1	50:50
4	I-51	NBS	PhMe:CHCl ₃ (2:1)	-40 °C	88	1.5:1	69:31

[a] *drs* were estimated by ¹H NMR (500 MHz) analysis. [b] *ers* were almost the same for two diastereomers.



A structural advantage of this catalyst is that there are many potential points of optimization that could lead to an increase in the enantioselectivity of the reaction. The general structure **I-52** highlights the domains for further studies. We could investigate steric and electronic perturbations, as well as the nature of the carbonyl linker between the aryl group and the alkaloid (carbamate/thiocarbamate, urea/thiourea). The influence of different substitutions on the quinoline ring could be probed, as well as modulation of the basicity of the quinuclidine nitrogen atom.

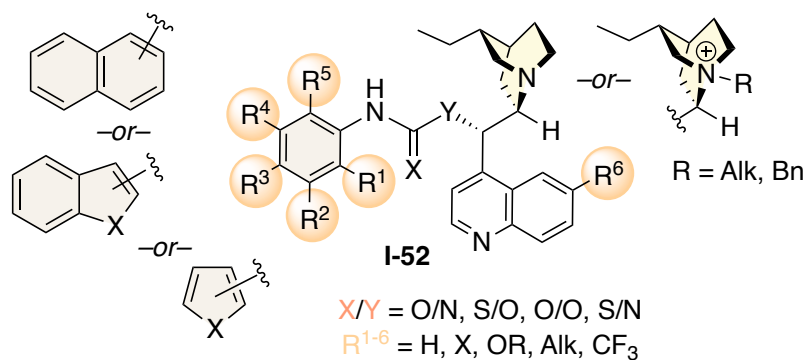
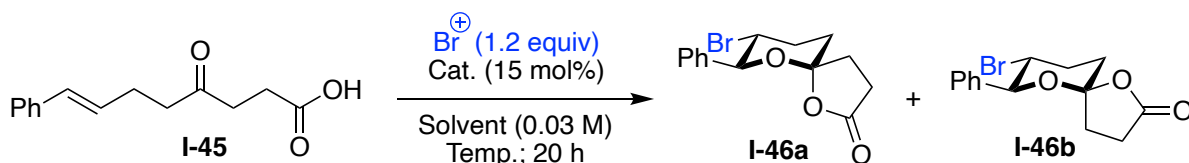


Figure I-17. Generalized structures for basic catalysts based on the cinchona alkaloid structure

Before optimizing the catalyst structure, we intended to study different conditions that may affect the enantiomeric ratio. As shown in Table I-3, we altered temperature (Table I-3, entry 2), solvent and bromine source, however, none of them improved the *er* to more than 69:31%.

Table I-3. Reaction optimization for cat. **I-51**; temperature, solvent and Br source were altered



Entry	Cat.	Br Source	Solvent	Temp.	<i>er</i> ^a (%)
1	I-51	NBS	PhMe:CHCl ₃ (2:1)	0 °C	66:34
2	I-51	NBS	PhMe:CHCl ₃ (2:1)	-40 °C	69:31
3	I-51	NBS	PhMe	-40 °C	52.5:47.5

Table I-3 (cont'd)

4	I-51	NBS	PhMe:CHCl ₃ (2:1)	-50 °C	65:35
5	I-51	NBS	CHCl ₃	-40 °C	60:40
6	I-51	DBDMH	PhMe:CHCl ₃ (2:1)	-40 °C	66.5:33.5
7	I-51	NBP	PhMe:CHCl ₃ (2:1)	-40 °C	66.5:33.5

Isolated yields are between 68-93%; *d*rs were estimated by ¹H NMR (500 MHz) analysis and were between (1.5:1 to 2:1); NBP is N-bromophthalimide. [*a*] *ers* were almost the same for two diastereomers.

The data demonstrated that -40 °C, NBS as bromine source, and a 2:1 mixture of PhMe:CHCl₃ gave the optimal enantiomeric outcome. Based on these initial results, we realized the need to alter the catalyst structure to further increase enantioselectivity. Our general strategy for synthesizing the catalysts are summarized in Figure I-18. Proper cinchona alkaloid derivatives was synthesized and reacted with functionalized isocyanate or isothiocyanate.

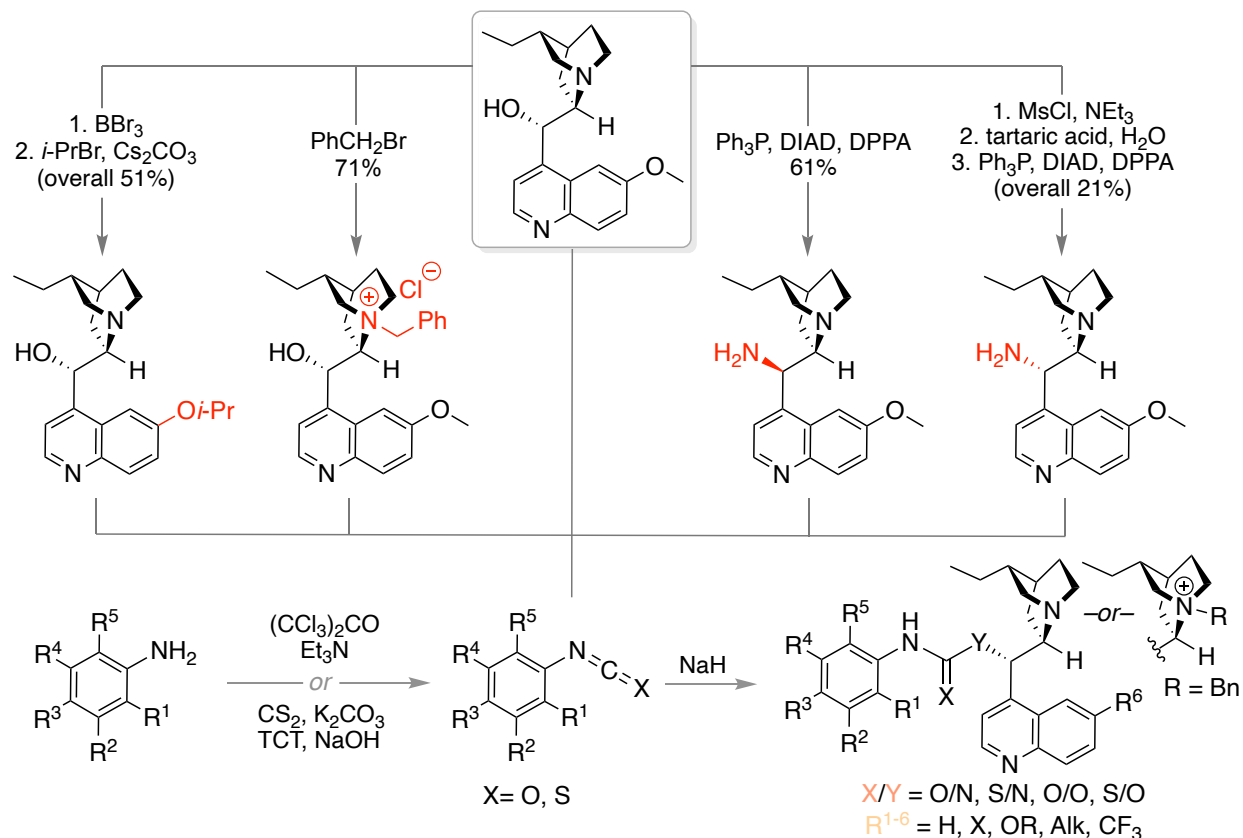
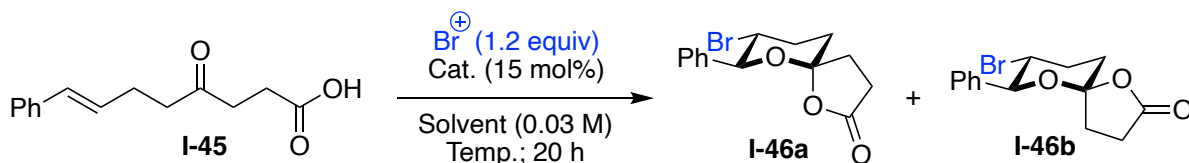


Figure I-18. General synthesis of basic catalysts

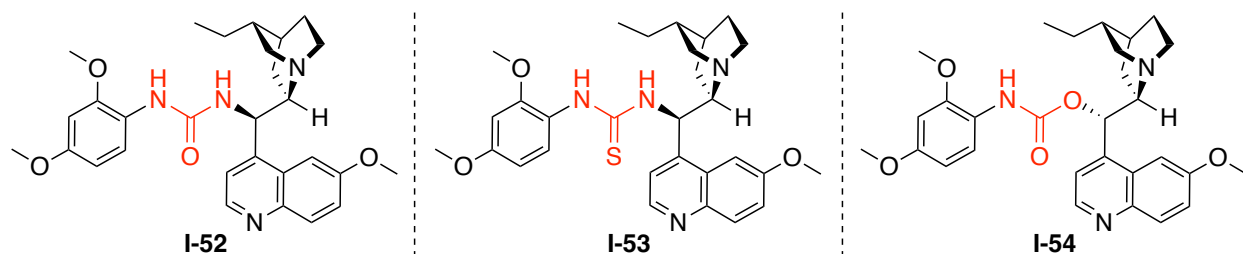
Our first attempt was focused on the carbonyl linker between the aryl group and the alkaloid. In addition, we synthesized the carbamate, urea, and thiourea version of thiocarbamate catalyst **I-51**. As illustrated in Table **I-4**, running the reaction in the presence of urea catalyst **I-52** and thiourea catalyst **I-53** dropped the enantiomeric ratio to 55:45% and 50:50%, respectively while carbamate catalyst **I-54** increased it drastically to 85:15%.

Table I-4. Study of the effects of different carbonyl linkers on asymmetric bromospirolactonization



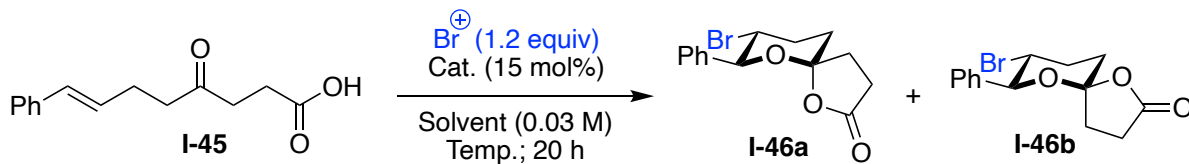
Entry	Cat.	Br Source	Solvent	Temp.	<i>dr</i> ^a (a:b)	<i>er</i> ^b (%)
1	I-51	NBS	PhMe:CHCl ₃ (2:1)	-40 °C	1.5:1	69:31
2	I-52	NBS	PhMe:CHCl ₃ (2:1)	-40 °C	1.1:1	55:45
3	I-53	NBS	PhMe:CHCl ₃ (2:1)	-40 °C	1:1.1	50:50
4	I-54	NBS	PhMe:CHCl ₃ (2:1)	-40 °C	1.7:1	85:15

Isolated yields were between 72-94%. [a] *drs* were estimated by ¹H NMR (500 MHz) analysis. [b] *ers* were almost the same for two diastereomers.



Catalyst **I-54** has the potential to be an ideal candidate for asymmetric bromospirolactonization; and as such, we sought to understand the different conditions that may influence the enantiomeric ratio. As shown in Table **I-5**, we altered temperature, solvent, and bromine source. Also, we studied the effect of different additives such as benzoic acid and 4-nitrobenzenesulfonamide (NsNH₂).

Table I-5. Reaction optimization for cat. **I-54**; temperature, solvent and Br source were altered



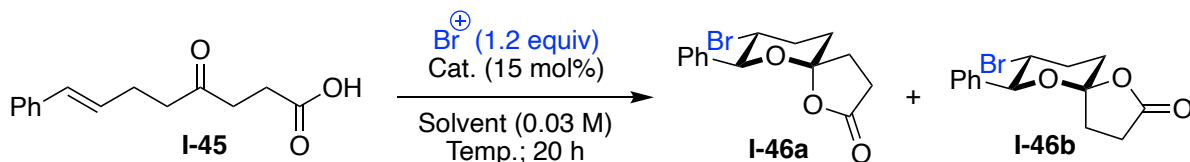
Entry	Cat.	Br Source	Solvent	Temp.	Time (h)	<i>er</i> ^a (%)
1	I-54	NBS	PhMe:CHCl ₃ (2:1)	0 °C	12	68:32
2	I-54	NBS	PhMe:CHCl ₃ (2:1)	-20 °C	20	74.5:25.5
3	I-54	NBS	PhMe:CHCl ₃ (2:1)	-30 °C	20	80:20
4	I-54	NBS	PhMe:CHCl ₃ (2:1)	-40 °C	20	85:15
5	I-54	NBS	PhMe:CHCl ₃ (2:1)	-50 °C	24	73:27
6 ^d	I-54	NBS	PhMe:CHCl ₃ (2:1)	-40 °C	20	73:27
7	I-54	NBS	PhMe:CHCl ₃ (2:1)	-70 °C	28	61.5:38.5
8	I-54	NBS	PhMe:CHCl ₃ (1:1)	-40 °C	20	82:18
9	I-54	NBS	PhCl	-40 °C	20	73.5:26.5
10	I-54	NBS	ACN	-40 °C	20	56:44
11	I-54	NBS	Toluene	-40 °C	20	62.5:37.5
12	I-54	NBS	CHCl ₃	-40 °C	16	80:20
13 ^e	I-54	NBS	PhMe:CHCl ₃ (2:1)	-40 °C	20	78:22
14 ^f	I-54	NBS	PhMe:CHCl ₃ (2:1)	-40 °C	20	77:23
15	I-54	DBDMH	PhMe:CHCl ₃ (2:1)	-40 °C	20	65.5:35.5

Table I-5 (cont'd)

16	I-54	NBA	PhMe:CHCl ₃ (2:1)	-40 °C	20	76:24
17	I-54	NBP	PhMe:CHCl ₃ (2:1)	-40 °C	20	73:27

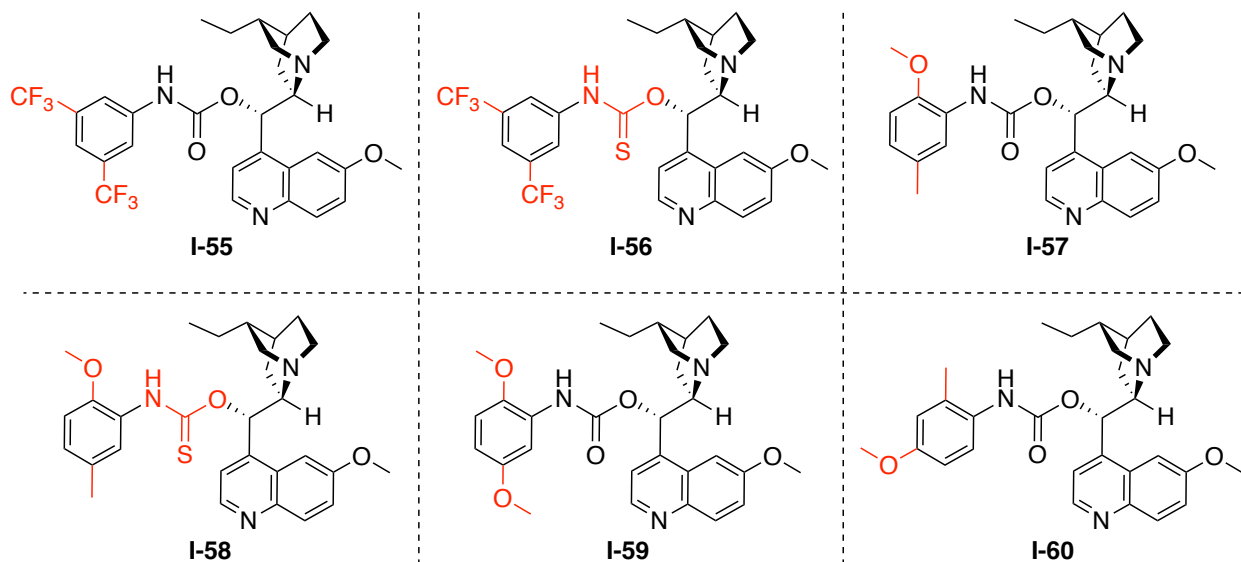
[a] *ers* were almost the same for two diastereomers. [b] *drs* were estimated by ¹H NMR (500 MHz) analysis and were between 1.1:1 to 2:1 [c] Isolated yields were between 66-94%. [d] Chloroform included 0.75% EtOH [e] Benzoic acid (1 equiv) was added as an additive. [f] NsNH₂ (1 equiv) was added as an additive. [g] NBA is N-bromoacetamide.

Between several evaluated bromine sources, NBS gave the best results, with an optimal temperature of -40°C. Higher temperatures reduced the *er* due to increasing rate of the background reactions. Lower temperature led to a decrease in *er* as well, which may suggest that the catalyst conformation is altered or catalyst is aggregated. Nonetheless, the 2:1 mixture of solvents (PhMe:CHCl₃) was optimal. At this point, we focused on the electronic and steric effects of the carbamate aryl group. First, we investigated the impact of electron-withdrawing groups (EWG) such as CF₃ on the phenyl ring (catalysts **I-55** and **I-56**, Table I-6), however these catalysts resulted in significantly lower enantiomeric ratio compared to the electron-rich dimethoxy aryl catalyst **I-54**. Based on this observation, we kept the methoxy group at the ortho position and introduced a methyl group at the meta position, which based on Hammett values, is slightly electron-donating (catalysts **I-57** and **I-58**, Table I-6). We also varied the meta-methyl group with methoxy, which is a weak EDG at this position (catalyst **I-59**). The other catalyst was made from 2-methyl-4-methoxy isocyanate: the methoxy and methyl at these positions act as a strong and weak EDG, respectively (catalyst **I-60**).

Table I-6. Catalyst optimization; study of electronic effect on the carbamate aryl group

Entry	Cat.	Br Source	Solvent	Temp.	<i>dr</i> ^a (a:b)	<i>er</i> ^b (%)
1	I-55	NBS	PhMe:CHCl ₃ (2:1)	-40 °C	1.7:1	62.5:37.5
2	I-56	NBS	PhMe:CHCl ₃ (2:1)	-40 °C	1.1:1	58:42
3	I-57	NBS	PhMe:CHCl ₃ (2:1)	-40 °C	1.8:1	64:36
4	I-58	NBS	PhMe:CHCl ₃ (2:1)	-40 °C	1:1.2	60:40
5 ^c	I-59	NBS	PhMe:CHCl ₃ (2:1)	-40 °C	1.1:1	52.5:47.5
6	I-60	NBS	PhMe:CHCl ₃ (2:1)	-40 °C	1.5:1	70:30

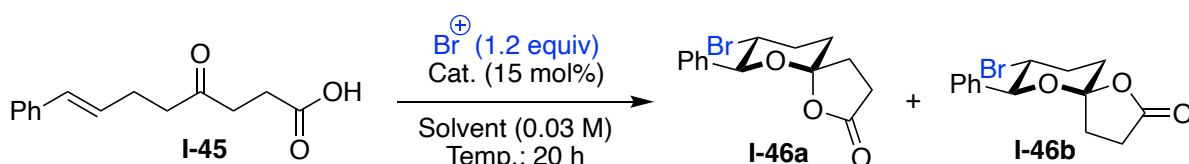
Isolated yields were between 72-94%. [a] *drs* were estimated by ¹H NMR (500 MHz) analysis. [b] *ers* were almost the same for two diastereomers. [c] yield was less than 30%.



All these changes decreased the enantiomeric ratio compared to the 2,4-dimethoxy catalyst **I-54**. As tabulated in Table I-7, we then investigated trimethoxy-

substituted synthesized ([2,3,4-],[2,4,6-] and [3,4,5-] trimethoxy catalysts) catalyst **I-61**, **I-62** and **I-63** respectively. The steric effect of functional groups was examined by means of introduction of bulky isopropyl relative to the methyl group, generating the 2,4-diisopropyl derivative (catalyst **I-64**). The influence of substitutions on the quinoline ring was additionally probed. To do this, we envisioned substituting the methoxy group with hydrogen to see if an EDG is obligatory for a functional catalyst (catalyst **I-65**). Previously, the steric effect of this functional group on the quinoline showed a large impact on the enantiomeric ratio for other reactions.²⁵ As such, we switched the methyl group with a bulky isobutyl to test the steric effect.

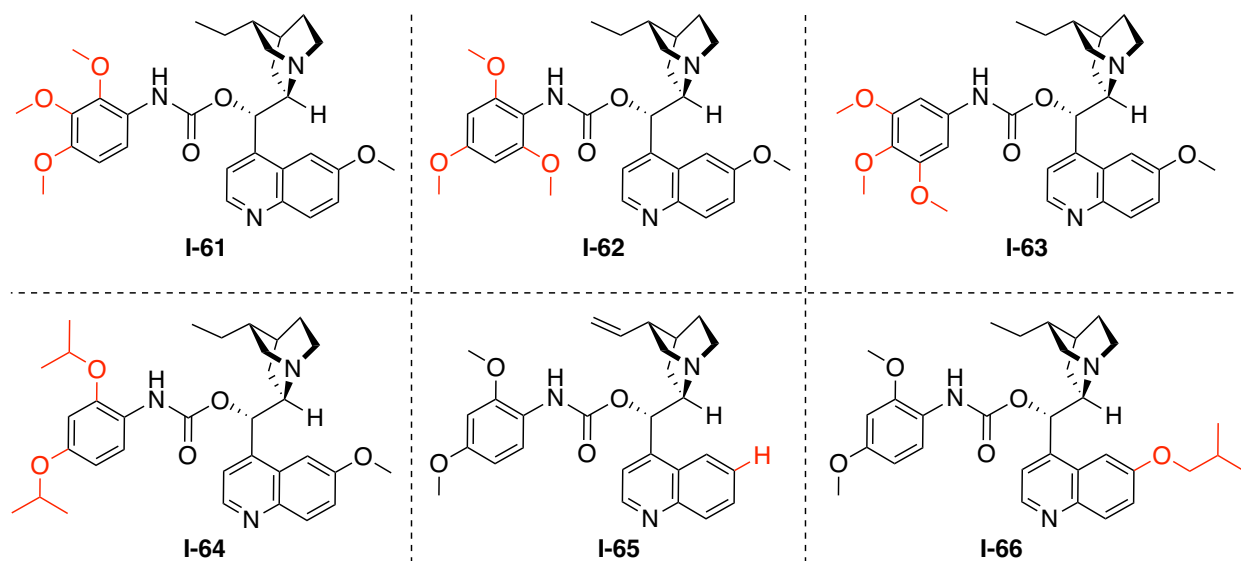
Table I-7. Catalyst optimization; electronic and steric effect on aryl carbamate and quinoline



Entry	Cat.	Br Source	Solvent	Temp.	<i>dr</i> ^a (a:b)	<i>er</i> ^b (%)
1 ^c	I-61	NBS	PhMe:CHCl ₃ (2:1)	-40 °C	2.2:1	52.5:47.5
2 ^c	I-62	NBS	PhMe:CHCl ₃ (2:1)	-40 °C	1.2:1	62:38
3 ^c	I-63	NBS	PhMe:CHCl ₃ (2:1)	-40 °C	1.6:1	56.5:43.5
4	I-64	NBS	PhMe:CHCl ₃ (2:1)	-40 °C	2:1	80.5:19.5
5	I-65	NBS	PhMe:CHCl ₃ (2:1)	-40 °C	2:1	79:21
6	I-66	NBS	PhMe:CHCl ₃ (2:1)	-40 °C	1.8:1	77.5:22.5

Isolated yields were between 63-84%. [a] *drs* were estimated by ¹H NMR (500 MHz) analysis. [b] *ers* were almost the same for two diastereomers. [c] yield was less than 30%.

Table I-7 (cont'd)

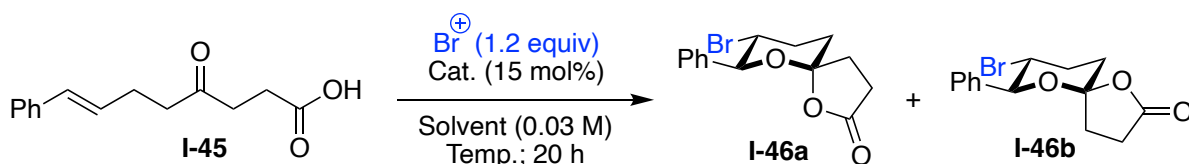


The trimethoxy substituted catalysts **I-61**, **I-62** and **I-63** did not lead to enantiomeric ratios higher than the 2,4-dimethoxy substituted catalyst **I-54**. The data showed that the sterics of the alkoxy group do not have an effect on enantiomeric excess of the reaction. Studies conducted on the quinoline moiety revealed that the functional group at C6 position does play a critical role in the enantiomeric excess of the reaction. Also, replacing the methoxy with hydrogen decreased the *er*. However, the sterics of that functional group did not affect the reaction to any appreciable extent.

In the next step, the pseudo-enantiomer of catalyst **I-54** was synthesized (catalyst **I-67**) and was examined in the enantioselective bromospirolactonization reaction, which led to opposite enantioinduction with a slightly lower *er* (Table I-8). Subsequently, we studied the amide derivative of cinchona alkaloid (catalyst **I-68**) which was utilized in prior asymmetric halofunctionalizations. Also, we tested catalyst **I-67** which was recently reported for the domino halocyclization reaction¹⁴ (Table I-8, entry 3) The urea and carbamate derivative of this catalyst was also synthesized (**I-68** and **I-69**) and examined

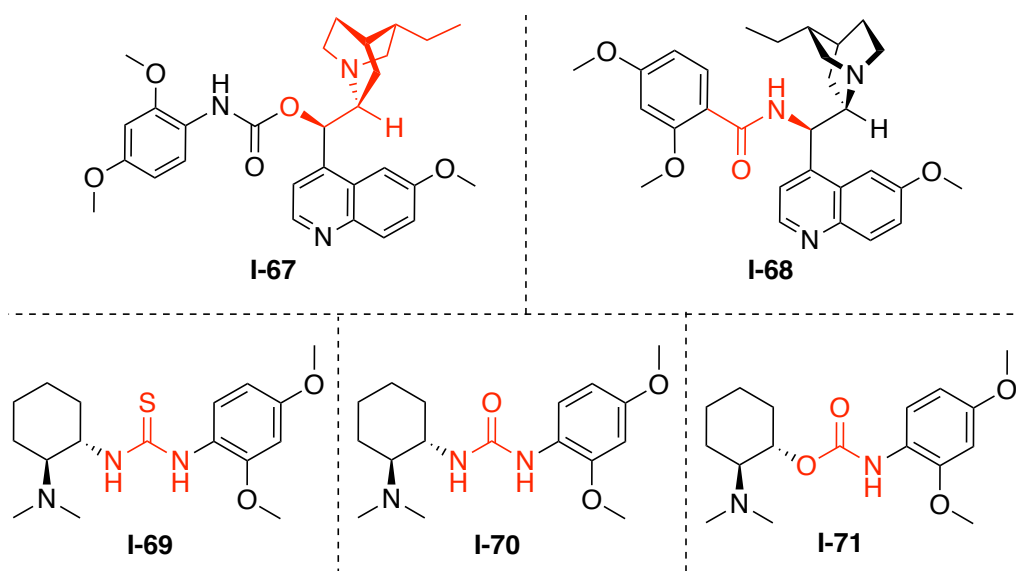
for asymmetric bromspirolactonization. These series of catalysts showed moderate to good yield (58-89%) and up to 1.5:1 *dr* but, none of these catalysts was able to improve the *er* compared to catalyst **I-54**.

Table I-8. Study of thiourea, urea and carbamate catalysts



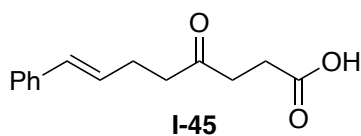
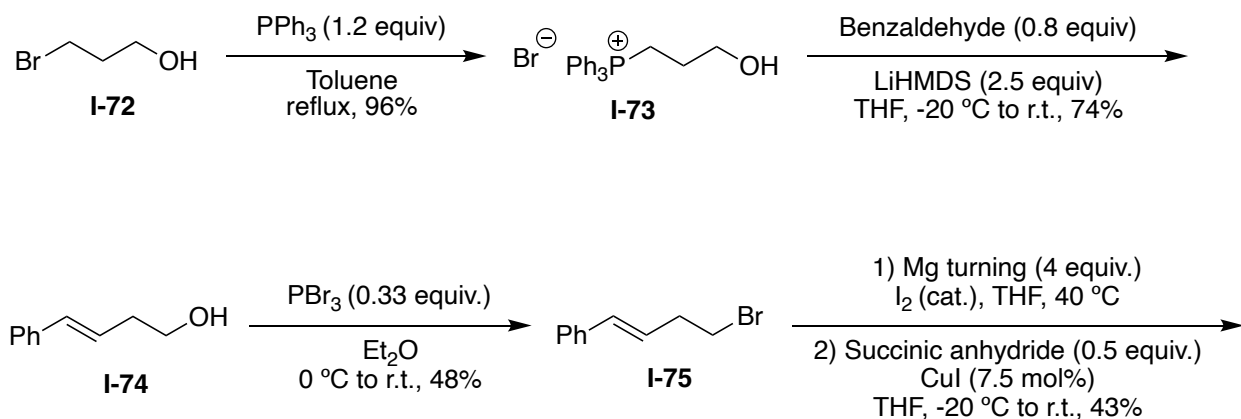
Entry	Cat.	Br Source	Solvent	Temp.	<i>dr</i> ^a (a:b)	<i>er</i> ^b (%)
1	I-67	NBS	PhMe:CHCl ₃ (2:1)	-40 °C	1.5:1	75:25
2	I-68	NBS	PhMe:CHCl ₃ (2:1)	-40 °C	1:1	52.5:47.5
3	I-69	NBS	PhMe:CHCl ₃ (2:1)	-40 °C	1.1:1	57:43
4	I-70	NBS	PhMe:CHCl ₃ (2:1)	-40 °C	1.1:1	52:48
5	I-71	NBS	PhMe:CHCl ₃ (2:1)	-40 °C	1:1	50:50

Isolated yields were between 58-89%. [a] *drs* were estimated by ¹H NMR (500 MHz) analysis. [b] *ers* were almost the same for two diastereomers.



The upshot of these studies is that catalyst **I-54** remained the best of the group. While we were actively seeking to optimize this catalyst and other parameters of the reaction condition to improve the enantiomeric ratio, we aimed to examine the generality of this method. In order to do this, we sought to synthesize a library of appropriate substrates. As shown in Figure **I-19** (method A), Our first method for generating the phenyl substrate **I-45** proceeded by generating the phosphonium ylide **I-73** from 3-bromopropanol, which underwent a Wittig reaction with benzaldehyde to generate homoallylic alcohol **I-74**. After bromination of alcohol in the presence of PBr_3 , we attempted to react with succinic anhydride via its corresponding Grignard. This method has two major drawbacks for making the substrate library; the first being that the final step is low yielding, and the yield tended to fluctuate. Secondly, the overall lack of atom and stepwise economy meant a laborious process to complete all 4 steps for each substrate. To mitigate this issue, we designed and develop a divergent method to make the starting materials. As shown in Figure **I-19** (method B), compound **I-80** was synthesized following the reported procedure.²⁶ The allyl bromide reacted with methyl acetoacetate in a basic condition to generate the keto ester **I-77**, which was converted to di-ester **I-79** in the presence of sodium hydride. Decarboxylation with potassium hydroxide led to the formation of a keto ester substrate with a terminal alkene **I-80** (we run large scale reactions for these 3 steps). Lastly, every substrate was stitched together with the terminal olefin, via a Grubbs cross metathesis reaction. The substrates that were successfully synthesized are listed in Table **I-9**.

Method A:



Method B:

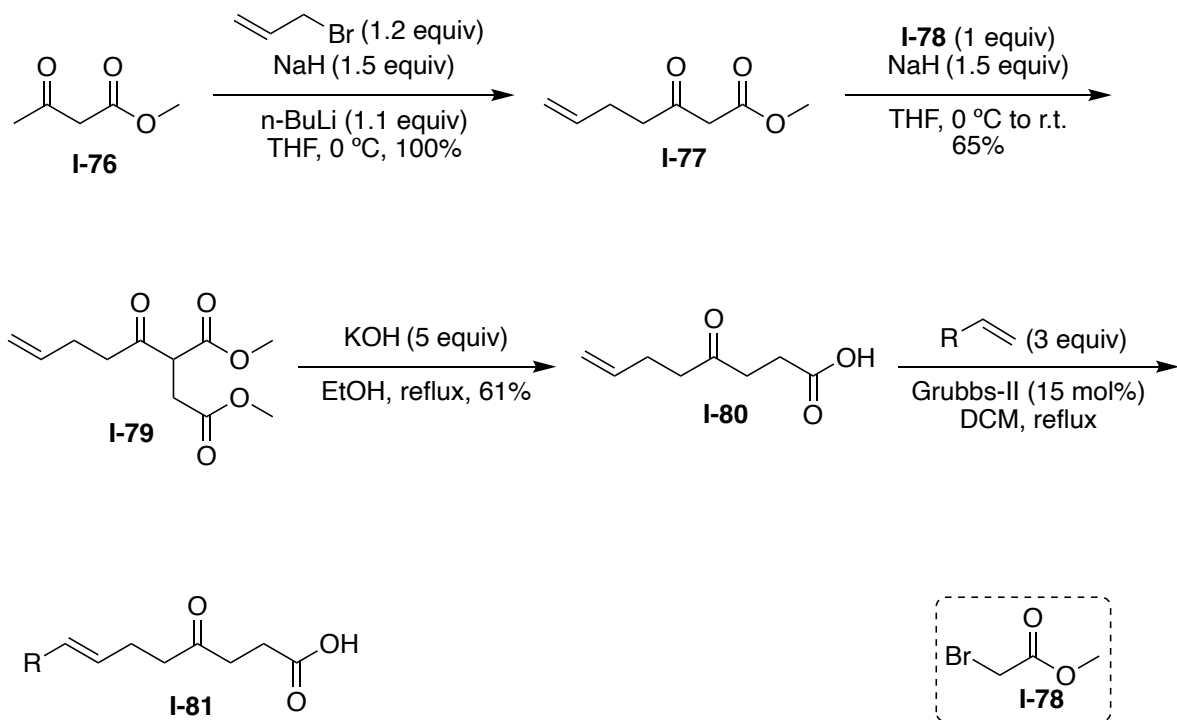
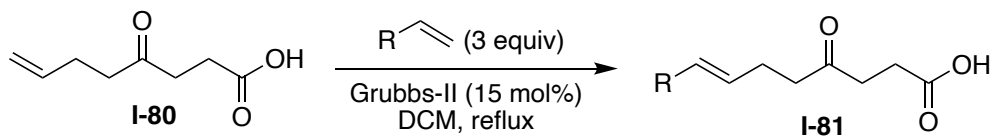
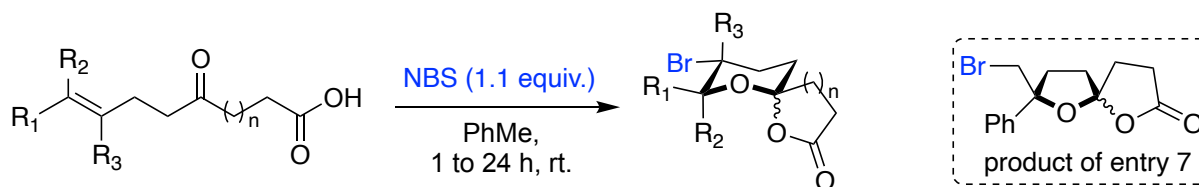


Figure I-19. Synthetic methods for making substrates

Table I-9. Grubbs cross metathesis results

Entry	R	Product	Yield (%)	Entry	R	Product	Yield (%)
1	Ph	I-45	71	7	4-CH ₃ CO ₂ -C ₆ H ₄	I-87	57
2	4-CH ₃ O-C ₆ H ₄	I-82	61	8	β -naphthyl	I-88	61
3	3-NO ₃ -C ₆ H ₄	I-83	33	9	4-CH ₃ CO-C ₆ H ₄	I-89	49
4	4-CF ₃ -C ₆ H ₄	I-84	42	10	<i>t</i> -Bu	I-90	54
5	4-CH ₃ -C ₆ H ₄	I-85	72	11	Cy	I-91	38
6	4-F-C ₆ H ₄	I-86	55	12	C ₄ H ₄ S	I-92	59

As summarized in Table I-10, the generality of the uncatalyzed bromospirolactonization reaction was investigated. The keto-acids presented in Table I-10 were subjected to halonium atom initiated cascade spirolactonization under optimized conditions. The crystal structure of product **I-45** was used to establish the relative stereochemistry in the halogenated spirolactone products. The reactions proceeded in moderate to high yield for different functional groups and different ring sizes. The rate was slower for the 4-chloro phenyl substrate and led to lower yield (Table I-10, entry 5) compared to phenyl substrate (Table I-10, entry 1). One hypothesis is that the electron withdrawing effect of chlorine at the para position decreases the nucleophilicity of the double bond toward abstracting the halogen. As shown in Table I-10 (entry 8), the [6,6]-

Table I-10. Substrate scope study of uncatalyzed bromspirolactonizations

Entry	R ¹	R ²	R ³	n	Product	Yield (%)	<i>dr</i> ^a
1	Ph	H	H	1	I-45	92	2.5:1
2	4-CH ₃ O-C ₆ H ₄	H	H	1	I-93	89	1:1.2
3	4-CH ₃ -C ₆ H ₄	H	H	1	I-94	90	1:1.5
4	4-F-C ₆ H ₄	H	H	1	I-95	81	1:1.85
5	4-Cl-C ₆ H ₄	H	H	1	I-96	40	1:1.1
6	C ₄ H ₄ S	H	H	1	I-97	58	1:1
7	H	H	Ph	1	I-98	84	1:1
8	Ph	H	H	2	I-99	79	10:1

[a] *drs* were estimated by ¹H NMR (500 MHz) analysis.

spirolactone core was obtained via diastereoselective bromspirolactonization (10:1 *dr*). The crystal structure of the major diastereomer of **I-99** product was obtained and showed the carboxylic acid residue in the axial position as anticipated due to anomeric stabilization (Figure I-20). The corresponding [5,5]-spirolactone **I-98** was formed in good yield by installing the phenyl group at the R₃ position (Table I-10, entry 7). The transition state of [5,5]-spirolactonization does not enjoy the same level of stability from the anomeric effect, thus leading to reduced *dr*.

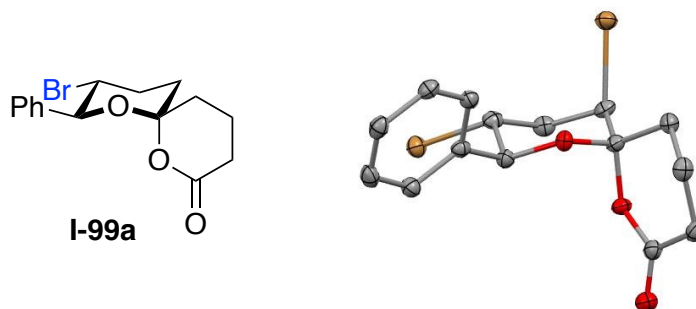
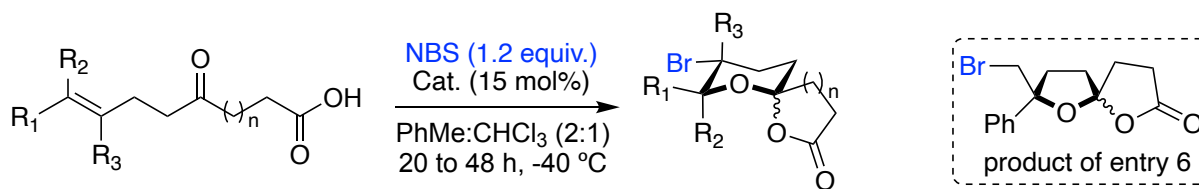


Figure I-20. X-ray crystal structure of I-99a

The generality of the asymmetric catalytic bromospirolactonization is reported in Table I-11. The enantioselective reaction of the above keto-acid substrates were exploited with catalyst **I-54** under optimized condition. The reactions proceeded in moderate to excellent yield for different functional groups and ring sizes. The distereoselectivity ranged from 1:1 to 1.9:1 and did not vary significantly between substrates. Modulating the electronic profile or the size of the substituents, had a significant effect on the enantiomeric ratio of the reactions. In case of electron rich 4-methoxy substrate (Table I-11, entry 2), the enantiomeric ratio dropped drastically to 57.5:42.5% relative to the phenyl substituted 85:15% (entry 1). Presumably, strong electron donating group at para position would increase the nucleophilicity of the olefin and not requiring the activation for bromonium capture. In this system, the oxacarbenium template dominated by *NAAA* would be absent. The enantiomeric ratio of the 4-fluorophenyl substrate was the same as for phenyl, since fluoro is slightly electron withdrawing at para position (entry 4) and, 4-chloro and 4-methyl reactions resulted in a slightly lower *er* (entry 3 and 4). This reaction was not compatible with different ring sizes and as shown in Table I-11, the *er* dropped dramatically for [5,5] and [6,6] substrates (entries 6 and 7).

Table I-11. Substrate scope study of catalytic asymmetric bromospirolactonizations

Entry	R ¹	R ²	R ³	n	Product	Yield (%)	<i>dr</i> ^a	<i>er</i> ^b
1	Ph	H	H	1	I-45	94	1.7:1	85:15
2	4-CH ₃ O-C ₆ H ₄	H	H	1	I-93	58	1.5:1	57.5:42.5
3	4-CH ₃ -C ₆ H ₄	H	H	1	I-94	89	1.9:1	76:24
4	4-F-C ₆ H ₄	H	H	1	I-95	78	1.7:1	84:16
5	4-Cl-C ₆ H ₄	H	H	1	I-96	69	1.7:1	75:25
6	H	H	Ph	1	I-98	81	1:1	60:40
7	Ph	H	H	2	I-99	83	1.5:1	57.5:42.5

a] *drs* were estimated by ¹H NMR (500 MHz) analysis. [b] *ers* were almost the same for two diastereomers.

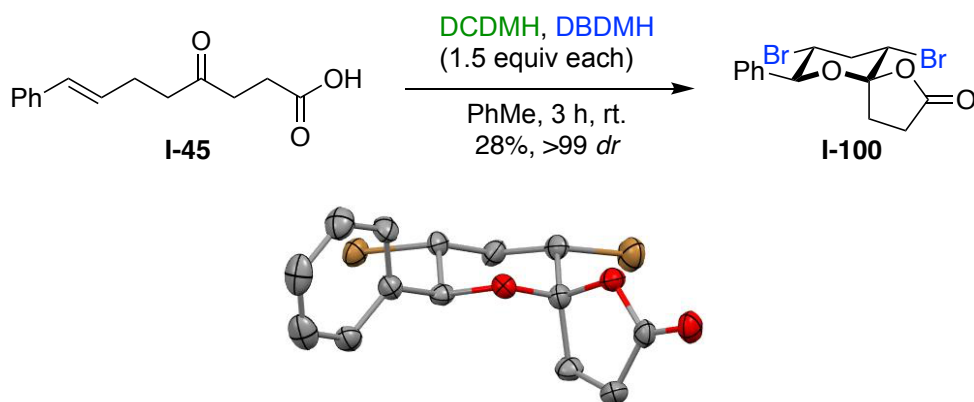
I-5 Future work

I-5-1 Development of di-bromospirolactonization

During reaction optimization studies on mono-bromospirolactonization, we found that an excess amount of a more reactive bromine source (toward halofunctionalization) led to a second bromination of the oxane ring. As shown in Figure I-21a, excess of 3-bromo-1-chloro-5,5-dimethylhydantoin (BCDMH); generated in situ by combining equimolar amounts of DBDMH and DCDMH was able to furnish the di-bromospirolactonization product. The relative stereochemistry of di-brominated spirolactone product was confirmed by an X-ray crystal structure. This reaction is currently under further

development and optimization. Also, in the case that a second bromine is substituted after generation of the mono-bromospirolactone, there is a great potential to develop di-halogenated spirolactones with different halogens (Figure I-21b). Lastly, we could study the first enantioselective di-bromospirolactone using the carbamate derivatives of cinchona alkaloid catalyst **I-54**.

a. di-bromospirolactonization result and X-ray crystal structure



b. proposed di-halospirolactonization



Figure I-21. Development of di-bromo and di-halospirolactonization

I-5-2 Toward the total synthesis of Obtusallenes V and VI

After developing the mono and di-bromospirolactonization reaction, we intended to extend our chemistry by applying this method to access Obtusallene VI, a dihalogenated C_{15} -macrocyclic ether. This macrocycle was isolated in 2000 from a red seaweed, *Laurencia obtuse*.^{27, 28} Since its isolation, its synthesis has not been reported and remains an elusive synthetic target. The synthesis of obtusallene VI will be pursued by first making

keto-acid **I-80** as described above, which will undergo a cross metathesis²⁹ with the known protected alcohol **I-102**³⁰ to afford **I-103**. This intermediate is then set up for the key bromo spirolactonization reaction to generate compound **I-104** (Figure I-22). As shown in Table I-11, we demonstrated the synthesis of the 5,5-spirolactone and the transformation of **I-103** to **I-104** would be carried out under the same conditions. Currently, this step is under investigative screening with different catalysts. We propose the use of the Comins reagent which was used to make the vinyl triflate of a similar compound previously³¹ followed by a Negishi cross-coupling with the Reformatsky derived zincated ethyl ester should presumably lead to **I-105**.³²⁻³⁴ The conjugated ester **I-106** would be generated via β -chlorination of the vinyl ether in the presence of a mild chlorenium source and subsequent deprotonation.³⁵⁻³⁷ The olefin **I-106** should be reduced by hydrogen atom transfer methods due to the susceptibility of the alkyl bromide and allylic chloride to reduction.³⁸⁻⁴⁰ Putatively, the reduction will occur syn to the chlorine, since in an energy minimized structure of **I-106**, the alternate face is sterically hindered. This is presumed to be mediated by interactions with the spiro oxygen atom. Reducing the ethyl ester to the aldehyde and subsequent Julia-Kocienski olefination results in enyne **I-110**,⁴¹ which, after deprotection of the alcohol will undergo an intramolecular bromoetherification,⁴² generating natural product **I-111**. It should however be noted that although the stereochemistry of the C4 ether bond originates from the olefin face-selectivity (calculation showed $\Delta E > 2.2$ kcal/mol for the **Z-110** rotomer that leads to the undesired face selectivity), the stereochemistry for the allenyl bromide is unpredictable.

Alternatively, the *E*-olefin of **I-110** can be synthesized with **I-109**,⁴¹ and tested for the bromoetherification that leads to obtusallene VI.

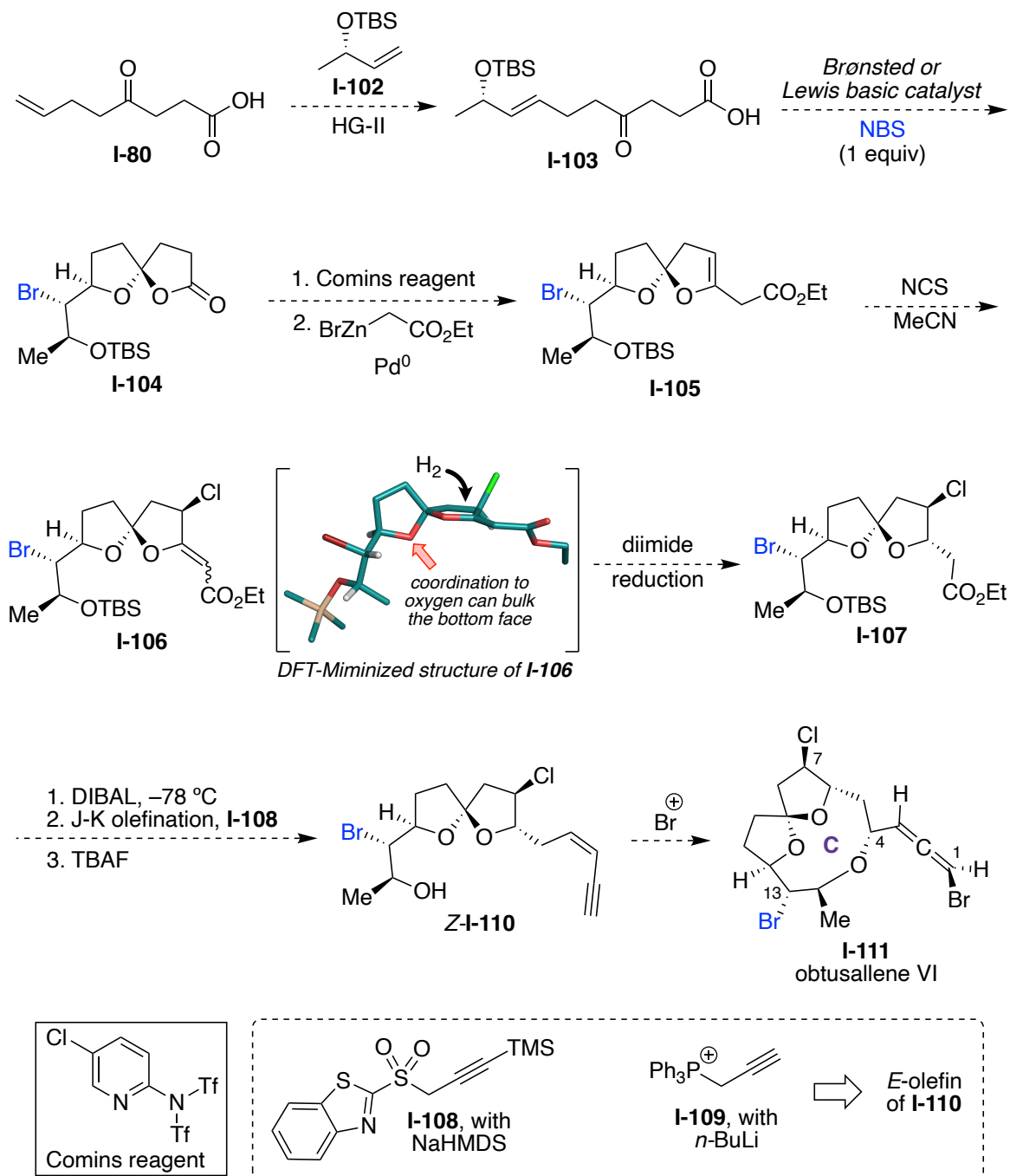


Figure I-22. Proposed total synthesis of obtusallenes VI

In summary, we have developed a bromospirolactonization method based on the application of halonium affinity (*HalA*) as a guiding tool in conjunction with Nucleophile Assisted Alkene Activation (NAAA). A series of acid/base catalysts were studied to develop a catalytic asymmetric bromospirolactonization reaction, and ultimately led to the conclusion that carbamate and thiocarbamate derivatives of cinchona alkaloid-based catalysts are able to induce chirality in the reaction. Further optimization revealed that a 2,4-methoxy functionalized carbamate would lead to the highest enantiomeric ratio. While further catalyst optimization is ongoing in our lab, we have tested and demonstrated the generality of the reaction.

I-6 Experimental section

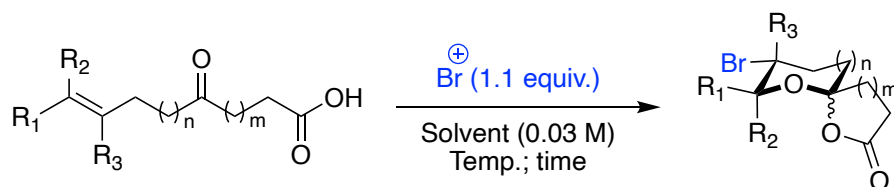
I-6-1 General remarks:

Molecular sieves (4Å) were dried at 160 °C under 0.25 mtorr vacuum prior to use. Unless otherwise mentioned, solvents were purified as follows. CHCl₃ (amylene stabilized) was purchased from Sigma Aldrich and incubated over 4 Å MS for 48 h prior to use. Toluene and CH₂Cl₂ were dried over CaH₂ whereas THF and Et₂O were dried over sodium (dryness was monitored by colorization of benzophenone ketyl radical); they were freshly distilled prior to use. NMR spectra were obtained using a 500 MHz or 600 MHz Varian NMR spectrometer and referenced using the residual ¹H peak from the deuterated solvent. Waters 2795 (Alliance HT) instrument was used for HRMS (ESI) analysis with polyethylene glycol (PEG-400-600) as a reference.

Column chromatography was performed using Silicycle 60 Å, 35-75 μm silica gel. Pre-coated 0.25 mm thick silica gel 60 F254 plates were used for analytical TLC and visualized using UV light, iodine, potassium permanganate stain, *p*-anisaldehyde stain or phosphomolybdic acid in EtOH stain.

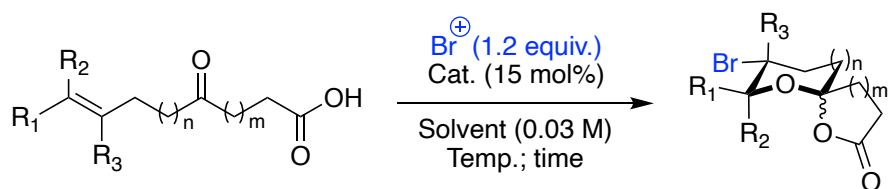
Halofunctionalization reactions were performed in the absence of light. N-bromosuccinimide (NBS), N-chlorosuccinimide (NCS), 1,3-dichloro-5,5-dimethylhydantoin (DCDMH), and 1,3-dibromo-5,5-dimethylhydantoin (DBDMH) were recrystallized prior to use. All other commercially available reagents and solvents were used as received unless otherwise mentioned.

I-6-2 General procedure for racemic bromo spirolactonization of keto-acids



The keto-acid substrate (0.1 mmol) and N-bromosuccinimide, NBS (0.11 mmol) were suspended in dry toluene (3 mL) in a 25 mL round bottom with a magnetic stir bar under a nitrogen balloon. The reaction mixture was stirred at room temperature and followed by TLC. Upon completion, the reaction mixture was diluted with hexanes (3 mL) and quenched by addition of sodium thiosulfate (3 ml of a 10% aqueous solution). The organic layer was separated, and the aqueous layer was extracted with hexanes (3 x 3 mL). The combined organic layers were dried with anhydrous Na_2SO_4 and concentrated under reduced pressure at room temperature to give the crude product. Crude 1H NMR was used to determine the diastereoselectivity of the reaction. The crude product was then purified by column chromatography (silica, ethyl acetate/hexanes = 1:10) leading to the pure bromo spirolactone products.

I-6-3 General procedure for catalytic asymmetric bromo spirolactonization of keto- acids



The N-bromosuccinimide, NBS (0.12 mmol) and catalyst (15 mol %) placed in a test tube with a magnetic stir bar and capped with a rubber septum under an argon balloon

in the dark (the reaction covered with aluminum foil). The reaction tube cooled to $-40\text{ }^{\circ}\text{C}$ and a mixture of dry toluene (2 mL) and dry chloroform (1 mL) was added via syringe. After 20 minutes, the keto-acid substrate (0.1 mmol) was added in one portion. The reaction stirred at this temperature and followed by TLC. Upon completion, the reaction mixture was diluted with hexanes (3 mL) and quenched by addition of sodium thiosulfate (3 ml of a 10% aqueous solution). The organic layer was separated, and the aqueous layer was extracted with hexanes (3 x 3 mL). The combined organic layers were dried with anhydrous Na_2SO_4 and concentrated under reduced pressure at room temperature to give the crude product. Crude ^1H NMR was used to determine the diastereoselectivity of the reaction. The crude product was then purified by column chromatography (silica, ethyl acetate/hexanes 10%) leading to the pure bromo spirolactone products.

I-6-3-1 Analytical data



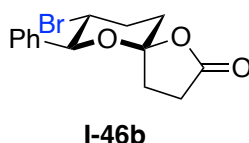
The title compound was prepared according to the general procedure at 0.1 mmol scale. Product was formed as a mixture of diastereomers **a** and **b** (1.7:1) and isolated as a white solid (29 mg, 94% yield, 85:15 *er*).

^1H NMR (500 MHz, Chloroform-*d*) δ 7.39 – 7.34 (m, 5H), 4.92 (d, $J = 10.5$ Hz, 1H), 4.03 (ddd, $J = 11.9, 10.5, 4.6$ Hz, 1H), 2.75 (dt, $J = 17.8, 10.6$, Hz, 1H), 2.62 – 2.45 (m, 3H), 2.33 – 2.27 (m, 1H), 2.16 – 2.04 (m, 3H).

^{13}C NMR (126 MHz, Chloroform-*d*) δ 175.96, 138.27, 128.86, 128.28, 127.85, 107.06, 79.25, 49.88, 41.75, 35.68, 33.95, 31.72, 27.93.

HPLC analysis: Chiralpak IA, 99:1 hexane/*i*-PrOH, flow rate = 1 mL/min, λ = 215 nm, retention time = 22.3 min (major), 26.2 min (minor).

HRMS: TOF MS AP⁺ (C₁₄H₁₆BrO₃): Calc. [M + H]⁺: 311.0285, Found [M + H]⁺: 311.0287.



^1H NMR (500 MHz, Chloroform-*d*) δ 7.47 – 7.33 (m, 5H), 4.68 (d, J = 9.8 Hz, 1H), 4.10 (td, J = 10.2, 4.6 Hz, 1H), 2.79 – 2.48 (m, 4H), 2.38 – 2.07 (m, 4H).

^{13}C NMR (126 MHz, Chloroform-*d*) δ 175.09, 138.00, 128.94, 128.37, 127.67, 107.33, 81.68, 49.70, 34.73, 31.49, 29.60, 27.70.

HRMS: TOF MS AP⁺ (C₁₄H₁₆BrO₃): Calc. [M + H]⁺: 311.0285, Found [M + H]⁺: 311.0287.



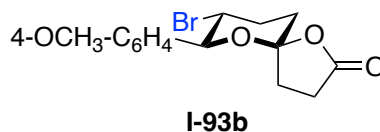
The title compound was prepared according to the general procedure at 0.1 mmol scale. Product was formed as a mixture of diastereomers **a** and **b** (1.5:1) and isolated as a white solid (20 mg, 58% yield, 57.5:42.5 *er*).

^1H NMR (500 MHz, Chloroform-*d*) δ 7.31 (d, J = 8.2 Hz, 2H), 6.92 (d, J = 8.1 Hz, 2H), 4.91 (d, J = 10.6 Hz, 1H), 4.05 (td, J = 10.6, 4.7 Hz, 1H), 3.83 (s, 3H), 2.83 – 2.72 (m, 1H) 2.64 – 2.46 (m, 3H), 2.31 (t, J = 11.5 Hz, 1H), 2.19 – 2.06 (m, 3H).

^{13}C NMR (126 MHz, Chloroform-*d*) δ 175.96, 159.88, 130.55, 129.01, 113.68, 107.12, 78.86, 55.27, 50.19, 35.71, 33.96, 31.77, 27.94.

HPLC analysis: Chiralpak IA, 98:2 hexane/*i*-PrOH, flow rate = 1 mL/min, λ = 215 nm, retention time = 31.5 min (major), 39.3 min (minor).

HRMS: TOF MS AP⁺ (C₁₅H₁₈BrO₄): Calc. [M + H]⁺: 341.0390, Found [M + H]⁺: 341.0392.



^1H NMR (500 MHz, Chloroform-*d*) δ 7.35 (d, J = 8.53 Hz, 2H), 6.92 (d, J = 8.82 Hz, 2H), 4.64 (d, J = 9.9 Hz, 1H), 4.09 (td, J = 10.2, 4.6 Hz, 1H), 3.83 (s, 3H), 2.80 – 2.51 (m, 4H), 2.34 – 2.05 (m, 4H).

^{13}C NMR (126 MHz, CDCl₃) δ 175.08, 159.95, 130.28, 128.87, 113.75, 107.36, 81.33, 55.29, 50.10, 34.82, 31.55, 29.59, 27.72.

HRMS: TOF MS AP⁺ (C₁₅H₁₈BrO₄): Calc. [M + H]⁺: 341.0390, Found [M + H]⁺: 341.0390.



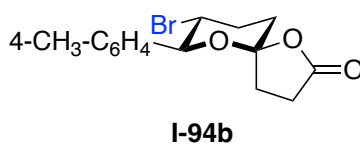
The title compound was prepared according to the general procedure at 0.1 mmol scale. Product was formed as a mixture of diastereomers **a** and **b** (1.9:1) and isolated as a white solid (29 mg, 89% yield, 76:24 *er*).

^1H NMR (500 MHz, Chloroform-*d*) δ 7.29 – 7.26 (m, 2H), 7.19 (d, $J = 7.9$ Hz, 2H), 4.90 (d, $J = 10.5$ Hz, 1H), 4.06 (ddd, $J = 12.0, 10.5, 4.7$ Hz, 1H), 2.76 (ddd, $J = 17.9, 10.7, 9.6$ Hz, 1H), 2.62 – 2.45 (m, 3H), 2.37 (s, 3H), 2.30 (ddd, $J = 13.3, 9.5, 2.2$ Hz, 1H), 2.16 – 2.06 (m, 3H).

^{13}C NMR (126 MHz, Chloroform-*d*) δ 176.02, 138.74, 135.36, 129.03, 127.73, 107.10, 79.07, 49.95, 35.68, 33.95, 31.74, 27.93, 21.29.

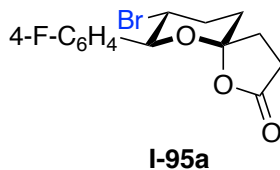
HPLC analysis: Chiralpak IA, 98:2 hexane/*i*-PrOH, flow rate = 1 mL/min, $\lambda = 215$ nm, retention time = 14.4 min (major), 18.2 min (minor).

HRMS: TOF MS AP⁺ (C₁₅H₁₈BrO₃): Calc. [M + H]⁺: 325.0441, Found [M + H]⁺: 325.0439.



^1H NMR (600 MHz, Chloroform-*d*) δ 7.32 (d, $J = 7.9$ Hz, 2H), 7.20 (d, $J = 7.9$ Hz, 2H), 4.65 (d, $J = 9.8$ Hz, 1H), 4.11 (ddd, $J = 10.7, 9.8, 4.6$ Hz, 1H), 2.78 – 2.66 (m, 2H), 2.65 – 2.59 (m, 1H), 2.65 – 2.60 (m, 1H), 2.38 (s, 3H), 2.32 – 2.21 (m, 2H), 2.15 – 2.07 (m, 2H).

^{13}C NMR (151 MHz, Chloroform-*d*) δ 175.09, 138.82, 135.10, 129.09, 127.56, 107.33, 81.56, 49.83, 34.76, 31.52, 29.62, 27.71, 21.25.



The title compound was prepared according to the general procedure at 0.1 mmol scale. Product was formed as a mixture of diastereomers **a** and **b** (1.7:1) and isolated as a white solid (25 mg, 78% yield, 84:16 *er*).

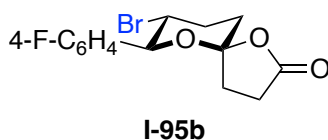
^1H NMR (500 MHz, Chloroform-*d*) δ 7.43 – 7.36 (m, 2H), 7.06 (t, J = 8.7 Hz, 2H), 4.65 (d, J = 9.9 Hz, 1H), 4.02 (td, J = 10.6, 4.5 Hz, 1H), 2.79 – 2.50 (m, 4H), 2.34 – 2.05 (m, 4H).

^{13}C NMR (126 MHz, Chloroform-*d*) δ 175.01, 162.89 (d, J = 247.6 Hz), 133.94 (d, J = 3.5 Hz), 129.43 (d, J = 8.7 Hz), 115.33 (d, J = 21.6 Hz), 107.32, 81.00, 49.83, 34.78, 31.47, 29.55, 27.67.

^{19}F NMR (470 MHz, Chloroform-*d*) δ -112.82 – -112.90 (m).

HPLC analysis: Chiralpak IA, 98:2 hexane/*i*-PrOH, flow rate = 1 mL/min, λ = 215 nm, retention time = 21.6 min (major), 24.0 min (minor).

HRMS: TOF MS AP⁺ (C₁₄H₁₅BrFO₃): Calc. [M + H]⁺: 329.0190, Found [M + H]⁺: 329.0194.

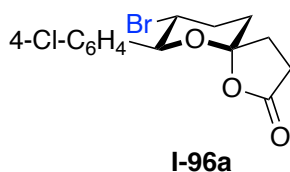


^1H NMR (500 MHz, Chloroform-*d*) δ 7.40 – 7.34 (m, 2H), 7.07 (t, J = 8.4 Hz, 2H), 4.94 (d, J = 10.5 Hz, 1H), 3.99 (td, J = 11.3, 4.5 Hz, 1H), 2.84 – 2.46 (m, 4H), 2.38 – 2.02 (m, 4H),

^{13}C NMR (201 MHz, Chloroform-*d*) δ 175.89, 162.84 (d, J = 248.08 Hz), 134.21, 129.56 (d, J = 8.3 Hz), 115.24 (d, J = 21.5 Hz), 107.03, 78.56, 50.02, 35.64, 33.93, 31.67, 27.90.

^{19}F NMR (470 MHz, Chloroform-*d*) δ -112.68 – -112.76 (m, 1F).

HRMS: TOF MS AP⁺ ($\text{C}_{14}\text{H}_{15}\text{BrFO}_3$): Calc. $[\text{M} + \text{H}]^+$: 329.0190, Found $[\text{M} + \text{H}]^+$: 329.0191.



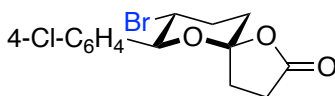
The title compound was prepared according to the general procedure at 0.1 mmol scale. Product was formed as a mixture of diastereomers **a** and **b** (1.7:1) and isolated as a white solid (24 mg, 69% yield, 75:25 *er*).

^1H NMR (500 MHz, Chloroform-*d*) δ 7.30 – 7.21 (m, 4H), 4.86 – 4.80 (d, J = 10.58, 1H), 3.89 (td, J = 11.6, 5.2 Hz, 1H), 2.71 – 2.61 (m, 1H), 2.53 – 2.37 (m, 3H), 2.22 (t, J = 11.9 Hz, 1H), 2.12 – 1.97 (m, 3H).

^{13}C NMR (126 MHz, Chloroform-*d*) δ 175.77, 136.81, 134.63, 129.21, 128.50, 106.94, 78.59, 49.70, 35.61, 33.92, 31.64, 27.85.

HPLC analysis: Chiralpak IA, 98:2 hexane/*i*-PrOH, flow rate = 1 mL/min, λ = 215 nm, retention time = 14.3 min (major), 18.0 min (minor).

HRMS: TOF MS AP⁺ (C₁₄H₁₅BrClO₃): Calc. [M + H]⁺: 344.9895, Found [M + H]⁺: 344.9895.

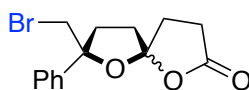


I-96b

¹H NMR (500 MHz, Chloroform-*d*) δ 7.40 – 7.35 (m, 4H), 4.67 (d, *J* = 9.8, 1H), 4.04 (td, *J* = 10.0, 5.2 Hz, 1H), 2.80 – 2.52 (m, 4H), 2.36 – 2.07 (m, 4H).

¹³C NMR (126 MHz, Chloroform-*d*) δ 174.90, 136.56, 134.73, 129.04, 128.57, 107.27, 80.99, 49.50, 34.66, 31.39, 29.64, 27.64.

HRMS: TOF MS AP⁺ (C₁₄H₁₅BrClO₃): Calc. [M + H]⁺: 344.9895, Found [M + H]⁺: 344.9897.



I-98a&b

The title compound was prepared according to the general procedure at 0.1 mmol scale. Product was formed as a mixture of diastereomers **a** and **b** (1:1) and isolated as a white solid (25 mg, 81% yield, 60:40 *er*).

Diastereomer **a**:

¹H NMR (500 MHz, Chloroform-*d*) δ 7.37 – 7.30 (m, 4H), 7.29 – 7.26 (m, 1H), 3.61 (d, *J* = 11.1 Hz, 1H), 3.55 (d, *J* = 11.1 Hz, 1H), 2.93 (dt, *J* = 17.6, 10.1 Hz, 1H), 2.71 – 2.28 (m, 7H).

^{13}C NMR (126 MHz, Chloroform-*d*) δ 175.69, 143.80, 128.41, 127.77, 125.06, 116.76, 88.58, 42.56, 37.30, 35.32, 31.79, 29.07.

HPLC analysis: Chiralpak IA, 98:2 hexane/*i*-PrOH, flow rate = 1 mL/min, λ = 215 nm, retention time = 17.7 min (major), 22.7 min (minor).

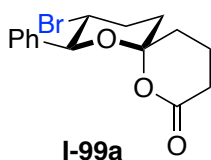
HRMS: TOF MS AP⁺ (C₁₅H₁₈BrO₃): Calc. [M + H]⁺: 311.0285, Found [M + H]⁺: 311.0285.

Diastereomer **b**:

^1H NMR (500 MHz, Chloroform-*d*) δ 7.41 – 7.35 (m, 4H), 7.34 – 7.29 (m, 1H), 3.77 (d, J = 10.7 Hz, 1H), 3.72 (d, J = 10.7 Hz, 1H), 2.93 (dt, J = 17.4, 9.6 Hz, 1H), 2.66 – 2.30 (m, 6H), 2.00 (td, J = 12.9, 8.0 Hz, 1H).

^{13}C NMR (126 MHz, cdCl₃) δ 175.47, 142.31, 128.29, 127.80, 125.39, 115.86, 88.68, 41.68, 36.39, 35.75, 31.71, 28.96.

HRMS: TOF MS AP⁺ (C₁₅H₁₈BrO₃): Calc. [M + H]⁺: 311.0285, Found [M + H]⁺: 311.0288.



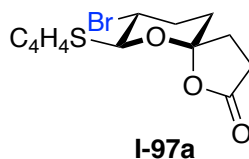
The title compound was prepared according to the general procedure at 0.1 mmol scale. Product was formed as a mixture of diastereomers **a** and **b** (1.5:1) and isolated as a white solid (27 mg, 83% yield, 57.5:42.5 *er*).

^1H NMR (500 MHz, Chloroform-*d*) δ 7.38 – 7.34 (m, 5H), 4.97 (d, J = 10.4 Hz, 1H), 3.99 (ddd, J = 12.2, 10.4, 4.4 Hz, 1H), 2.74 – 2.64 (m, 1H), 2.62 – 2.54 (m, 1H), 2.47 – 2.36 (m, 2H), 2.12 – 1.91 (m, 4H), 1.84 – 1.76 (m, 1H), 1.76 – 1.67 (m, 1H).

^{13}C NMR (126 MHz, Chloroform-*d*) δ 170.77, 138.49, 128.68, 128.17, 127.88, 102.61, 78.08, 50.47, 36.78, 32.66, 30.26, 29.33, 15.26.

HPLC analysis: Chiralpak AD-H, 98:2 hexane/*i*-PrOH, flow rate = 1 mL/min, λ = 215 nm, retention time = 15.2 min (minor), 17.3 min (major).

HRMS: TOF MS AP⁺ ($\text{C}_{15}\text{H}_{19}\text{BrO}_3$): Calc. $[\text{M} - \text{H}]^+$: 323.0281, Found $[\text{M} + \text{H}]^+$: 323.0280.

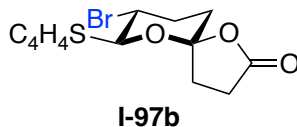


The title compound was prepared according to the general procedure **I-6-2** at 0.1 mmol scale. Product was formed as a mixture of diastereomers **a** and **b** (1:1) and isolated as a white solid (18 mg, 58% yield).

^1H NMR (500 MHz, Chloroform-*d*) δ 7.24 (d, J = 5.0 Hz, 1H), 7.05 (d, J = 3.5 Hz, 1H), 6.92 (dd, J = 5.3, 4.0 Hz, 1H), 5.15 (d, J = 10.5 Hz, 1H), 3.96 (td, J = 11.2, 4.6 Hz, 1H), 2.79 – 2.64 (m, 1H), 2.53 – 2.37 (m, 3H), 2.29 – 2.20 (m, 1H), 2.11 – 1.91 (m, 3H).

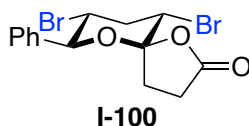
^{13}C NMR (126 MHz, Chloroform-*d*) δ 175.78, 141.36, 127.58, 126.41, 125.71, 106.95, 75.06, 50.54, 35.44, 33.85, 31.70, 27.88.

HRMS: TOF MS AP⁺ (C₁₂H₁₄BrO₃S): Calc. [M + H]⁺: 316.9849, Found [M + H]⁺: 316.9847.



¹H NMR (500 MHz, Chloroform-*d*) δ 7.32 (d, *J* = 5.5 Hz, 1H), 7.08 (d, *J* = 3.5 Hz, 1H), 7.02 – 6.95 (m, 1H), 5.08 (d, *J* = 8.0 Hz, 1H), 4.33 – 4.26 (m, 1H), 2.83 – 2.70 (m, 1H), 2.66 – 2.50 (m, 3H), 2.25 – 2.10 (m, 4H).

¹³C NMR (126 MHz, Chloroform-*d*) δ 175.04, 141.52, 126.40, 126.32, 126.01, 107.11, 49.66, 33.27, 30.90, 29.99, 27.79.



The title compound was prepared according to the general procedure **I-6-2** at 0.1 mmol scale, except using DCDMH, DBDMH (1 equiv. each) as bromine source. Product was formed as a single diastereomer and isolated as a white solid (11 mg, 28% yield).

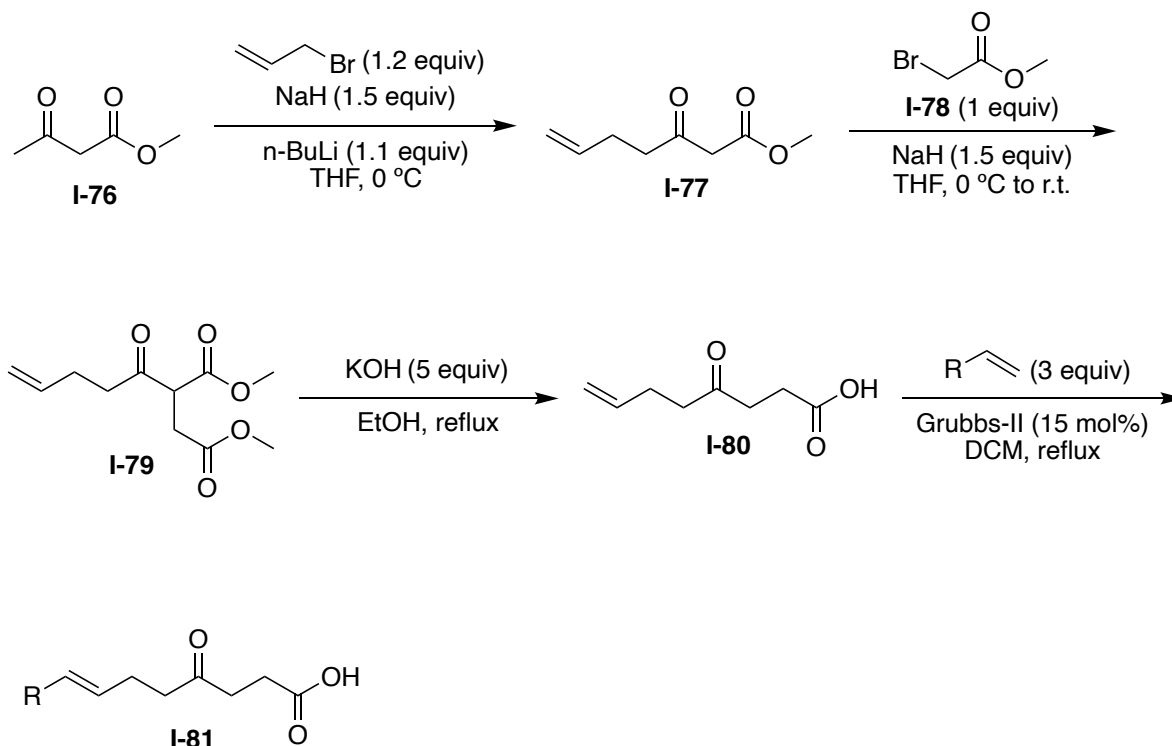
¹H NMR (500 MHz, Chloroform-*d*) δ 7.46 – 7.37 (m, 5H), 4.97 (d, *J* = 10.7 Hz, 1H), 4.50 (ddd, *J* = 11.9, 10.7, 4.3 Hz, 1H), 4.25 (t, *J* = 3.1 Hz, 1H), 3.12 – 3.03 (m, 1H), 2.88 – 2.71 (m, 2H), 2.59 – 2.43 (m, 2H), 2.29 – 2.19 (m, 1H).

¹³C NMR (126 MHz, Chloroform-*d*) δ 175.26, 137.57, 129.13, 128.39, 127.92, 106.29, 79.33, 51.52, 45.77, 39.72, 34.43, 29.71, 28.23.

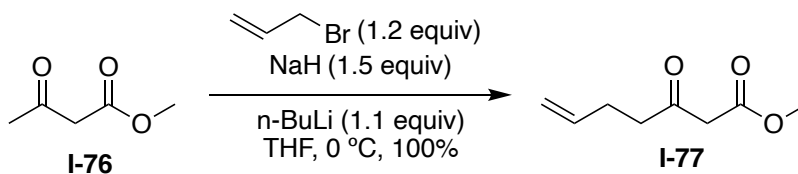
HRMS: TOF MS AP⁺ (C₁₂H₁₄BrO₃S): Calc. [M + H]⁺: 388.9390, Found [M + H]⁺: 388.9391.

I-6-4 Synthesis of keto-acid substrates I-45, I-82 to I-92

The ketone substrates were synthesized according to the following general scheme:



I-6-4-1 Synthesis of keto-ester I-77



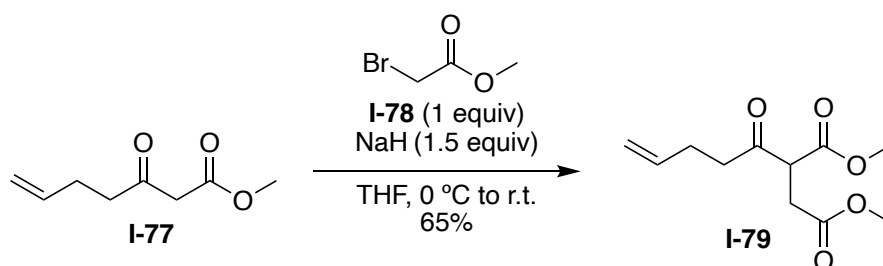
Following the reported procedure²⁶, methyl acetoacetate (4.45 mL, 41.3 mmol) was added dropwise under nitrogen to a suspension of NaH (60% on mineral oil, 2.48 g, 62 mmol) in dry THF (100 mL) at 0 °C. The resulting mixture was stirred for 30 min at this temperature and *n*-BuLi (18.17 mL, 2.50 M, 45.43 mmol) was added dropwise. The

mixture was stirred for another 30 min and allyl bromide (4.28 mL, 49.56 mmol) was added. The reaction stirred for 45 minutes before cautiously, quenched by 2 M HCl (30 mL). The reaction was extracted with diethyl ether (3 x 75 mL). The combined organic layers were washed with saturated NaHCO₃ and NaCl. The combined organic extracts dried with anhydrous Na₂SO₄ and concentrated under reduced pressure at room temperature to give the product **I-77** as an orange liquid (6.45 g, 100%).

¹H NMR (500 MHz, Chloroform-*d*) δ 5.79 (ddt, *J* = 16.9, 10.2, 6.5 Hz, 1H), 5.10 – 4.95 (m, 2H), 3.73 (s, 3H), 3.46 (s, 2H), 2.65 (t, *J* = 7.3 Hz, 2H), 2.38 – 2.31 (m, 2H).

¹³C NMR (126 MHz, Chloroform-*d*) δ 201.87, 167.57, 136.49, 115.61, 52.37, 49.06, 42.06, 27.38.

I-6-4-2 Synthesis of di-ester I-79



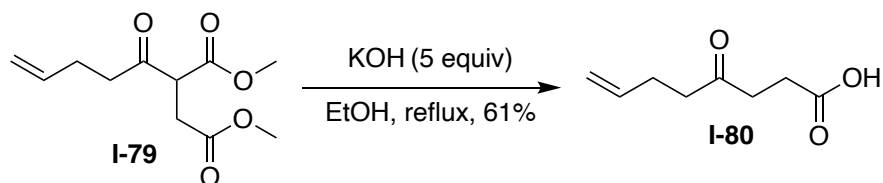
Following the reported procedure²⁶, NaH (60% on mineral oil, 2.48 g, 62 mmol) was added portionwise to a solution of compound **I-77** (6.45 g, 41.3 mmol) at 0 °C. The resulting mixture was stirred for 30 min at this temperature and methyl bromoacetate **I-78** (3.94 mL, 41.3 mmol) was added dropwise. The reaction was warmed up to the room temperature and stirred for 2 hours before cautiously, quenched by 1 M HCl (50 mL). The reaction was extracted with diethyl ether (3 x 100 mL). The combined organic layers dried

with anhydrous Na₂SO₄ and concentrated under reduced pressure at room temperature. The crude product was then purified by column chromatography (silica, ethyl acetate/hexanes 10% to 30%) leading to the pure product **I-79** as a yellow liquid (6.12 g, 65%).

¹H NMR (500 MHz, Chloroform-*d*) δ 5.69 (ddt, *J* = 16.8, 10.2, 6.5 Hz, 1H), 4.97 – 4.84 (m, 2H), 3.91 (dd, *J* = 8.4, 6.1 Hz, 1H), 3.64 (s, 3H), 3.56 (s, 3H), 2.88 (dd, *J* = 17.6, 8.3 Hz, 1H), 2.79 – 2.69 (m, 2H), 2.68 – 2.61 (m, 1H), 2.29 – 2.19 (m, 2H).

¹³C NMR (126 MHz, Chloroform-*d*) δ 202.94, 171.64, 168.67, 136.60, 115.22, 53.59, 52.58, 51.87, 41.72, 31.99, 27.22.

I-6-4-3 Synthesis of acid I-80



Following the reported procedure²⁶, To a solution of compound **I-79** (3.65 g, 16 mmol) in ethanol (75 mL) was added potassium hydroxide (4.48 g, 80 mmol) and heated at reflux for 4 hours. The reaction was cooled and concentrated under reduced pressure. Then water (50 mL) was added to the solution and acidified to PH 1 by 2 M HCl. The reaction stirred for 10 minutes and extracted with diethyl ether (3 x 50 mL). The combined organic layers dried with anhydrous Na₂SO₄ and concentrated under reduced pressure at room temperature. The crude product was then purified by column chromatography

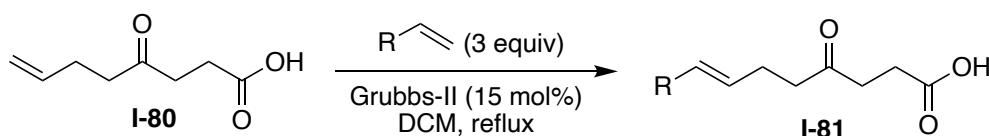
(silica, ethyl acetate/hexanes 20% to 40%, acetic acid 0.5% was added to solvent mixture) leading to the pure product **I-80** as a yellow solid (1.52 g, 61%).

^1H NMR (500 MHz, Chloroform-*d*) δ 10.44 (br s, 1H), 5.80 (ddt, $J = 16.8, 10.2, 6.5$ Hz, 1H), 5.10 – 4.89 (m, 2H), 2.75 – 2.61 (m, 4H), 2.56 (t, $J = 7.4$ Hz, 2H), 2.37 – 2.32 (m, 2H).

^{13}C NMR (126 MHz, Chloroform-*d*) δ 208.06, 178.90, 136.87, 115.38, 41.69, 36.83, 27.74, 27.66.

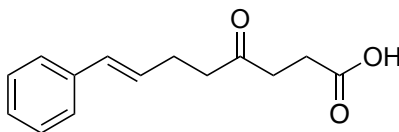
HRMS: TOF MS ES⁺ (C₈H₁₁O₃): Calc. [M - H]⁺: 155.0708, Found [M - H]⁺: 155.0711.

I-6-4-4 General procedure for Grubbs cross metathesis



Following the reported procedure,⁴³ to a solution of keto-acid **I-80** (2 mmol) and vinyl derivatives (6 mmol) in DCM (20 mL) was added Grubbs-II (15 mol%) and heated at reflux overnight under argon. The completion of the reaction monitored by TLC and then, solvent was evaporated under reduced pressure at room temperature. The crude product was then purified by column chromatography (silica, ethyl acetate/hexanes 20% to 30%) leading to the pure derivatives of keto-acid products.

I-6-4-5 Analytical data



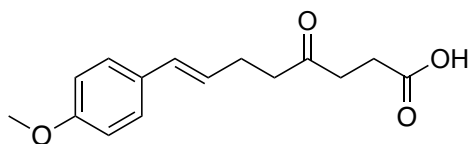
I-45

The title compound was prepared according to the general procedure at 2 mmol scale. Product was isolated as a white solid (329 mg, 71% yield)

^1H NMR (500 MHz, Chloroform-*d*) δ 7.36 – 7.26 (m, 4H), 7.23 – 7.19 (m, 1H), 6.42 (dt, J = 15.9, 1.6 Hz, 1H), 6.20 (dt, J = 15.8, 6.9 Hz, 1H), 2.78 – 2.73 (m, 2H), 2.69 – 2.63 (m, 4H), 2.54 – 2.49 (m, 2H).

^{13}C NMR (126 MHz, Chloroform-*d*) δ 207.94, 178.59, 137.36, 130.86, 128.66, 128.52, 127.12, 126.03, 42.18, 36.92, 27.78, 27.06.

HRMS: TOF MS ES⁺ (C₁₄H₁₅O₃): Calc. [M - H]⁻ : 231.1021, Found [M - H]⁻ : 231.1025.



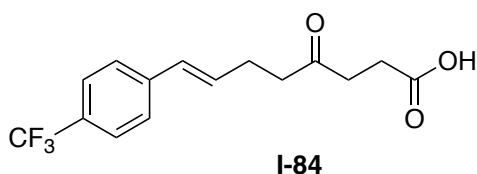
I-82

The title compound was prepared according to the general procedure at 2 mmol scale. Product was isolated as a white solid (320 mg, 61% yield)

^1H NMR (500 MHz, Chloroform-*d*) δ 7.25 (d, $J = 8.7$ Hz, 2H), 6.83 (d, $J = 8.7$ Hz, 2H), 6.34 (d, $J = 15.8$ Hz, 1H), 6.04 (dt, $J = 15.8, 6.9$ Hz, 1H), 3.79 (s, 3H), 2.76 – 2.70 (m, J , 2H), 2.66 – 2.60 (m, 4H), 2.51 – 2.44 (m, 2H).

^{13}C NMR (126 MHz, cdCl_3) δ 208.12, 178.70, 158.82, 130.19, 127.13, 126.45, 113.92, 55.28, 42.34, 36.91, 27.76, 27.07.

HRMS: TOF MS ES^+ ($\text{C}_{15}\text{H}_{17}\text{O}_4$): Calc. $[\text{M} - \text{H}]^-$: 261.1127, Found $[\text{M} - \text{H}]^-$: 261.1130.



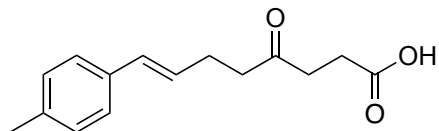
The title compound was prepared according to the general procedure at 2 mmol scale. Product was isolated as a white solid (252 mg, 42% yield)

^1H NMR (500 MHz, Chloroform-*d*) δ 10.65 (br s, 1H) 7.53 (d, $J = 8.2$ Hz, 2H), 7.40 (d, $J = 8.1$ Hz, 2H), 6.43 (d, $J = 15.7$ Hz, 1H), 6.29 (dt, $J = 15.8, 6.7$ Hz, 1H), 2.78 – 2.70 (M, 2H), 2.70 – 2.62 (m, 4H), 2.57 – 2.48 (m, 2H).

^{13}C NMR (126 MHz, Chloroform-*d*) δ 207.75, 178.91, 140.87, 131.55, 129.65, 128.82 (q, $J = 32.3$ Hz), 126.17, 125.42 (q, $J = 3.8$ Hz), 41.76, 36.86, 27.75, 26.96.

^{19}F NMR (470 MHz, Chloroform-*d*) δ -62.42 (s, 3F).

HRMS: TOF MS ES^+ ($\text{C}_{15}\text{H}_{14}\text{F}_3\text{O}_3$): Calc. $[\text{M} - \text{H}]^-$: 299.0895, Found $[\text{M} - \text{H}]^-$: 299.0899.



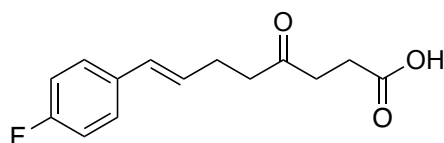
I-85

The title compound was prepared according to the general procedure at 2 mmol scale. Product was isolated as a white solid (354 mg, 72% yield)

^1H NMR (500 MHz, Chloroform-*d*) δ 10.90 (br s, 1H), 7.24 (d, $J = 7.9$ Hz, 2H), 7.11 (d, $J = 7.8$ Hz, 2H), 6.38 (d, $J = 15.8$ Hz, 1H), 6.14 (dt, $J = 15.8, 6.8$ Hz, 1H), 2.74 (t, $J = 6.4$ Hz, 2H), 2.68 – 2.59 (m, 4H), 2.49 (q, $J = 7.5$ Hz, 2H), 2.33 (s, 3H).

^{13}C NMR (126 MHz, Chloroform-*d*) δ 208.17, 178.71, 136.84, 134.60, 130.66, 129.22, 127.64, 125.94, 42.24, 36.95, 27.86, 27.09, 21.17.

HRMS: TOF MS ES⁺ (C₁₅H₁₇O₃): Calc. [M - H]⁻ : 245.1178, Found [M - H]⁻ : 245.1176.



I-86

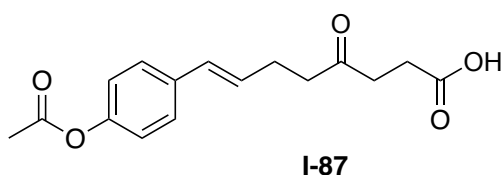
The title compound was prepared according to the general procedure at 2 mmol scale. Product was isolated as a white solid (275 mg, 55% yield)

^1H NMR (500 MHz, Chloroform-*d*) δ 10.16 (br s, 1H), 7.28 (dd, $J = 8.5, 5.5$ Hz, 2H), 6.97 (t, $J = 8.6$ Hz, 2H), 6.36 (d, $J = 15.8$ Hz, 1H), 6.10 (dt, $J = 15.8, 6.8$ Hz, 1H), 2.74 (t, $J = 6.2$ Hz, 2H), 2.68 – 2.60 (m, 4H), 2.49 (q, $J = 7.1$ Hz, 2H).

^{13}C NMR (126 MHz, Chloroform-*d*) δ 207.93, 178.79, 162.01 (d, $J = 246.0$ Hz), 133.52 (d, $J = 3.3$ Hz), 129.68, 128.39 (d, $J = 2.3$ Hz), 127.47 (d, $J = 7.9$ Hz), 115.34 (d, $J = 21.5$ Hz), 42.10, 36.89, 27.75, 26.96.

^{19}F NMR (470 MHz, Chloroform-*d*) δ -115.35 (m, 1F).

HRMS: TOF MS ES⁺ (C₁₄H₁₄FO₃): Calc. [M - H]⁻ : 249.0894, Found [M - H]⁻ : 249.0902.

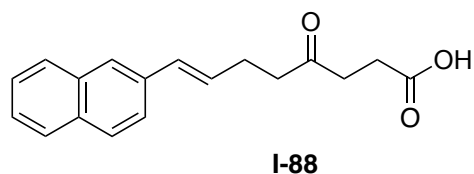


The title compound was prepared according to the general procedure at 2 mmol scale. Product was isolated as a white solid (330 mg, 57% yield)

^1H NMR (500 MHz, Chloroform-*d*) δ 7.32 (d, $J = 8.5$ Hz, 2H), 7.01 (d, $J = 8.5$ Hz, 2H), 6.39 (d, $J = 15.8$ Hz, 1H), 6.14 (dt, $J = 15.8, 6.9$ Hz, 1H), 2.79 – 2.73 (m, 2H), 2.69 – 2.61 (m, 4H), 2.50 (q, $J = 7.0$ Hz, 2H), 2.29 (s, 3H).

^{13}C NMR (126 MHz, Chloroform-*d*) δ 209.46, 175.05, 169.79, 149.78, 135.38, 129.39, 128.99, 126.47, 126.47, 121.32, 41.44, 36.61, 27.26, 26.69, 19.50.

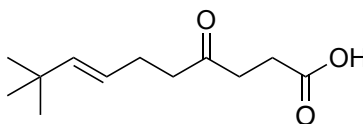
HRMS: TOF MS ES⁺ (C₁₆H₁₇O₅): Calc. [M - H]⁻ : 289.1076, Found [M - H]⁻ : 289.1072.



The title compound was prepared according to the general procedure at 2 mmol scale. Product was isolated as a white solid (344 mg, 61% yield)

^1H NMR (500 MHz, Chloroform-*d*) δ 7.78 (t, 3H), 7.68 (s, 1H), 7.56 (dd, $J = 8.5, 1.8$ Hz, 1H), 7.49 – 7.39 (m, 2H), 6.58 (d, $J = 15.9$ Hz, 1H), 6.33 (dt, $J = 15.9, 6.8$ Hz, 1H), 2.80 (t, $J = 6.4$ Hz, 2H), 2.74 – 2.65 (m, 4H), 2.58 (q, $J = 7.2$ Hz, 2H).

^{13}C NMR (126 MHz, cdCl_3) δ 207.92, 178.18, 134.82, 133.64, 132.76, 130.98, 129.11, 128.11, 127.89, 127.63, 126.18, 125.66, 125.62, 123.48, 42.19, 36.94, 27.68, 27.16.



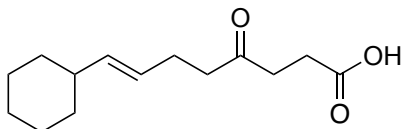
I-90

The title compound was prepared according to the general procedure at 2 mmol scale. Product was isolated as a white solid (229 mg, 54% yield)

^1H NMR (500 MHz, Chloroform-*d*) δ 5.46 (dt, $J = 15.6, 1.4$ Hz, 1H), 5.28 (dt, $J = 15.5, 6.6$ Hz, 1H), 2.73 – 2.68 (m, 2H), 2.66 – 2.60 (m, 2H), 2.50 (t, $J = 7.5$ Hz, 3H), 2.33 – 2.23 (m, 3H), 0.96 (s, 12H).

^{13}C NMR (126 MHz, Chloroform-*d*) δ 208.50, 176.21, 142.76, 122.59, 42.75, 36.99, 32.80, 29.64, 27.37, 26.89.

HRMS: TOF MS ES^+ ($\text{C}_{12}\text{H}_{19}\text{O}_3$): Calc. $[\text{M} - \text{H}]^-$: 211.1334, Found $[\text{M} - \text{H}]^-$: 211.1330.

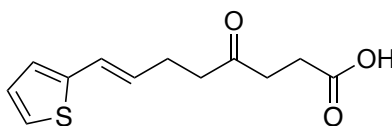


I-91

The title compound was prepared according to the general procedure at 2 mmol scale. Product was isolated as a white solid (180 mg, 38% yield)

^1H NMR (500 MHz, Chloroform-*d*) δ 5.44 – 5.28 (m, 2H), 2.73 (t, $J = 6.9\text{ Hz}$, 2H), 2.7 – 2.62 (m, 2H), 2.51 (t, $J = 7.6\text{ Hz}$, 2H), 2.31 – 2.24 (m, 2H), 1.92 – 1.84 (m, 1H), 1.71 – 1.63 (m, 4H), 1.29 – 0.98 (m, 6H).

HRMS: TOF MS ES⁺ (C₁₄H₂₁O₃): Calc. [M - H]⁻ : 237.1490, Found [M - H]⁻ : 237.1491.



I-92

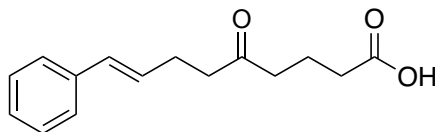
The title compound was prepared according to the general procedure at 2 mmol scale.

Product was isolated as a white solid (180 mg, 59% yield)

^1H NMR (500 MHz, Chloroform-*d*) δ 11.34 (s, 1H), 7.08 (d, $J = 5.3\text{ Hz}$, 1H), 6.94 – 6.90 (m, 1H), 6.87 (t, $J = 2.7\text{ Hz}$, 1H), 6.52 (d, $J = 15.7\text{ Hz}$, 1H), 6.05 – 6.97 (m, 1H), 2.72 (t, $J = 6.4\text{ Hz}$, 2H), 2.65 – 2.57 (m, 4H), 2.45 (q, $J = 7.0\text{ Hz}$, 2H).

^{13}C NMR (126 MHz, Chloroform-*d*) δ 207.93, 178.66, 142.51, 128.58, 127.27, 124.73, 124.10, 123.48, 41.97, 36.93, 27.86, 26.81.

HRMS: TOF MS ES⁺ (C₁₂H₁₃O₃S): Calc. [M - H]⁻ : 237.0585, Found [M - H]⁻ : 237.0591.



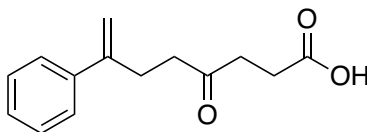
I-112

The title compound was prepared according to the procedure I-6-4-3 at 2 mmol scale. Product was isolated as a white solid (261 mg, 53% yield)

¹H NMR (500 MHz, Chloroform-*d*) δ 10.80 (s, 1H), 7.37 – 7.26 (m, 4H), 7.24 – 7.18 (m, 1H), 6.41 (dt, *J* = 15.8, 1.6 Hz, 1H), 6.19 (dt, *J* = 15.8, 6.8 Hz, 1H), 2.60 (t, *J* = 7.5 Hz, 2H), 2.57 – 2.46 (m, 4H), 2.41 (t, *J* = 7.2 Hz, 2H), 1.93 (p, *J* = 7.2 Hz, 2H).

¹³C NMR (126 MHz, Chloroform-*d*) δ 209.40, 179.52, 137.36, 130.82, 128.76, 128.53, 127.14, 126.02, 42.29, 41.48, 33.00, 27.10, 18.50.

HRMS: TOF MS ES⁺ (C₁₅H₁₇O₃): Calc. [M - H]⁻ : 245.1178, Found [M - H]⁻ : 245.1174.



I-113

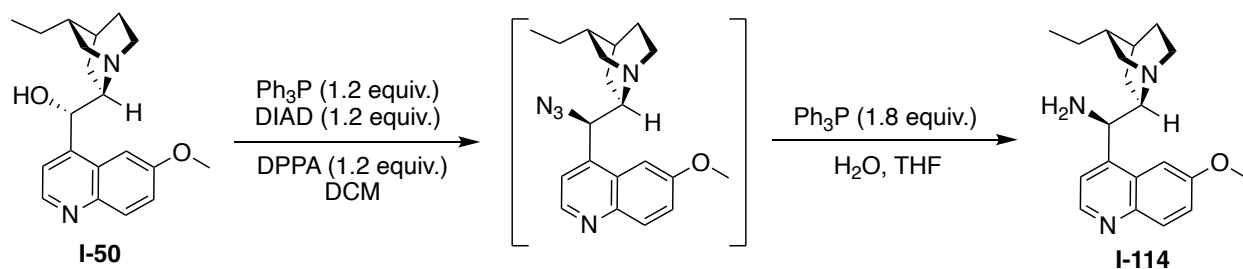
The title compound was prepared according to the procedure I-6-4-3 at 2 mmol scale. Product was isolated as a white solid (218 mg, 47% yield)

¹H NMR (500 MHz, Chloroform-*d*) δ 11.12 (s, 1H), 7.42 – 7.25 (m, 5H), 5.30 (s, 1H), 5.07 (d, *J* = 1.6 Hz, 1H), 2.81 (t, *J* = 7.85 Hz, 2H), 2.72 – 2.58 (m, 6H).

^{13}C NMR (126 MHz, Chloroform-*d*) δ 208.02, 178.73, 146.99, 140.49, 128.44, 127.64, 126.10, 112.92, 41.36, 36.93, 29.18, 27.74.

HRMS: TOF MS ES⁺ (C₁₄H₁₅O₃): Calc. [M - H]⁻ : 231.1021, Found [M - H]⁻ : 231.1017.

I-6-5 Synthesis of the amine derivative of dihydroquinidine I-114



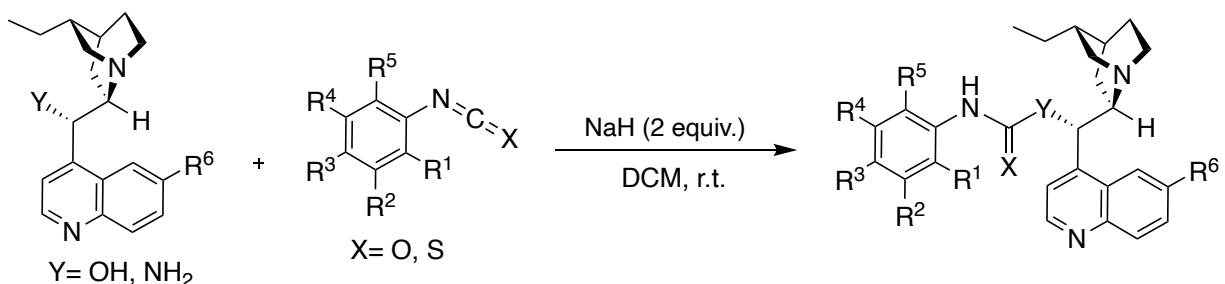
Following the reported procedure,⁴⁴ to a solution of dihydroquinidine, DHQD (6g, 18.4 mmol) in DCM (36 mL) was added Ph₃P (5.79 g, 22.05 mmol). The reaction mixture was stirred at room temperature for 30 minutes under nitrogen balloon. The solution cooled to 0 °C and the diisopropyl azodicarboxylate, DIAD (4.33 mL, 22.05 mmol) was added dropwise and kept the solution temperature below 5 °C. After 5 minutes, a solution of diphenyl phosphoryl azide, DPPA (4.75 mL, 22.05 mmol) in DCM (8 mL) was added dropwise while the solution temperature kept around 0 °C. The mixture was warmed up to 20 °C and stirred for 2 hours to form the azide derivative intermediate. Next, H₂O (8.1 mL) and a solution of Ph₃P (8.7 g, 33.12 mmol) in DCM (8 mL) was added and the reaction stirred overnight at room temperature. The reaction quenched by 3N HCl to pH 2.2 and the product was in upper aqueous layer which washed with DCM. After discarding the organic layer, 28% aqueous ammonia was added to the aqueous layer to adjust pH to above 10. The solution was extracted with DCM (3 x 20 mL). The combined organic layers

dried with anhydrous Na_2SO_4 and concentrated under reduced pressure at room temperature. The crude product was then purified by column chromatography (silica, ethyl acetate/methanol/ammonium hydroxide 50:49.5:0.5%) leading to the pure product **I-114** as a yellow oil (3.65 g, 61%).

^1H NMR (500 MHz, Methanol- d_4) δ 8.69 (d, $J = 4.7$ Hz, 1H), 7.97 (d, $J = 9.2$ Hz, 1H), 7.69 – 7.61 (m, 2H), 7.46 (dd, $J = 9.2, 2.7$ Hz, 1H), 4.86 – 4.78 (d, 10.1 Hz, 1H), 4.01 (s, 3H), 3.35 (s, 1H), 3.14 – 2.95 (m, 4H), 2.87 – 2.78 (m, 1H), 1.55 – 1.38 (m, 6H), 1.06 – 0.98 (m, 1H), 0.90 (t, $J = 7.1$, 3H).

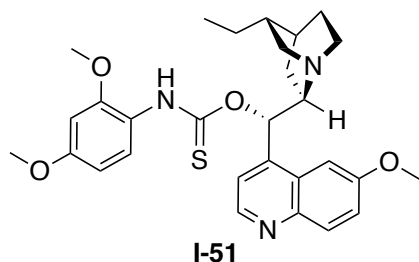
^{13}C NMR (126 MHz, Methanol- d_4) δ 158.39, 148.22, 147.00, 143.63, 131.63, 130.11, 128.90, 122.23, 101.04, 62.65, 54.77, 48.98, 48.61, 48.45, 37.04, 26.56, 25.80, 25.50, 24.31, 10.77.

I-6-6 General procedure for the synthesis of cinchona alkaloid derivatives



Following the reported procedure,²⁴ NaH (60% on mineral oil, 80 mg, 2 mmol) was added to a solution of cinchona derivative (1 mmol) and isocyanate/isothiocyanate derivative (1 mmol) in THF (5 mL). The reaction was stirred at room temperature for overnight and the completion of the reaction monitored by TLC. After quenching the reaction with water (10 mL), the solution was extracted with DCM (3 x 20 mL). The

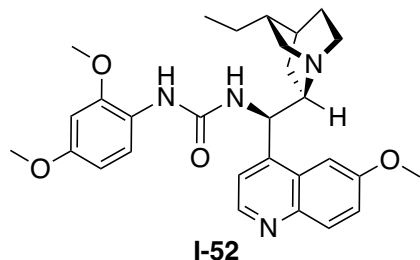
combined organic layers washed with NaCl, dried with anhydrous Na₂SO₄ and concentrated under reduced pressure at room temperature. The crude product was then purified by column chromatography (silica, methanol/DCM 10%) leading to the pure catalyst products as white solids.



The compound existed as a mixture of rotamers. ¹H NMR (500 MHz, DMSO-*d*₆) δ 10.56 – 10.47 (m, 1H), 8.78 – 8.67 (m, 1H), 7.99 – 7.90 (m, 1H), 7.57 – 7.06 (m, 5H), 6.63 – 6.45 (m, 2H), 3.82 – 3.47 (m, 9H), 3.19 – 3.10 (m, 1H), 2.78 – 2.60 (m, 2H), 2.53 – 2.43 (m, 2H), 1.70 – 1.36 (m, 5H), 1.31 – 1.21 (m, 3H), 0.90 – 0.79 (m, 3H).

¹³C NMR (126 MHz, DMSO-*d*₆) δ 190.23, 188.36, 160.00, 159.62, 157.60, 157.41, 155.21, 148.00, 147.87, 144.96, 144.56, 144.51, 131.69, 131.65, 129.38, 128.39, 127.62, 127.27, 121.90, 121.72, 120.46, 120.24, 120.09, 118.99, 104.81, 102.96, 99.51, 99.32, 79.77, 79.66, 77.77, 60.07, 59.78, 56.08, 55.98, 55.83, 55.78, 55.66, 55.56, 50.65, 50.59, 49.39, 49.36, 37.47, 37.36, 27.35, 27.10, 26.08, 25.85, 25.54, 25.29, 23.81, 23.66, 12.43, 12.42.

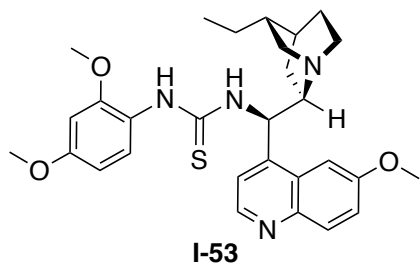
HRMS: TOF MS ES⁺ (C₂₉H₃₆N₃O₄S): Calc. [M + H]⁺: 522.2427, Found [M + H]⁺: 522.2421.



^1H NMR (500 MHz, Methanol- d_4) δ 8.61 (d, $J = 4.7$ Hz, 1H), 7.92 (d, $J = 9.2$ Hz, 1H), 7.81 (d, $J = 2.7$ Hz, 1H), 7.71 (d, $J = 8.8$ Hz, 1H), 7.42 (d, $J = 4.7$ Hz, 1H), 7.34 (dd, $J = 9.3$, 2.6 Hz, 1H), 6.39 (d, $J = 2.6$ Hz, 1H), 6.30 (dd, $J = 8.9$, 2.6 Hz, 1H), 5.59 (br s, 1H), 3.96 (s, 3H), 3.64 (s, 3H), 3.60 (s, 3H), 3.11 – 3.00 (m, 1H), 2.91 – 2.71 (m, 4H), 1.46 – 1.15 (m, 7H), 1.05 – 0.95 (m, 1H), 0.87 (t, $J = 9.6$ Hz, 3H).

^{13}C NMR (126 MHz, Methanol- d_4) δ 158.21, 156.35, 155.67, 149.76, 147.69, 147.00, 143.71, 130.11, 128.73, 122.35, 121.81, 120.22, 119.28, 103.58, 101.61, 98.14, 59.89, 54.95, 54.80, 54.54, 48.91, 48.85, 37.04, 26.69, 25.73, 24.88, 19.83, 11.04.

HRMS: TOF MS ES⁺ (C₂₉H₃₇N₄O₄): Calc. [M + H]⁺: 505.2815, Found [M + H]⁺: 505.2812.

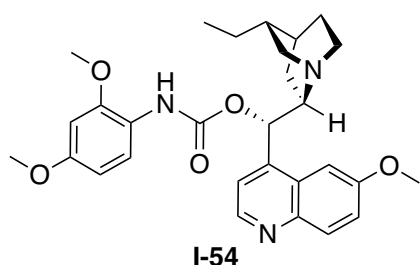


^1H NMR (500 MHz, Methanol- d_4) δ 8.58 (d, $J = 4.7$ Hz, 1H), 8.02 (br s, 1H), 7.91 (d, $J = 9.2$ Hz, 1H), 7.44 (d, $J = 4.7$ Hz, 1H), 7.39 (dd, $J = 9.2$, 2.6 Hz, 2H), 6.49 (d, $J = 2.6$ Hz, 1H), 6.45 (dd, $J = 8.7$, 2.6 Hz, 1H), 6.21 (br s, 1H), 3.97 (s, 3H), 3.75 (s, 3H), 3.54 (s, 3H),

3.18 (ddd, $J = 10.6, 9.7, 9.3$ Hz, 1H), 2.95 (d, $J = 8.4$ Hz, 2H), 2.84 (m, 2H), 1.54 – 1.32 (m, 6H), 1.13 (dd, $J = 12.5, 8.2$ Hz, 1H), 0.89 (t, $J = 7.2$ Hz, 3H).

^{13}C NMR (126 MHz, Methanol- d_4) δ 181.20, 159.37, 158.01, 154.24, 147.33, 146.83, 143.63, 129.75, 128.81, 127.47, 122.38, 119.80, 119.35, 103.97, 102.60, 98.50, 59.88, 54.98, 54.61, 54.58, 49.27, 48.60, 37.16, 26.68, 25.82, 24.74, 10.93.

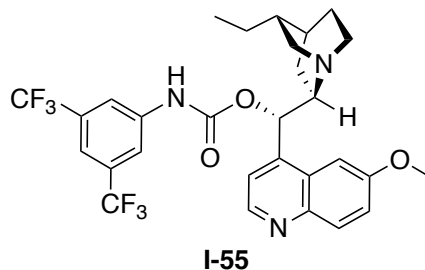
HRMS: TOF MS ES⁺ ($\text{C}_{29}\text{H}_{37}\text{N}_4\text{O}_3\text{S}$): Calc. $[\text{M} + \text{H}]^+$: 521.2578, Found $[\text{M} + \text{H}]^+$: 521.2586.



^1H NMR (500 MHz, Methanol- d_4) δ 8.65 (d, $J = 4.6$ Hz, 1H), 7.94 (d, $J = 9.2$ Hz, 1H), 7.63 – 7.42 (m, 3H), 7.38 (dd, $J = 9.3, 2.6$ Hz, 1H), 6.68 – 6.27 (m, 3H), 3.94 (s, 3H), 3.75 (s, 3H), 3.66 (s, 3H), 3.20 (br s, 1H), 2.89 – 2.59 (m, 4H), 2.07 – 1.90 (m, 1H), 1.59 – 1.24 (m, 7H), 0.93 – 0.82 (m, 3H).

^{13}C NMR (126 MHz, Methanol- d_4) δ 158.41, 157.28, 153.58, 151.33, 146.79, 145.02, 143.65, 130.20, 126.96, 122.34, 121.91, 119.79, 118.56, 103.72, 101.11, 98.39, 73.17, 58.78, 55.09, 54.87, 54.55, 50.34, 49.37, 36.87, 26.32, 25.87, 25.03, 21.74, 11.09.

HRMS: TOF MS ES⁺ ($\text{C}_{29}\text{H}_{36}\text{N}_3\text{O}_5$): Calc. $[\text{M} + \text{H}]^+$: 506.2655, Found $[\text{M} + \text{H}]^+$: 506.2652.

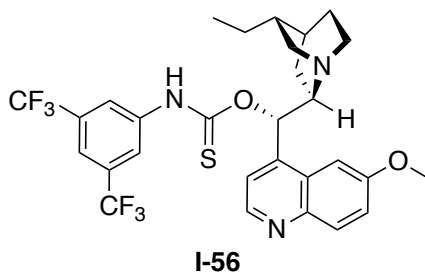


^1H NMR (500 MHz, Methanol- d_4) δ 8.65 (d, $J = 4.6$ Hz, 1H), 8.06 (s, 2H), 7.91 (d, $J = 9.2$ Hz, 1H), 7.57 (d, $J = 4.7$ Hz, 1H), 7.54 (d, $J = 2.7$ Hz, 1H), 7.49 (s, 1H), 7.35 (dd, $J = 9.2, 2.6$ Hz, 1H), 6.75 (d, $J = 5.4$ Hz, 1H), 3.98 (s, 3H), 3.37 – 3.27 (m, 1H), 2.93 – 2.63 (m, 4H), 2.06 – 1.99 (m, 1H), 1.69 – 1.63 (m, 1H), 1.56 – 1.36 (m, 6H), 0.85 (t, $J = 7.3$ Hz, 3H).

^{13}C NMR (126 MHz, Methanol- d_4) δ 158.53, 152.81, 146.72, 144.38, 143.65, 140.80, 131.86 (q, $J = 33.2$ Hz), 130.17, 126.91, 123.14 (q, $J = 272$, Hz), 122.38, 118.50, 117.87, 115.45, 101.03, 73.57, 58.88, 55.07, 50.33, 49.30, 36.72, 26.05, 25.66, 24.77, 21.79, 10.87.

^{19}F NMR (470 MHz, Methanol- d_4) δ -64.48 (s, 6F).

HRMS: TOF MS ES⁺ ($\text{C}_{29}\text{H}_{30}\text{F}_6\text{N}_3\text{O}_3$): Calc. $[\text{M} + \text{H}]^+$: 582.219, Found $[\text{M} + \text{H}]^+$: 582.2197.

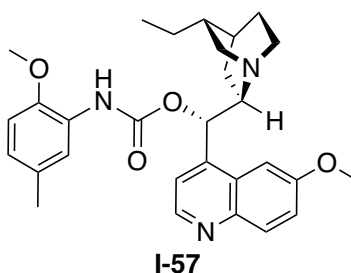


^1H NMR (500 MHz, Methanol- d_4) δ 8.67 (d, J = 4.7 Hz, 1H), 8.33 (br s, 2H), 7.91 (d, J = 9.2 Hz, 1H), 7.74 – 7.51 (m, 3H), 7.48 (d, J = 6.4 Hz, 1H), 7.35 (dd, J = 9.2, 2.6 Hz, 1H), 5.09 (br s, 2H), 3.95 (s, 3H), 3.44 (ddd, J = 9.2, 8.5, 7.0 Hz, 1H), 2.91 – 2.57 (m, 4H), 2.14 – 1.94 (m, 1H), 1.72 – 1.30 (m, 7H), 0.91 – 0.70 (m, 3H).

^{13}C NMR (126 MHz, Methanol- d_4) δ 187.19, 158.42, 146.73, 144.18, 143.76, 140.51, 131.68, 130.11, 127.25, 123.15, 122.40, 122.15, 119.10, 117.81, 101.56, 77.18, 59.49, 55.06, 50.45, 49.13, 36.80, 26.17, 25.64, 24.96, 22.50, 10.87.

^{19}F NMR (470 MHz, Methanol- d_4) δ -64.30 (s, 6F).

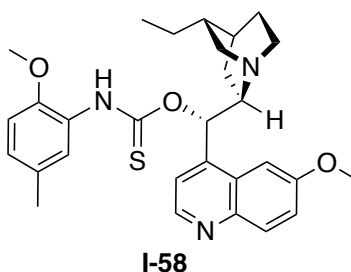
HRMS: TOF MS ES⁺ ($\text{C}_{29}\text{H}_{30}\text{F}_6\text{N}_3\text{O}_2\text{S}$): Calc. $[\text{M} + \text{H}]^+$: 598.1963, Found $[\text{M} + \text{H}]^+$: 598.1964.



^1H NMR (500 MHz, Methanol- d_4) δ 8.63 (d, J = 4.7 Hz, 1H), 7.93 (d, J = 9.2 Hz, 1H), 7.60 (br s, 1H), 7.54 (d, J = 4.7 Hz, 1H), 7.50 (d, J = 2.7 Hz, 1H), 7.37 (dd, J = 9.2, 2.7 Hz, 1H), 6.73 (s, 2H), 6.61 (d, J = 5.4 Hz, 1H), 3.94 (s, 3H), 3.74 (s, 3H), 3.16 (td, J = 8.9, 5.3 Hz, 1H), 2.84 – 2.56 (m, 4H), 2.13 (s, 3H), 1.98 – 1.90 (m, 1H), 1.60 – 1.54 (m, 1H), 1.49 – 1.24 (m, 6H), 0.89 – 0.81 (m, 3H).

^{13}C NMR (126 MHz, Methanol- d_4) δ 158.43, 153.01, 147.23, 146.79, 144.96, 143.65, 130.19, 129.71, 127.00, 126.37, 124.03, 122.33, 120.46, 118.59, 110.17, 101.08, 73.40, 58.77, 55.05, 54.92, 50.32, 49.35, 36.87, 26.37, 25.86, 25.02, 21.86, 19.67, 11.03.

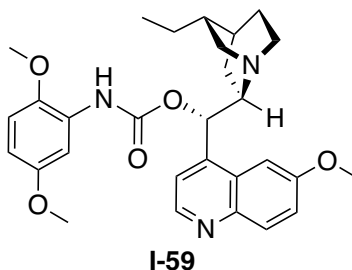
HRMS: TOF MS ES⁺ ($\text{C}_{29}\text{H}_{36}\text{N}_3\text{O}_4$): Calc. $[\text{M} + \text{H}]^+$: 490.2706, Found $[\text{M} + \text{H}]^+$: 490.2694.



The compound existed as a mixture of rotamers. ^1H NMR (500 MHz, Methanol- d_4) δ 8.74 – 8.60 (m, 1H), 7.99 – 7.90 (m, 1H), 7.71 – 7.29 (m, 4H), 7.10 – 6.73 (m, 2H), 4.04 – 3.49 (m, 6H), 3.36 – 3.15 (m, 1H), 2.92 – 2.43 (m, 4H), 2.30 – 2.04 (m, 3H), 1.90 – 1.76 (m, 1H), 1.60 – 1.19 (m, 6H), 1.09 – 0.64 (m, 4H).

^{13}C NMR (126 MHz, Methanol- d_4) δ 188.11, 187.34, 158.27, 150.82, 149.88, 146.79, 144.88, 144.49, 143.84, 130.25, 129.71, 129.23, 128.22, 127.21, 127.04, 126.76, 125.38, 122.35, 119.62, 119.06, 111.28, 110.82, 101.83, 80.32, 77.31, 59.12, 55.24, 55.08, 54.88, 53.77, 53.74, 50.46, 49.21, 36.97, 26.41, 25.71, 25.22, 24.58, 22.20, 19.63, 11.35, 11.33.

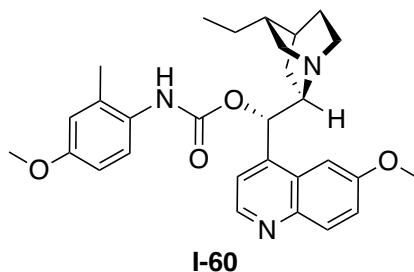
HRMS: TOF MS ES⁺ ($\text{C}_{29}\text{H}_{36}\text{N}_3\text{O}_3\text{S}$): Calc. $[\text{M} + \text{H}]^+$: 506.2477, Found $[\text{M} + \text{H}]^+$: 506.2475.



^1H NMR (500 MHz, Methanol- d_4) δ 8.65 (d, $J = 4.6$ Hz, 1H), 7.94 (d, $J = 9.2$ Hz, 1H), 7.60 (d, $J = 4.7$ Hz, 1H), 7.50 (d, $J = 2.7$ Hz, 1H), 7.45 (br s, 1H), 7.41 (dd, $J = 9.3, 2.6$ Hz, 1H), 6.84 (d, $J = 8.9$ Hz, 1H), 6.62 (d, $J = 5.4$ Hz, 1H), 6.57 – 6.52 (m, 1H), 3.97 (s, 3H), 3.79 (s, 3H), 3.65 (s, 3H), 3.25 (td, $J = 9.0, 5.3$ Hz, 1H), 2.91 – 2.65 (m, 4H), 2.05 – 1.96 (m, 1H), 1.71 – 1.64 (m, 1H), 1.58 – 1.36 (m, 6H), 0.93 – 0.84 (m, 3H).

^{13}C NMR (126 MHz, Methanol- d_4) δ 158.49, 153.73, 152.93, 146.75, 144.85, 143.59, 130.10, 127.43, 126.94, 122.37, 118.56, 111.05, 107.74, 100.98, 73.54, 58.74, 55.33, 55.00, 54.58, 50.34, 49.35, 36.88, 26.28, 25.88, 24.98, 21.81, 10.91.

HRMS: TOF MS ES⁺ (C₂₉H₃₆N₃O₅): Calc. [M + H]⁺: 506.2655, Found [M + H]⁺: 506.2651.

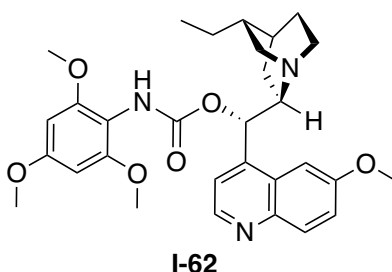


^1H NMR (500 MHz, Methanol- d_4) δ 8.70 (d, $J = 4.6$ Hz, 1H), 7.96 (d, $J = 9.1$ Hz, 1H), 7.70 – 7.47 (m, 2H), 7.43 (dd, $J = 9.2, 2.6$ Hz, 1H), 7.10 (d, $J = 8.6$ Hz, 1H), 6.86 – 6.59 (m,

3H), 3.97 (s, 3H), 3.71 (s, 3H), 3.32 – 3.25 (m, 1H), 3.03 – 2.66 (m, 4H), 2.18 (s, 3H), 1.80 – 1.25 (m, 8H), 1.01 – 0.88 (m, 3H).

^{13}C NMR (126 MHz, Methanol- d_4) δ 158.49, 157.96, 154.90, 146.71, 145.23, 143.65, 134.92, 130.09, 128.20, 126.97, 126.91, 122.42, 118.39, 115.30, 111.15, 101.02, 73.51, 58.77, 55.01, 54.35, 50.45, 49.34, 36.96, 26.36, 25.91, 25.02, 21.58, 16.91, 11.04.

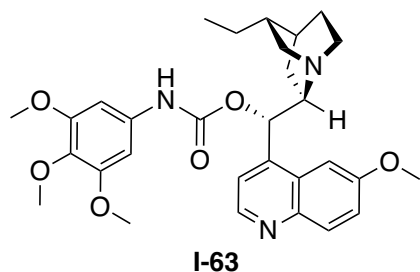
HRMS: TOF MS ES⁺ (C₂₉H₃₆N₃O₄): Calc. [M + H]⁺: 490.2706, Found [M + H]⁺: 490.2695.



The compound existed as a mixture of rotamers. ^1H NMR (500 MHz, Methanol- d_4) δ 8.72 (d, $J = 4.6$ Hz, 1H), 7.95 (d, $J = 9.2$ Hz, 1H), 7.65 (br s, 1H), 7.49 – 7.32 (m, 2H), 6.68 (m, 1H), 6.24 (m, 2H), 3.96 – 3.66 (m, 12H), 3.47 – 3.21 (m, 1H), 3.09 – 2.65 (m, 4H), 1.82 – 1.33 (m, 7H), 0.97 – 0.64 (m, 4H).

^{13}C NMR (126 MHz, cd_3od) δ 160.60, 160.36, 158.50, 157.13, 155.43, 155.08, 146.71, 146.58, 144.29, 143.61, 130.18, 126.73, 126.28, 122.40, 118.61, 106.82, 100.99, 90.58, 74.29, 72.57, 58.80, 58.15, 55.17, 55.01, 54.61, 53.56, 50.37, 50.19, 49.39, 48.19, 48.02, 47.85, 47.67, 47.50, 47.33, 47.16, 36.47, 36.21, 25.70, 25.59, 25.17, 24.92, 24.70, 23.84, 20.83, 19.75, 11.11, 10.97.

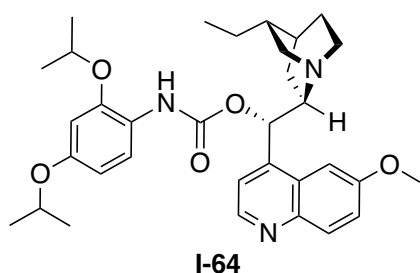
HRMS: TOF MS ES⁺ (C₃₀H₃₈N₃O₆): Calc. [M + H]⁺: 536.2759, Found [M + H]⁺: 536.2761.



¹H NMR (500 MHz, Methanol-*d*₄) δ 8.67 (d, *J* = 4.6 Hz, 1H), 7.94 (d, *J* = 9.2 Hz, 1H), 7.57 (d, *J* = 4.7 Hz, 1H), 7.53 (d, *J* = 2.7 Hz, 1H), 7.42 (dd, *J* = 9.2, 2.6 Hz, 1H), 6.81 (s, 2H), 6.68 (d, *J* = 5.4 Hz, 1H), 3.99 (s, 3H), 3.75 (s, 6H), 3.68 (s, 3H), 3.34 (td, *J* = 9.0, 5.3 Hz, 1H), 3.01 – 2.70 (m, 4H), 2.11 – 2.03 (m, 1H), 1.78 – 1.72 (m, 1H), 1.60 – 1.48 (m, 5H), 1.29 – 1.22 (m, 1H), 0.91 (t, *J* = 7.1 Hz, 3H).

¹³C NMR (126 MHz, Methanol-*d*₄) δ 158.55, 153.18, 152.98, 146.75, 144.78, 143.63, 134.80, 130.14, 126.91, 122.39, 118.48, 102.46, 101.06, 96.16, 72.82, 59.78, 58.94, 55.07, 55.06, 50.33, 49.29, 36.69, 25.94, 25.70, 24.75, 21.74, 10.89.

HRMS: TOF MS ES⁺ (C₃₀H₃₈N₃O₆): Calc. [M + H]⁺: 536.2761, Found [M + H]⁺: 536.2769.

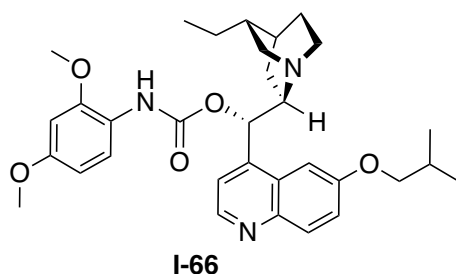


¹H NMR (500 MHz, Methanol-*d*₄) δ 8.66 (d, *J* = 4.6 Hz, 1H), 7.95 (d, *J* = 9.2 Hz, 1H), 7.60 (d, *J* = 4.7 Hz, 1H), 7.56 – 7.42 (m, 2H), 7.40 (dd, *J* = 9.2, 2.6 Hz, 1H), 6.71 (d, *J* = 4.4

Hz, 1H), 6.52 (s, 1H), 6.40 – 6.29 (m, 1H), 4.57 – 4.39 (m, 2H), 3.96 (s, 3H), 3.37 – 3.28 (m, 1H), 3.05 – 2.72 (m, 4H), 2.16 – 2.05 (m, 1H), 1.77 – 1.15 (m, 19H), 0.90 (m, 3H).

¹³C NMR (126 MHz, Methanol-*d*₄) δ 158.58, 155.46, 153.15, 149.56, 146.77, 144.38, 143.66, 130.24, 126.70, 122.47, 122.31, 120.45, 118.47, 106.46, 102.79, 101.02, 72.98, 70.91, 69.84, 58.55, 55.24, 50.42, 49.42, 36.48, 26.60, 25.73, 25.43, 24.84, 21.11, 21.06, 11.08.

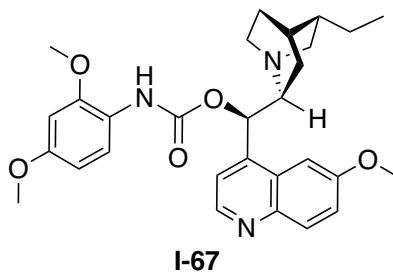
HRMS: TOF MS ES⁺ (C₃₃H₄₄N₃O₅): Calc. [M + H]⁺: 562.3281, Found [M + H]⁺: 562.3283.



¹H NMR (500 MHz, Methanol-*d*₄) δ 8.65 (d, *J* = 4.7 Hz, 1H), 7.94 (d, *J* = 9.2 Hz, 1H), 7.62 – 7.43 (m, 3H), 7.41 (dd, *J* = 9.2, 2.5 Hz, 1H), 6.68 – 6.31 (m, 3H), 3.96 – 3.84 (m, 2H), 3.76 (s, 3H), 3.68 (s, 3H), 3.29 – 3.28 (m, 1H), 2.95 – 2.65 (m, 4H), 2.15 – 1.97 (m, 2H), 1.71 – 1.34 (m, 7H), 1.06 (d, *J* = 2.9 Hz, 3H), 1.05 (d, *J* = 2.9 Hz, 3H), 0.95 – 0.85 (m, 3H).

¹³C NMR (126 MHz, Methanol-*d*₄) δ 158.00, 157.44, 153.63, 151.45, 146.66, 144.75, 143.55, 130.12, 127.00, 122.63, 122.18, 119.71, 118.53, 103.72, 101.68, 98.38, 74.60, 72.77, 58.82, 54.83, 54.52, 50.31, 49.35, 36.70, 28.13, 26.07, 25.83, 24.96, 21.64, 18.31, 11.00.

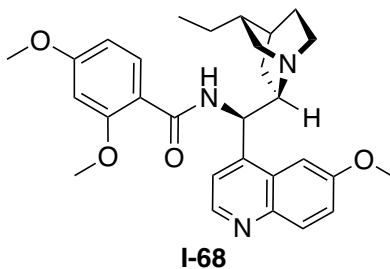
HRMS: TOF MS ES⁺ (C₃₂H₄₂N₃O₅): Calc. [M + H]⁺: 548.3127, Found [M + H]⁺: 548.3124.



The compound existed as a mixture of rotamers. ¹H NMR (500 MHz, Methanol-*d*₄) δ 8.67 (d, *J* = 4.6 Hz, 1H), 7.96 (d, *J* = 9.2 Hz, 1H), 7.65 – 7.39 (m, 4H), 6.67 – 6.34 (m, 3H), 3.97 (s, 3H), 3.80 (s, 3H), 3.72 (s, 3H), 3.38 – 3.23 (m, 2H), 3.06 (t, *J* = 11.9 Hz, 1H), 2.80 – 2.61 (m, 1H), 2.42 – 2.31 (m, 1H), 1.97 – 1.45 (m, 6H), 1.31 – 1.18 (m, 2H), 0.86 – 0.75 (m, 3H).

¹³C NMR (126 MHz, cd₃od) δ 158.57, 158.53, 157.72, 153.90, 152.02, 146.71, 144.94, 143.61, 143.59, 130.15, 130.10, 126.75, 123.00, 122.37, 119.57, 118.47, 118.37, 103.72, 101.02, 98.40, 73.61, 58.70, 57.80, 57.34, 55.12, 55.09, 54.79, 54.52, 48.13, 47.96, 47.79, 47.62, 47.45, 47.28, 47.11, 43.38, 42.63, 36.87, 27.12, 27.00, 25.65, 25.48, 25.12, 21.62, 10.90, 10.83.

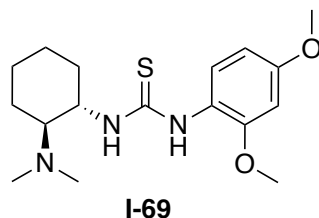
HRMS: TOF MS ES⁺ (C₂₉H₃₆N₃O₅): Calc. [M + H]⁺: 506.2655, Found [M + H]⁺: 506.2653.



^1H NMR (500 MHz, Methanol- d_4) δ 8.64 (d, $J = 4.6$ Hz, 1H), 7.95 (d, $J = 9.2$ Hz, 1H), 7.83 – 7.77 (m, 2H), 7.57 (d, $J = 4.7$ Hz, 1H), 7.40 (dd, $J = 9.2, 2.6$ Hz, 1H), 6.55 (d, $J = 2.3$ Hz, 1H), 6.49 (dd, $J = 8.8, 2.3$ Hz, 1H), 5.76 – 5.59 (m, 1H), 3.96 (s, 3H), 3.90 (s, 3H), 3.74 (s, 3H), 3.36 – 3.28 (m, 1H), 3.05 – 2.89 (m, 3H), 2.82 – 2.75 (m, 1H), 1.53 – 1.32 (m, 6H), 1.26 – 1.18 (m, 1H), 1.01 – 0.94 (m, 1H), 0.86 (t, $J = 7.1$ Hz, 3H).

^{13}C NMR (126 MHz, Methanol- d_4) δ 165.86, 164.07, 159.54, 158.14, 146.97, 146.79, 143.73, 132.61, 130.16, 128.44, 122.25, 119.68, 113.43, 105.43, 101.52, 98.09, 59.77, 55.28, 54.80, 54.68, 48.89, 37.03, 26.64, 25.70, 25.68, 24.80, 10.95.

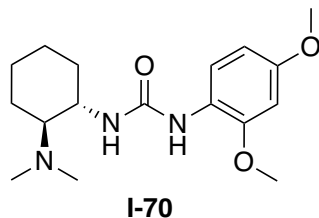
HRMS: TOF MS ES⁺ (C₂₉H₃₆N₃O₄): Calc. [M + H]⁺: 490.2706, Found [M + H]⁺: 490.2705.



^1H NMR (500 MHz, Methanol- d_4) δ 7.44 (d, $J = 8.7$ Hz, 1H), 6.58 (d, $J = 2.6$ Hz, 1H), 6.50 (dd, $J = 8.7, 2.6$ Hz, 1H), 4.96 – 4.68 (m, 1H), 4.28 – 4.11 (m, 1H), 3.79 (s, 3H), 3.78 (s, 3H), 2.64 – 2.51 (m, 1H), 2.32 (s, 6H), 1.91 – 1.63 (m, 3H), 1.34 – 1.07 (m, 4H).

^{13}C NMR (126 MHz, cd_3od) δ 180.23, 159.31, 154.39, 127.62, 119.33, 104.22, 98.76, 66.02, 55.41, 55.14, 54.95, 53.90, 39.44, 32.64, 24.82, 24.62, 22.56.

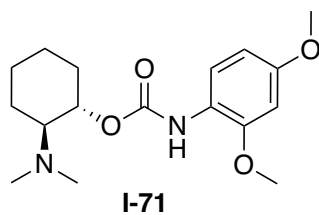
HRMS: TOF MS ES⁺ (C₁₇H₂₈N₃O₂S): Calc. [M + H]⁺: 338.1902, Found [M + H]⁺: 338.1903.



^1H NMR (500 MHz, Methanol- d_4) δ 7.76 (d, J = 8.8 Hz, 1H), 6.54 (d, J = 2.7 Hz, 1H), 6.44 (dd, J = 8.8, 2.7 Hz, 1H), 3.82 (s, 3H), 3.74 (s, 3H), 3.70 – 3.62 (m, 1H), 2.60 (td, J = 10.8, 3.3 Hz, 1H), 2.47 (s, 6H), 2.11 – 2.03 (m, 1H), 1.96 – 1.89 (m, 1H), 1.83 – 1.75 (m, 1H), 1.72 – 1.66 (m, 1H), 1.34 – 1.20 (m, 4H).

^{13}C NMR (126 MHz, Methanol- d_4) δ 156.81, 156.04, 150.39, 150.31, 121.76, 121.70, 121.09, 120.96, 103.75, 98.24, 67.14, 54.95, 54.65, 49.99, 49.90, 39.25, 33.59, 24.53, 24.45, 22.86.

HRMS: TOF MS ES⁺ ($\text{C}_{17}\text{H}_{28}\text{N}_3\text{O}_3$): Calc. $[\text{M} + \text{H}]^+$: 322.2131, Found $[\text{M} + \text{H}]^+$: 322.2125.



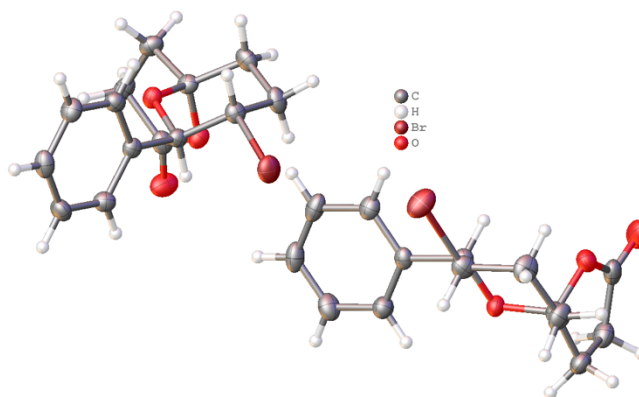
^1H NMR (500 MHz, Methylene Chloride- d_2) δ 7.92 (d, J = 8.5 Hz, 1H), 6.53 – 6.45 (m, 2H), 4.73 (td, J = 10.0, 4.4 Hz, 1H), 3.84 (s, 3H), 3.78 (s, 3H), 2.57 (ddd, J = 11.3, 10.0, 3.7 Hz, 1H), 2.33 (s, 6H), 2.22 – 2.14 (m, 1H), 1.93 – 1.86 (m, 1H), 1.81 – 1.70 (m, 2H), 1.43 – 1.16 (m, 4H).

^{13}C NMR (126 MHz, Methylene Chloride- d_2) δ 155.82, 153.29, 149.31, 121.33, 119.09, 103.73, 98.53, 73.07, 66.05, 55.59, 55.35, 40.25, 32.25, 24.74, 24.27, 23.00.

HRMS: TOF MS ES⁺ ($\text{C}_{17}\text{H}_{27}\text{N}_2\text{O}_4$): Calc. $[\text{M} + \text{H}]^+$: 323.1971, Found $[\text{M} + \text{H}]^+$: 323.1961.

I-6-7 General data

I-6-7-1 Crystal data for I-46a



Experimental. Single colorless needle-shaped crystals of **I-46a** were used as received. A suitable crystal 0.31×0.06×0.05 mm³ was selected and mounted on a nylon loop with paratone oil on a Bruker APEX-II CCD diffractometer. The crystal was kept at a steady $T = 173(2)$ K during data collection. The structure was solved with the ShelXT (Sheldrick, G.M. (2015). Acta Cryst. A71, 3-8) structure solution program using the Intrinsic Phasing solution method and by using **Olex2** (Dolomanov et al., 2009) as the graphical interface. The model was refined with version 2018/3 of ShelXL (Sheldrick, Acta Cryst. A64 2008, 112-122) using Least Squares minimization.

Crystal Data. C₁₄H₁₅BrO₃, $M_r = 311.17$, monoclinic, $P2_1/c$ (No. 14), $a = 5.6807(4)$ Å, $b = 17.3739(9)$ Å, $c = 26.0214(15)$ Å, $\beta = 90.501(4)^\circ$, $\alpha = \gamma = 90^\circ$, $V = 2568.1(3)$ Å³, $T = 173(2)$ K, $Z = 8$, $Z' = 2$, $\mu(\text{CuK}\alpha) = 4.355$, 26476 reflections measured, 5018 unique ($R_{int} = 0.0710$) which were used in all calculations. The final wR_2 was 0.0855 (all data) and R_1 was 0.0337 ($I > 2(I)$).

Compound	I-46a
CCDC	1939189
Formula	C ₁₄ H ₁₅ BrO ₃
<i>D</i> _{calc.} / g cm ⁻³	1.610
<i>μ</i> /mm ⁻¹	4.355
Formula Weight	311.17
Color	colorless
Shape	needle
Size/mm ³	0.31×0.06×0.05
<i>T</i> /K	173(2)
Crystal System	monoclinic
Space Group	<i>P</i> 2 ₁ / <i>c</i>
<i>a</i> /Å	5.6807(4)
<i>b</i> /Å	17.3739(9)
<i>c</i> /Å	26.0214(15)
<i>α</i> /°	90
<i>β</i> /°	90.501(4)
<i>γ</i> /°	90
<i>V</i> /Å ³	2568.1(3)
<i>Z</i>	8
<i>Z</i> '	2
Wavelength/Å	1.541838
Radiation type	CuK _α
<i>θ</i> _{min} /°	3.058
<i>θ</i> _{max} /°	72.329
Measured Refl.	26476
Independent Refl.	5018
Reflections with <i>I</i> > 2(<i>I</i>)	3962
<i>R</i> _{int}	0.0710
Parameters	325
Restraints	0
Largest Peak	0.460
Deepest Hole	-0.581
Goof	1.049
<i>wR</i> ₂ (all data)	0.0855
<i>wR</i> ₂	0.0769
<i>R</i> ₁ (all data)	0.0502
<i>R</i> ₁	0.0337

Structure Quality Indicators

Reflections: d min (Cu) 0.81 | I/σ 21.4 | Rint 7.10% | complete 100%

Refinement: Shift 0.001 | Max Peak 0.5 | Min Peak -0.6 | Goof 1.049

A colourless needle-shaped crystal with dimensions 0.31×0.06×0.05 mm³ was mounted on a nylon loop with paratone oil. Data were collected using a Bruker APEX-II CCD diffractometer equipped with an Oxford Cryosystems low-temperature device, operating at $T = 173(2)$ K.

Data were measured using ω and ϕ of 1.00° per frame for 75.00 s using CuK α radiation (sealed tube, 40 kV, 30 mA). The total number of runs and images was based on the strategy calculation from the program **COSMO** (BRUKER, V1.61, 2009). The actually achieved resolution was $\theta = 72.329$.

Cell parameters were retrieved using the **SAINT** (Bruker, V8.38A, after 2013) software and refined using **SAINT** (Bruker, V8.38A, after 2013) on 8310 reflections, 31 % of the observed reflections. Data reduction was performed using the **SAINT** (Bruker, V8.38A, after 2013) software which corrects for Lorentz polarization. The final completeness is 99.90 out to 72.329 in θ **SADABS**-2016/2 (Bruker, 2016/2) was used for absorption correction. $wR_2(\text{int})$ was 0.0930 before and 0.0607 after correction. The Ratio of minimum to maximum transmission is 0.7816. The $\lambda/2$ correction factor is Not present. The structure was solved in the space group $P2_1/c$ (# 14) by Intrinsic Phasing using the ShelXT (Sheldrick, G.M. (2015). Acta Cryst. A71, 3-8) structure solution program. The structure was refined by Least Squares using version 2014/6 of **XL** (Sheldrick, 2008) incorporated in **Olex2** (Dolomanov et al., 2009). All non-hydrogen atoms were refined

anisotropically. Hydrogen atom positions were calculated geometrically and refined using the riding model, except for the hydrogen atom on the non-carbon atom(s) which was found by difference Fourier methods and refined isotropically.

The value of Z' is 2. This means that there are two independent molecules in the asymmetric unit.

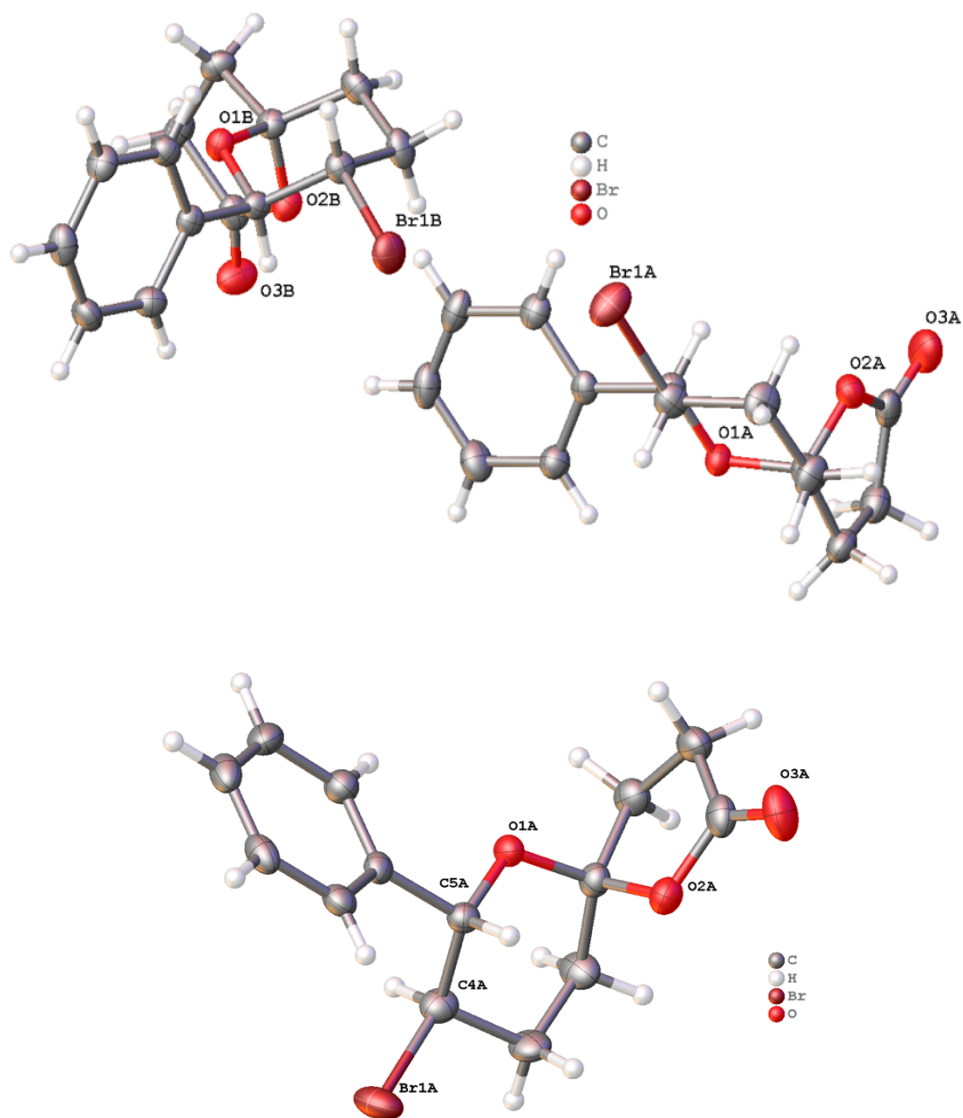
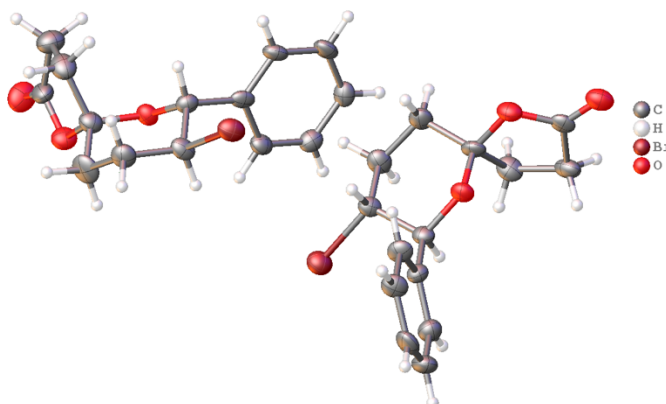


Figure I-23. X-ray structure of I-46a (different views)

I-6-7-2 Crystal data for I-46b



Experimental. Single colourless needle-shaped crystals of **I-46b** were used as received. A suitable crystal $0.31 \times 0.07 \times 0.04 \text{ mm}^3$ was selected and mounted on a nylon loop with paratone oil on a Bruker APEX-II CCD diffractometer. The crystal was kept at a steady $T = 173(2) \text{ K}$ during data collection. The structure was solved with the ShelXT (Sheldrick, G.M. (2015). Acta Cryst. A71, 3-8) structure solution program using the Intrinsic Phasing solution method and by using **Olex2** (Dolomanov et al., 2009) as the graphical interface. The model was refined with version 2018/3 of ShelXL (Sheldrick, Acta Cryst. A64 2008, 112-122) using Least Squares minimization.

Crystal Data. $\text{C}_{14}\text{H}_{15}\text{BrO}_3$, $M_r = 311.17$, monoclinic, $P2_1/n$ (No. 14), $a = 21.3782(10) \text{ \AA}$, $b = 5.8155(3) \text{ \AA}$, $c = 21.6027(12) \text{ \AA}$, $\beta = 102.604(4)^\circ$, $\alpha = \gamma = 90^\circ$, $V = 2621.0(2) \text{ \AA}^3$, $T = 173(2) \text{ K}$, $Z = 8$, $Z' = 2$, $\mu(\text{CuK}\alpha) = 4.267$, 19675 reflections measured, 4921 unique ($R_{int} = 0.1967$) which were used in all calculations. The final wR_2 was 0.1496 (all data) and R_1 was 0.0614 ($I > 2(I)$).

Compound	I-46b
CCDC	1942944
Formula	C ₁₄ H ₁₅ BrO ₃
<i>D</i> _{calc.} / g cm ⁻³	1.577
<i>μ</i> /mm ⁻¹	4.267
Formula Weight	311.17
Color	colourless
Shape	needle
Size/mm ³	0.31×0.07×0.04
<i>T</i> /K	173(2)
Crystal System	monoclinic
Space Group	<i>P</i> 2 ₁ / <i>n</i>
<i>a</i> /Å	21.3782(10)
<i>b</i> /Å	5.8155(3)
<i>c</i> /Å	21.6027(12)
<i>α</i> /°	90
<i>β</i> /°	102.604(4)
<i>γ</i> /°	90
<i>V</i> /Å ³	2621.0(2)
<i>Z</i>	8
<i>Z</i> '	2
Wavelength/Å	1.541838
Radiation type	CuK _α
<i>θ</i> _{min} /°	2.634
<i>θ</i> _{max} /°	70.141
Measured Refl.	19675
Independent Refl.	4921
Reflections with <i>I</i> > 2(<i>I</i>)	2486
<i>R</i> _{int}	0.1967
Parameters	325
Restraints	0
Largest Peak	0.975
Deepest Hole	-0.551
GooF	0.966
<i>wR</i> ₂ (all data)	0.1496
<i>wR</i> ₂	0.1189
<i>R</i> ₁ (all data)	0.1438
<i>R</i> ₁	0.0614

Structure Quality Indicators

Reflections: d min (Cu) 0.82 I/σ 6.9 R_{int} 19.67% complete 99%

Refinement: Shift 0.001 Max Peak 1.0 Min Peak -0.6 $Goof$ 0.966

A colourless needle-shaped crystal with dimensions 0.31×0.07×0.04 mm³ was mounted on a nylon loop with paratone oil. Data were collected using a Bruker APEX-II CCD diffractometer equipped with an Oxford Cryosystems low-temperature device, operating at $T = 173(2)$ K.

Data were measured using ω and ϕ of 1.00° per frame for 225.00 s using CuK α radiation (sealed tube, 40 kV, 30 mA). The total number of runs and images was based on the strategy calculation from the program **COSMO** (BRUKER, V1.61, 2009). The actually achieved resolution was $\theta = 70.141$.

Cell parameters were retrieved using the **SAINT** (Bruker, V8.38A, after 2013) software and refined using **SAINT** (Bruker, V8.38A, after 2013) on 1667 reflections, 8 % of the observed reflections. Data reduction was performed using the **SAINT** (Bruker, V8.38A, after 2013) software which corrects for Lorentz polarization. The final completeness is 99.40 out to 70.141 in θ **SADABS**-2016/2 (Bruker, 2016/2) was used for absorption correction. $wR_2(int)$ was 0.0981 before and 0.0754 after correction. The Ratio of minimum to maximum transmission is 0.7378. The $\lambda/2$ correction factor is Not present. The structure was solved in the space group $P2_1/n$ (# 14) by Intrinsic Phasing using the ShelXT (Sheldrick, G.M. (2015). Acta Cryst. A71, 3-8) structure solution program. The structure was refined by Least Squares using version 2014/6 of **XL** (Sheldrick, 2008) incorporated in **Olex2** (Dolomanov et al., 2009). All non-hydrogen atoms were refined

anisotropically. Hydrogen atom positions were calculated geometrically and refined using the riding model, except for the hydrogen atom on the non-carbon atom(s) which was found by difference Fourier methods and refined isotropically.

The value of Z' is 2. This means that there are two independent molecules in the asymmetric unit.

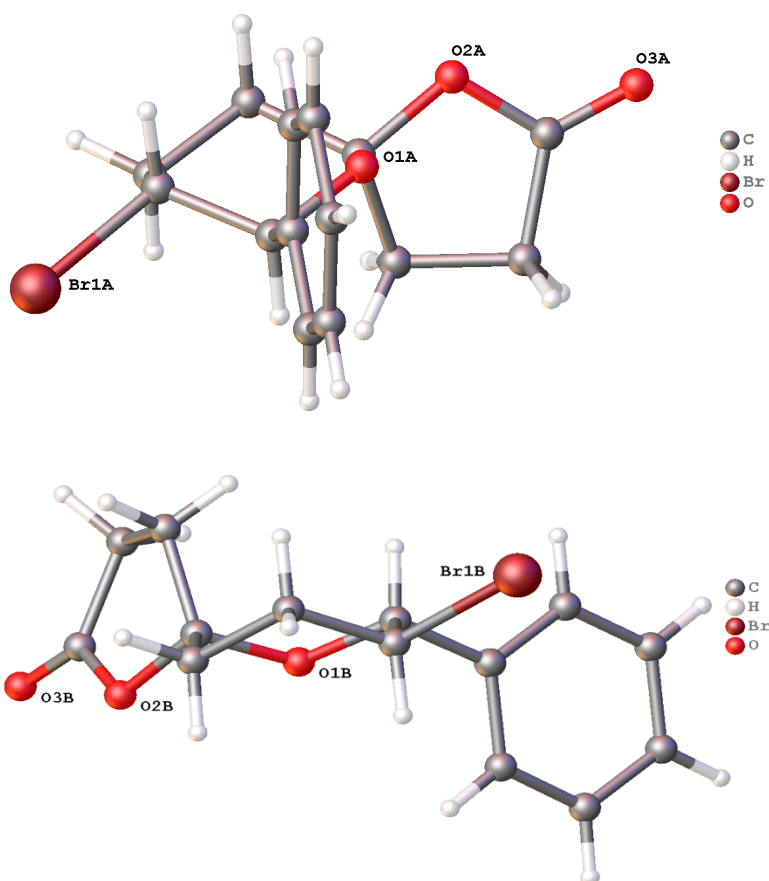
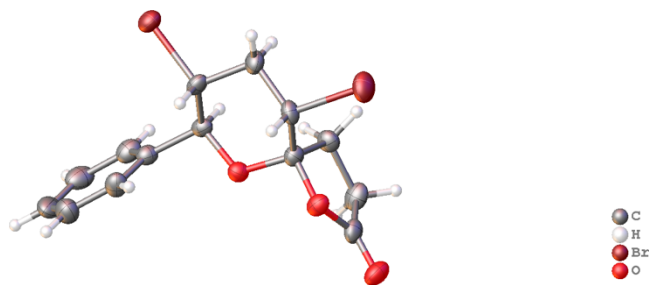


Figure I-24. X-ray structure of I-46b (different views)

I-6-7-3 Crystal data for I-100



Experimental. Single colourless needle-shaped crystals of **I-100** were used as received. A suitable crystal 0.40×0.07×0.05 mm³ was selected and mounted on a nylon loop with paratone oil on a Bruker APEX-II CCD diffractometer. The crystal was kept at a steady $T = 173(2)$ K during data collection. The structure was solved with the ShelXT (Sheldrick, G.M. (2015). Acta Cryst. A71, 3-8) structure solution program using the Intrinsic Phasing solution method and by using **Olex2** (Dolomanov et al., 2009) as the graphical interface. The model was refined with version 2018/3 of ShelXL (Sheldrick, Acta Cryst. A64 2008, 112-122) using Least Squares minimization.

Crystal Data. C₁₄H₁₄Br₂O₃, $M_r = 390.07$, monoclinic, $P2_1/c$ (No. 14), $a = 9.4982(2)$ Å, $b = 5.70550(10)$ Å, $c = 26.4310(6)$ Å, $\beta = 100.057(2)^\circ$, $\alpha = \gamma = 90^\circ$, $V = 1410.34(5)$ Å³, $T = 173(2)$ K, $Z = 4$, $Z' = 1$, $\mu(\text{CuK}\alpha) = 7.312$, 7919 reflections measured, 2553 unique ($R_{int} = 0.0546$) which were used in all calculations. The final wR_2 was 0.1059 (all data) and R_1 was 0.0418 ($I > 2(I)$).

Compound	I-100
CCDC	1942945
Formula	C ₁₄ H ₁₄ Br ₂ O ₃
<i>D</i> _{calc.} / g cm ⁻³	1.837
<i>μ</i> /mm ⁻¹	7.312
Formula Weight	390.07
Color	colourless
Shape	needle
Size/mm ³	0.40×0.07×0.05
<i>T</i> /K	173(2)
Crystal System	monoclinic
Space Group	<i>P</i> 2 ₁ / <i>c</i>
<i>a</i> /Å	9.4982(2)
<i>b</i> /Å	5.70550(10)
<i>c</i> /Å	26.4310(6)
<i>α</i> /°	90
<i>β</i> /°	100.057(2)
<i>γ</i> /°	90
<i>V</i> /Å ³	1410.34(5)
<i>Z</i>	4
<i>Z</i> '	1
Wavelength/Å	1.541838
Radiation type	CuK _α
<i>θ</i> _{min} /°	3.396
<i>θ</i> _{max} /°	70.108
Measured Refl.	7919
Independent Refl.	2553
Reflections with <i>I</i> > 2(<i>I</i>)	1940
<i>R</i> _{int}	0.0546
Parameters	172
Restraints	0
Largest Peak	0.917
Deepest Hole	-0.634
Goof	1.002
<i>wR</i> ₂ (all data)	0.1059
<i>wR</i> ₂	0.0967
<i>R</i> ₁ (all data)	0.0623
<i>R</i> ₁	0.0418

Structure Quality Indicators

Reflections:	d min (Cu) 0.82	I/ σ 18.0	R _{int} 5.46%	complete 96%
Refinement:	Shift 0.000	Max Peak 0.9	Min Peak -0.6	Goof 1.002

A colourless needle-shaped crystal with dimensions 0.40×0.07×0.05 mm³ was mounted on a nylon loop with paratone oil. Data were collected using a Bruker APEX-II CCD diffractometer equipped with an Oxford Cryosystems low-temperature device, operating at $T = 173(2)$ K.

Data were measured using ω and ϕ of 1.00° per frame for 100.00 s using CuK α radiation (sealed tube, 40 kV, 30 mA). The total number of runs and images was based on the strategy calculation from the program **COSMO** (BRUKER, V1.61, 2009). The actually achieved resolution was $\theta = 70.108$.

Cell parameters were retrieved using the **SAINT** (Bruker, V8.38A, after 2013) software and refined using **SAINT** (Bruker, V8.38A, after 2013) on 2647 reflections, 33 % of the observed reflections. Data reduction was performed using the **SAINT** (Bruker, V8.38A, after 2013) software which corrects for Lorentz polarization. The final completeness is 96.10 out to 70.108 in θ **SADABS**-2016/2 (Bruker,2016/2) was used for absorption correction. $wR_2(\text{int})$ was 0.0771 before and 0.0537 after correction. The Ratio of minimum to maximum transmission is 0.7349. The $\lambda/2$ correction factor is Not present. The structure was solved in the space group $P2_1/c$ (# 14) by Intrinsic Phasing using the ShelXT (Sheldrick, G.M. (2015). Acta Cryst. A71, 3-8) structure solution program. The structure was refined by Least Squares using version 2014/6 of **XL** (Sheldrick, 2008) incorporated in **Olex2** (Dolomanov et al., 2009). All non-hydrogen atoms were refined

anisotropically. Hydrogen atom positions were calculated geometrically and refined using the riding model, except for the hydrogen atom on the non-carbon atom(s) which was found by difference Fourier methods and refined isotropically.

There is a single molecule in the asymmetric unit, which is represented by the reported sum formula. In other words: Z is 4 and Z' is 1.

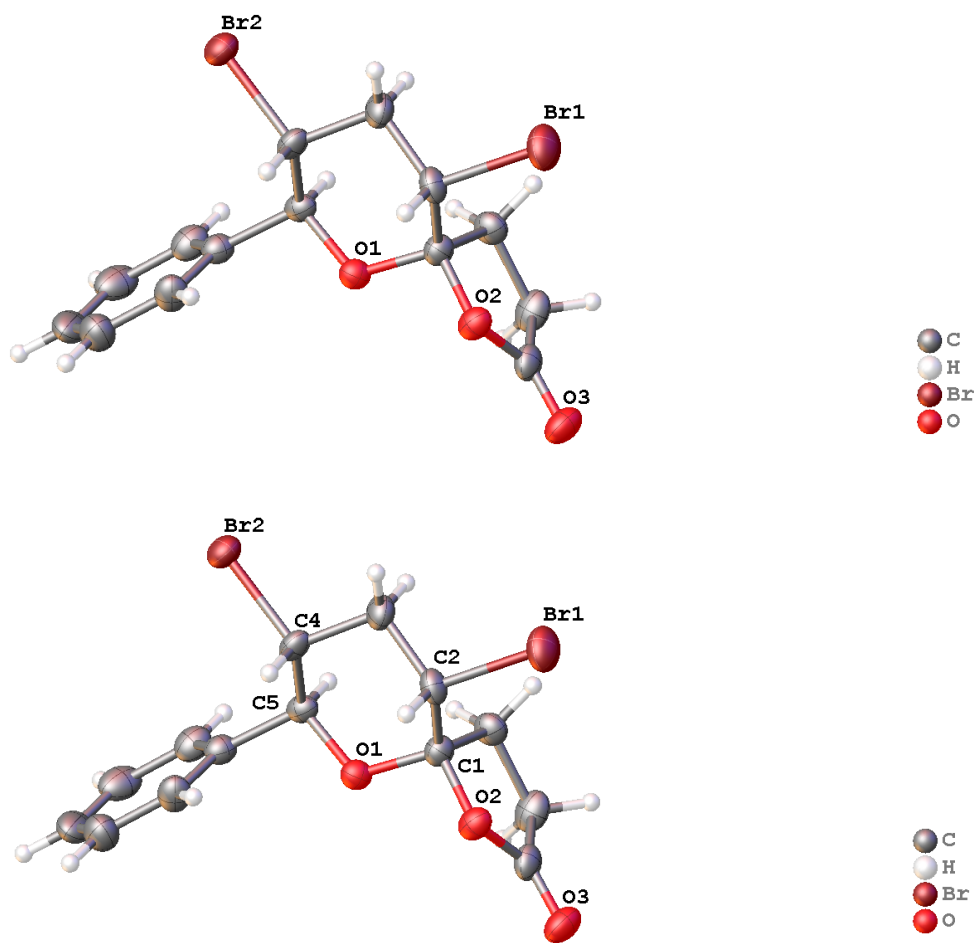
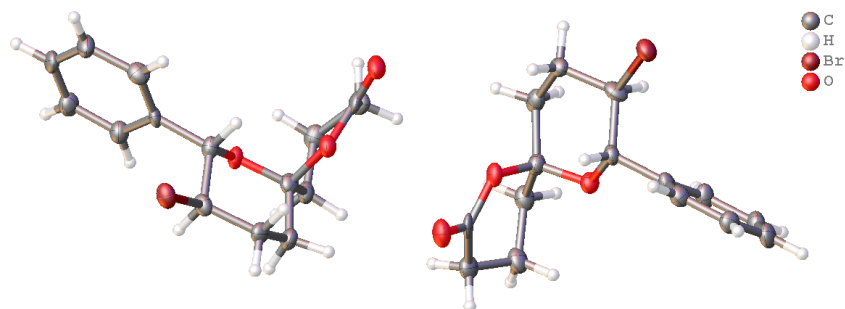


Figure I-25. X-ray structure of I-100 (different views)

I-6-7-4 Crystal data for I-99a



Experimental. Single colourless needle crystals of **I-99a** used as received. A suitable crystal with dimensions $0.31 \times 0.04 \times 0.02 \text{ mm}^3$ was selected and mounted on a nylon loop with paratone oil on a XtaLAB Synergy, Dualflex, HyPix diffractometer. The crystal was kept at a steady $T = 100.00(10) \text{ K}$ during data collection. The structure was solved with the ShelXS (Sheldrick, 2008) solution program using direct methods and by using Olex2 (Dolomanov et al., 2009) as the graphical interface. The model was refined with ShelXL 2018/3 (Sheldrick, 2015) using full matrix least squares minimisation on F^2 .

Crystal Data. $\text{C}_{15}\text{H}_{17}\text{BrO}_3$, $M_r = 325.20$, orthorhombic, $Pca2_1$ (No. 29), $a = 12.2672(5) \text{ \AA}$, $b = 6.3114(3) \text{ \AA}$, $c = 35.3845(15) \text{ \AA}$, $\alpha = \beta = \gamma = 90^\circ$, $V = 2739.6(2) \text{ \AA}^3$, $T = 100.00(10) \text{ K}$, $Z = 8$, $Z' = 2$, $\mu(\text{Cu K}\alpha) = 4.109$, 13914 reflections measured, 4587 unique ($R_{\text{int}} = 0.0678$) which were used in all calculations. The final wR_2 was 0.1874 (all data) and R_1 was 0.0681 ($I \geq 2 \sigma(I)$).

Compound	I-99a
Formula	C ₁₅ H ₁₇ BrO ₃
CCDC	2036932
<i>D</i> _{calc.} / g cm ⁻³	1.577
<i>μ</i> /mm ⁻¹	4.109
Formula Weight	325.20
Colour	colourless
Shape	needle
Size/mm ³	0.31×0.04×0.02
<i>T</i> /K	100.00(10)
Crystal System	orthorhombic
Flack Parameter	0.03(5)
Hooft Parameter	0.01(2)
Space Group	<i>Pca</i> 2 ₁
<i>a</i> /Å	12.2672(5)
<i>b</i> /Å	6.3114(3)
<i>c</i> /Å	35.3845(15)
<i>α</i> /°	90
<i>β</i> /°	90
<i>γ</i> /°	90
<i>V</i> /Å ³	2739.6(2)
<i>Z</i>	8
<i>Z</i> '	2
Wavelength/Å	1.54184
Radiation type	Cu K _α
<i>θ</i> _{min} /°	2.497
<i>θ</i> _{max} /°	77.860
Measured Refl's.	13914
Indep't Refl's	4587
Refl's I≥2 σ(I)	4177
<i>R</i> _{int}	0.0678
Parameters	343
Restraints	1
Largest Peak	0.824
Deepest Hole	-0.822
Goof	1.077
<i>wR</i> ₂ (all data)	0.1874
<i>wR</i> ₂	0.1832
<i>R</i> ₁ (all data)	0.0723
<i>R</i> ₁	0.0681

Structure Quality Indicators

Reflections: d min (Cu) 0.79 | $I/\sigma(I)$ 15.3 | Rint 6.78% | complete 100% (IUCr) 83%

Refinement: Shift 0.000 | Max Peak 0.8 | Min Peak -0.8 | GooF 1.077 | Flack -.04(8)

A colourless needle-shaped crystal with dimensions 0.31×0.04×0.02 mm³ was mounted on a nylon loop with paratone oil. Data were collected using a XtaLAB Synergy, Dualflex, HyPix diffractometer equipped with an Oxford Cryosystems low-temperature device, operating at $T = 100.00(10)$ K.

Data were measured using ω scans of 0.5° per frame for 3.5/14.0 s using Cu K_{α} radiation (micro-focus sealed X-ray tube, 50 kV, 1 mA). The total number of runs and images was based on the strategy calculation from the program CrysAlisPro (Rigaku, V1.171.40.84a, 2020). The actually achieved resolution was $\theta = 77.860$.

Cell parameters were retrieved using the CrysAlisPro (Rigaku, V1.171.40.84a, 2020) software and refined using CrysAlisPro (Rigaku, V1.171.40.84a, 2020) on 5380 reflections, 39 % of the observed reflections. Data reduction was performed using the CrysAlisPro (Rigaku, V1.171.40.84a, 2020) software which corrects for Lorentz polarization. The final completeness is 99.80 out to 77.860 in θ CrysAlisPro 1.171.40.84a (Rigaku Oxford Diffraction, 2020) Empirical absorption correction using spherical harmonics, implemented in SCALE3 ABSPACK scaling algorithm.

The structure was solved in the space group $Pca2_1$ (# 29) by using direct methods using the ShelXS (Sheldrick, 2008) structure solution program. The structure was refined by Least Squares using version 2018/2 of XL (Sheldrick, 2008) incorporated in Olex2 (Dolomanov et al., 2009). All non-hydrogen atoms were refined anisotropically. Hydrogen

atom positions were calculated geometrically and refined using the riding model, except for the hydrogen atom on the non-carbon atom(s) which were found by difference Fourier methods and refined isotropically when data permits.

The value of Z' is 2. This means that there are two independent molecules in the asymmetric unit.

The Flack parameter was refined to 0.03(5). Determination of absolute structure using Bayesian statistics on Bijvoet differences using the Olex2 results in 0.01(2). Note: The Flack parameter is used to determine chirality of the crystal studied, the value should be near 0, a value of 1 means that the stereochemistry is wrong and the model should be inverted. A value of 0.5 means that the crystal consists of a racemic mixture of the two enantiomers.

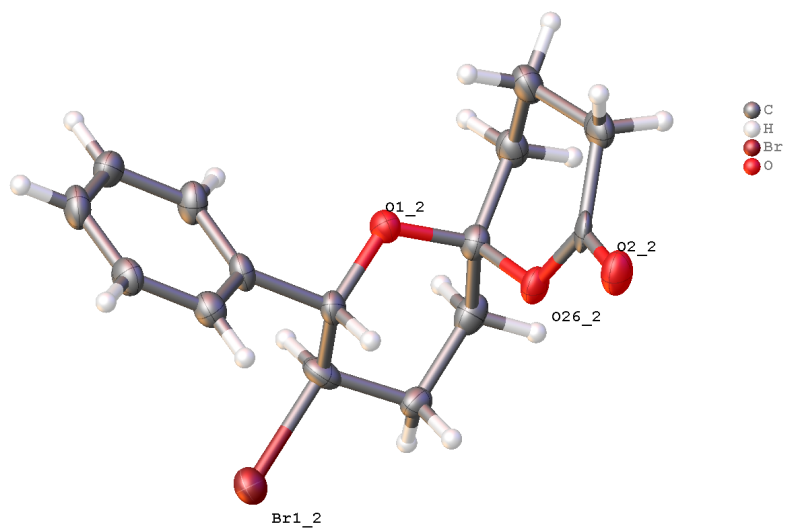
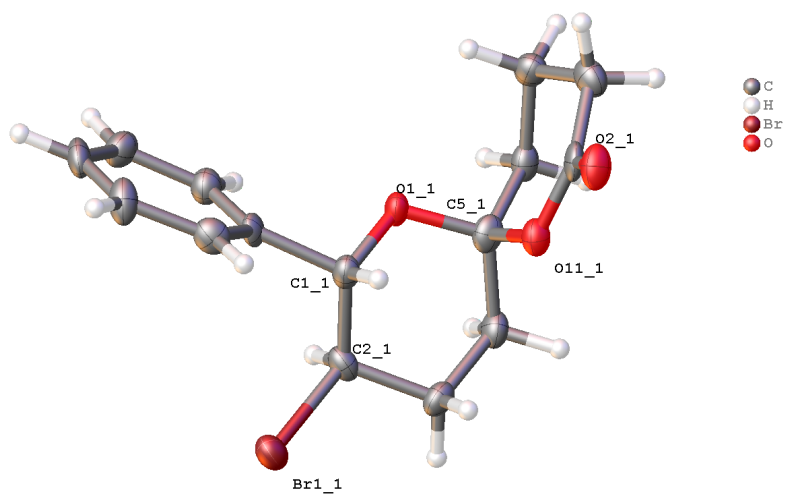


Figure I-26. X-ray structure of I-99a (different views)

REFERENCES

- (1) Oh, H.; Gloer, J. B.; Shearer, C. A. Massarinolins A-C: New bioactive sesquiterpenoids from the aquatic fungus *Massarina tunicata*. *J Nat Prod* **1999**, *62* (3), 497-501. DOI: DOI 10.1021/np980447+.
- (2) Xiao, W. L.; Zhu, H. J.; Shen, Y. H.; Li, R. T.; Li, S. H.; Sun, H. D.; Zheng, Y. T.; Wang, R. R.; Lu, Y.; Wang, C.; et al. Lancifodilactone G: A unique nortriterpenoid isolated from *Schisandra lancifolia* and its anti-HIV activity. *Org Lett* **2005**, *7* (11), 2145-2148. DOI: 10.1021/ol050502n.
- (3) Fan, Y. Y.; Zhang, H.; Zhou, Y.; Liu, H. B.; Tang, W.; Zhou, B.; Zuo, J. P.; Yue, J. M. Phainanoids A-F, A New Class of Potent Immunosuppressive Triterpenoids with an Unprecedented Carbon Skeleton from *Phyllanthus hainanensis*. *J Am Chem Soc* **2015**, *137* (1), 138-141. DOI: 10.1021/ja511813g.
- (4) Brimble, M. A.; Robinson, S. G. Synthesis of tricyclic aryl spiroacetals related to the papulacandins. *Tetrahedron* **1996**, *52* (28), 9553-9562. DOI: Doi 10.1016/0040-4020(96)00492-9.
- (5) Davis, D. C.; Walker, K. L.; Hu, C. H.; Zare, R. N.; Waymouth, R. M.; Dai, M. J. Catalytic Carbonylative Spirolactonization of Hydroxycyclopropanols. *J Am Chem Soc* **2016**, *138* (33), 10693-10699. DOI: 10.1021/jacs.6b06573.
- (6) Fukuda, H.; Takeda, M.; Sato, Y.; Mitsunobu, O. Convenient Method for the Formation of 2-Oxo-1,6-Dioxaspiroalkene Rings. *Synthesis-Stuttgart* **1979**, (5), 368-370.
- (7) Kambale, D. A.; Thorat, S. S.; Pratapure, M. S.; Gonnade, R. G.; Kontham, R. Lewis acid catalyzed cascade annulation of alkynols with alpha-ketoesters: a facile access to gamma-spiroketal-gamma-lactones. *Chem Commun* **2017**, *53* (49), 6641-6644. DOI: 10.1039/c7cc03668j.
- (8) Yamamoto, M.; Yoshitake, M.; Yamada, K. Cyclization of Alkynecarboxylic Acids - a Route to an Oxaspirolactone. *J Chem Soc Chem Comm* **1983**, (18), 991-992. DOI: DOI 10.1039/c39830000991.
- (9) Thorat, S. S.; Kontham, R. Recent advances in the synthesis of oxaspirolactones and their application in the total synthesis of related natural products. *Org Biomol Chem* **2019**, *17* (31), 7270-7292. DOI: 10.1039/c9ob01212e.
- (10) Haruki, F. M. T. Y. S. O. M. A Convenient Method for the Formation of 2-Oxo-1,6-dioxaspiroalkene Rings. *Synthesis* **1979**, *5*, 368-370. DOI: 10.1055/s-1979-28684.

- (11) Yoshida, J.; Sakaguchi, K.; Isoe, S. Oxidative [3+2] Cycloaddition of 1,3-Diketone and Olefin Using Electroorganic Chemistry. *Tetrahedron Lett* **1986**, *27* (50), 6075-6078. DOI: Doi 10.1016/S0040-4039(00)85402-7.
- (12) Gore, V. G.; Chordia, M. D.; Narasimhan, N. S. Improved Syntheses of Shihunine, the Spiro Phthalide Pyrrolidine Alkaloid. *Tetrahedron* **1990**, *46* (7), 2483-2494.
- (13) Cala, L.; Mendoza, A.; Fananas, F. J.; Rodriguez, F. A catalytic multicomponent coupling reaction for the enantioselective synthesis of spiroacetals. *Chem Commun* **2013**, *49* (26), 2715-2717. DOI: 10.1039/c3cc00118k.
- (14) heng, T. W., X.; Ng, W.-H.; Tse, Y.-L. S.; Yeung, Y.-Y. . Catalytic enantio- and diastereoselective domino halocyclization and spiroketalization. *Nature Catalysis* **2020**, *3*, 993-1001.
- (15) Whitehead, D. C.; Yousefi, R.; Jaganathan, A.; Borhan, B. An Organocatalytic Asymmetric Chlorolactonization. *J Am Chem Soc* **2010**, *132* (10), 3298-+. DOI: 10.1021/ja100502f.
- (16) Jaganathan, A.; Garzan, A.; Whitehead, D. C.; Staples, R. J.; Borhan, B. A Catalytic Asymmetric Chlorocyclization of Unsaturated Amides. *Angew Chem Int Edit* **2011**, *50* (11), 2593-2596. DOI: 10.1002/anie.201006910.
- (17) Garzan, A.; Jaganathan, A.; Marzijarani, N. S.; Yousefi, R.; Whitehead, D. C.; Jackson, J. E.; Borhan, B. Solvent-Dependent Enantiodivergence in the Chlorocyclization of Unsaturated Carbamates. *Chem-Eur J* **2013**, *19* (27), 9015-9021. DOI: 10.1002/chem.201300189.
- (18) Ashtekar, K. D.; Marzijarani, N. S.; Jaganathan, A.; Holmes, D.; Jackson, J. E.; Borhan, B. A New Tool To Guide Halofunctionalization Reactions: The Halenium Affinity (HalA) Scale. *J Am Chem Soc* **2014**, *136* (38), 13355-13362. DOI: 10.1021/ja506889c.
- (19) Ashtekar, K. D.; Vetticatt, M.; Yousefi, R.; Jackson, J. E.; Borhan, B. Nucleophile-Assisted Alkene Activation: Olefins Alone Are Often Incompetent. *J Am Chem Soc* **2016**, *138* (26), 8114-8119. DOI: 10.1021/jacs.6b02877.
- (20) Ashtekar, K. D.; Gholami, H.; Moemeni, M.; Chakraborty, A.; Kiiskila, L.; Ding, X. L.; Toma, E.; Rahn, C.; Borhan, B. A Mechanistically Inspired Halenium Ion Initiated Spiroketalization: Entry to Mono- and Dibromospiroketals. *Angew Chem Int Edit* **2022**, *61* (8). DOI: ARTN e20211517310.1002/anie.202115173.
- (21) Kitching, W.; Lewis, J. A.; Fletcher, M. T.; Devoss, J. J.; Drew, R. A. I.; Moore, C. J. Spiroacetals from Dienones and Hydroxyenones by Mercury(II) Cyclization. *J Chem Soc Chem Comm* **1986**, (11), 855-856. DOI: DOI 10.1039/c39860000855.

- (22) Holson, E. B.; Roush, W. R. Diastereoselective synthesis of the C(17)-C(28) fragment (The C-D spiroketal unit) of spongistatin 1 (altohrytin A) via a kinetically controlled iodo-spiroketalization reaction. *Org Lett* **2002**, *4* (21), 3719-3722. DOI: 10.1021/ol0266875.
- (23) Commandeur, M.; Commandeur, C.; Cossy, J. Synthesis of a Platform To Access Bistramides and Their Analogues. *Org Lett* **2011**, *13* (22), 6018-6021. DOI: 10.1021/ol202483u.
- (24) Zhou, L.; Tan, C. K.; Jiang, X. J.; Chen, F.; Yeung, Y. Y. Asymmetric Bromolactonization Using Amino-thiocarbamate Catalyst. *J Am Chem Soc* **2010**, *132* (44), 15474-15476. DOI: 10.1021/ja1048972.
- (25) Zhou, L.; Tay, D. W.; Chen, J.; Leung, G. Y. C.; Yeung, Y. Y. Enantioselective synthesis of 2-substituted and 3-substituted piperidines through a bromoaminocyclization process. *Chem Commun* **2013**, *49* (39), 4412-4414. DOI: 10.1039/c2cc36578b.
- (26) Resek, J. E. Intramolecular Ene Reaction of a Chiral Bicyclic Lactam. *J Org Chem* **2008**, *73* (24), 9792-9794. DOI: 10.1021/jo801696r.
- (27) Braddock, D. C.; Millan, D. S.; Perez-Fuertes, Y.; Pouwer, R. H.; Sheppard, R. N.; Solanki, S.; White, A. J. P. Bromonium Ion Induced Transannular Oxonium Ion Formation-Fragmentation in Model Obtusallene Systems and Structural Reassignment of Obtusallenes V-VII. *J Org Chem* **2009**, *74* (5), 1835-1841. DOI: 10.1021/jo8026577.
- (28) Guella, G.; Mancinci, I.; Oztunc, A.; Pietra, F. Conformational bias in macrocyclic ethers and observation of high solvolytic reactivity at a masked furfuryl (=2-furylmethyl) C-atom. *Helv Chim Acta* **2000**, *83* (2), 336-348. DOI: 10.1002/(Sici)1522-2675(20000216)83:2<336::Aid-Hlca336>3.0.Co;2-R.
- (29) Uenishi, J.; Fujikura, Y.; Kawai, N. Pd-II-Catalyzed Cascade Reaction with 1,3-Chirality Transfer; Stereoselective Synthesis of Chiral Nonracemic 2,2'-THF-THF Ring Units. *Org Lett* **2011**, *13* (9), 2350-2353. DOI: 10.1021/ol2005984.
- (30) Sun, Z. K.; Winschel, G. A.; Borovika, A.; Nagorny, P. Chiral Phosphoric Acid-Catalyzed Enantioselective and Diastereoselective Spiroketalizations. *J Am Chem Soc* **2012**, *134* (19), 8074-8077. DOI: 10.1021/ja302704m.
- (31) Shimizu, T.; Murakoshi, K.; Yasui, K.; Sodeoka, M. A New Route for the Preparation of Succinates. *Synthesis-Stuttgart* **2008**, (20), 3209-3218. DOI: 10.1055/s-0028-1083140.

- (32) Orsini, F.; Pelizzoni, F. Pd(0)-Mediated Cross-Coupling of Reformatsky Reagents with Vinyl Triflates and Aryl Triflates. *Synthetic Commun* **1987**, *17* (12), 1389-1402. DOI: Doi 10.1080/00397918708057763.
- (33) Sun, W.; Yuan, Y.; Lee, B.; Jun, H. S.; Shin, D.; Seo, S. Y. Short Synthesis of the Antidiabetic Octaketide Ethyl 2-(2,3,4-Trimethoxy-6-octanoylphenyl) acetate. *Synlett* **2018**, *29* (3), 326-329. DOI: 10.1055/s-0036-1592062.
- (34) Wong, B.; Xin, L. H.; Crawford, J. J.; Drobnick, J.; Lee, W.; Zhang, H. M. A chemoselective Reformatsky-Negishi approach to alpha-haloaryl esters. *Tetrahedron* **2014**, *70* (7), 1508-1515. DOI: 10.1016/j.tet.2013.12.053.
- (35) Chou, S. S. P.; Yang, K. S.; Chin, T. H. Synthesis of the Precursors of Pumiliotoxin 251d and Awajanomycin and Related Studies. *Heterocycles* **2014**, *89* (3), 679-691. DOI: 10.3987/Com-14-12930.
- (36) Tunge, J. A.; Mellegaard, S. R. Selective selenocatalytic allylic chlorination. *Org Lett* **2004**, *6* (8), 1205-1207. DOI: 10.1021/ol036525o.
- (37) Vilsmaier, E.; Adam, R.; Tetzlaff, C.; Cronauer, R. Functionalized Chloroenamines in Aminocyclopropane Synthesis .3. Synthesis and Assignment of Configuration of 2 Isomeric Morpholinobicyclo[3.1.0]Hexane Derivatives. *Tetrahedron* **1989**, *45* (12), 3683-3694. DOI: Doi 10.1016/S0040-4020(01)89230-9.
- (38) Mcdonald, R. N.; Davis, G. E. Strained Ring Systems .8. An Alternate Synthesis of 2-Oxy Derivatives of Bicyclo[2.2.0]Hexane and Rearrangement of Endo-Bicyclo[2.2.0]Hex-2-Yl Acetate. *J Org Chem* **1969**, *34* (6), 1916-&. DOI: DOI 10.1021/jo01258a086.
- (39) Mock, W. L. Orbital Symmetry Forbiddenness in a Suprafacial 1,6 Cycloelimination of Sulfur Dioxide. *J Am Chem Soc* **1970**, *92* (12), 3807-&. DOI: DOI 10.1021/ja00715a055.
- (40) Uemura, S.; Onoe, A.; Okazaki, H.; Okano, M.; Ichikawa, K. Chlorination of 1,3-Cyclooctadienes and 1,5-Cyclooctadienes with Various Chlorinating Agents. *B Chem Soc Jpn* **1976**, *49* (5), 1437-1438. DOI: DOI 10.1246/bcsj.49.1437.
- (41) Zhang, Y. A.; Yaw, N.; Snyder, S. A. General Synthetic Approach for the Laurencia Family of Natural Products Empowered by a Potentially Biomimetic Ring Expansion. *J Am Chem Soc* **2019**, *141* (19), 7776-7788. DOI: 10.1021/jacs.9b01088.
- (42) Ishihara, J.; Shimada, Y.; Kanoh, N.; Takasugi, Y.; Fukuzawa, A.; Murai, A. Conversion of prelaureatin into laurallene, a bromo-allene compound, by enzymatic and chemical bromo-etherification reactions. *Tetrahedron* **1997**, *53* (25), 8371-8382. DOI: Doi 10.1016/S0040-4020(97)00542-5.

- (43) Chatupheeraphat, A.; Soorukram, D.; Kuhakarn, C.; Tuchinda, P.; Reutrakul, V.; Pakawatchai, C.; Saithong, S.; Pohmakotr, M. Synthesis of gem-Difluoromethylenated Spiro-gamma-butyrolactones by Employing PhSCF₂Si(CH₃)₃ as a gem-Difluoromethylenating Agent. *Eur J Org Chem* **2013**, *2013* (30), 6844-6858. DOI: 10.1002/ejoc.201300998.
- (44) Wang, Y.; Milkiewicz, K. L.; Kaufman, M. L.; He, L. L.; Landmesser, N. G.; Levy, D. V.; Allwein, S. P.; Christie, M. A.; Olsen, M. A.; Neville, C. J.; et al. Plant Process for the Preparation of Cinchona Alkaloid-Based Thiourea Catalysts. *Org Process Res Dev* **2017**, *21* (3), 408-413. DOI: 10.1021/acs.oprd.7b00049.

**Chapter II: Design and Development of Organic Dyes for Transparent
Luminescent Solar Concentrators (TLSCs)**

II-1 Introduction of Transparent Luminescent Solar Concentrators (TLSCs)

Mitigating the world's growing global demand for energy remains a challenge, but harvesting solar energy is a key part of the solution to this problem. Many systems have been invented and developed with the aim of harvesting this sustainable energy source by converting the sun's solar spectrum into electric power.¹ In the last decade, solar cells have been installed in mass numbers on rural farmlands or building rooftops. Other potential options to absorb the sun's light, still unutilized, are the vast amounts of building surfaces in urban and dense high-rise areas.² Therefore, fabrication of light harvesting devices on window surfaces remains a highly desired target for solar harvesting. Low cost and flexible Transparent Luminescent Solar Concentrators (LSCs) dispersed within glass in the windows have attracted much attention due to their potential to convert a building into an efficient power generating source via solar to current conversion.³⁻⁶

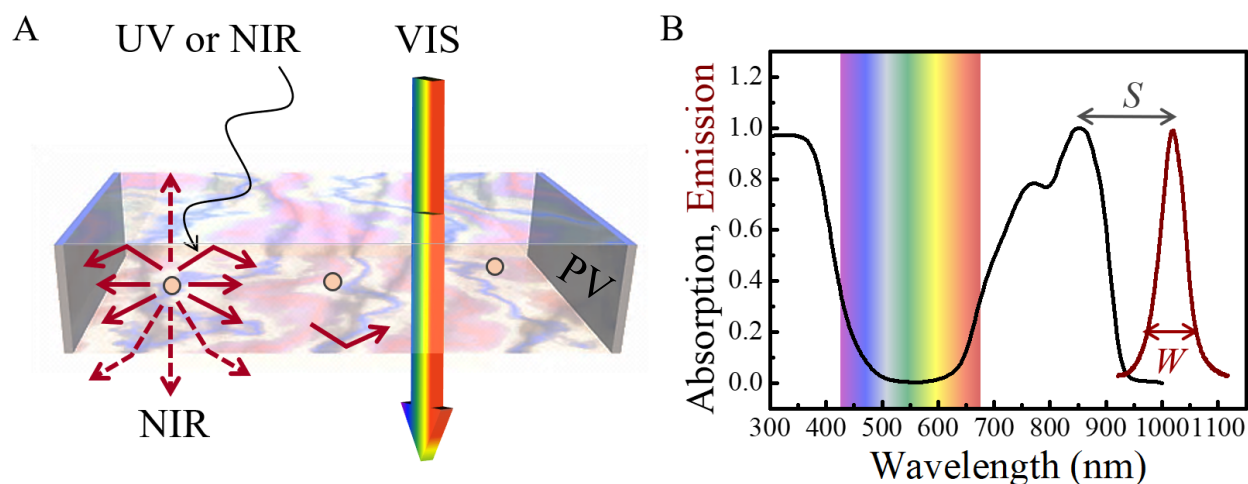


Figure II-1. A. TLSC model in which both UV and NIR light is absorbed while visible light passes through. B. Spectra of chromophore; S stand for Stokes shift, W is the width of the emission peak (Permission to reproduce this figure is kindly provided by Prof. Lunt and Dr. Yang)⁷

Transparent luminescent solar concentrators selectively convert non-visible light, such as UV light and Near-infrared (NIR) light, into electricity while the vast majority of visible light would pass through, which translates to a high level of visible transparency. As such, a vital design parameter is to minimize the chromophore's absorption and emission in the range of 400 nm to 700 nm (visible wavelength). Working principle of TLSC is to employ the chromophoric materials within the window to absorb the UV or/and NIR light, and re-emit the light to the edge of the window (by total internal reflection) that is lined with photovoltaics (PV) (Figure II-1).

This project is a collaboration with professor Richard Lunt's group (Chemical Engineering Department, Michigan State University) which pioneered this work. Our group has previously and currently engineered and synthesized light harvesting organic dyes and studied their application in transparent luminescent solar concentrators.

II-2 Important parameters for investigating TLSC devices

The key parameter to compare the performance of various solar cells is the power conversion efficiency (PCE), which is the ratio of maximum output energy density ($P_{max.out}$) to the sun light's energy input density (P_0). In order to quantify the PCE of TLSC devices, we need to address three important parameters, all of which can be extracted through the corresponding current density (J) - voltage (V) curve. The first is the short-circuit current density (J_{sc}), which defines the current (I_{sc}) value at zero voltage bias ($V = 0$) divided by A , which is the active area of the solar cell ($J_{sc} = I_{sc}/A$). The second is V_{oc} , which is the voltage at open-circuit condition ($I = 0$). The third parameter we need is the fill factor (FF),

this represents the “squareness” of the J - V curve (see Figure II-2A for an example of a J - V curve for two different solar cell).

$$PCE = \frac{P_{max,out}}{P_0} = \frac{V_{OC} \cdot J_{SC} \cdot FF}{P_0} \quad (2.1)$$

The other important parameters for the characterization of solar cells are the external quantum efficiency (EQE_{PV}) and the internal quantum efficiency (IQE_{PV}). The EQE_{PV} is the ratio of the number of photogenerated electrons collected at the solar cell to the number of photons which shine on the device at each wavelength. The IQE_{PV} is the ratio of the number of photogenerated electrons collected at the solar cell to the number of photons which shine on the device and are absorbed at each wavelength.

$$EQE_{PV} = \frac{\text{electrons/sec}}{\text{photons/sec}} \quad (2.2)$$

$$IQE_{PV} = \frac{\text{electrons/sec}}{\text{absorbed photons/sec}} \quad (2.3)$$

The EQE_{PV} is related to IQE_{PV} according to below equation:

$$EQE_{PV}(\lambda) = \eta_{Abs}(\lambda) \cdot IQE_{PV}(\lambda) \quad (2.4)$$

which η_{Abs} is the photovoltaic absorption efficiency at each wavelength. (see Figure II-2B for EQE_{PV} spectra of a silicon and a Gallium Arsenide (GaAs) photovoltaic cells) .

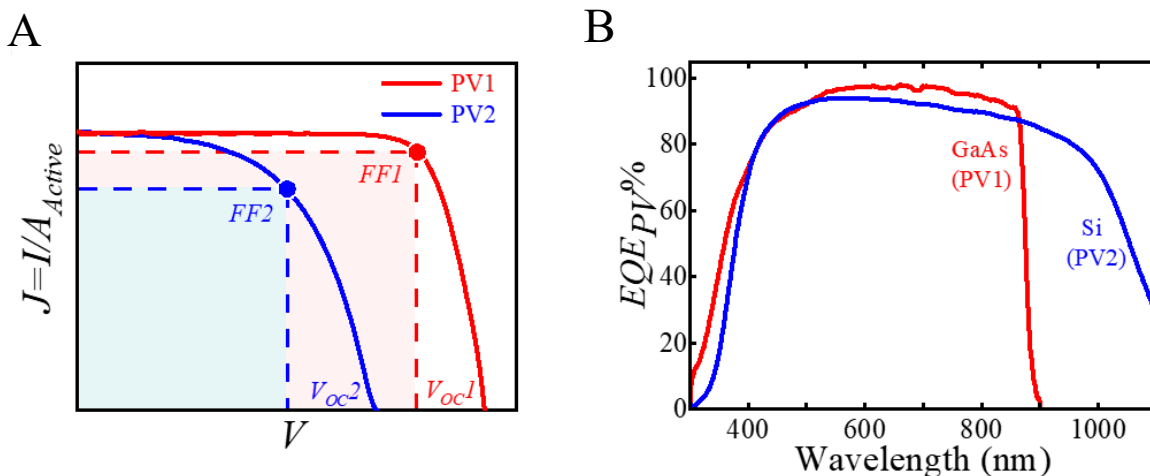


Figure II-2 A. Examples of J - V curves for two different solar cells. B. External quantum efficiency spectra of a silicon and GaAs PV cells (Permission to reproduce this figure is kindly provided by Prof. Lunt and Dr. Yang)⁷

The main parameter utilized to study the transparency performance of a solar cell is coined as the average visible transmission (AVT) which defines the percentage of visible light that passes through the device. The combination of PCE and AVT which together is called Light Utilization Efficiency ($LUE = PCE \times AVT$), defines the last factor for evaluation of transparent photovoltaic devices.⁷

II-3 Development of organic dyes for use with TLSC devices

II-3-1 General strategy for tuning the Stokes shift of cyanine dyes

In a TLSC, the organic chromophores should absorb sun light selectively in UV or NIR region, while maintaining minimal visible transmission, in order to generate a transparent solar concentrator. Lunt's group has successfully studied highly efficient nanoclusters for harvesting light in the UV region.^{8, 9} In this chapter we mainly focus on the NIR portion of the spectrum. We explored various NIR fluorophores after which we turned to heptamethine cyanine dyes. These dyes have the potential to be excellent

candidates for harvesting the NIR light, due to their high quantum yield (QY), brightness and their narrow emission profile in a region that is devoid of many spectral interferences.¹⁰⁻¹² However, most cyanine dyes exhibit a small Stokes shift, which negatively impacts their application in optical imaging due to significant background, light scattering and internal absorbance interferences. We also found that there is a direct relationship between the dye's Stokes shift and the corresponding TLSC device's efficiency. As illustrated in Figure II-3, the calculated optical efficiency as a function of LSC device length has a direct correlation with the Stokes shift of the organic dyes and as such, implementation of materials possessing a small Stokes shift would lead to lower system efficiency.^{7,13, 14} This effect of Stokes shift on the optical efficiency is higher with increasing the length of the device (Figure II-3).

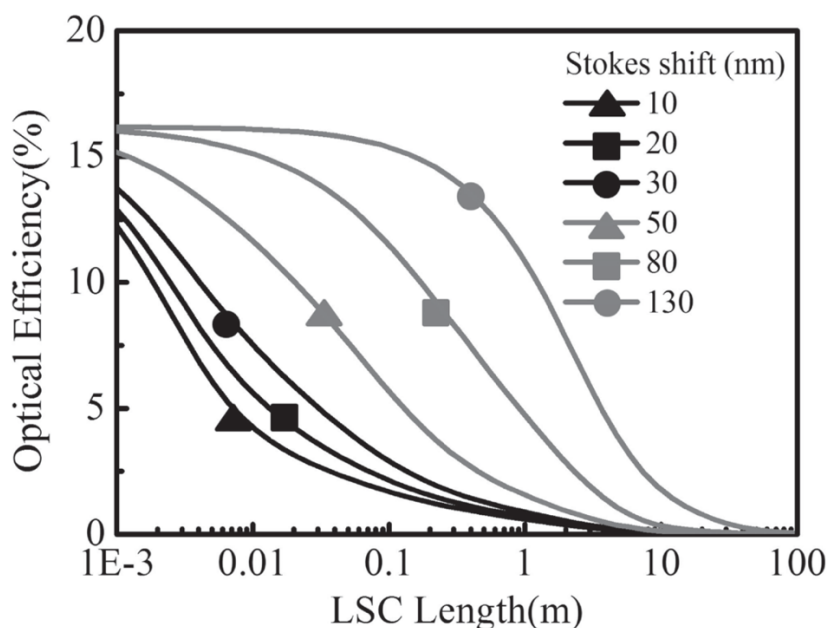


Figure II-3. LSC system as a function of calculated Stokes shift (Permission to reproduce this figure is kindly provided by Prof. Lunt and Dr. Yang)⁷

The primary factor in efficiency loss, stems from the self-quenching process of small Stokes shift organic dyes installed on the device. With the maximum absorption and emission overlap (see Figure II-4a), the emission of one dye is reabsorbed by another proximal dye which hinders the photon output to PV material located in the window's edge. Increasing the Stokes shift would decrease this spectral overlap region resulting in diminished self-quenching (Figure II-4b). With this knowledge in hand, we aim to develop a general strategy to tune the Stokes shift of heptamethine cyanine dyes.

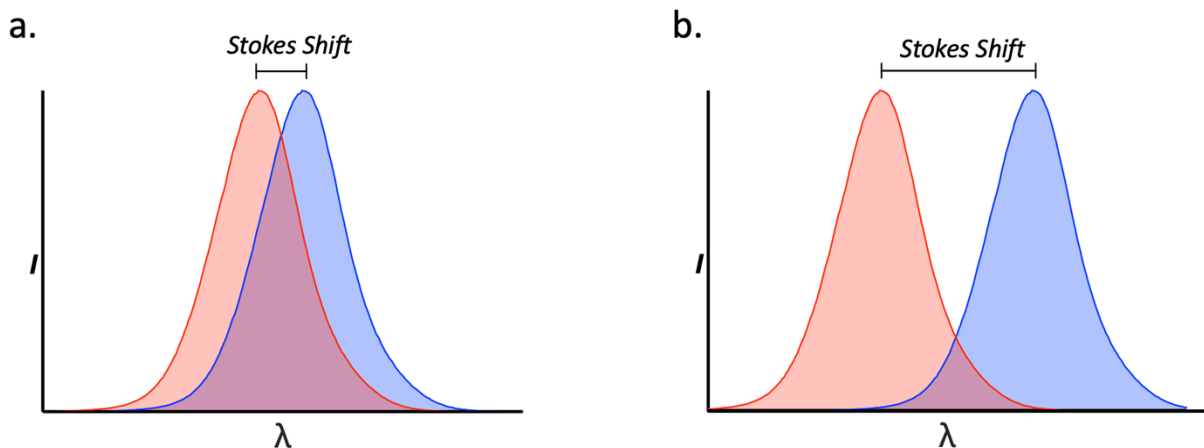
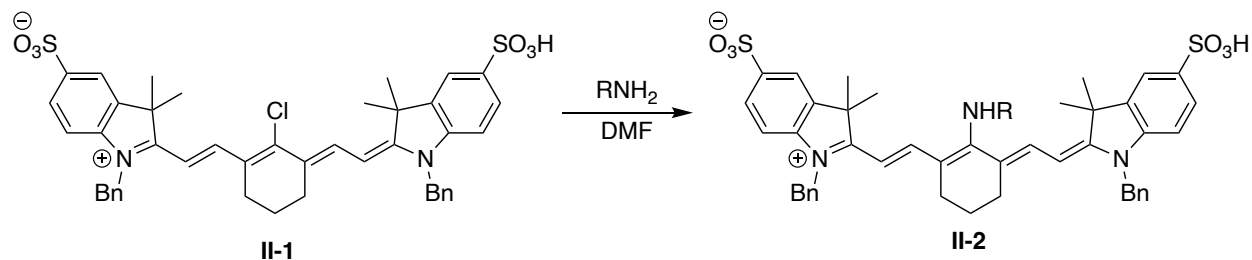
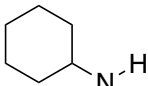
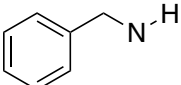


Figure II-4. Correlation of Stokes shift and self-quenching

In 2005, the Peng group reported the first large Stokes shift heptamethine cyanines.¹⁵ Nucleophilic addition/elimination of the meso chloro group at the C4 position of Cy7 (**II-1**) by simple primary amines resulted in a massive Stokes shift. As is shown in Table II-1, the cyclohexanemethylamine **II-2** and benzyl amine **II-3** yield a Stokes shift of 150 nm and 140 nm, respectively. With limited mechanistic understanding for this observation it was suggested that a change of the amine's pyramidal geometry in the excited state leads to the observed increase in Stokes shift.

Table II-1. Strategy to achieve large Stokes shift cyanine dyes

Dye	NHR	λ_{\max} (nm) ^a	λ_{em} (nm) ^a	Stokes Shift (nm)	Φ (%) ^a
II-1	---	783	803	20	17
II-2		602	757	155	47
II-3		617	757	140	38

[a] Absorption, emission and absolute quantum yield data were obtained in methanol.

Other seminal work by the Maury group studied the effect of various substitutions at the C4 position of multiple polymethine dyes, leading to the development of a new bis-dipole structure for cyanine dyes.¹⁶ As shown in Figure II-5, the absorption properties of a cyanine would be affected by electronic character of its C4-substituent. It was observed that groups such as halogens or thioethers exhibit absorption profiles similar to general cyanines, while strong electron donating groups like ketone (hydroxyl) or imines (amines) could break the cyanine's conjugation with its heterocyclic ends, blue shifting the absorption by generation of a bis-dipole type structure. However, the impact of these substituents on the Stokes shift was not investigated in this work.

affect the spectroscopic characteristics, and in particular, the Stokes shift. In doing so, we have identified a simple strategy to tune the Stokes shift of heptamethine cyanine dyes by tuning the relative energies of conformers of the dye differentiated by rotation about the central amine group.

A conventional heptamethine cyanine dye **II-6** was chosen to investigate the effects of different nitrogen substituents on the observed Stokes shift. The general synthesis of different heptamethine cyanine backbones is shown in Figure II-6.¹⁷

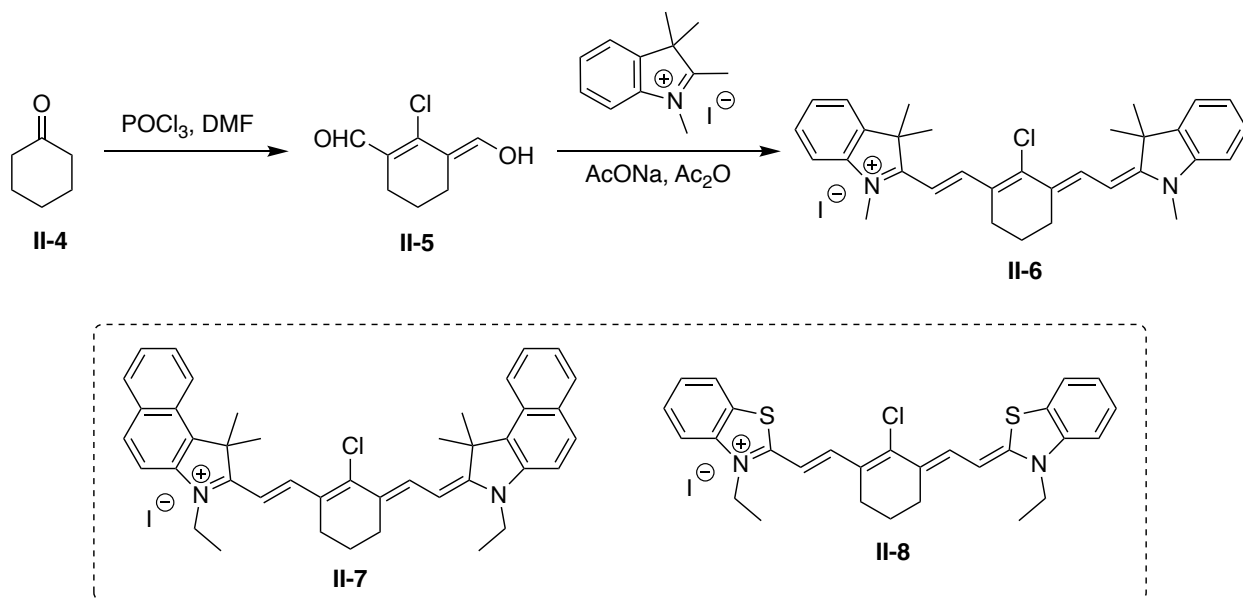


Figure II-6. Synthesis of heptamethine cyanine dyes

Two categories of cyanine dyes (substituted with acyclic and cyclic amines) were synthesized via addition–elimination, promoted by diisopropylethylamine (DIPEA) and excess amine in acetonitrile (Figure II-7). Acyclic amine substituted cyanine dyes include dimethyl amino (**II-10**), methyl ethyl amino (**II-11**) and diethyl amino groups (**II-12**), whereas heterocyclic groups include methyl aziridine (**II-13**), azetidine (**II-14**), pyrrolidine (**II-15**) and piperidine (**II-16**).

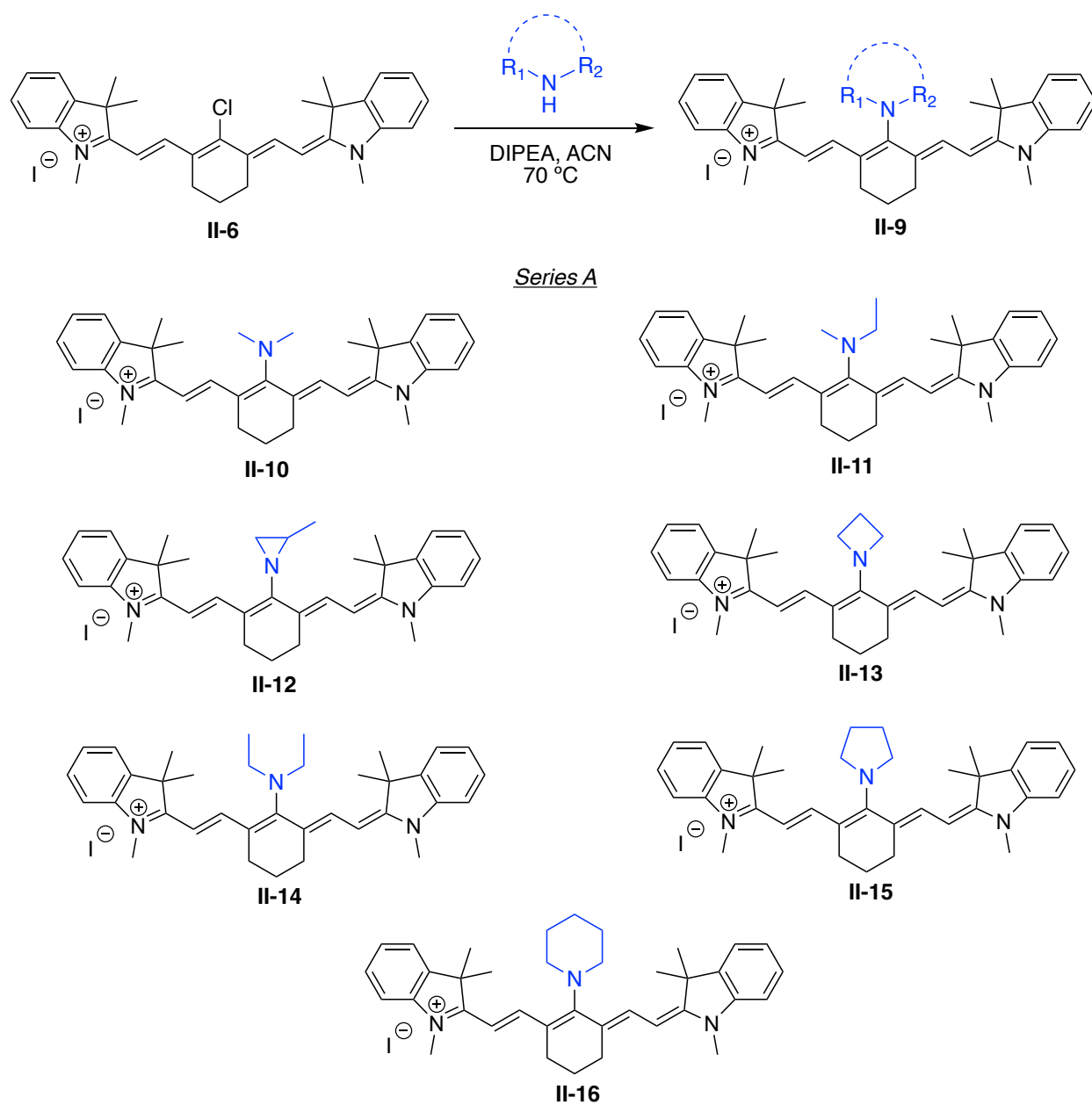


Figure II-7. Synthesis of first series of amine substituted heptamethine cyanine dyes

Attempts to synthesize the seven membered azepane substituted cyanine were not fruitful, as the product could not be isolated in its pure form. Table II-2 summarizes spectroscopic properties for dyes **II-9** to **II-16**.

Table II-2. Spectroscopic data of amine substituted heptamethine cyanines

Dye	NR ₂	λ_{\max} (nm) ^a	λ_{em} (nm) ^a	Stokes Shift (nm)	FWHM (nm)	Φ (%) ^b
II-6	-	785	806	21	-	15
II-10		664	777	113	117	28
II-11		684	778	94	110	29
II-12		742	766	24	94	25
II-13		615	704	89	80	26
II-14		699	778	79	98	31
II-15		604	784	180	85	33
II-16		668	785	117	133	23

FWHM, full width at half maximum; λ_{\max} , absorption maximum; λ_{em} , emission maximum; ϕ , quantum yield. [a] Absorptions and emissions were recorded in DCM at rt; [b] Absolute quantum yields were measured by Hamamatsu Quantaaurus fluorimeter in DCM at rt.

Cyanine dye **II-6** exhibits an absorption maximum in the NIR region ($\lambda_{\max} = 785$ nm), emission maximum ($\lambda_{\text{em}} = 806$ nm), with a small Stokes shift (21 nm) in DCM. To our surprise, while dyes **II-10** and **II-12** share a similar structure, they are quite different spectroscopically (Figure II-8 top). Dye **II-10** absorbs at 664 nm and emits at 777 nm in DCM, leading to a 113 nm Stokes shift. In contrast, aziridinyl substrate dye **II-12** shows a 24 nm Stokes shift. Interestingly, the quantum yield is not improved by using aziridinyl or azetidinyl rings (25% for dye **II-12** and 26% for dye **II-3**).

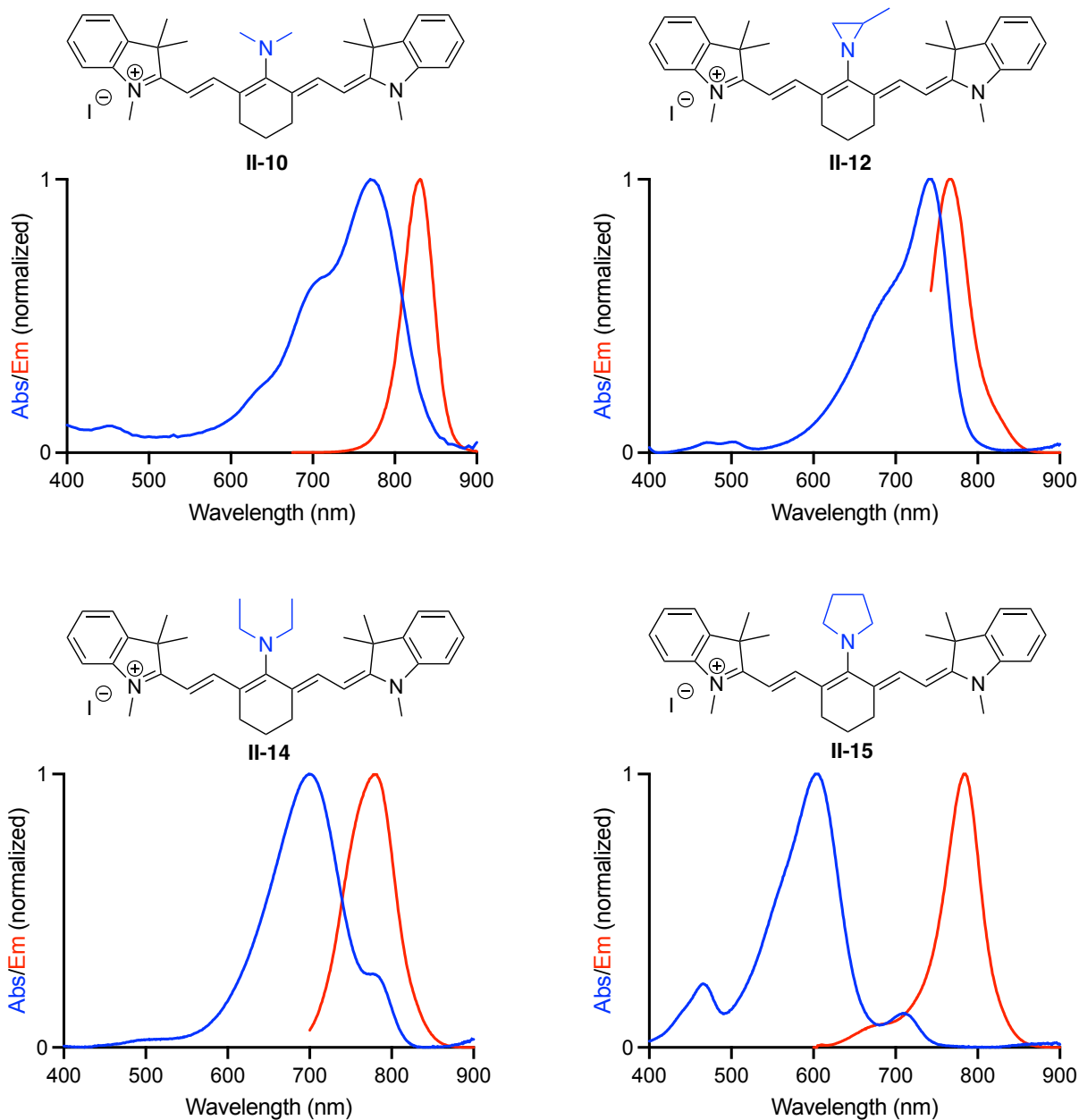


Figure II-8. Normalized absorption and fluorescence emission spectra (measured in DCM) for dyes **II-10** (top left) and **II-12** (top right), and dyes **II-14** (bottom left) and **II-15** (bottom right)

In contrast, the opposite trend is observed for dyes **II-14** and **II-15** (Figure II-8 bottom). Diethylamine substrate **II-14** yields a moderate 79 nm Stokes shift (absorption at 699 nm and emission at 778 nm), while the cyclic pyrrolidine substituted cyanine **7**

leads to an even larger Stokes shift (180 nm). Notably, the quantum yields are similar (31% for dye **II-14** and 33% for dye **II-15**). These observations indicate that the Stokes shift of cyanine dyes can be easily tuned by varying the amine substituents ranging from 24 nm up to 180 nm. Based on the collective data obtained, some trends can be observed amongst the series. Cyclic and acyclic amines appear to behave differently; the smaller acyclic amines lead to a larger Stokes shifts, while smaller cyclic amines yield a smaller Stokes shift. Another notable observation is that most of these dyes (except dye **II-13**) share similar emission profiles (around 770 nm). The change in Stokes shift is dictated mainly by the blueshift of the absorption. Thus, we speculated that these dyes may have different ground state geometries. It is notable that the azetidine substituted dye **II-13** possesses strong solvatochromic properties in various solvents. The photophysical properties of dye **II-13** in different solvents are reported in Table II-3.

Table II-3. Spectroscopic data of dye **II-13** in different solvents

Solvent	λ_{\max} (nm) ^a	λ_{em} (nm) ^a	Stokes Shift (nm)
DCM	615	704	89
Methanol	589	701	112
Acetone	585	704	119
Toluene	574	679	105

λ_{\max} , absorption maximum; λ_{em} , emission maximum.

To examine the generality of the trend described above, similar amine substitutions were made with other series of cyanine dyes. The second series that was synthesized contained indocyanine green (ICG) as the head group (Figure II-9).

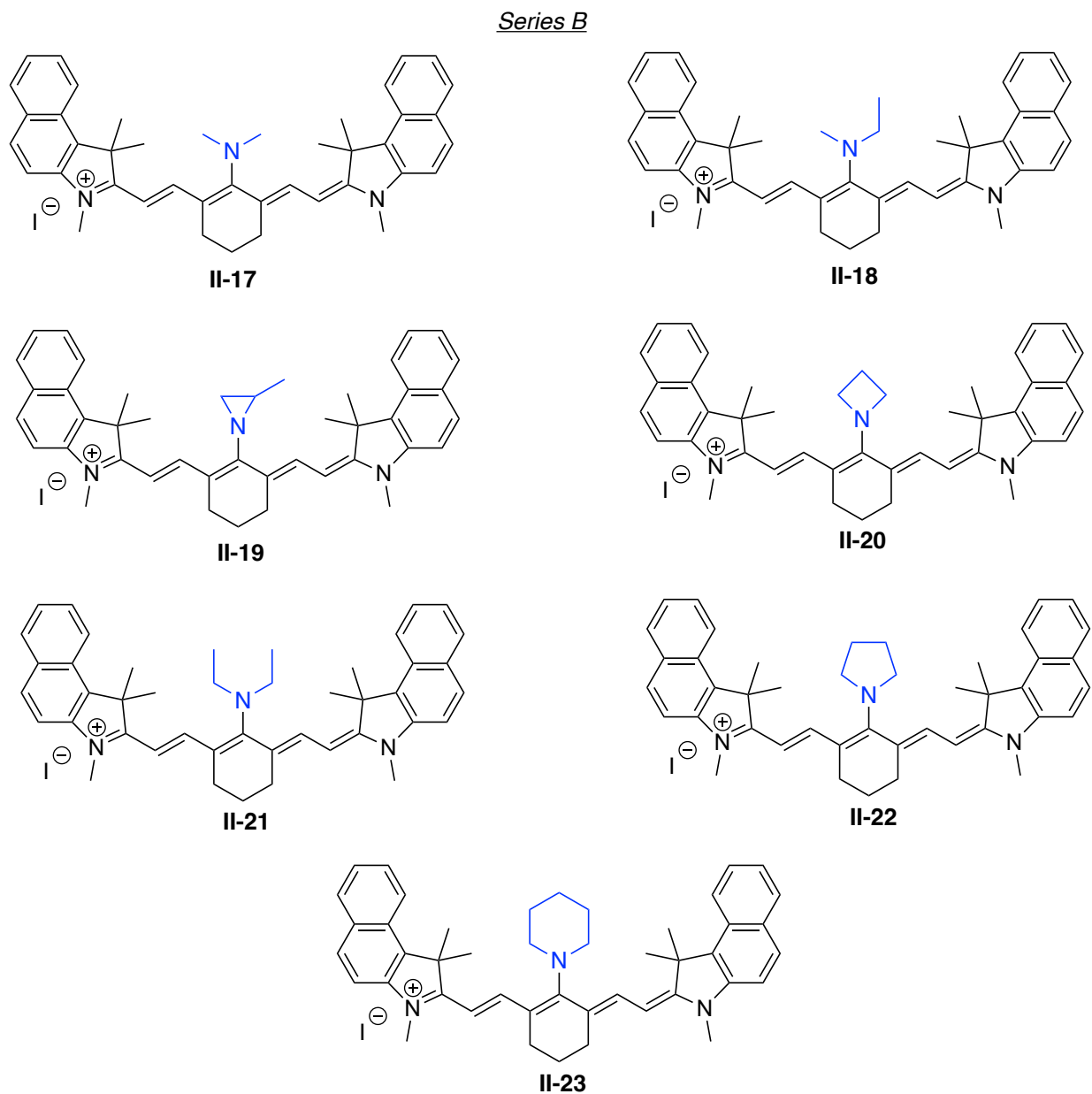


Figure II-9. Structure of second series of amine substituted heptamethine cyanine dyes

Photophysical characteristics of these dyes are listed in Table II-4. In comparison to cyanine dyes **II-10** – **II-16** in Table II-3, ICG type dyes **II-17** – **II-23** possess a larger

conjugated aryl ring, and are red shifted by around 40 nm, while maintaining the same Stokes shift trend. The largest Stokes shift was seen with dye **II-22** containing the pyrrolidine ring substitution (187 nm), while the smallest Stokes shift was the aziridinyl functionalized dye **II-19** (56 nm).

Table II-4. Spectroscopic data of amine substituted ICG based cyanine dyes

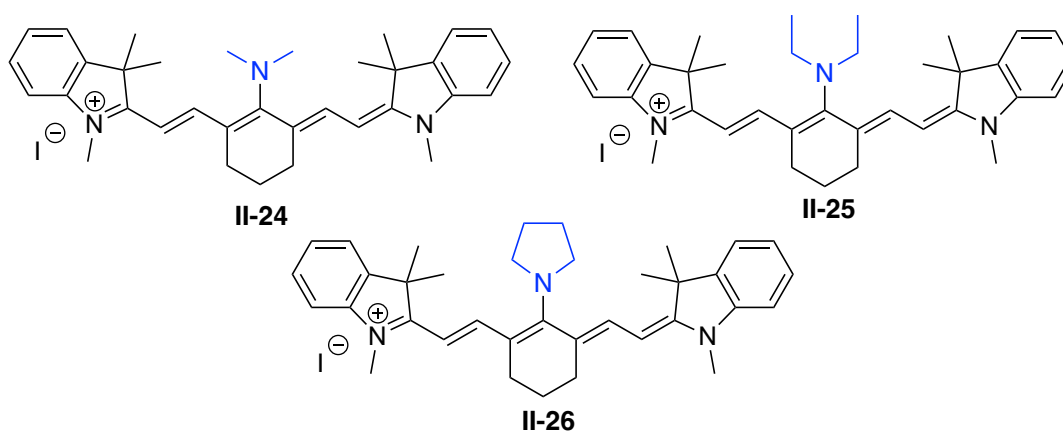
Dye	NR ₂	λ_{\max} (nm) ^a	λ_{em} (nm) ^a	Stokes Shift (nm)	FWHM (nm)	ϕ (%) ^b
II-17		705	818	113	124	24
II-18		724	816	92	116	26
II-19		746	802	56	128	24
II-20		649	737	88	84	30
II-21		739	819	80	107	24
II-22		636	823	187	85	25
II-23		708	824	116	143	21

FWHM, full width at half maximum; λ_{\max} , absorption maximum; λ_{em} , emission maximum; ϕ , quantum yield. [a] Absorptions and emissions were recorded in DCM at rt; [b] Absolute quantum yields were measured by Hamamatsu Quantaurus fluorimeter in DCM at rt.

Most of the dyes listed in Table II-4 have a slightly lower quantum yield than their analogs in Table II-3, with the azetidino substituted dye **II-20** having a slightly higher quantum yield (30%). In continuation of this study, we also synthesized benzothiazole based cyanine dyes and chose 3 representative substituents: dimethyl, diethyl, and pyrrolidinyl groups to examine their photophysical properties (Table II-5). Gratifyingly, the

same trend was also observed in these dyes featuring a large Stokes shift with pyrrolidinyl (171 nm for dye **II-26**) and a moderate Stokes shift with diethyl (69 nm for dye **II-25**).

Table II-5. Structure and spectroscopic data of amine substituted benzothiazole based cyanines



Dye	NR ₂	λ_{\max} (nm) ^a	λ_{em} (nm) ^a	Stokes Shift (nm)	FWHM (nm)	Φ (%) ^b
II-24		703	801	98	123	26
II-25		733	802	69	129	27
II-26		636	807	171	105	35

FWHM, full width at half maximum; λ_{\max} , absorption maximum; λ_{em} , emission maximum; Φ , quantum yield. [a] Absorptions and emissions were recorded in DCM at rt; [b] Absolute quantum yields were measured by Hamamatsu Quantaaurus fluorimeter in DCM at rt.

To investigate the mechanism underlying the observed change in the Stokes shift we carried a computational study of dyes **II-10** – **II-16**. Calculating the spectroscopic properties of cyanine dyes remains challenging. For example, commonly used time-dependent density functional theory (TD-DFT) functionals cannot provide accurate transition energies for cyanine dyes, overestimating excitation energies by 0.5 – 1.0 eV.

Nonetheless, TD-DFT is established to provide an accurate description of the shape of the excited potential energy surfaces of these molecules.^{18, 19} Thus, one can expect TD-DFT to provide an accurate description of the Stokes shift and the associated displacement coordinate, with the caveat that it does not provide quantitative predictions of the excitations energies themselves.

Before turning our attention to the excited state, we examined the ground state conformer. Geometry optimizations at the CAM-B3LYP/6-31G* level²⁰ (performed with the TeraChem software package^{21, 22} show the *s-trans* conformer having a lower energy than the *s-cis* structure (differentiate by flipping of the indolium ring) for all dyes in the series **II-9** to **II-16**. Interestingly, all seven of the amine-substituted dyes **II-10** to **II-16** have two distinct *s-trans* ground state minimum structures that differ in the rotation angle of the amine group (Figure II-10). In one minimum, the amine is rotated to be roughly in plane with the heptamethine chain, which we refer to as the parallel conformer. In the other structure, referred to as the perpendicular conformer, the amine is rotated approximately 90° with respect to the heptamethine chain. Structures for all optimized systems can be found in experimental section.

The existence of two conformers is closely related to the concept elaborated upon in an elegant work by Guennic, Andraud, Maury and coworkers.¹⁶ Their conformational approach was used to determine the spectroscopic properties of substituted cyanine dyes: the distinction between bis-dipolar and cyanine-like electronic structures (Figure II-10). A bis-dipolar system is characterized by alternating double and single bond character, which would occur when an amine nitrogen conjugates to the π system of the

chain (Figure II-10, left). In a cyanine-like system, bond orders of all carbon-carbon bonds in the heptamethine chain are roughly 1.5 (Figure II-10, right). The excitation energy, or extent of absorption blue shifting, tends to increase with increasing bis-dipolar character.

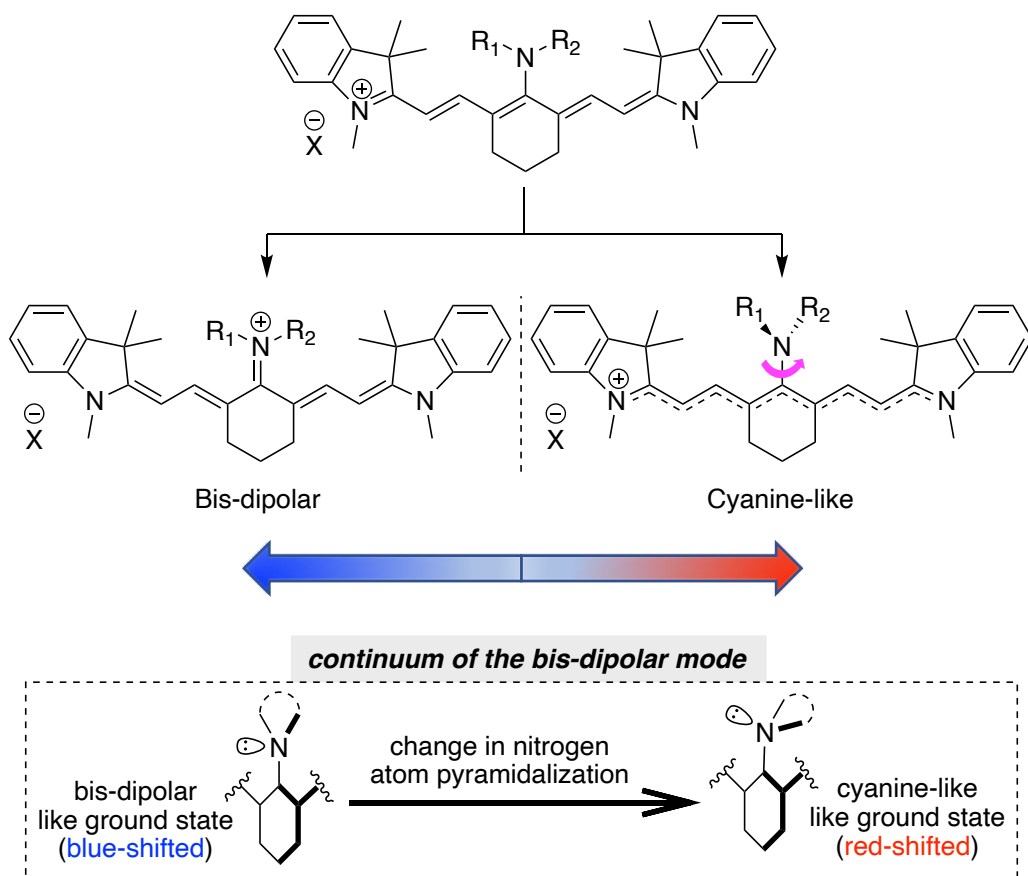


Figure II-10. Generalized cyanine-like and bis-dipolar structures of cyanine dyes

It is important to note that all perpendicular structures will exhibit cyanine-like character, because twisting about the amine bond breaks conjugation with the chain. Parallel structures, however, may exhibit a continuum of electronic character, from more bis-dipolar to more cyanine-like character, depending on the degree of π electron donation from the amine to the chain (see dashed box, Figure II-10).

Interestingly, several of the amine-substituted dyes (**II-10**, **II-11**, **II-14** and **II-16**) favor a perpendicular conformation, while the minority (**II-12** and **II-13**) favor a parallel

conformation. Only those dyes with relatively narrow amine substituents (**II-12** and **II-13**) favor the parallel conformation. Analysis of the C–C distance between the carbon atoms in the amine substituent and those in the polymethine chain suggests that steric interaction between these groups determines the ground state conformation. The parallel conformers of **II-10**, **II-11**, **II-14** and **II-16** all have C–C contacts between the amine substituent and the polymethine chain in the range 2.91–2.93 Å. These close contacts suggest that the parallel conformers of these dyes are sterically destabilized. On the other hand, the parallel conformers of **II-12** and **II-13** have no contacts shorter than 3.00 Å, and therefore are not sterically destabilized. For **II-15**, the calculations predict the difference in energy to be <1.5 kcal/mol, which is effectively equal, given the margin of error for this DFT approach. In this case, the closest C–C contact between the amine substituent and the polymethine chain is 2.94 Å, which is between the two extremes. For molecules with a clear lowest energy conformer (**II-10** – **II-14** and **II-16**), computing a Stokes shift is more straightforward. In each of these cases, two excited state minima (parallel and perpendicular) were optimized at the TD-CAM-B3LYP/6-31G* level, and in all cases the energetically favored conformer was the same as in the ground state.

Figure II-11 is a scatter plot with the computed excitation energies on the x-axis and the experimentally measured spectral maxima on the y-axis. Blue marks indicate the experimental absorption maxima as a function of the computed vertical excitation energies from the ground state minimum structure. Red marks indicate the experimental emission maxima as a function of the computed vertical excitation energy at the excited state minimum structure.

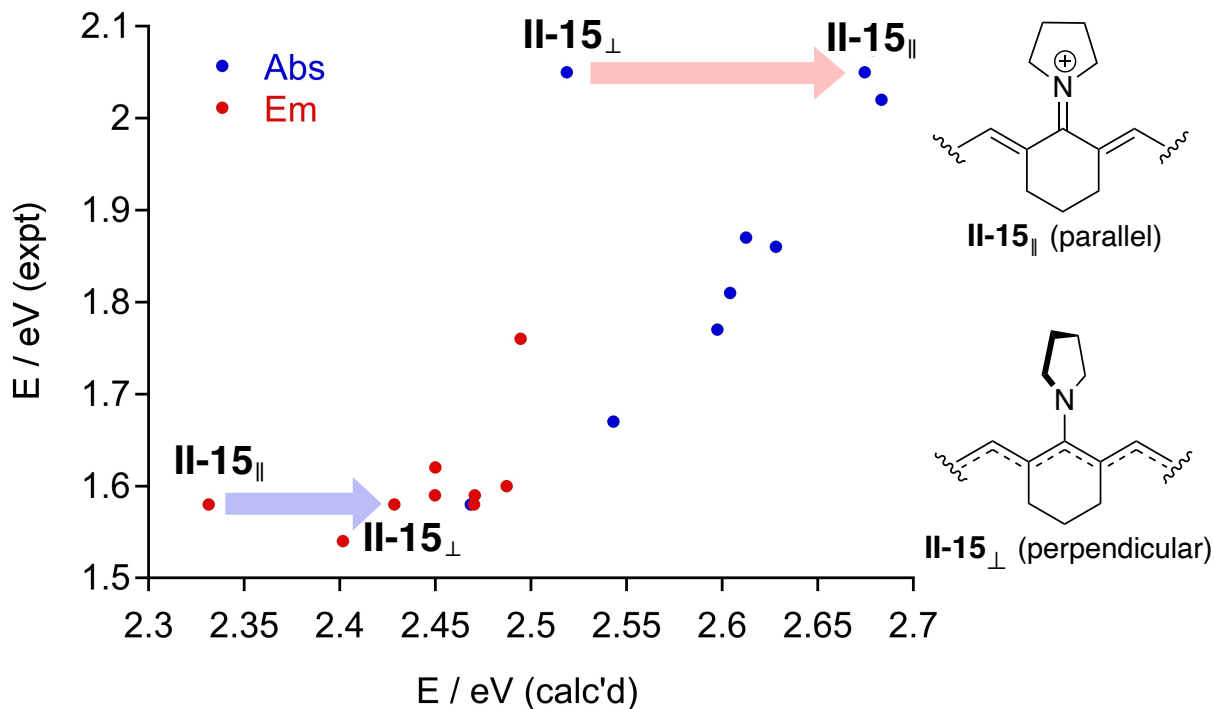


Figure II-11. Scatter plot of the experimental spectral energy maxima as a function of the DFT-computed theoretical excitation energies. Absorption and emission energies are shown by blue and red dots, respectively. The lowest energy conformer is chosen for **II-9 – II-14** and **II-16**, while for **II-15**, both the parallel (**II-15_{||}**) and perpendicular (**II-15_⊥**) conformers are shown

Though DFT consistently overestimates the experimental energies by 0.6 – 0.7 eV, a compelling pseudo linear relationship between experiment and theory is observed for molecules **II-10 – II-12**, **II-14** and **II-16**. This suggests that the basic physics underlying the Stokes shift is well described. As will be discussed below, molecules **II-13** and **II-15** do not follow the trends due to other factors. As shown in Figure II-12, the experimental excitation energies correlate strongly with displacement along a bond length alternation coordinate (BLA) as determined from the calculated structures, supporting the

assignment of variances in the excitation energies to a shift between cyanine-like and bis-dipolar electronic character.

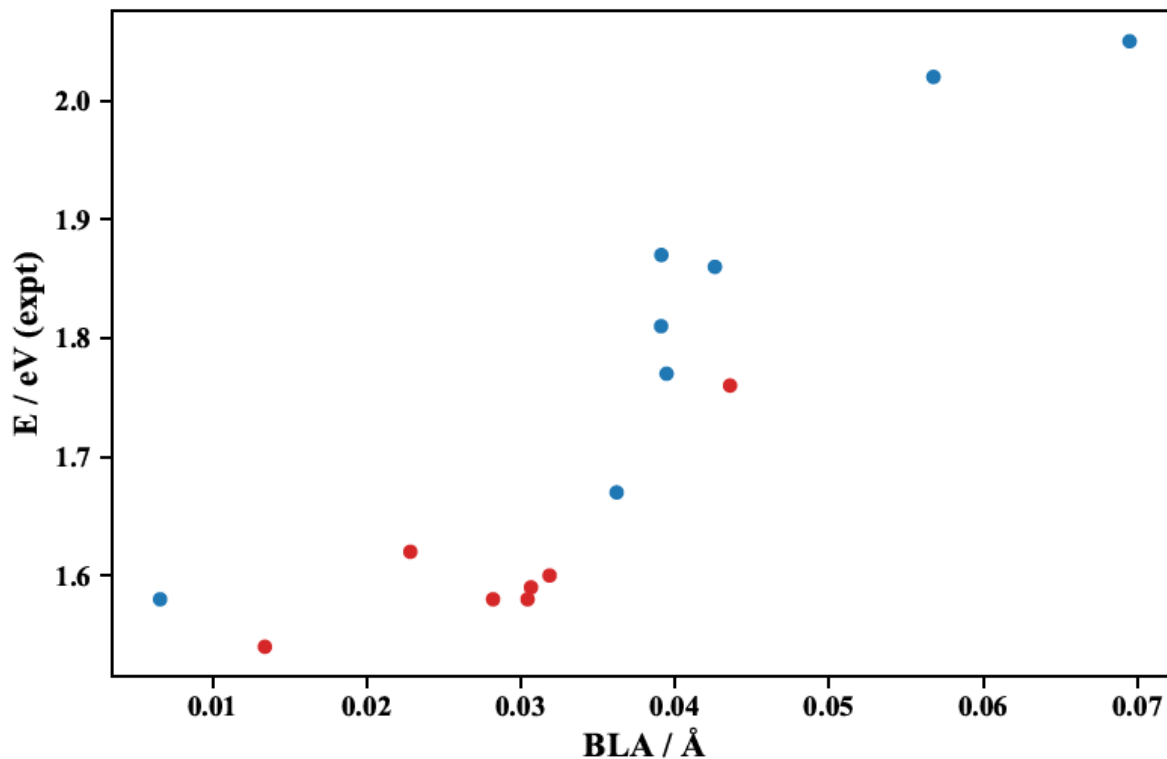


Figure II-12. Scatter plot of the experimental spectral energy maxima as a function of the DFT-optimized bond length alternation coordinate (in angstrom). Absorption and emission energies are shown by blue and red dots, respectively

Applying the same analysis to **II-15**, the molecule with the largest Stokes shift does not result in good agreement with experimental data (see Figure II-8). The fit is poor regardless of whether the perpendicular (**II-15_⊥**) or parallel (**II-15_∥**) conformer is chosen. In the parallel case, the absorption point falls on the line, but the emission point does not. On the other hand, in the perpendicular case, the emission point falls on the line, but the absorption point does not. This suggests the intriguing possibility that the molecule converts from the parallel to the perpendicular conformation upon excitation. A shift from

a strongly bis-dipolar character in the ground state to more cyanine-like character in the excited state is indicated by a reduction in BLA from 0.089 Å (the largest of all dyes studied here) to 0.034 Å. Such a reorganization mechanism has previously been recognized, but here we demonstrate the delicate energy balance that determines whether such rotation occurs or not.^{16, 23}

As noted above, all perpendicular structures exhibit cyanine-like electronic structure. This includes both ground and excited states structures for **II-10**, **II-11**, **II-14** and **II-16** as well as the excited state structure for **II-15**. To determine the nature of the electronic structure of the parallel structures (both ground and excited states structures of **II-12** and **II-13**, and the ground state structure of **II-15**), we must consider additional coordinates. Table II-6 presents the computed BLA displacement and pyramidalization angle about the amine nitrogen atom of these five structures (A Table containing these parameters for all structures can be found in the experimental section, along with explicit definitions of the BLA and pyramidalization angle coordinates). The computed ground state pyramidalization angles increase as the amine ring become more constrained, with dyes **II-15**, **II-13**, and **II-12** having angles of 2.1°, 7.2°, and 43.4°, respectively. This change in hybridization from a nearly planar sp² conformation in **II-15** to a more sp³ conformation in **II-12** results in decreased coupling of the amine lone pair to the π system of the heptamethine chain (see dashed box, Figure II-10). The reduction in the bis-dipolar character is evidenced by a decrease in the computed BLA (respectively 0.069, 0.057, and 0.036 Å) and increasing experimental λ_{max} (respectively 604, 615, and 742 nm). A similar trend is seen in the excited state structures, with **II-13** being the dye with more bis-

dipolar character upon excitation (BLA of 0.044 Å) and a correspondingly high emission energy ($\lambda_{em} = 704$ nm).

Table II-6. Important geometric parameters that determine the electronic character (bis-dipolar vs. cyanine-like) of the five structures in the parallel conformation^a

Dye	NR ₂	State ^b	BLA (Å)	Pyr. Ang. (°)
II-12		GS	0.036	43.3
		ES	0.023	49.4
II-13		GS	0.057	7.2
		ES	0.044	15.9
II-15		GS ^c	0.069	2.1

BLA, bond length alternation; Pyr. Ang., pyramidalization angle. [a] Geometric parameters are computed at the TD-CAM-B3LYP/6-31G* level. [b] Ground and excited state structures are abbreviated GS and ES, respectively. [c] Only the GS structure is presented for **II-15**, because the ES minimum energy structure has a perpendicular conformation.

With the latter experimental and computational results, a physical description of the trends observed in Table II-2 can be summarized as follows. Dyes with small amine substitutions orient such that the nitrogen atom lone pair may participate in conjugation (bis-dipolar), thus leading to the observed blue-shift in absorption. To clarify, the meaning of “size” in this context, it is the width of the substituent, not necessarily the smallest overall moiety. Therefore, the width of the pyrrolidine substituent is less than dimethylamine (dye **II-15** vs. **II-10**). As the lateral size of the substituent increases, the degree of blue-shift is reduced as the bis-dipolar orientation is more difficult to achieve. The observed trend in Stokes shift (**II-16** > **II-10** > **II-11** > **II-14**) follows the size trend with

the anticipated increasing difficulty in adopting the necessary orientation to have the nitrogen atom lone pair in conjugation with the polyene.

Dyes **II-12** and **II-13** (as well as the analogous **II-19** and **II-20**), however, defy the latter description; though they are both smaller than **II-15**, they do not have higher-energy absorption. Aziridine nitrogen atom's donating ability to form the bis-dipolar electronic structure would require it to adopt the more strained sp^2 hybridization, which is energetically disfavored.²⁴ Thus, dye **II-12** has the lowest Stokes shift as it exists in a more cyanine-like conformation in both the ground and excited state, even though it adopts the 'bis-dipolar' state by rotation about the C–N bond. Based on the absorption and emission spectra of dye **II-13** (both blue-shifted), the azetidone substituent present a unique case. It is small, and thus can adopt the bis-dipolar conformation, and in contrast to the aziridine, rehybridization of its nitrogen atom is not as energetically costly. In fact, iminium formation of azetidines is well documented.²⁵ Yet, it resists conformational change to the structure that favors cyanine-like character in the excited state, presumably because rehybridization is costlier in a small ring, and therefore emits from the bis-dipolar conformation. Dye **II-15** finds itself with the correct balance of size, and conformational flexibility to easily traverse from a more bis-dipolar conformer to a more cyanine-like conformations upon excitation, leading to the observed large Stokes shift.

In summary, we demonstrate a simple strategy to selectively engineer Stokes shifts for cyanine dyes, important in biomedical engineering and energy capture.²⁶ Stokes shifts of different cyanine dyes can be easily tuned via nitrogen substituents (from 24 nm up to 180 nm). Rotation of the amine substituent upon excitation is responsible for the

largest Stokes shifts, and an enhanced Stokes shift is observed when the dye may convert from the bis-dipolar form to the cyanine-like form upon excitation. Some of these dyes applied on TLSC devices demonstrated good results. The large Stokes shift cyanine candidate showed 0.6% *PCE* with excellent visible transparency >80%.¹⁴

II-3-2 Broad absorbing NIR fluorophores for TLCS devices

The features of the desired fluorophores for TLCS device are: NIR absorption wavelength, high quantum yield, large Stokes shift and broad absorption profile. In continuation of our efforts to improve the power conversion efficiency of TLSCs, we explored new candidates fitting the criteria of the abovementioned properties. The synthesized cyanine dyes demonstrated good results on the device, since they absorb in NIR with large Stokes shift and high quantum yield. In a new class of dyes, we look for NIR fluorophores that in addition to the high quantum yield and large Stokes shift, have a broad absorption band. As shown in Figure II-13, broad absorption would increase the probability of absorbing more photons, which results in higher system efficiency.

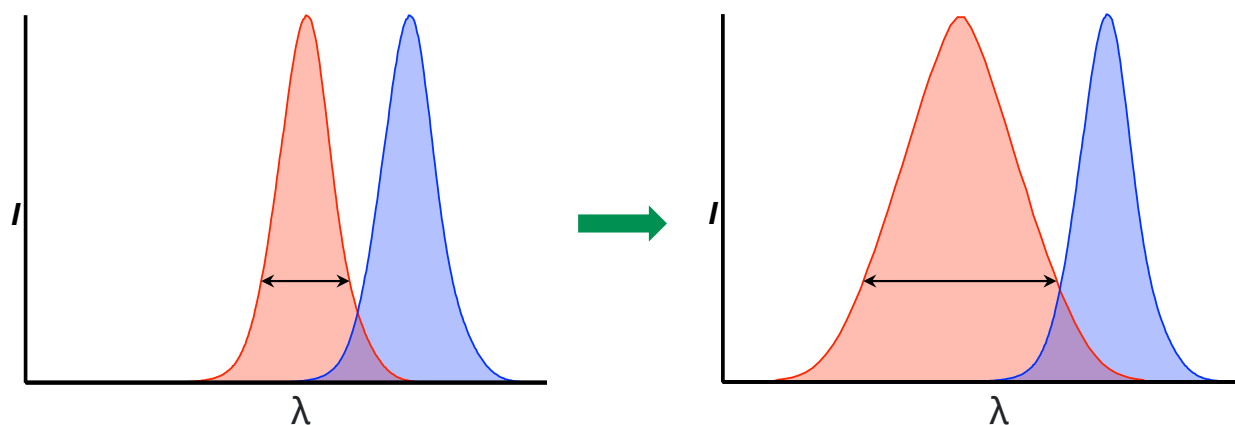


Figure II-13. Broad absorbing spectra leads to harvesting higher photon numbers

During our investigation we found that the acceptor–donor–acceptor (A–D–A) small molecules that are used widely in organic photovoltaic solar cells, have broad absorption spectra. The **DRCN7T** compound shown in Figure II-14, is an ideal example reported by Chen and co-workers.²⁷ This small molecule with oligothiophene-like backbone and two terminal acceptors, shows broad absorption spectra in solution and film (fluorescent properties were not reported in this work). These dyes usually absorb in the visible region, which can be simply tuned by putting electron donating groups, such as alkoxy, on the thiophene rings and also replacing the terminal groups with stronger molecular acceptors. More recent example of this A–D–A dyes is **CO₈DFIC** (also referred to as O6T-4F, Figure II-14), which has been developed as a nonfullerene acceptor in organic photovoltaics with unprecedented performance.^{28, 29} Alkoxy electron donating groups on the thieno[3,2-*b*]thiophene rings of **CO₈DFIC** along with the strong **DFIC** acceptors led to absorption in the NIR region. There are two important factors in the design of this dye that affect the quantum yield; with the first being the three thieno[3,2-*b*]thiophene rings in the backbone. These are rigidified via the 6-member rings, which inhibit free rotation, limiting non-radiative pathways in the excited state and resulting in a higher quantum yield, 2. The flat backbone of these dyes could lead to aggregation and lower the quantum yield, but the two geminal di-aryl groups (*p*(C₆H₁₃)-Ph-) on the 6-member rings rotate out of plane and hinder. In this work we planned to introduce nonfullerene acceptor **CO₈DFIC** as the luminescent emitters in NIR-selective harvesting TLSCs.

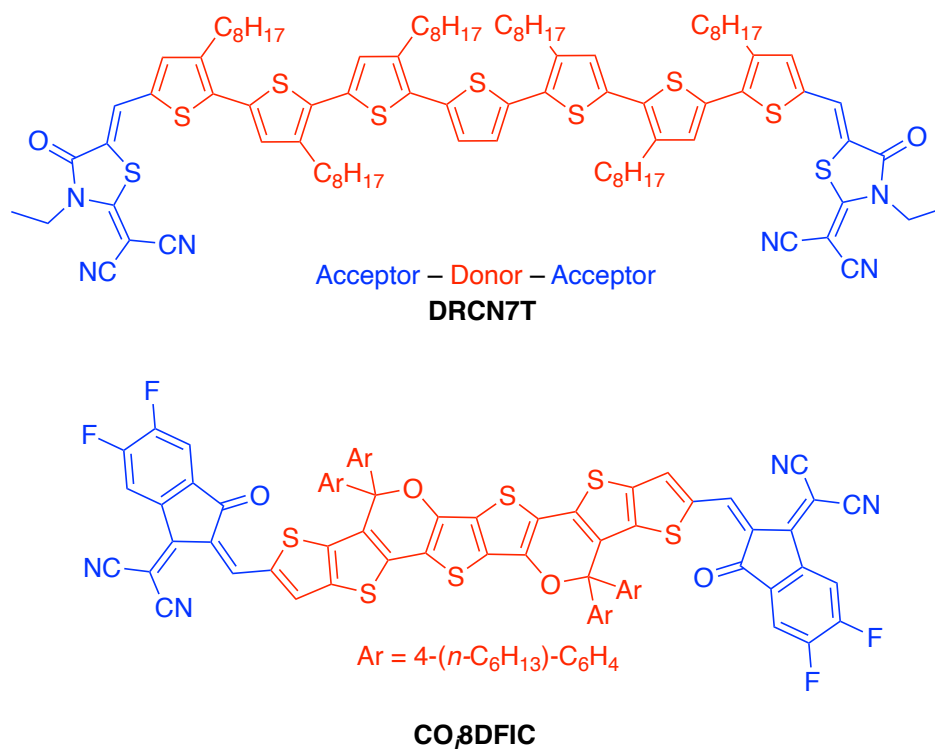


Figure II-14. Structures of D-A-D dyes; DRCN7T and CO₈DFIC

The synthesis of **CO₈DFIC** closely followed the procedure reported previously with small alterations to a few procedures as described in the experimental section^{30, 31} (Figure II-15). The synthesis commenced with 3-bromothieno[3,2-*b*]thiophene **II-27**, and in two steps, bromo ester **II-30** was obtained. Meanwhile, the bis(trimethyltin) compound **II-33** was made in two steps from dibromide **II-31** and reacted with **II-30** to furnish the **II-34**. Later, demethylation and acidification resulted in di-lactone structure **II-36**, which following ring opening with 127yrrolid and recyclization, generated the fully cyclized backbone **II-38**. After a formylation reaction, the di-aldehyde **II-39** in the of **DFIC** acceptor (**II-40**) was converted to the **CO₈DFIC** as the final product.

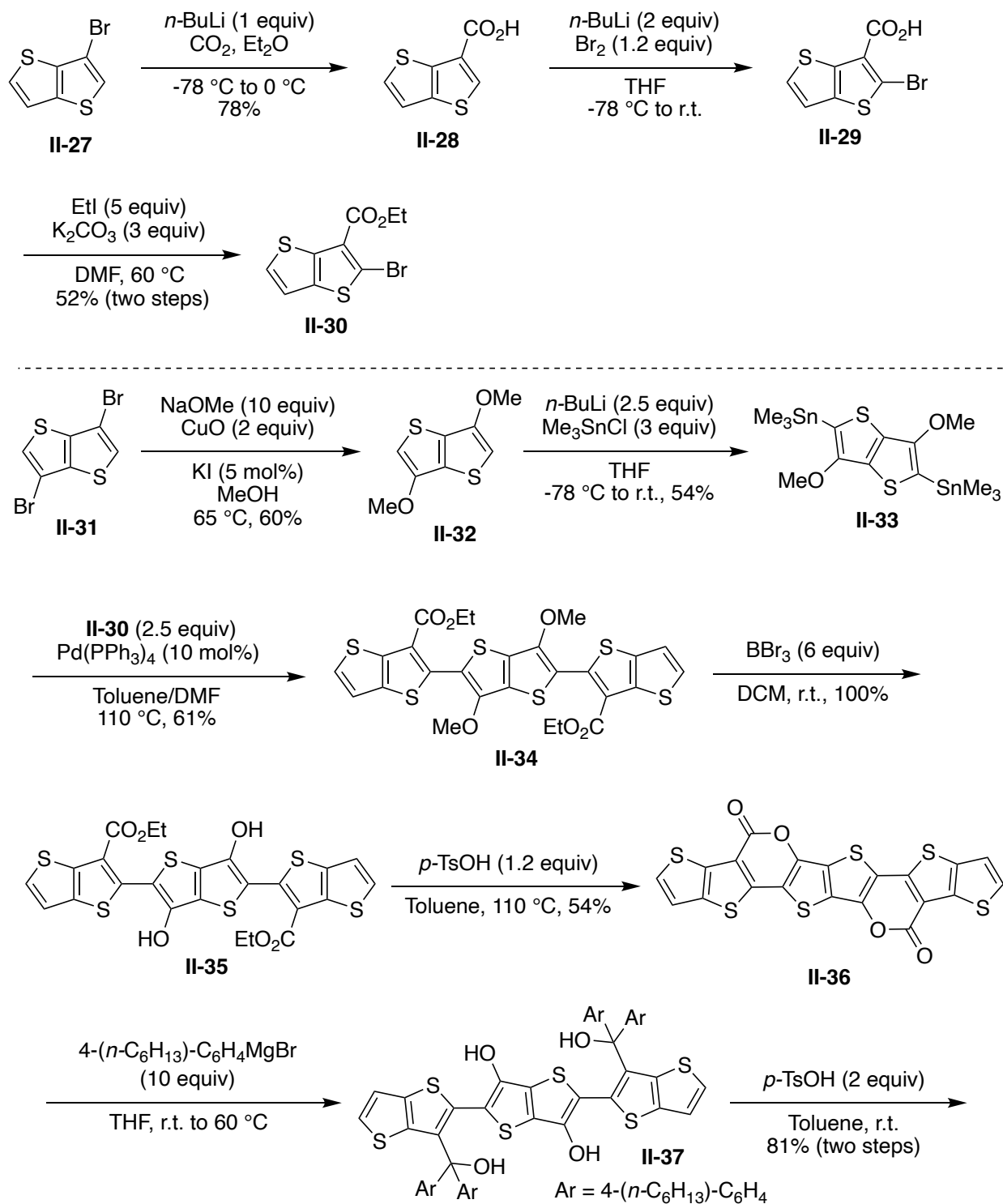
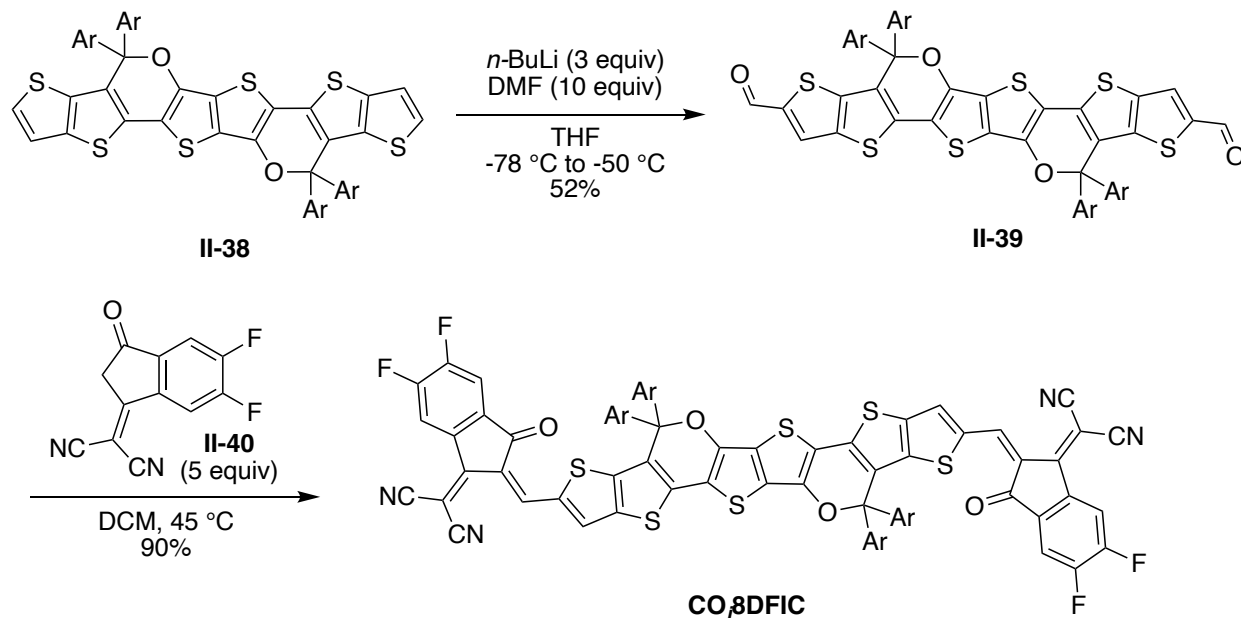


Figure II-15. Synthesis of CO8DFIC

Figure II-15 (cont'd)



The normalized absorption and emission spectra of **CO₈DFIC** dissolved in chlorobenzene solution and embedded in polymer matrix are plotted in Figure II-16a and II-16b. From solution to polymer matrix, there is a hypsochromic shift of both the absorption and emission spectra: the absorption peak shifts from 770 nm to 745 nm and the emission peak shifts from 831 nm to 808 nm, exhibiting Stokes shift of ~60 nm. The measured quantum yield is $23 \pm 1\%$ in chlorobenzene solution and $25 \pm 3\%$ in the polymer matrix. The relatively high Stokes shift values as well as high quantum yield demonstrate the potential for these NIR dyes, suggesting that **CO₈DFIC** may be a proper candidate for fabricating on TLSC.

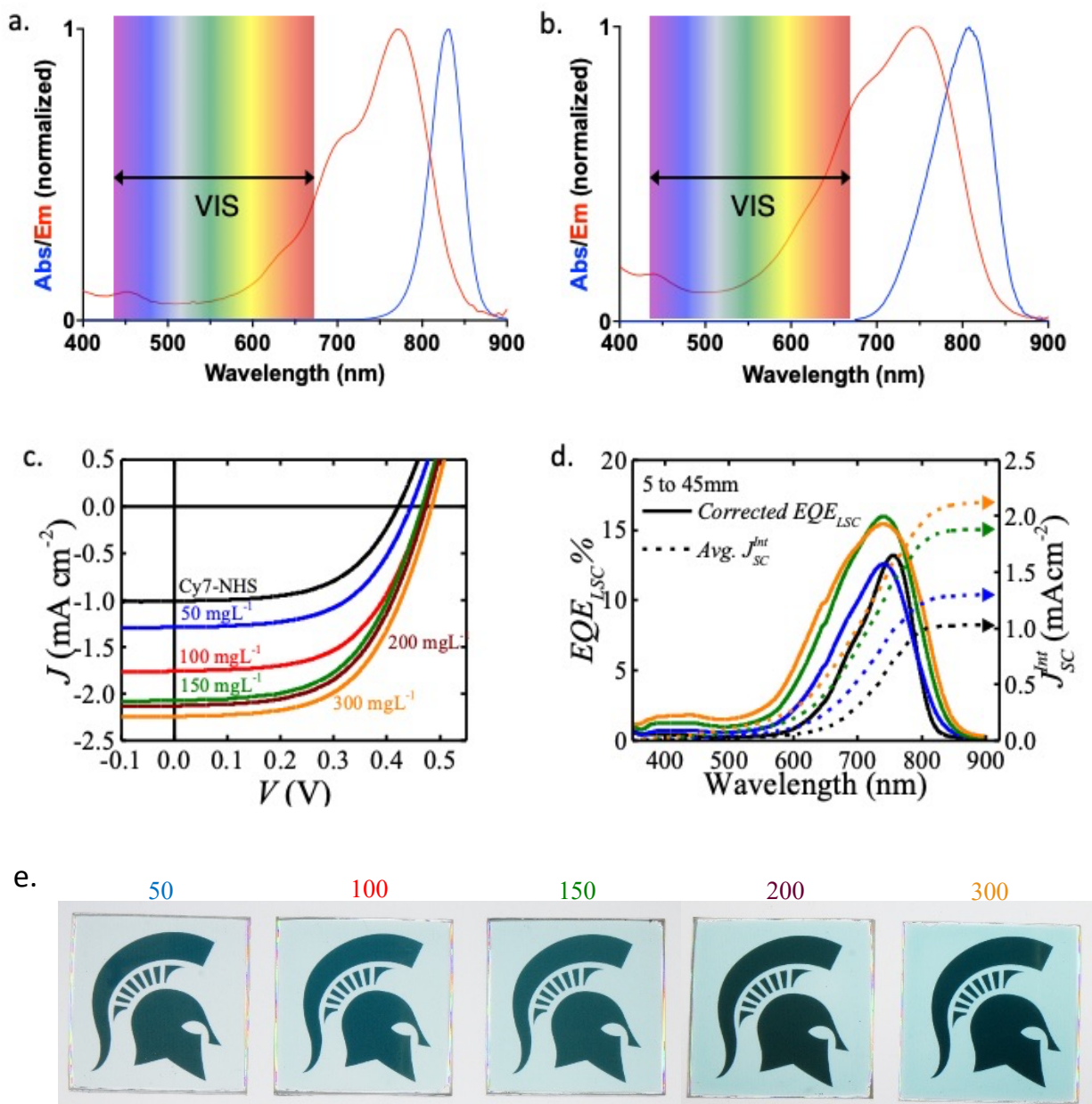


Figure II-16. Data for Coi8DFIC; a. Normalized absorption and emission spectra in chlorobenzene solution, b. Normalized absorption and emission spectra in polymer matrix, c. Current density versus voltage (J - V) characteristics of TLSCs with different concentrations, d. Average EQELSC(λ) spectra of TLSCs with different concentrations, e. Photographs of all the TLSC devices (Permission to utilize the Spartan helmet logo is kindly provided by MSU)

TLSC devices with five different **CO₈DFIC** concentrations were made by our collaborator Dr. Chenchen Yang in Prof. Lunt's group and their photovoltaic performance was characterized. For comparison, TLSC with cyanine dye (Cy7- NHS) was added as a reference device. The current density versus voltage ($J-V$) characteristics of these TLSCs is shown in Figure II-16c along with average position-dependent external quantum efficiency ($EQE_{LSC}(\lambda)$) spectra in Figure II-16d. Photographs of all the TLSC devices are shown in Figure II-16e (Permission to utilize the Spartan helmet logo is kindly provided by MSU). The TLSC with **CO₈DFIC** yielded a PCE of 1.24% with an AVT of 74.4%. The spectroscopic properties and extracted photovoltaic parameters are summarized in Table II-7.

Table II-7. Spectroscopic properties and TLSC photovoltaic parameters of **CO₈DFIC**

Dye	λ_{max} (nm) ^a	λ_{em} (nm) ^a	Stokes Shift (nm)	ϕ (%) ^b	PCE (%) ^c	AVT (%) ^c
CO₈DFIC	770	831	61	25	1.24	74.4

λ_{max} , absorption maximum; λ_{em} , emission maximum; ϕ , quantum yield; PCE, power conversion efficiency; AVT, average visible transmittance. [a] Absorptions and emissions were recorded in chlorobenzene at rt. [b] Absolute quantum yields were measured by Hamamatsu Quantaurus fluorimeter. [c] PCE and AVT reported for 150 mgL⁻¹.

In summary, we have synthesized the nonfullerene acceptor **CO₈DFIC** and utilized it in TLSCs as the luminophore. After device optimization, the TLSCs are shown to achieve a PCE of over 1.2% while the AVT exceeds 74%. This work reports the highest TLSC device efficiency at the highest visible transparency at the time of the report.³² Also, we highlight that the photoluminescent properties of these emerging low bandgap organic molecules provide a promising path for to higher TLSC performance.

II-3-3 Ultraviolet and near-infrared dual-band selective-harvesting TLSC

Multiple luminophores with various wavelength-selectivity can be incorporated into the LSC waveguide to maximize the spectral coverage of light harvesting³³⁻³⁵, and enhance photovoltaic performance.^{36, 37} However, coupling or reabsorption between different luminophores often leads to a reduction in the efficacy of this approach.³⁸ In this work, we introduce highly luminescent phosphorescent nanoclusters (NCs) and fluorescent organic molecules into TLSCs as isolated UV and NIR selective-harvesting luminophores, respectively. The NCs selectively harvest UV photons while exhibiting near-unity PL quantum yields (QY) and massive downshift of the luminescence into the NIR, without the use of heavy or toxic elements such as lead.⁹ To effectively pair these emitters and prevent deleterious reabsorption loss of the nanocluster emission in the NIR absorbing organic fluorophore, we demonstrate a strategy to isolate the absorption/emission bands. The dual-band TLSC device is composed of two distinct waveguides as shown in Figure II-17 with the UV component coated in polymer matrix on one waveguide and the NIR component on the other. An air gap is utilized to optically isolate the waveguided luminescence in each panel to prevent reabsorption.

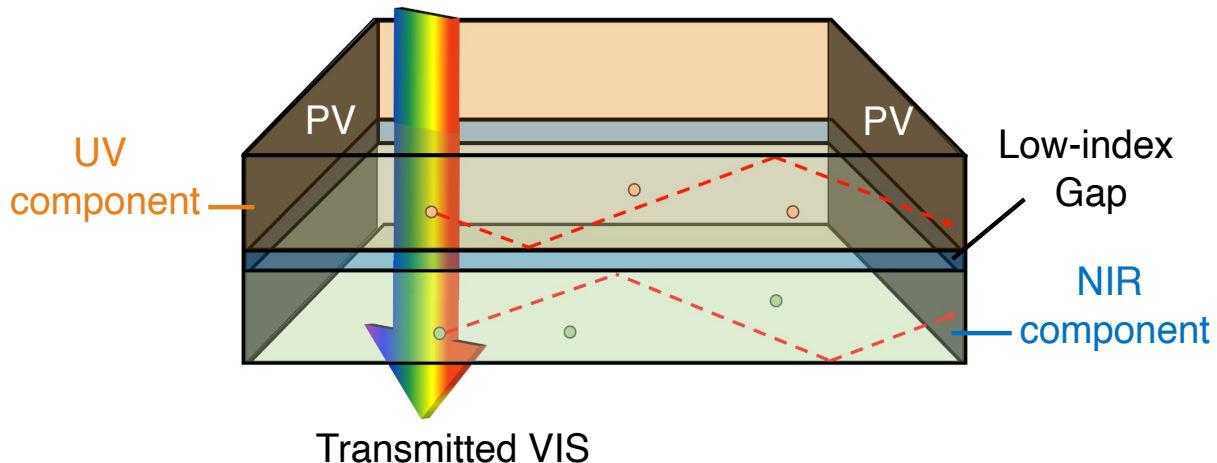


Figure II-17. Schematic of the working principle of the dual-band selective harvesting TLSC

The top UV component is based on phosphorescent hexanuclear NCs, where the chemical structure of $\text{Cs}_2\text{Mo}_6\text{l}_8(\text{CF}_3\text{CF}_2\text{COO})_6$ NC is shown in Figure II-18 (The NCs were synthesized by our collaborators in chemical engineering). Substitution of the apical halide positions has been shown previously to be an effective approach to increase quantum yields above 50%.^{9, 39} Various terminating ligands ($(\text{CF}_3)_n$ chain length) were synthesized and tested to maximize the QY with the composition above providing the highest value. We note that the chemical composition of the NC does not contain any hazardous heavy metal ions, which makes the deployment more environment friendly. The normalized absorption and emission spectra of the NC in polymer are shown in Figure II-18. The spectra show absorption cut-off at the UV/VIS border and NIR emission onset at the VIS/NIR border with a massive downshift over 300 nm and a corresponding QY of 80 ± 5 in the polymer matrix ($75 \pm 5\%$ in acetonitrile), which makes these NCs a practical UV selective-harvesting luminophore for TLSC applications.

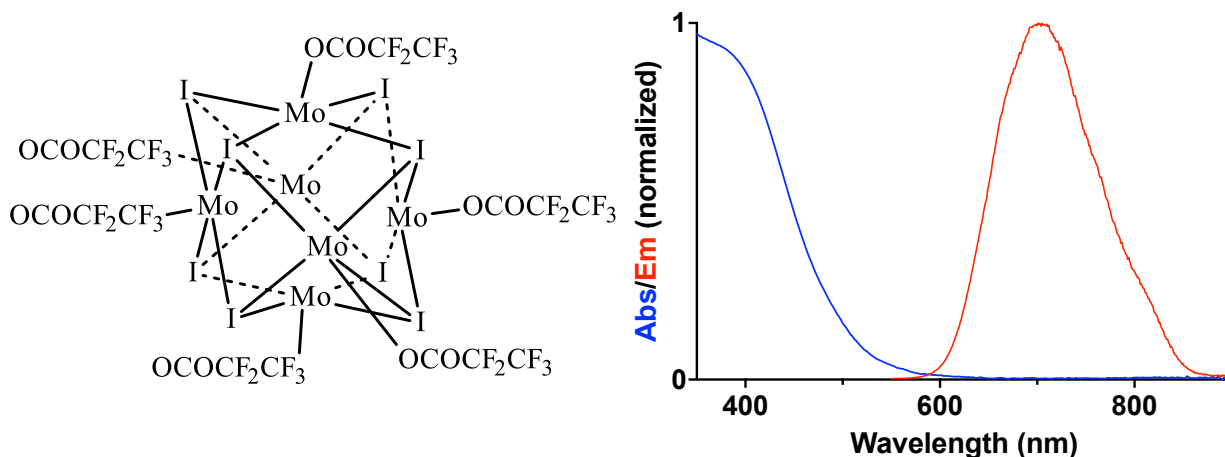


Figure II-18. Molecular structure, normalized absorption and emission spectra of $\text{Cs}_2\text{Mo}_6\text{I}_8(\text{CF}_3\text{CF}_2\text{COO})_6$ nanocluster

The bottom waveguide is based on NIR fluorescent small molecules. Two different organic luminophores are demonstrated as NIR selective harvesters. The first being **CO8DFIC**, as discussed in a previous section (II-3-2). The absorption peak is 745 nm while the emission peak is at 808 nm, resulting in a Stokes shift of ~60 nm and QY of $25 \pm 3\%$ in polymer matrix ($23 \pm 1\%$ in chlorobenzene). The second dye is a **BODIPY** derivative with high QY in the NIR.⁴⁰ The molecular structure, normalized absorption, and emission spectra of **BODIPY** in polymer matrix is shown in Figure II-19. Compared to **CO8DFIC**, the absorption and emissions peaks of **BODIPY** are narrower with a smaller Stokes shift (10 nm), but the significantly higher QY of $40 \pm 3\%$ in polymer matrix ($41 \pm 2\%$ in hexane) is among the highest values for this NIR emission range.

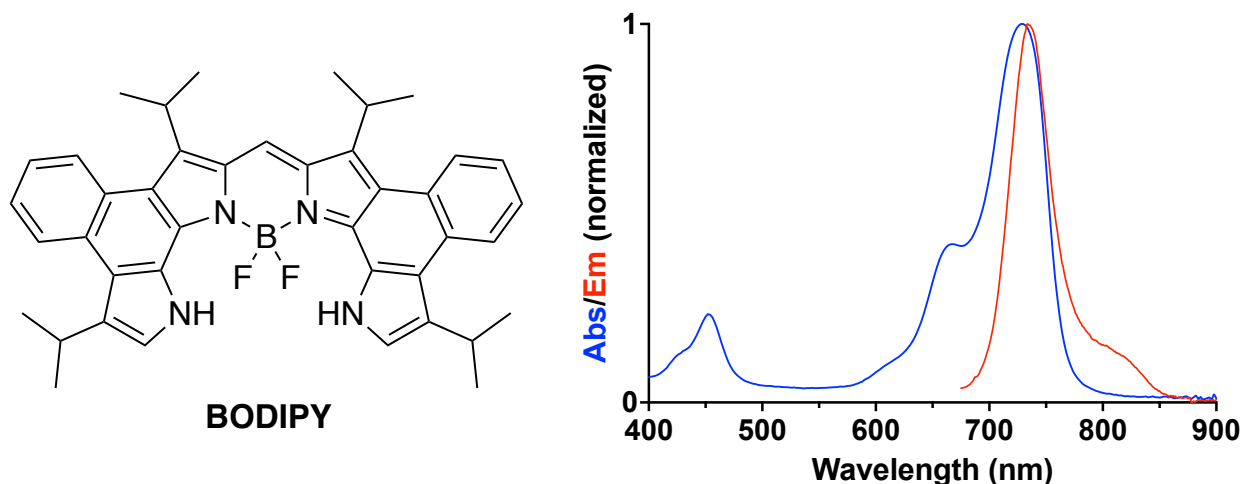


Figure II-19. Molecular structure, normalized absorption and emission spectra of **BODIPY**

After optimization of concentration, dual-band TLSC devices with two luminophore combinations (NC+CO₂DFIC and NC+BODIPY) were fabricated and their photovoltaic performance was characterized. For comparison, the TLSC with NC-only was added as a reference device. The current density versus voltage (J - V) characteristics of these TLSCs are shown in Figure II-20a along with average position-dependent external quantum efficiency ($EQE_{LSC}(\lambda)$) spectra in Figure II-20b.

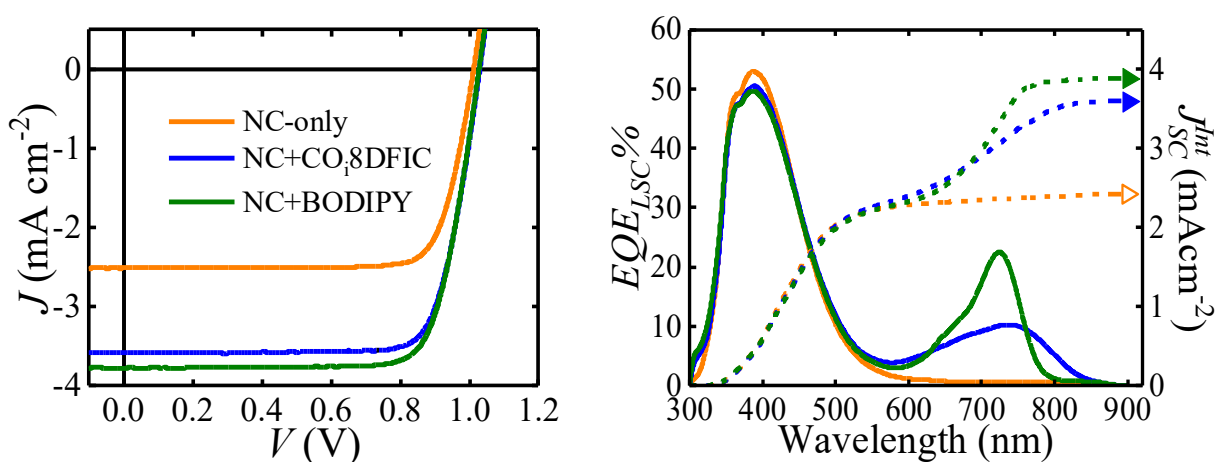


Figure II- 20. A. J - V characteristics of TLSCs, b. Average $EQE_{LSC}(\lambda)$ spectra of TLSCs

The quantum yield and extracted photovoltaic parameters are summarized in Table II-8. PCEs reach $2.9 \pm 0.1\%$ and $3.01 \pm 0.07\%$ for **NC+CO₈DFIC** and NC+**BODIPY** TLSCs, respectively, with color metrics suitable for the window industry.

Table II-8. Spectroscopic properties and TLSC photovoltaic parameters of **CO₈DFIC**

TLSCs	Dyes	Φ (%) ^a	PCE (%)	AVT (%)
1	NC	80	2.9	65.6
	+ CO ₈ DFIC	25		
2	NC	80	3.1	75.8
	+ BODIPY	40		

[a] Quantum yields were measured in polymer matrix.

In summary, by combining highly emissive phosphorescent hexanuclear metal halide NCs and organic luminophores as isolated UV and NIR selective-harvesting luminophores, we have designed and demonstrated dual-band selective-harvesting TLSC devices. Harvesting non-visible photons from both UV and NIR portions of solar spectrum leads to PCE > 3%, with good wavelength-selectivity that results in AVT > 75%. This work reports the highest PCE of any transparent photovoltaic (TPV) devices with AVT greater than 70% at the time of publication.⁴¹

II-4 Future work

II-4-1 Further investigations on tuning the Stokes shift and QY of cyanines

We previously reported a general strategy to tune the Stokes shift of the cyanine dyes by substitution of different amines at C4 position which would maintain or break conjugation leading to two distinct ground state conformations. As shown in Figure II-21a, the C2 position on cyanine's methine backbone has the potential to affect more than the C-4 (**II-41**). Amination at this position could also disrupt conjugation, leading to a greater extent of blue shifting, as compared to C-4, because it would shorten the conjugation to a greater extent. The synthesis of C2-halogenated cyanines is under study in our lab. In a parallel study our computational collaborator, Professor Levine hypothesized that, locking the pyrrolidine ring to the methine chain backbone such as that shown in structure (**II-42**), could lead to a massive Stokes shift (Figure II-21b). The synthetic strategy toward making this molecule is under study.

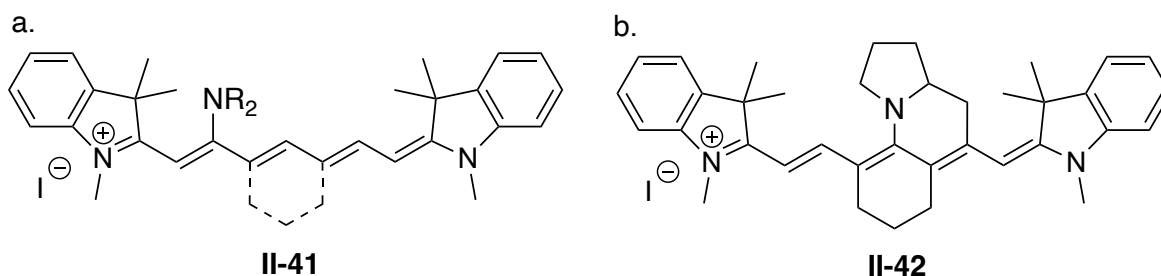


Figure II-21. a. Amine C2-substituted cyanines, b. asymmetric cyclized aminated cyanine

We have previously discussed cyanine's wide utility due to their unique structural characteristics. Although improving the quantum yield of cyanines was evaluated with different approaches, for most cases the efficiency does not rise above 25-35% beyond 700 nm. Schnermann and coworkers have shown a QY increase of more than 4-fold upon

restricting bond rotations of the Cy5 methine chain, although this approach fails when the methine length increases from five to seven.^{42, 43} Since Cy5 absorption is primarily in the visible region, they fall short of what is required for transparent solar concentrators. In addition, red-shifted fluorophores are more suitable for bio imaging as well. Our plan entails modification of the indoline based head groups (with higher donor strength) on Cy5, in order to optimize the absorption in the NIR region. Next, we would restrain the conformation to increase the QY. Five proposed head groups are depicted in Figure II-22; two full structures with the head groups are shown as examples. In addition, we would install an amine at the center of the chain to increase the stokes shift and minimize the integral overlap.

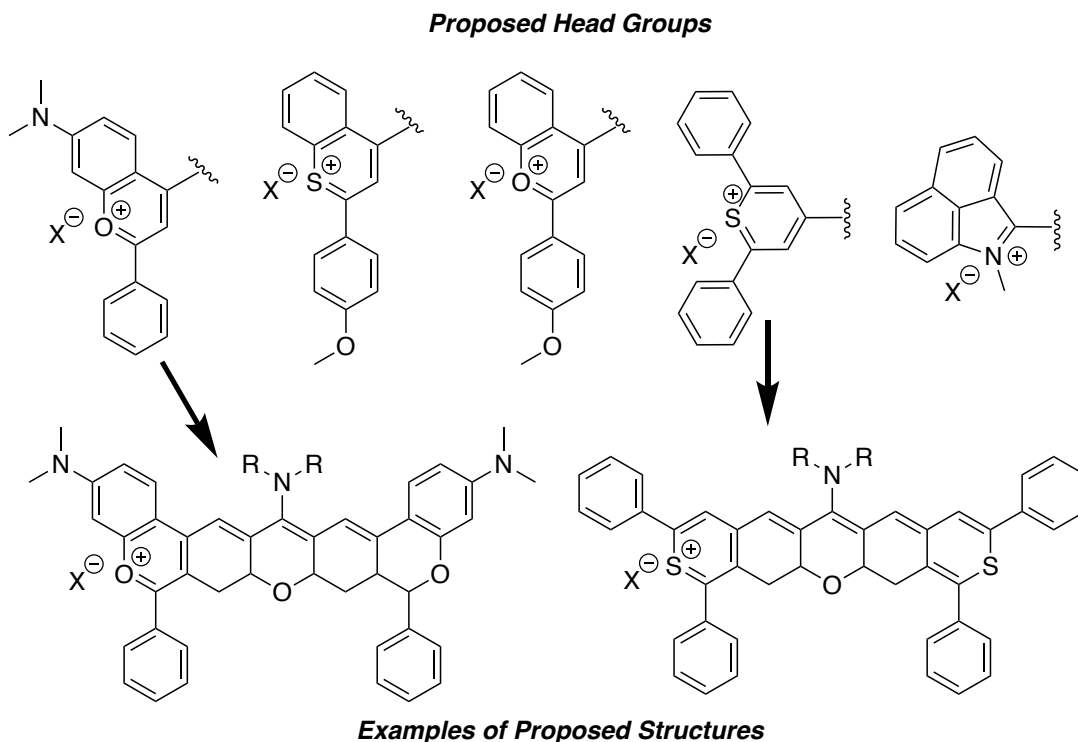
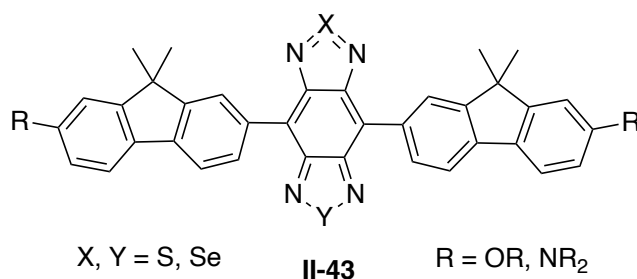


Figure II-22. Proposed head groups to redshift the Cy5 core and, proposed new Cy5 structures

II-4-2 Donor-acceptor-donor dyes as a potential tools in TLSCs and bio imaging

We have shown the application of acceptor–donor–acceptor (A–D–A) fluorophore **CO:8DFIC** as the luminescent emitters in NIR-selective harvesting TLSCs. The other potential candidate could be donor–acceptor–donor (D–A–D) NIR I/II chromophores which have gained considerable attention as a result of their unique structural and photophysical properties. These include high quantum yields, a high stokes shift, high coefficient of absorption, all while absorbing and emitting outside the visible spectrum.⁴⁴ The general structure of D–A–D that are under evaluation in our lab is depicted in Figure II-23. Our goal is to make a library of these dyes by tuning the donating ability of the substituents and perturbing the electronic structure of acceptor by having different atoms at X and Y.



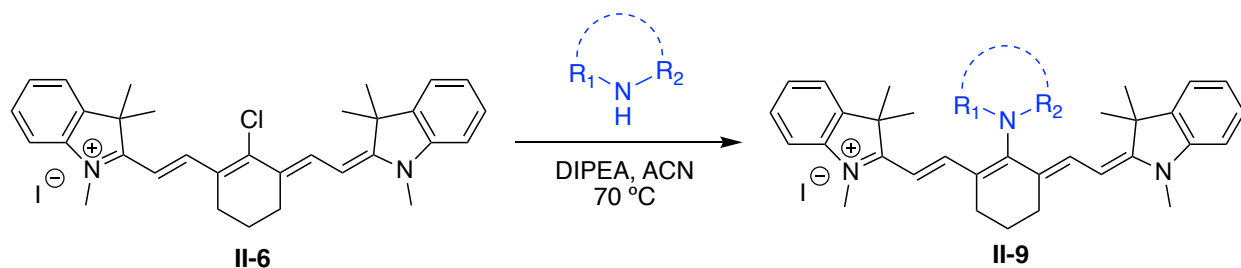
II-5 Experimental section

II-5-1 General remarks:

Molecular sieves (4Å) were dried at 160 °C under 0.25 mtorr vacuum prior to use. Unless otherwise mentioned, solvents were purified as follows. CHCl₃ (amylene stabilized) was purchased from Sigma Aldrich and incubated over 4Å MS for 48 h prior to use. Toluene and CH₂Cl₂ were dried over CaH₂ whereas THF and Et₂O were dried over sodium (dryness was monitored by colorization of benzophenone ketyl radical); they were freshly distilled prior to use. Acetonitrile and DMF for reactions was HPLC grade from Sigma-Aldrich. NMR spectra were obtained using a 500 MHz Varian NMR spectrometer and referenced using the residual ¹H peak from the deuterated solvent. Waters 2795 (Alliance HT) instrument was used for HRMS (ESI) analysis with polyethylene glycol (PEG-400-600) as a reference. UV-Vis was performed on Agilent Cary 100 series machine and PL was recorded on Fluorolog by ISA instrument. Quantum yield measurement was performed on absolute PL quantum yield spectrometer C11347 by Hamamatsu.

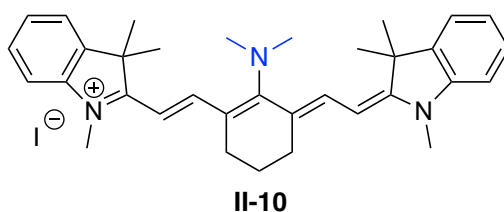
Column chromatography was performed using Silicycle 60Å, 35-75 μm silica gel. Pre-coated 0.25 mm thick silica gel 60 F254 plates were used for analytical TLC and visualized using UV light, potassium permanganate stain, *p*-anisaldehyde stain or phosphomolybdic acid in EtOH stain.

II-5-2 General synthesis of amine substituted cyanines:



Amine substituted cyanines **II-9** were synthesized according to the previous reported procedures.¹⁷ To a solution of **II-6** (74 mg, 0.10 mmol), diisopropylethylamine (DIPEA) (35 μ L, 2 equiv, 0.20 mmol) in acetonitrile (2 mL) was added amine (20 equiv, 2.0 mmol) under nitrogen in a sealed tube. The mixture was stirred at 70 °C and the reaction was monitored by LC-MS. Upon completion, typically in 48 h, the mixture was concentrated under reduced pressure and purified by flash column (100% DCM gradually to 5% MeOH/DCM). The products were isolated as a dark solids.

II-5-2-1 Analytical Data



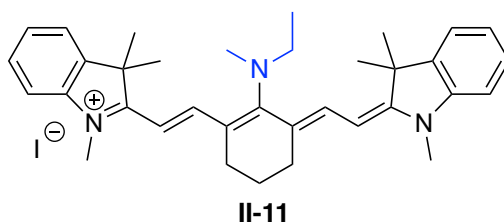
2-(CAN-2-(CAN-2-(dimethylamino)-3-(2-(CAN-1,3,3-trimethylindolin-2-ylidene)ethylidene)cyclohex-1-en-1-yl)vinyl)-1,3,3-trimethyl-3H-indol-1-ium iodide.

The title compound was prepared according to the general procedure at 0.1 mmol scale. Product was isolated as a dark green solid (40 mg, 0.064 mmol, 64%).

$^1\text{H-NMR}$ (500 MHz, Chloroform-*d*): δ 7.40 (d, $J = 13.1$ Hz, 2H), 7.23 (td, $J = 8.1, 7.4, 1.5$ Hz, 4H), 7.01 (t, $J = 7.4$ Hz, 2H), 6.88 (d, $J = 7.9$ Hz, 2H), 5.56 (d, $J = 13.1$ Hz, 2H), 3.61 (s, 6H), 3.39 (s, 6H), 2.46 (t, $J = 6.6$ Hz, 4H), 1.79 (p, $J = 6.6$ Hz, 2H), 1.59 (s, 12H).

$^{13}\text{C-NMR}$ (126 MHz, Chloroform-*d*): δ 175.55, 167.84, 143.54, 140.28, 139.84, 128.22, 122.73, 122.08, 121.97, 108.50, 94.06, 53.53, 47.86, 47.60, 29.48, 25.40, 21.56.

HRMS(ESI⁺): calcd for $\text{C}_{34}\text{H}_{42}\text{N}_3^+$ [M]⁺ 492.3379, found 492.3378.



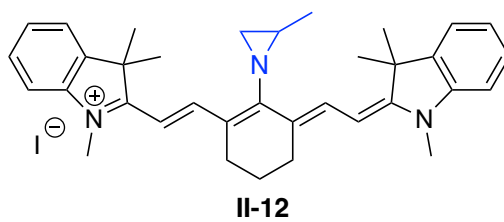
2-(CAN-2-(CAN-2-(ethyl(methyl)amino)-3-(2-(CAN-1,3,3-trimethylindolin-2-ylidene)ethylidene)cyclohex-1-en-1-yl)vinyl)-1,3,3-trimethyl-3H-indol-1-ium iodide.

The title compound was prepared according to the general procedure at 0.1 mmol scale. Product was isolated as a dark solid (39 mg, 0.062 mmol, 62%).

$^1\text{H-NMR}$ (500 MHz, Chloroform-*d*): δ 7.46 (d, $J = 13.4$ Hz, 2H), 7.33 – 7.24 (m, 4H), 7.08 (t, $J = 7.4$ Hz, 2H), 6.97 (d, $J = 7.9$ Hz, 2H), 5.72 (d, $J = 13.4$ Hz, 2H), 3.79 (q, $J = 7.0$ Hz, 2H), 3.48 (s, 6H), 3.41 (s, 3H), 2.47 (t, $J = 6.5$ Hz, 4H), 1.81 (p, $J = 6.6$ Hz, 2H), 1.60 (s, 12H), 1.37 (t, $J = 7.0$ Hz, 3H).

^{13}C -NMR (126 MHz, Chloroform-*d*): δ 175.03, 169.15, 143.30, 141.83, 139.94, 128.44, 124.26, 123.41, 121.97, 109.15, 95.86, 53.52, 47.90, 44.73, 31.24, 29.27, 24.94, 21.83, 14.98.

HRMS(ESI⁺): calcd for $\text{C}_{35}\text{H}_{44}\text{N}_3^+$ [M]⁺ 506.3535, found 506.3525.



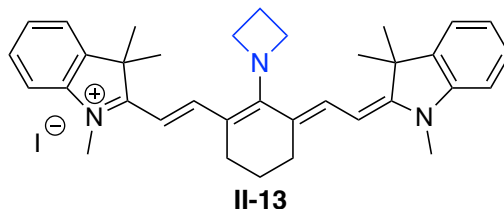
1,3,3-Trimethyl-2-(CAN-2-(CAN-2-(2-methylaziridin-1-yl)-3-(2-(CAN-1,3,3-trimethylindolin-2-ylidene)ethylidene)cyclohex-1-en-1-yl)vinyl)-3H-indol-1-ium iodide.

The title compound was prepared according to the general procedure at 0.1 mmol scale. Product was isolated as a dark solid (30 mg, 0.047 mmol, 47%).

^1H -NMR (500 MHz, Chloroform-*d*): δ 8.01 (d, $J = 13.7$ Hz, 2H), 7.38 – 7.26 (m, 4H), 7.14 (t, $J = 7.4$ Hz, 2H), 7.05 (d, $J = 7.9$ Hz, 2H), 5.88 (d, $J = 13.7$ Hz, 2H), 3.57 (s, 6H), 2.57 (t, $J = 6.0$ Hz, 4H), 1.84 – 1.76 (m, 3H), 1.69 – 1.59 (m, 14H), 1.46 (d, $J = 5.4$ Hz, 3H).

^{13}C -NMR (126 MHz, Chloroform-*d*): δ 170.91, 170.12, 143.07, 140.20, 139.76, 128.61, 124.61, 124.14, 121.99, 109.76, 98.11, 48.27, 39.06, 36.94, 31.66, 28.61, 28.47, 25.95, 20.86, 18.09.

HRMS(ESI⁺): calcd for $\text{C}_{35}\text{H}_{42}\text{N}_3^+$ [M]⁺ 504.3379, found 504.3375.



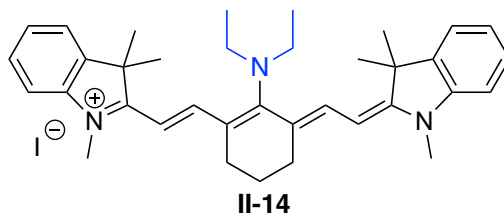
2-(CAN-2-(CAN-2-(144yrrolidi-1-yl)-3-(2-(CAN-1,3,3-trimethylindolin-2-ylidene)ethylidene)cyclohex-1-en-1-yl)vinyl)-1,3,3-trimethyl-3H-indol-1-ium iodide.

The title compound was prepared according to the general procedure at 0.1 mmol scale. Product was isolated as a dark solid (49 mg, 0.078 mmol, 78%).

¹H-NMR (500 MHz, Chloroform-*d*): δ 7.24 – 7.16 (m, 6H), 6.96 (t, *J* = 7.5 Hz, 2H), 6.77 (d, *J* = 7.7 Hz, 2H), 5.32 (d, *J* = 12.8 Hz, 2H), 4.93 (t, *J* = 7.6 Hz, 4H), 3.25 (s, 6H), 2.71 (p, *J* = 7.6 Hz, 2H), 2.56 – 2.49 (m, 4H), 1.86 – 1.83 (m, 2H), 1.64 (s, 12H).

¹³C-NMR (126 MHz, Chloroform-*d*): δ 169.77, 165.86, 143.70, 139.75, 134.78, 127.96, 121.99, 121.95, 107.61, 92.32, 62.46, 47.02, 29.83, 29.27, 27.22, 20.79, 19.31.

HRMS(ESI⁺): calcd for C₃₅H₄₂N₃⁺ [M]⁺ 504.3379, found 504.3382.



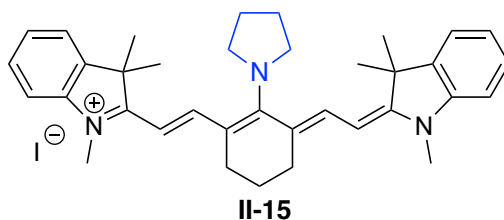
2-(CAN-2-(CAN-2-(diethylamino)-3-(2-(CAN-1,3,3-trimethylindolin-2-ylidene)ethylidene)cyclohex-1-en-1-yl)vinyl)-1,3,3-trimethyl-3H-indol-1-ium iodide.

The title compound was prepared according to the general procedure at 0.1 mmol scale. Product was isolated as a dark solid (21 mg, 0.032 mmol, 32%).

$^1\text{H-NMR}$ (500 MHz, Chloroform- d): δ 7.52 (d, J = 13.6 Hz, 2H), 7.34 – 7.26 (m, 4H), 7.11 (m, 2H), 7.02 (d, J = 7.9 Hz, 2H), 5.80 (d, J = 13.6 Hz, 2H), 3.65 (q, J = 6.9 Hz, 4H), 3.52 (s, 6H), 2.49 (t, J = 6.5 Hz, 4H), 1.82 (p, J = 6.5 Hz, 2H), 1.60 (s, 12H), 1.28 (t, J = 6.9 Hz, 6H).

$^{13}\text{C-NMR}$ (126 MHz, Chloroform- d): δ 174.15, 169.83, 143.19, 142.52, 140.06, 128.57, 125.76, 123.76, 121.97, 109.50, 96.95, 49.47, 48.03, 31.36, 29.07, 24.88, 21.98, 14.84.

HRMS(ESI $^+$): calcd for $\text{C}_{36}\text{H}_{46}\text{N}_3^+$ $[\text{M}]^+$ 520.3690, found 520.3692.



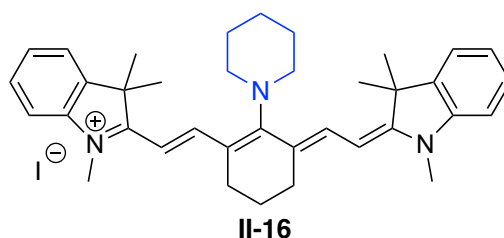
1,3,3-Trimethyl-2-(CAN-2-(CAN-2-(145yrrolidine-1-yl)-3-(2-(CAN-1,3,3-trimethylindolin-2-ylidene)ethylidene)cyclohex-1-en-1-yl)vinyl)-3H-indol-1-ium iodide.

The title compound was prepared according to the general procedure at 0.1 mmol scale. Product was isolated as a dark solid (15 mg, 0.023 mmol, 23%).

$^1\text{H-NMR}$ (500 MHz, Chloroform- d): δ 7.42 (d, J = 12.7 Hz, 2H), 7.19 (m, 4H), 6.94 (t, J = 7.4 Hz, 2H), 6.73 (d, J = 8.0 Hz, 2H), 5.27 (d, J = 12.7 Hz, 2H), 4.32 (d, J = 6.5 Hz, 4H), 3.22 (s, 6H), 2.59 (t, J = 6.2 Hz, 4H), 2.10 (m, 4H), 1.79 (t, J = 6.3 Hz, 2H), 1.70 (s, 12H).

^{13}C -NMR (126 MHz, cdcl_3): δ 173.07, 165.22, 143.92, 140.02, 135.14, 127.72, 122.03, 121.53, 121.22, 107.08, 91.76, 55.86, 46.98, 29.58, 29.43, 28.77, 24.16, 20.91.

HRMS(ESI+): calcd for $\text{C}_{36}\text{H}_{44}\text{N}_3^+$ [M] $^+$ 518.3535, found 518.3536.



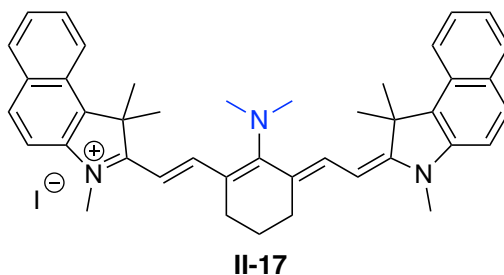
1,3,3-Trimethyl-2-(CAN-2-(CAN-2-(piperidin-1-yl)-3-(2-(CAN-1,3,3-trimethylindolin-2-ylidene)ethylidene)cyclohex-1-en-1-yl)vinyl)-3H-indol-1-ium iodide.

The title compound was prepared according to the general procedure at 0.1 mmol scale. Product was isolated as a dark solid (72 mg, 0.054 mmol, 54%).

^1H -NMR (500 MHz, Chloroform-*d*): δ 7.50 (d, J = 13.2 Hz, 2H), 7.33 – 7.22 (m, 4H), 7.06 (t, J = 7.4 Hz, 2H), 6.95 (d, J = 7.9 Hz, 2H), 5.68 (d, J = 13.2 Hz, 2H), 3.85 (t, J = 5.0 Hz, 4H), 3.46 (s, 6H), 2.47 (t, J = 6.7 Hz, 4H), 1.96-1.92 (m, 2H), 1.90-1.86 (m, 4H), 1.84-1.82 (m, 2H), 1.62 (s, 12H).

^{13}C -NMR (126 MHz, Chloroform-*d*): δ 175.57, 168.39, 143.43, 140.15, 139.75, 128.36, 123.79, 123.06, 121.89, 108.84, 95.03, 56.80, 47.63, 28.96, 28.15, 24.94, 24.28, 21.63, 18.91.

HRMS(ESI+): calcd for $\text{C}_{37}\text{H}_{46}\text{N}_3^+$ [M] $^+$ 532.3692, found 532.3690.



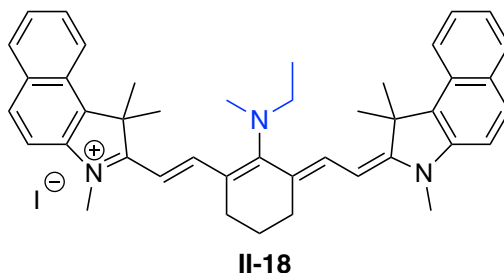
2-(CAN-2-(CAN-2-(dimethylamino)-3-(CAN-2-(3-ethyl-1,1-dimethyl-1,3-dihydro-2H-benzo[e]indol-2-ylidene)ethylidene)cyclohex-1-en-1-yl)vinyl)-3-ethyl-1,1-dimethyl-1H-benzo[e]indol-3-ium iodide.

The title compound was prepared according to the general procedure at 0.1 mmol scale. Product was isolated as a dark solid (41 mg, 0.055 mmol, 55%).

¹H-NMR (500 MHz, Chloroform-*d*): δ 8.07 (d, *J* = 8.5 Hz, 2H), 7.83 (dd, *J* = 8.5, 4.4 Hz, 4H), 7.57 (d, *J* = 13.3 Hz, 2H), 7.51 (ddd, *J* = 8.3, 6.8, 1.3 Hz, 2H), 7.34 (t, *J* = 7.5 Hz, 2H), 7.23 (d, *J* = 8.4 Hz, 2H), 5.69 (d, *J* = 13.3 Hz, 2H), 4.04 (q, *J* = 7.2 Hz, 4H), 3.65 (s, 6H), 2.50 (t, *J* = 6.6 Hz, 4H), 1.93 (s, 12H), 1.86 – 1.81 (m, 2H), 1.40 (t, *J* = 7.2 Hz, 6H).

¹³C-NMR (126 MHz, Chloroform-*d*): δ 174.46, 168.95, 140.52, 139.85, 131.82, 130.89, 130.18, 129.89, 128.49, 127.41, 123.90, 122.00, 121.91, 109.74, 93.65, 49.72, 47.83, 38.59, 28.97, 25.34, 21.74, 12.03.

HRMS(ESI⁺): calcd for C₄₄H₅₀N₃⁺ [M]⁺ 620.4005, found 620.4008.



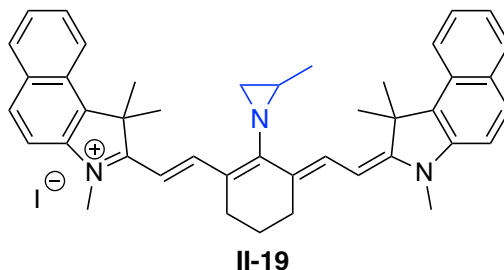
3-Ethyl-2-(CAN-2-(CAN-2-(ethyl(methyl)amino)-3-(CAN-2-(3-ethyl-1,1-dimethyl-1,3-dihydro-2H-benzo[e]indol-2-ylidene)ethylidene)cyclohex-1-en-1-yl)vinyl)-1,1-dimethyl-1H-benzo[e]indol-3-ium iodide.

The title compound was prepared according to the general procedure at 0.1 mmol scale. Product was isolated as a dark solid (57 mg, 0.075 mmol, 75%).

¹H-NMR (500 MHz, Chloroform-*d*): δ 8.06 (d, *J* = 8.4 Hz, 2H), 7.86 (dd, *J* = 8.7, 2.1 Hz, 4H), 7.63 (d, *J* = 13.6 Hz, 2H), 7.53 (ddd, *J* = 8.4, 6.8, 1.3 Hz, 2H), 7.36 (ddd, *J* = 8.1, 6.9, 1.1 Hz, 2H), 7.30 (d, *J* = 8.8 Hz, 2H), 5.82 (d, *J* = 13.6 Hz, 2H), 4.11 (q, *J* = 7.2 Hz, 4H), 3.80 (q, *J* = 7.0 Hz, 2H), 3.42 (s, 3H), 2.50 (t, *J* = 6.4 Hz, 4H), 1.92 (s, 12H), 1.85 (p, *J* = 6.5 Hz, 2H), 1.43 – 1.40 (m, 9H).

¹³C-NMR (126 MHz, Chloroform-*d*): δ 173.76, 170.16, 141.76, 139.68, 132.27, 131.18, 130.46, 130.02, 128.35, 127.53, 124.33, 124.23, 121.83, 110.09, 95.39, 53.44, 49.99, 44.59, 39.03, 24.99, 21.96, 15.12, 12.24.

HRMS(ESI⁺): calcd for C₄₅H₅₂N₃⁺ [M]⁺ 634.4161, found 634.4171.



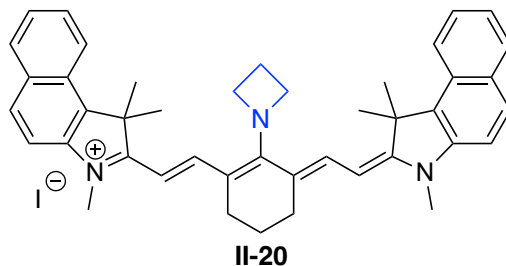
3-Ethyl-2-(CAN-2-(CAN-3-(CAN-2-(3-ethyl-1,1-dimethyl-1,3-dihydro-2H-benzo[e]indol-2-ylidene)ethylidene)-2-(2-methylaziridin-1-yl)cyclohex-1-en-1-yl)vinyl)-1,1-dimethyl-1H-benzo[e]indol-3-ium iodide.

The title compound was prepared according to the general procedure at 0.1 mmol scale. Product was isolated as a dark solid (36 mg, 0.047 mmol, 47%).

¹H-NMR (500 MHz, Chloroform-*d*): δ 8.14 (d, *J* = 13.7 Hz, 2H), 8.10 – 8.04 (m, 2H), 7.88 (dd, *J* = 8.5, 4.2 Hz, 4H), 7.55 (ddd, *J* = 8.3, 6.8, 1.3 Hz, 2H), 7.39 (ddd, *J* = 8.0, 6.8, 1.0 Hz, 2H), 7.35 (d, *J* = 8.8 Hz, 2H), 5.94 (d, *J* = 13.7 Hz, 2H), 4.18 (q, *J* = 7.3 Hz, 4H), 2.79 – 2.77 (m, 1H), 2.70 (d, *J* = 5.8 Hz, 1H), 2.58 (t, *J* = 6.2 Hz, 4H), 2.43 (d, *J* = 3.5 Hz, 1H), 1.98 (d, *J* = 7.4 Hz, 13H), 1.86 – 1.82 (m, 2H), 1.56 (d, *J* = 5.4 Hz, 3H), 1.44 (t, *J* = 7.2 Hz, 6H).

¹³C-NMR (126 MHz, Chloroform-*d*): δ 170.68, 170.28, 139.50, 139.11, 132.75, 131.45, 130.61, 130.07, 128.30, 127.64, 124.54, 124.01, 121.93, 110.27, 97.17, 50.26, 39.37, 37.12, 28.16, 28.04, 25.94, 20.92, 18.37, 12.33.

HRMS(ESI⁺): calcd for C₄₅H₅₀N₃⁺ [M]⁺ 632.4005, found 632.4009.



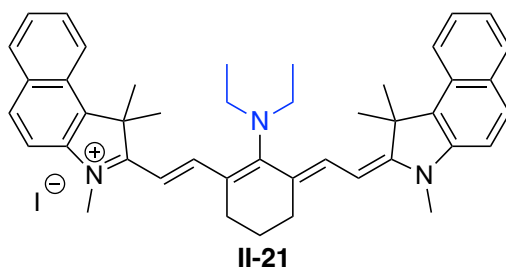
2-(CAN-2-(CAN-2-(150yrrolidi-1-yl)-3-(CAN-2-(3-ethyl-1,1-dimethyl-1,3-dihydro-2H-benzo[e]indol-2-ylidene)ethylidene)cyclohex-1-en-1-yl)vinyl)-3-ethyl-1,1-dimethyl-1H-benzo[e]indol-3-ium iodide.

The title compound was prepared according to the general procedure at 0.1 mmol scale. Product was isolated as a dark solid (64 mg, 0.084 mmol, 84%).

¹H-NMR (500 MHz, Chloroform-*d*): δ 8.07 (d, *J* = 8.6 Hz, 2H), 7.78 (dd, *J* = 13.7, 8.4 Hz, 4H), 7.48 (ddd, *J* = 8.3, 6.8, 1.3 Hz, 2H), 7.38 (d, *J* = 12.8 Hz, 2H), 7.29 (ddd, *J* = 8.0, 6.8, 1.0 Hz, 2H), 7.11 (d, *J* = 8.7 Hz, 2H), 5.43 (d, *J* = 12.7 Hz, 2H), 5.01 (t, *J* = 7.5 Hz, 4H), 3.88 (q, *J* = 7.2 Hz, 4H), 2.75 (p, *J* = 7.5 Hz, 2H), 2.55 (t, *J* = 6.2 Hz, 4H), 1.96 (s, 12H), 1.90 – 1.84 (m, 2H), 1.31 (t, *J* = 7.2 Hz, 6H).

¹³C-NMR (126 MHz, Chloroform-*d*): δ 169.26, 166.64, 140.07, 134.72, 131.06, 130.49, 129.81, 129.72, 128.65, 127.24, 123.39, 122.06, 117.62, 109.25, 91.46, 62.48, 49.04, 37.71, 28.66, 27.22, 20.84, 19.31, 11.59.

HRMS(ESI⁺): calcd for C₄₅H₅₀N₃⁺ [M]⁺ 632.4005, found 632.4007.



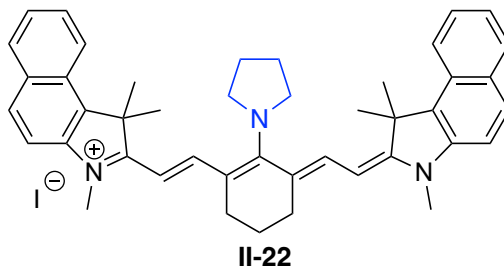
2-(CAN-2-(CAN-2-(diethylamino)-3-(CAN-2-(3-ethyl-1,1-dimethyl-1,3-dihydro-2H-benzo[e]indol-2-ylidene)ethylidene)cyclohex-1-en-1-yl)vinyl)-3-ethyl-1,1-dimethyl-1H-benzo[e]indol-3-ium iodide

The title compound was prepared according to the general procedure at 0.1 mmol scale. Product was isolated as a dark solid (36 mg, 0.046 mmol, 46%).

¹H-NMR (500 MHz, Chloroform-*d*): δ 8.07 (d, *J* = 8.5 Hz, 2H), 7.89 (d, *J* = 8.9 Hz, 4H), 7.69 (d, *J* = 13.7 Hz, 2H), 7.58 – 7.51 (m, 2H), 7.42 – 7.37 (m, 2H), 7.34 (d, *J* = 8.8 Hz, 2H), 5.89 (d, *J* = 13.7 Hz, 2H), 4.15 (q, *J* = 7.2 Hz, 4H), 3.70 (q, *J* = 6.9 Hz, 4H), 2.53 (t, *J* = 6.4 Hz, 4H), 1.93 (s, 12H), 1.89 – 1.85 (m, 2H), 1.44 (t, *J* = 7.2 Hz, 6H), 1.35 (t, *J* = 6.9 Hz, 6H).

¹³C-NMR (126 MHz, Chloroform-*d*): δ 173.00, 170.56, 142.05, 139.64, 132.46, 131.29, 130.56, 130.10, 128.33, 127.57, 125.62, 124.37, 121.82, 110.20, 96.22, 50.06, 49.39, 39.18, 28.59, 28.44, 25.01, 22.05, 14.96, 12.31.

HRMS (ESI+): calcd for C₄₆H₅₄N₃⁺ [M]⁺ 648.4319, found 648.4318.



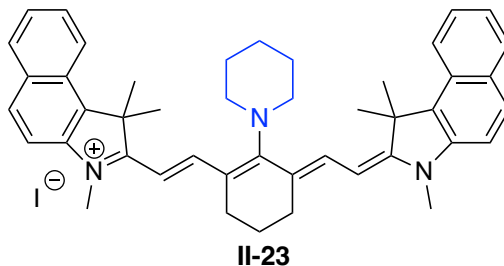
3-Ethyl-2-(CAN-2-(CAN-3-(CAN-2-(3-ethyl-1,1-dimethyl-1,3-dihydro-2H-benzo[e]indol-2-ylidene)ethylidene)-2-(152yrrolidine-1-yl)cyclohex-1-en-1-yl)vinyl)-1,1-dimethyl-1H-benzo[e]indol-3-ium iodide.

The title compound was prepared according to the general procedure at 0.1 mmol scale. Product was isolated as a dark solid (56 mg, 0.072 mmol, 72%).

¹H-NMR (500 MHz, Chloroform-*d*): δ 8.08 (d, *J* = 8.6 Hz, 2H), 7.75 (dd, *J* = 16.0, 8.4 Hz, 4H), 7.53 (d, *J* = 12.7 Hz, 2H), 7.44 (dd, *J* = 8.4, 6.8 Hz, 2H), 7.25 (t, *J* = 7.5 Hz, 2H), 7.08 (d, *J* = 8.7 Hz, 2H), 5.38 (d, *J* = 12.7 Hz, 2H), 4.34 (d, *J* = 6.4 Hz, 4H), 3.84 (q, *J* = 7.6, 7.0 Hz, 4H), 2.62 (t, *J* = 6.1 Hz, 4H), 2.12 (q, *J* = 4.7, 3.1 Hz, 4H), 1.99 (s, 12H), 1.81 (p, *J* = 6.4 Hz, 2H), 1.29 (t, *J* = 7.3 Hz, 6H).

¹³C-NMR (126 MHz, Chloroform-*d*): δ 172.74, 165.92, 140.25, 135.05, 130.89, 130.28, 129.65, 129.62, 128.76, 127.03, 123.10, 122.11, 120.64, 109.17, 91.03, 55.93, 48.99, 37.51, 28.81, 28.78, 24.30, 20.89, 11.50.

HRMS (ESI+): calcd for C₄₆H₅₂N₃⁺ [M]⁺ 646.4161, found 646.4163.



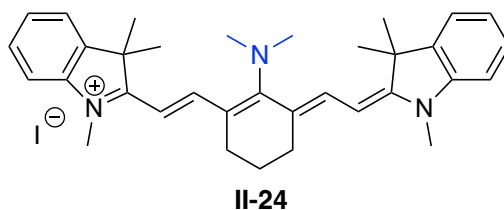
3-Ethyl-2-(CAN-2-(CAN-3-(CAN-2-(3-ethyl-1,1-dimethyl-1,3-dihydro-2H-benzo[e]indol-2-ylidene)ethylidene)-2-(piperidin-1-yl)cyclohex-1-en-1-yl)vinyl)-1,1-dimethyl-1H-benzo[e]indol-3-ium iodide.

The title compound was prepared according to the general procedure at 0.1 mmol scale. Product was isolated as a dark solid (66 mg, 0.084 mmol, 84%).

¹H-NMR (500 MHz, Chloroform-*d*): δ 8.06 (d, *J* = 8.6 Hz, 2H), 7.84 (d, *J* = 8.5 Hz, 4H), 7.68 (d, *J* = 13.3 Hz, 2H), 7.51 (ddd, *J* = 8.3, 6.8, 1.3 Hz, 2H), 7.34 (ddd, *J* = 8.0, 6.8, 1.0 Hz, 2H), 7.27 (d, *J* = 8.7 Hz, 2H), 5.78 (d, *J* = 13.3 Hz, 2H), 4.07 (q, *J* = 7.2 Hz, 4H), 3.79 (t, *J* = 4.8 Hz, 4H), 2.48 (t, *J* = 6.6 Hz, 4H), 1.95 – 1.80 (m, 20H), 1.40 (t, *J* = 7.2 Hz, 6H).

¹³C-NMR (126 MHz, Chloroform-*d*): δ 174.14, 169.56, 140.35, 139.77, 131.99, 131.07, 130.38, 129.99, 128.39, 127.46, 124.08, 124.04, 121.86, 110.03, 94.84, 56.78, 49.78, 38.85, 28.48, 28.23, 25.07, 24.57, 21.83, 12.18.

HRMS (ESI+): calcd for C₄₇H₅₄N₃⁺ [M]⁺ 660.4318, found 660.4318.

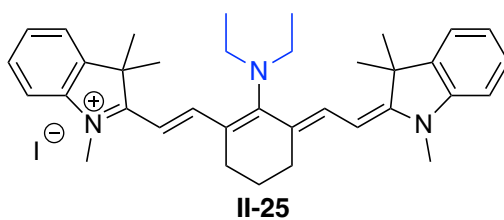


3-Ethyl-2-(CAN-2-(CAN-3-((Z)-2-(3-ethylbenzo[d]thiazol-2(3H)-ylidene)ethylidene)-2-(154yrrolidine-1-yl)cyclohex-1-en-1-yl)vinyl)benzo[d]thiazol-3-ium iodide.

The title compound was prepared according to the general procedure at 0.1 mmol scale. Product was isolated as a dark solid (29 mg, 0.046 mmol, 46%).

¹H NMR (500 MHz, Chloroform-*d*) δ 7.58 (dd, *J* = 8.3, 1.2 Hz, 2H), 7.42 (ddd, *J* = 8.6, 7.6, 1.2 Hz, 2H), 7.36 – 7.31 (m, 2H), 7.27 – 7.20 (m, 4H), 5.87 (d, *J* = 12.7 Hz, 2H), 4.24 (q, *J* = 7.3 Hz, 4H), 3.46 (s, 6H), 2.45 (t, *J* = 6.5 Hz, 4H), 1.84 – 1.80 (m, 2H), 1.47 (t, *J* = 7.2 Hz, 6H).

¹³C NMR (126 MHz, Chloroform-*d*) δ 141.48, 127.63, 124.71, 124.07, 122.31, 111.13, 92.69, 47.76, 41.33, 29.71, 22.01, 12.31.

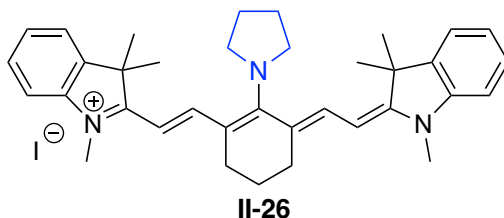


2-(CAN-2-(CAN-2-(diethylamino)-3-((Z)-2-(3-ethylbenzo[d]thiazol-2(3H)-ylidene)ethylidene)cyclohex-1-en-1-yl)vinyl)-3-ethylbenzo[d]thiazol-3-ium iodide.

The title compound was prepared according to the general procedure at 0.1 mmol scale. Product was isolated as a dark solid (38 mg, 0.058 mmol, 58%).

^1H NMR (500 MHz, Chloroform-*d*) δ 7.59 (d, $J = 8.0$, 1.2 Hz, 2H), 7.48 – 7.39 (m, 4H), 7.32 (d, $J = 8.2$ Hz, 2H), 7.26 – 7.20 (m, 2H), 6.02 (d, $J = 13.0$ Hz, 2H), 4.33 (q, $J = 7.3$ Hz, 4H), 3.59 (q, $J = 7.1$ Hz, 4H), 2.51 (t, $J = 6.3$ Hz, 4H), 1.85 (q, $J = 6.4$ Hz, 2H), 1.48 (t, $J = 7.3$ Hz, 6H), 1.31 (t, $J = 7.0$ Hz, 6H).

^{13}C NMR (126 MHz, Chloroform-*d*) δ 161.30, 142.65, 141.53, 127.87, 124.93, 124.41, 122.31, 122.21, 111.69, 111.14, 94.81, 49.60, 41.79, 29.71, 25.77, 21.93, 14.22.



3-Ethyl-2-(CAN-2-(CAN-3-((Z)-2-(3-ethylbenzo[d]thiazol-2(3H)-ylidene)ethylidene)-2-(155yrrolidine-1-yl)cyclohex-1-en-1-yl)vinyl)benzo[d]thiazol-3-ium iodide.

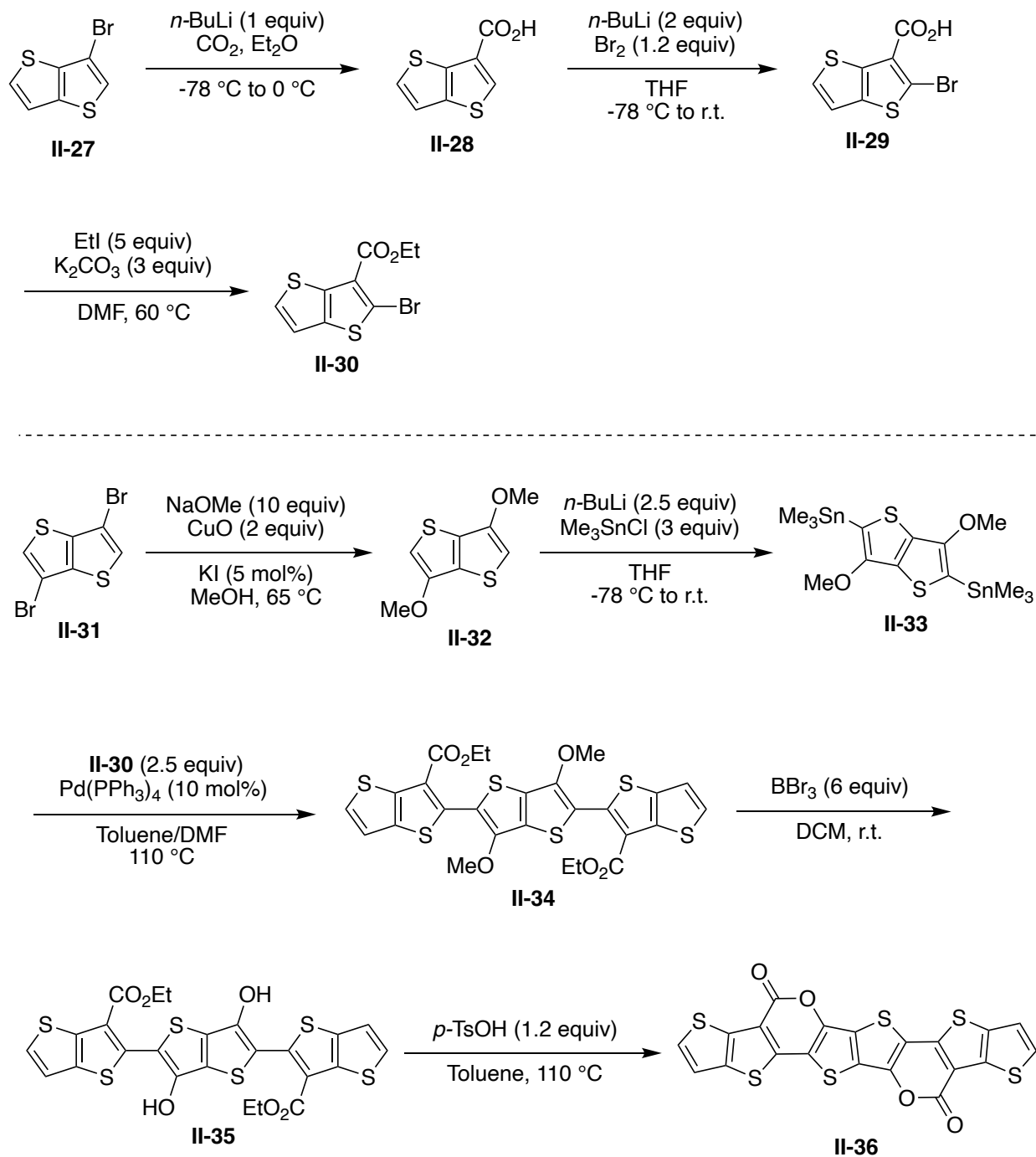
The title compound was prepared according to the general procedure at 0.1 mmol scale. Product was isolated as a dark solid (54 mg, 0.082 mmol, 82%).

^1H NMR (500 MHz, Chloroform-*d*): δ 7.47 (d, $J = 7.7$ Hz, 2H), 7.31 (t, $J = 7.7$ Hz, 2H), 7.14 – 7.05 (m, 4H), 7.02 (d, $J = 8.2$ Hz, 2H), 5.51 (d, $J = 12.0$ Hz, 2H), 4.17 (s, 4H), 4.04 (q, $J = 7.2$ Hz, 4H), 2.61 – 2.53 (m, 4H), 2.11 (s, 4H), 1.86 – 1.81 (m, 2H), 1.38 (t, $J = 7.2$ Hz, 6H).

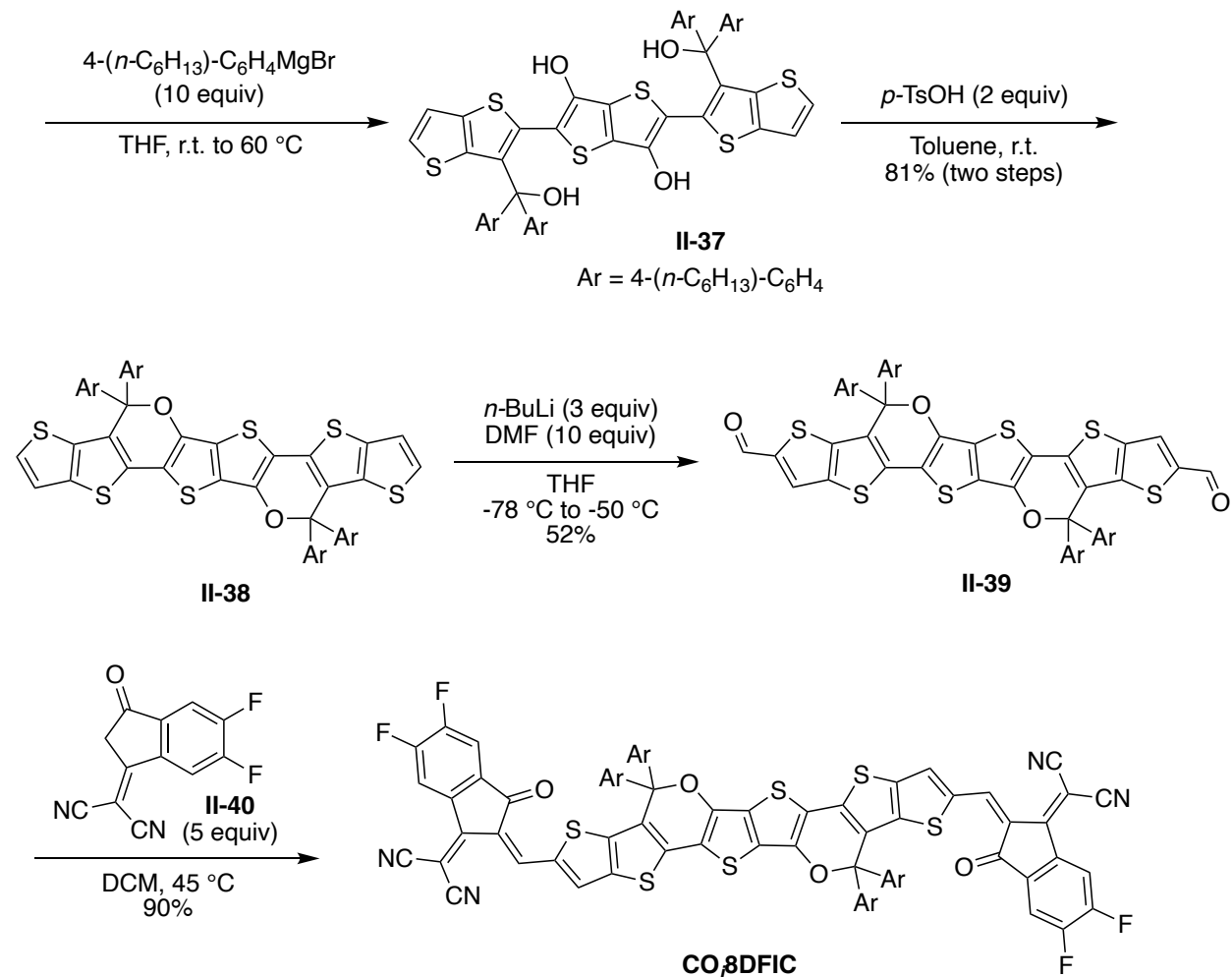
^{13}C NMR (126 MHz, Chloroform-*d*): δ 156.88, 141.65, 137.22, 126.98, 124.54, 122.91, 122.15, 119.87, 109.86, 88.91, 55.99, 40.37, 28.82, 24.62, 20.94, 11.73.

II-5-3 Synthesis of CO₈DFIC

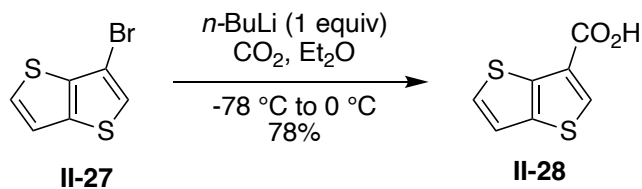
The dye **CO₈DFIC** was synthesized according to the following scheme:



II-5-3 Synthesis of CO₂DFIC (cont'd)



II-5-3-1 Synthesis of compound II-28



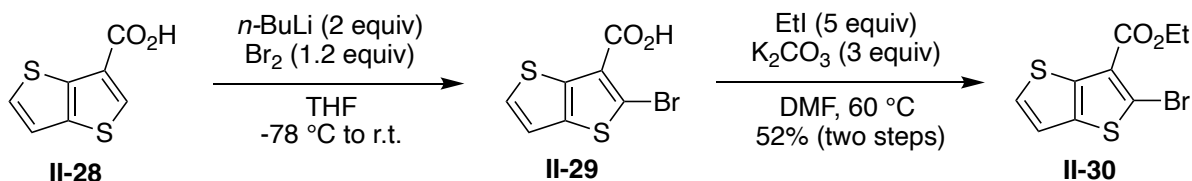
Following the reported procedure³¹ *n*-BuLi (2.5 M in hexane, 4 mL, 10 mmol) was added dropwise to a solution of 3-bromothiopheno[3,2-*b*]thiophene **II-27** (2.19 g, 10 mmol) in dry diethyl ether (30 mL) at -78 °C. The mixture stirred for 1 hour at this temperature and

then CO₂ gas was bubbled in the reaction for 30 minutes. The reaction warmed up to 0°C and 1 M, NaOH (100 mL) was added to quench it. The solution was extracted with diethyl ether (2 x 50 mL). The organic layers were discarded and 3 M, HCl was added to aqueous layer to adjust the pH at 3. The white solid was filtered and dried to give the product (1.43 g, 78%)

¹H NMR (500 MHz, Chloroform-*d*) δ 8.35 (d, *J* = 1.6 Hz, 1H), 7.53 (dd, *J* = 5.3, 1.6 Hz, 1H), 7.31 (d, *J* = 5.3 Hz, 1H).

¹³C NMR (126 MHz, Chloroform-*d*) δ 166.88, 139.08, 138.77, 136.79, 129.76, 124.94, 119.11.

II-5-3-2 Synthesis of compound II-30



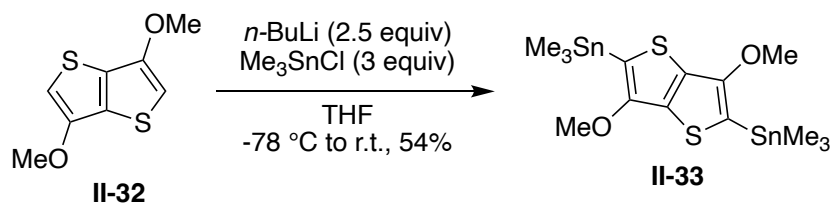
Following the reported procedure³¹ *n*-BuLi (2.5 M in hexane, 4.96 mL, 12.4 mmol) was added dropwise to a solution of **II-28** (1.14 g, 6.2 mmol) in dry THF (25 mL) at -78 °C. After stirring for 30 minutes at this temperature, bromine was added dropwise (333 μL, 7.5 mmol). The solution slowly warmed up to the room temperature and stirred overnight. The reaction was quenched with 3 M, HCl (10 mL) and extracted with diethyl ether (3 x 30 mL). The combined organic layers washed with NaCl, dried with anhydrous Na₂SO₄ and concentrated under reduced pressure to give the acid as a white solid. The

acid crude was dissolved in DMF (10 mL) and, ethyl iodide (4.85 g, 31 mmol) and K_2CO_3 (2.55 g, 18.6 mmol), were added. The reaction heated at 60 °C and stirred for 5 hours at this temperature. The solution cooled to room temperature then, the mixture extracted with DCM (25 mL) and H_2O (25 mL). The organic layer dried with anhydrous Na_2SO_4 and concentrated under reduced pressure. The crude product was then purified by column chromatography (silica, DCM/petroleum ether 30%) leading to bromo ester **II-30** with its regioisomer in a ~2:1 ratio. Recrystallization of the mixture was done by dissolving the material in pure DCM at room temperature, followed by slow addition of diethyl ether to a final 3:1 ratio in volume. The crystals formed after overnight standing at room temperature was collected and washed with cold diethyl ether to afford **II-30** (938 mg, 52%).

1H NMR (500 MHz, Chloroform-*d*): δ 7.52 (d, $J = 5.4$ Hz, 1H), 7.19 (d, $J = 5.4$ Hz, 1H), 4.46 (q, $J = 7.1$ Hz, 2H), 1.48 (t, $J = 7.1$ Hz, 3H).

^{13}C NMR (126 MHz, Chloroform-*d*): δ 161.12, 138.25, 136.43, 128.62, 124.04, 121.43, 118.57, 61.48, 14.27.

II-5-3-3 Synthesis of compound II-33



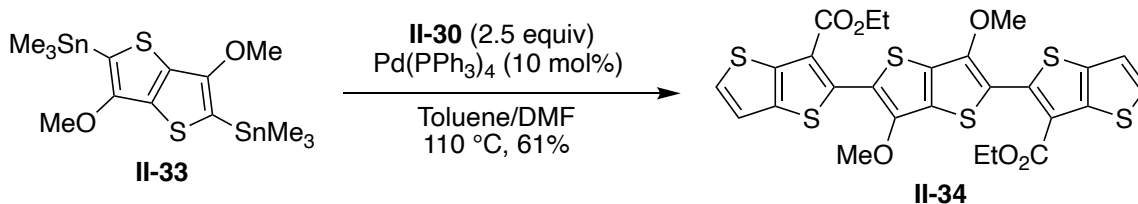
Following the reported procedure³⁰ compound **II-32** (1 g, 5 mmol) was dissolved in dry THF (100 mL) and $n\text{-BuLi}$ (2.5 M in hexane, 5 mL, 12.5 mmol) was added dropwise

at -78 °C under argon balloon. The mixture stirred for 1 hour at this temperature and then, warmed up to room temperature and stirred for additional 2 hours. The reaction brought to -78 °C before adding trimethyltin chloride (1 M in THF, 15 mL, 15 mmol). The solution was brought to the room temperature and stirred 16 hours. After completion, the mixture was poured into water (100 mL) and extracted with petroleum ether (3 × 100 mL). The combined organic layers dried with anhydrous Na₂SO₄ and concentrated under reduced pressure. The crude washed with cold methanol to give compound **II-33** as gray product (1.41 g, 54%)

¹H NMR (500 MHz, Chloroform-*d*): δ 3.98 (s, 6H), 0.38 (s, 18H).

¹³C NMR (126 MHz, Chloroform-*d*): δ 155.25, 136.09, 118.04, 59.58, 8.25.

II-5-3-4 Synthesis of compound II-34



Following the reported procedure³⁰ to a solution of **II-33** (736 mg, 1.4 mmol) and **II-30** (1.01 g, 3.5 mmol) in a mixture solvents of toluene (50 mL) and DMF (3.8 mL) was added Pd(PPh₃)₄ (162 mg, 0.14 mmol) under argon balloon. The reaction stirred at reflux for 48 hours and monitored by TLC. After the completion, the solution concentrated under reduced pressure. The crude product was then purified by column chromatography (silica, chloroform) leading to the pure product **II-34** as a yellow solid (530 mg, 61%).

^1H NMR (500 MHz, Chloroform-*d*) δ 7.50 (d, J = 5.3 Hz, 2H), 7.27 (d, J = 5.3 Hz, 2H), 4.39 (q, J = 7.1 Hz, 4H), 4.03 (s, 6H), 1.36 (t, J = 7.1 Hz, 6H).

^{13}C NMR (126 MHz, Chloroform-*d*) δ 161.90, 148.30, 141.28, 140.09, 137.35, 129.31, 128.28, 123.41, 118.91, 114.77, 61.15, 59.49, 14.23.

II-5-3-5 Synthesis of compound II-35

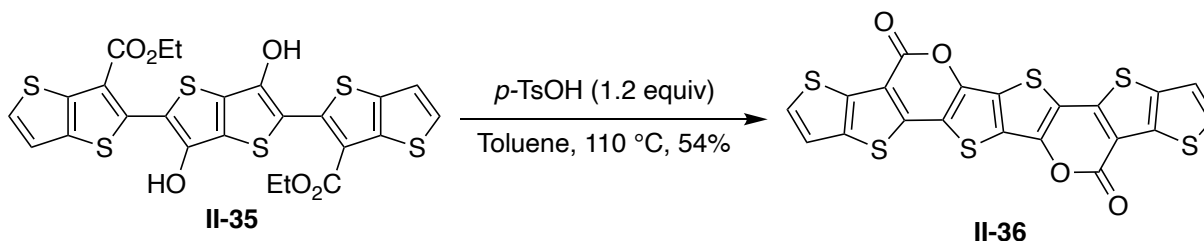


Following the reported procedure³⁰ In a flame dried flask, compound **II-34** (397 mg, 0.64 mmol) was dissolved in dry DCM (80 mL) and BBr_3 (1.75 M in DCM , 2.2 mL, 3.84 mmol) was added dropwise at room temperature under argon balloon. The reaction stirred for 2.5 hours and monitored by TLC. After completion, the solution was poured into methanol. A yellow precipitate was formed, filtered and dried to give compound **II-35** as a yellow solid (380 mg, 100%).

^1H NMR (500 MHz, $\text{DMSO-}d_6$) δ 10.78 (s, 2H), 7.77 (d, J = 5.3 Hz, 2H), 7.48 (d, J = 5.3 Hz, 2H), 4.27 (q, J = 7.1 Hz, 4H), 1.24 (t, J = 7.1 Hz, 6H).

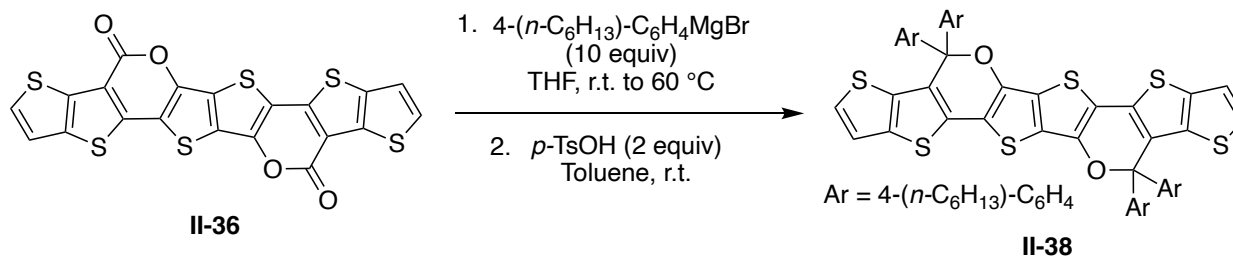
^{13}C NMR (126 MHz, $\text{DMSO-}d_6$) δ 166.78, 151.15, 147.27, 144.55, 141.70, 135.01, 133.02, 127.09, 125.09, 114.64, 65.93, 19.17.

II-5-3-6 Synthesis of compound II-36



Following the reported procedure³⁰ *p*-toluenesulfonic acid (133 mg, 0.7 mmol) was added in one portion to a suspension of di-ester **II-35** (380 mg, 0.64 mmol) in toluene (20 mL) at room temperature. The reaction heated to 110 °C and stirred for 1 hour. After that, the reaction solution was poured into methanol and the precipitate was filtered and dried to give product **II-36** as a dark red solid (173 mg, 54%). The analytical data didn't provided because of low solubility in solvents.

II-5-3-7 Synthesis of compound II-38



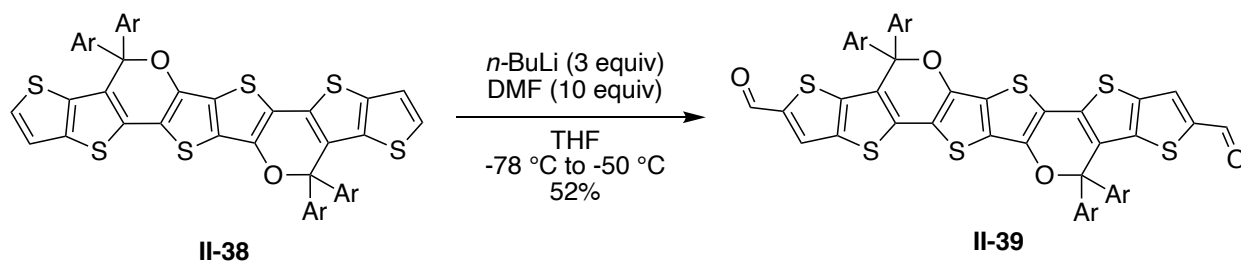
Following the reported procedure³⁰ In a flame dried flask, compound **II-36** (173 mg, 0.34 mmol) was suspended in dry THF (8 mL) under argon balloon. Then, 4-(*n*-C₆H₁₃)-C₆H₄MgBr (3.4 mL, 1M in THF, 3.4 mmol) was added dropwise at room temperature. The reaction heated at 60 °C and stirred for 12 hours. After completion, the solution cooled to the room temperature and was poured into ice water. The reaction was extracted with

DCM (3 x 15 mL). The combined organic layers dried with anhydrous Na₂SO₄ and concentrated under reduced pressure to give the tetra-hydroxy compound **II-37** which used in the next step without furthered purification. Crude compound **II-37** was dissolved in toluene (10 mL) and *p*-toluenesulfonic acid (129 mg, 0.68 mmol) was added in one portion. After stirring for 2 hours, the mixture was poured into methanol and formed a precipitate. The crude product was then purified by column chromatography (silica, chloroform) leading to the pure product **II-38** as a dark yellow solid (306 mg, 81%).

¹H NMR (500 MHz, Chloroform-*d*) δ 7.23 (d, *J* = 8.2 Hz, 8H), 7.18 (d, *J* = 5.3 Hz, 2H), 7.12 (d, *J* = 8.2 Hz, 8H), 7.10 (d, *J* = 5.3 Hz, 2H), 2.59 (t, *J* = 7.7 Hz, 9H), 1.62 – 1.58 (m, 8H), 1.33 – 1.26 (m, 24H), 0.88 (t, *J* = 6.5 Hz, 12H).

¹³C NMR (126 MHz, Chloroform-*d*) δ 143.79, 143.46, 139.76, 139.20, 135.14, 131.92, 128.27, 128.10, 126.82, 125.51, 124.71, 119.17, 114.45, 88.61, 35.65, 31.70, 31.23, 29.01, 22.61, 14.10.

II-5-3-8 Synthesis of compound II-39



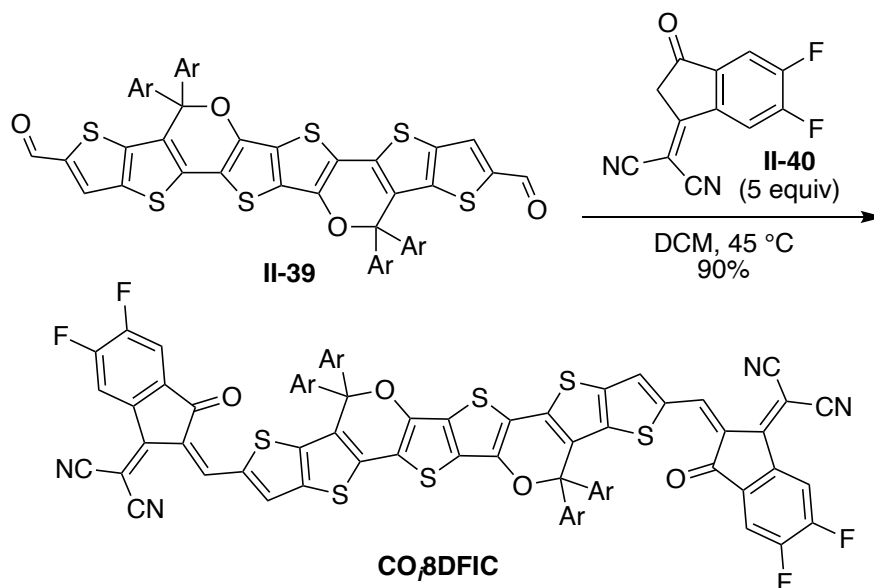
Following the reported procedure³⁰ compound **II-38** (275 mg, 0.24 mmol) was placed in dry THF (50 mL) at -78 °C under argon balloon and *n*-BuLi (0.3 mL, 2.5 M, 0.72

mmol) was added dropwise. The reaction warmed up to -50 °C and kept for 2 hours at this temperature and then, DMF (185 μ L, 2.4 mmol) was added slowly. After stirring for additional 1 hour, the reaction mixture quenched by addition of water. The reaction was extracted with DCM (3 x 70 mL). The combined organic layers dried with anhydrous Na_2SO_4 and concentrated under reduced pressure. The crude product was then purified by column chromatography (silica, DCM/petroleum ether 30%) leading to the pure product **I-39** as a red solid (145 mg, 52%).

^1H NMR (500 MHz, Chloroform-*d*) δ 9.80 (s, 2H), 7.82 (s, 2H), 7.21 (d, $J = 8.3$ Hz, 8H), 7.15 (d, $J = 8.3$ Hz, 8H), 2.61 (t, $J = 7.8$ Hz, 8H), 1.64 – 1.57 (m, 8H), 1.37 – 1.27 (m, 24H), 0.91 – 0.86 (t, $J = 6.2$ Hz, 12H).

^{13}C NMR (126 MHz, Chloroform-*d*) δ 182.64, 146.36, 145.37, 144.13, 144.07, 138.21, 138.12, 135.03, 128.76, 128.38, 128.13, 126.96, 124.85, 115.11, 88.91, 35.66, 31.69, 31.15, 29.05, 22.59, 14.11.

II-5-3-9 Synthesis of CO₈DFIC



Following the reported procedure³⁰ In a flame dried flask, compound **II-39** (80 mg, 0.068 mmol) was dissolved in dry DCM (20 mL) under argon balloon and compound **II-40** (78.2 mg, 0.34 mmol) and pyridine (0.5 mL) was added at room temperature and the reaction refluxed for 3 hours. The solvent removed under reduced pressure and the crude product was then purified by column chromatography (silica, chloroform) leading to the pure product **CO₈DFIC** as a black solid (98 mg, 91%).

¹H NMR (500 MHz, Chloroform-*d*) δ 8.66 (s, 2H), 8.49 (dd, *J* = 9.9, 6.4 Hz, 2H), 7.98 (s, 2H), 7.56 (t, *J* = 7.5 Hz, 2H), 7.27 (d, *J* = 8.3 Hz, 8H), 7.22 (d, *J* = 8.3 Hz, 8H), 2.64 (t, *J* = 7.8 Hz, 8H), 1.67 – 1.58 (m, 8H), 1.32 – 1.21 (m, 24H), 0.85 (t, *J* = 7.2 Hz, 12H).

¹³C NMR (126 MHz, cdcl₃) δ 185.17, 158.22, 155.42, 155.30, 153.96, 153.33, 153.21, 146.76, 144.43, 141.59, 137.87, 137.64, 137.21, 136.52, 136.46, 135.86, 134.40, 134.32,

128.58, 128.22, 128.06, 125.73, 121.48, 116.76, 114.91, 114.74, 114.37, 114.22, 112.50, 112.36, 89.27, 69.32, 35.73, 31.77, 31.31, 29.10, 22.62, 14.09.

II-5-4 Computational Supplementary

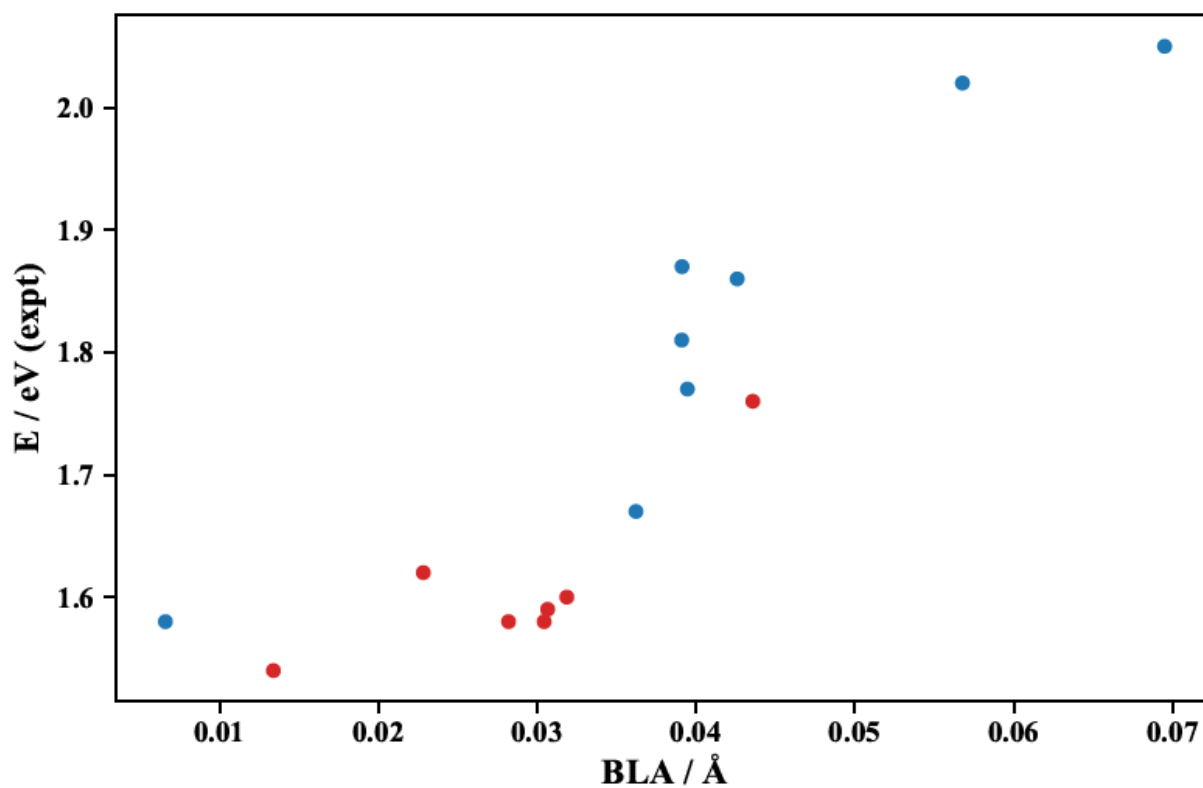


Figure II-24. Scatter plot of the experimental spectral energy maxima as a function of the DFT-optimized bond length alternation coordinate (in angstrom). Absorption and emission energies are shown by blue and red dots, respectively

Table II-9. Absolute energies of optimized geometries on the DFT level of theory (CAM-B3LYP/6-31G*)

Dye	Conformers	Geometries	S ₀ Energy / a.u.	S ₁ Energy / a.u.	S ₁ -S ₀ Gap / a.u.
1	-	Franck-Condon point	-1809.801264	-1809.710549	0.090715
		S ₁ minimum	-1809.800022	-1809.711759	0.088263
2	Bis-dipole	Franck-Condon point	-1484.092954	-1483.994624	0.098330
		S ₁ minimum	-1484.088437	-1483.998166	0.090271
	Cyanine-like	Franck-Condon point	-1484.098962	-1484.002956	0.096006
		S ₁ minimum	-1484.073807	-1484.010546	0.066895
3	Bis-dipole	Franck-Condon point	-1523.376682	-1523.280279	0.096404
		S ₁ minimum	-1523.355859	-1523.287972	0.067887
	Cyanine-like	Franck-Condon point	-1523.388981	-1523.293277	0.095704
		S ₁ minimum	-1523.386699	-1523.295906	0.090793
4	Bis-dipole	Franck-Condon point	-1522.160161	-1522.066705	0.093456
		S ₁ minimum	-1522.158405	-1522.068372	0.090032
	Cyanine-like	Franck-Condon point	-1522.144393	-1522.053229	0.091164
		S ₁ minimum	-1522.143264	-1522.054359	0.088905
5	Bis-dipole	Franck-Condon point	-1522.167762	-1522.069148	0.098614
		S ₁ minimum	-1522.164092	-1522.072413	0.091678
	Cyanine-like	Franck-Condon point	-1522.15922	-1522.06249	0.096730
		S ₁ minimum	-1522.156756	-1522.065402	0.091353
6	Bis-dipole	Franck-Condon point	-1562.663326	-1562.567549	0.095776
		S ₁ minimum	-1562.638213	-1562.577772	0.060441
	Cyanine-like	Franck-Condon point	-1562.679046	-1562.583593	0.095453
		S ₁ minimum	-1562.676662	-1562.586636	0.090026

Table II-9 (cont'd)

7	Bis-dipole	Franck-Condon point	-1561.475774	-1561.377488	0.098285
		S ₁ minimum	-1561.467923	-1561.382244	0.085679
	Cyanine-like	Franck-Condon point	-1561.476323	-1561.383757	0.092565
		S ₁ minimum	-1561.474749	-1561.385506	0.089244
8	Bis-dipole	Franck-Condon point	-1600.75445	-1600.657514	0.096936
		S ₁ minimum	-1600.735358	-1600.666551	0.068807
	Cyanine-like	Franck-Condon point	-1600.764007	-1600.667421	0.096586
		S ₁ minimum	-1600.761831	-1600.671054	0.090777

Table II-10. Important geometric parameters for CAM-B3LYP/6-31G* structures^a

Dye	State ^b	BLA (Å) ^c	Pyr. Ang. (°) ^d
2	GS	0.03912	0.002
	ES	0.03187	0.001
3	GS	0.03910	0.014
	ES	0.03066	0.177
4	GS	0.03622	43.354
	ES	0.02284	49.371
5	GS	0.05677	7.156
	ES	0.04358	15.927
6	GS	0.03948	0.002
	ES	0.03046	0.162
7	GS	0.06949	2.115
	ES	0.02820	0.1421
8	GS	0.04259	0.011
	ES	0.03044	0.002

[a] Geometric parameters are computed at the TD-CAM-B3LYP/6-31G* level.

[b] Ground and excited state structures are abbreviated GS and ES, respectively.

[c] BLA is defined:

$$BLA = (r_{2-3} + r_{4-5} + r_{5-6} + r_{7-8}) - (r_{1-2} + r_{3-4} + r_{6-7} + r_{8-9})$$

where r_{m-n} is the distance between carbon atoms m and n of the heptamethine chain.

[d] Pyramidalization angle is defined:

$$\text{Pyr. Ang.} = 360 - (\theta_{C_a-N-C_b} + \theta_{C_a-N-C_c} + \theta_{C_b-N-C_c})$$

where $\theta_{C_m-N-C_n}$ is the angle formed by carbon atom m , the amine nitrogen atom, and carbon atom n . Carbon atoms a, b, and c are the three atoms bound to the amine nitrogen.

Optimized Geometries (In Angstrom) (CAM-B3LYP/6-31G*)

Dye II-6

Franck-Condon point

H	-1.8122047363	7.8617759991	-4.0734638064	H	-0.5058554220	0.1762746719	-3.4647046816
C	-1.8885658517	7.7571257269	-2.9973907038	C	0.8274638321	-1.9281220617	-2.1372975518
C	-2.0977123043	7.5195855010	-0.1943131131	H	1.5401348873	-2.7572357300	-2.1432805184
C	-1.5805410273	6.5780285207	-2.3396678174	H	-0.1072651408	-2.3153014421	-2.5655569153
C	-2.3097886635	8.8313210674	-2.2157363357	C	1.3637691501	-0.7991433504	-3.0070891423
C	-2.4145080632	8.7186427030	-0.8326841532	H	2.3592303343	-0.5105714808	-2.6511314735
C	-1.6790260316	6.4475976258	-0.9601939778	H	1.4771424668	-1.1375048655	-4.0408753162
H	-2.5590540209	9.7698981915	-2.6989994384	H	1.5758340317	-8.7045217548	1.8190082965
H	-2.7445781100	9.5695668987	-0.2469190732	C	1.4527127162	-7.9816488751	2.6171381168
H	-2.1801280010	7.4365187621	0.8852505761	C	1.1494634786	-6.1236986440	4.7177388518
N	-1.1359439550	5.3464790509	-2.8765985895	C	1.2446640308	-6.6340116734	2.3756319053
C	-0.9387562285	4.4246386930	-1.9133545507	C	1.5055398628	-8.3895241746	3.9487167137
C	-1.2744680110	5.0457991120	-0.5529266509	C	1.3557432969	-7.4765064793	4.9881711833
H	-1.1551375073	6.0086721239	-4.8500764667	C	1.0967381914	-5.7080187554	3.4004053067
C	-0.9174701179	5.1068385910	-4.2909018971	H	1.6677492483	-9.4382214228	4.1735790517
H	0.1276003042	4.8444456937	-4.4778789502	H	1.4014334988	-7.8190314629	6.0161303798
H	-1.5610139722	4.2968443002	-4.6450756158	H	1.0344842690	-5.4151223072	5.5325471140
C	-0.5017049820	3.1374727919	-2.2094924200	C	0.8863612996	-4.3284344901	2.8109007433
H	-0.3360393304	2.9025363361	-3.2531726356	C	0.9583644703	-4.6308128373	1.3099608594
C	-0.2798926230	2.1399929468	-1.2605499057	C	0.8727221603	-3.7566275751	0.2315561753
H	-0.4665483542	2.3886580210	-0.2264750225	H	0.9806089092	-4.1831337698	-0.7575574117
C	0.1454077917	0.8390089862	-1.5253280819	N	1.1449076117	-5.9547676222	1.1385293714
C	0.2794583552	-0.1178267988	-0.5026038540	Cl	0.0120114314	0.4141819222	1.1538988063
C	0.5903489564	-1.4743302652	-0.7115233929	C	1.2437514955	-6.6043483577	-0.1550247418
C	0.6536917349	-2.3836175520	0.3427695877	H	2.1508599693	-6.2900184855	-0.6798795186
H	0.5043600367	-1.9852434443	1.3352902400	H	0.3713736927	-6.3607615168	-0.7665754440
C	0.4363151090	0.4064599149	-2.9482137777	H	1.2751958137	-7.6824307864	-0.0149812576
H	0.8922958286	1.2384331164	-3.4929264928	C	-2.4578987655	4.3284773985	0.1237101245
				H	-2.2025001414	3.3121237346	0.4306222355
				H	-3.3221027256	4.2792217449	-0.5437393294

H	-2.7545389226	4.8839698407	1.0176428033	C	1.6027491931	-8.4435386555	3.9019884434
C	-0.0438630977	5.0971373052	0.3724897326	C	1.4594250338	-7.5425672459	4.9573821272
H	0.7984062891	5.5902284603	-0.1195417588	C	1.1406978672	-5.7584722433	3.3973434203
H	0.2760956659	4.1018117033	0.6876470504	H	1.7859037933	-9.4917905491	4.1138613671
H	-0.2910738697	5.6703325922	1.2702073256	H	1.5315707359	-7.8964312555	5.9801586427
C	-0.4987013169	-3.7899176515	3.2194589581	H	1.1167938018	-5.4920828683	5.5315395721
H	-0.5503939565	-3.7226099313	4.3095047813	C	0.8961334508	-4.3756805601	2.8327114093
H	-1.2953986228	-4.4597538971	2.8857935991	C	0.9497463554	-4.6550051288	1.3313256540
H	-0.6926494535	-2.7950278773	2.8128676601	C	0.8382922812	-3.7697383551	0.2662583029
C	2.0130656832	-3.3790876646	3.2597204089	H	0.9400264854	-4.1871259063	-0.7284633812
H	2.9911838790	-3.7504596551	2.9433988209	N	1.1537932546	-5.9894019185	1.1384975327
H	2.0155832364	-3.3124722575	4.3510355982	Cl	-0.0684044162	0.4126970597	1.1854427190
H	1.8832463071	-2.3702311327	2.8623844067	C	1.2334987925	-6.6182348829	-0.1643407009
S₁ minimum				H	2.1215136949	-6.2787607268	-0.7077420939
H	-1.7241524533	7.8930069682	-4.1316849236	H	0.3428397738	-6.3811331555	-0.7532101028
C	-1.8260832499	7.7949377547	-3.0571133251	H	1.2886490736	-7.6978361355	-0.0433265298
C	-2.1029990560	7.5739591453	-0.2543158667	C	-2.5104927074	4.3927952959	0.0873717461
C	-1.5445436713	6.6086944850	-2.3861205184	H	-2.2744222423	3.3726702553	0.3970955130
C	-2.2518489680	8.8749753254	-2.2921565627	H	-3.3637699928	4.3561344407	-0.5945885533
C	-2.3906397709	8.7726115231	-0.9079041561	H	-2.8128869295	4.9521698583	0.9772567524
C	-1.6792274520	6.4917050975	-1.0008073740	C	-0.0971289943	5.1341926226	0.3905908313
H	-2.4793540858	9.8142764470	-2.7852696682	H	0.7627859309	5.6192217414	-0.0780556902
H	-2.7244412866	9.6316545439	-0.3358828787	H	0.2050981685	4.1358413974	0.7133761356
H	-2.2117474073	7.4987183821	0.8234939032	H	-0.3647665304	5.7084017766	1.2820895302
N	-1.1054072088	5.3843068006	-2.8984719857	C	-0.4923947328	-3.8660635922	3.2744820293
C	-0.9413415946	4.4562093194	-1.9140516424	H	-0.5224269534	-3.8011437447	4.3657582562
C	-1.3024613236	5.0904276637	-0.5715751863	H	-1.2826200326	-4.5501261224	2.9549363730
H	-1.0517800776	6.0316862379	-4.8765022882	H	-0.7132935131	-2.8743323284	2.8734518010
C	-0.8525848635	5.1297153301	-4.3024375016	C	2.0076547691	-3.4067169122	3.2847932551
H	0.1913878298	4.8401872717	-4.4572698724	H	2.9908702025	-3.7542081746	2.9578437105
H	-1.5030233524	4.3302340316	-4.6704664546	H	2.0154437800	-3.3479934562	4.3767681087
C	-0.5136058327	3.1624174296	-2.1900467168	H	1.8530012353	-2.3980600949	2.8962004464
H	-0.3288967220	2.9201599333	-3.2298873522	Dye II-10			
C	-0.3197106793	2.1589897674	-1.2319493192	Bis-dipole Franck-Condon point			
H	-0.5196159596	2.4083152150	-0.2007049485	H	6.3215188475	5.2264514052	2.1358302896
C	0.0966863475	0.8482053819	-1.4921153764	C	6.1269240781	4.3127500461	2.6858437135
C	0.2203687965	-0.1151037525	-0.4650101192	C	5.6481488793	1.9475159330	4.1400563841
C	0.5350985785	-1.4791998609	-0.6712131395	C	4.9542238981	3.5916666244	2.5321672990
C	0.6035534205	-2.3927176160	0.3852771127	C	7.0686429214	3.8231802533	3.5901424000
H	0.4503401196	-1.9981098223	1.3786186673	C	6.8378971539	2.6568304957	4.3115582237
C	0.3973315399	0.4092694466	-2.9081701072	C	4.7084307916	2.4236246717	3.2458439196
H	0.8494602025	1.2382766894	-3.4599477924	H	7.9958032916	4.3683442955	3.7323458773
H	-0.5445845793	0.1702478955	-3.4227719088	H	7.5850434739	2.2976902929	5.0106645933
C	0.7763829264	-1.9256021368	-2.0957294985	H	5.4697101027	1.0371917864	4.7051846563
H	1.4769579096	-2.7644348934	-2.1066405211	N	3.8486140666	3.8574264656	1.7000103461
H	-0.1638342362	-2.2956809243	-2.5291760769	C	2.8700943747	2.9211343375	1.8484456025
C	1.3246374855	-0.7971955320	-2.9593686595	C	3.3501037935	1.8707404110	2.8596199716
H	2.3183915629	-0.5116069223	-2.5966035916	H	4.6868880383	5.5382607524	0.8066374368
H	1.4425301115	-1.1358833387	-3.9925776808	C	3.7489759976	4.9867668484	0.8024484355
H	1.6371710632	-8.7379443644	1.7713074575	H	3.5533467437	4.6461386758	-0.2190520522
C	1.5177820321	-8.0251180489	2.5789972098	H	2.9439288453	5.6619464684	1.1106797833
C	1.2266384319	-6.1898442552	4.7067251560	C	1.6830060082	2.9938809261	1.1605693252
C	1.2832808435	-6.6724250524	2.3507318899				

H	1.5484799781	3.8397382323	0.4986545677	H	2.3125016016	2.7792075235	4.5539871532
C	0.6130511729	2.0647857587	1.2445386823	H	2.8895242416	1.1324792229	4.8418232955
H	0.7545608521	1.2119530056	1.8954050845	C	3.5130845349	0.4890972641	2.1999459214
C	-0.5394581445	2.1320713466	0.5059629066	H	4.1687145231	0.5480041277	1.3275681592
C	-1.5224544028	1.0588295908	0.5172710949	H	2.5555626630	0.0719361146	1.8778855322
C	-2.0283064989	0.6538850000	-0.7858666546	H	3.9626554266	-0.2071867880	2.9135717077
C	-2.1337696566	-0.6661759609	-1.1389490185	H	-2.3292483128	0.8298112021	3.6692245379
H	-1.8958576847	-1.4150077323	-0.3949327601	H	-3.5737903434	-0.3907413097	2.5951343671
C	-0.7223370154	3.2292361447	-0.5259077088	Bis-dipole S₁ minimum			
H	0.0827933283	3.1810717003	-1.2722333782	H	6.2944724021	5.2700623033	2.1738075222
H	-0.6240377296	4.2021997322	-0.0302970623	C	6.1159697783	4.3449909334	2.7097477896
C	-2.2196011665	1.7412271147	-1.8261153981	C	5.6809946465	1.9436900340	4.1263940721
H	-1.4955150932	1.6137252512	-2.6430152198	C	4.9489631451	3.6067236002	2.5499563118
H	-3.2127908390	1.6290215187	-2.2765976841	C	7.0674585898	3.8550344990	3.5990521876
C	-2.0674735268	3.1318115977	-1.2291149152	C	6.8595781457	2.6702952739	4.3020482201
H	-2.1469717956	3.8937491290	-2.0088085038	C	4.7270369559	2.4185210046	3.2478866723
H	-2.8775068505	3.3216225170	-0.5139709873	H	7.9874803581	4.4108962050	3.7457530566
H	-3.3141529468	-4.5092885177	-6.3566313334	H	7.6175654992	2.3112952746	4.9896047000
C	-3.0610030773	-4.9628087878	-5.4051925557	H	5.5217270798	1.0203958240	4.6757287419
C	-2.4095736757	-6.1770295345	-2.9475415726	N	3.8412265205	3.8673581456	1.7375857120
C	-2.7961652364	-4.2107803283	-4.2724655018	C	2.8792513357	2.9018284268	1.8704704128
C	-2.9937929818	-6.3505866767	-5.2855427082	C	3.3783455557	1.8484001071	2.8605876884
C	-2.6732464333	-6.9557245063	-4.0752128776	H	4.6279695639	5.6074657642	0.9117437325
C	-2.4733758141	-4.8008281260	-3.0552623514	C	3.7181550208	5.0132102830	0.8637192406
H	-3.1993080818	-6.9651415074	-6.1556623327	H	3.5685964175	4.6910939639	-0.1718063269
H	-2.6287691375	-8.0372477398	-4.0074773609	H	2.8732985834	5.6419105456	1.1639390162
H	-2.1598696571	-6.6517475750	-2.0029487630	C	1.6903028115	2.9590635877	1.1736690867
C	-2.2370934370	-3.7219056130	-2.0162456894	H	1.5450007948	3.8198111841	0.5318619846
C	-2.4932474604	-2.4493495848	-2.8352614130	C	0.6405629208	2.0074368296	1.2063559355
C	-2.4497027580	-1.1339522930	-2.4411741920	H	0.7662675307	1.1326004042	1.8318516237
H	-2.6740125141	-0.3867533100	-3.1916146488	C	-0.5289922578	2.1133096296	0.4748553140
N	-2.7955859667	-2.8106208773	-4.1136429689	C	-1.5761216493	1.1090073508	0.5213241513
N	-1.9274524637	0.4726691006	1.6558644866	C	-1.9918855208	0.6588668658	-0.7951063673
C	-1.4848551160	0.9032436024	2.9822399895	C	-2.0561722059	-0.6807338324	-1.1343076607
C	-2.9665741377	-0.5561501123	1.7041261233	H	-1.7873457226	-1.4048723601	-0.3749789816
H	-3.6023906478	-0.4935225088	0.8237057186	C	-0.7026193655	3.2245845651	-0.5422291651
H	-2.5373485092	-1.5611841516	1.7686316615	H	0.1144685821	3.1904070001	-1.2761281288
H	-1.1425072106	1.9352108877	2.9499542564	H	-0.6177252757	4.1943457865	-0.0359407534
H	-0.6806665694	0.2674224255	3.3659974103	C	-2.2057661612	1.7323639370	-1.8435466018
C	-3.0797554117	-1.8628860803	-5.1683426102	H	-1.4993896670	1.5917301524	-2.6735890103
H	-2.2337505338	-1.1830320633	-5.3107272104	H	-3.2086891674	1.6211510530	-2.2746373751
H	-3.9714878804	-1.2734453146	-4.9317505492	C	-2.0413558183	3.1297129207	-1.2614419011
H	-3.2542690222	-2.3967960613	-6.1000179403	H	-2.1040393383	3.8825158953	-2.0518452081
C	-0.7846582708	-3.7898074986	-1.5109326697	H	-2.8550742037	3.3348783475	-0.5565518198
H	-0.0782838078	-3.6795224159	-2.3374733078	H	-3.3653181364	-4.4946063491	-6.3577917813
H	-0.6052433715	-4.7615694186	-1.0422796804	C	-3.0902335136	-4.9576037353	-5.4171315638
H	-0.5677217574	-3.0142346887	-0.7720212631	C	-2.3837605445	-6.1971547799	-2.9824869073
C	-3.2403691337	-3.8751764339	-0.8600061976	C	-2.8061775901	-4.2143868300	-4.2772229871
H	-3.1004093136	-4.8480321425	-0.3805460626	C	-3.0133887492	-6.3431831644	-5.3141212270
H	-4.2697913759	-3.8234138254	-1.2234872705	C	-2.6653642312	-6.9620075113	-4.1154290450
H	-3.1097947914	-3.1032088409	-0.0975863704	C	-2.4561961114	-4.8207673062	-3.0698052354
C	2.4395273569	1.7946574543	4.0968085643	H	-3.2312528780	-6.9496361739	-6.1869791819
H	1.4500405630	1.4006210534	3.8537393142	H	-2.6137669246	-8.0440505651	-4.0626508143

H	-2.1132967775	-6.6825961504	-2.0492823849	C	3.2464804299	0.0600079245	-2.0724514297
C	-2.2064414034	-3.7557824937	-2.0221464206	H	3.0756938026	-0.5655453879	-2.9395131120
C	-2.4805291429	-2.4797493499	-2.8191056731	C	2.2120324196	0.1413881802	-1.1212948336
C	-2.4244964557	-1.1622885345	-2.4149020090	H	2.3960672273	0.7180832264	-0.2241229486
H	-2.6795144812	-0.4164233483	-3.1584308599	C	0.9487403591	-0.4021460087	-1.2672166687
N	-2.8107485067	-2.8273393918	-4.1017984256	C	-0.0312733741	-0.1984542065	-0.2438649364
N	-1.9954739498	0.5157664020	1.6787091377	C	-1.4223956996	-0.2281738623	-0.5865117230
C	-1.5754592741	0.9782354697	2.9921946294	C	-2.3835831770	-0.4582513256	0.3776812687
C	-3.0747941454	-0.4593876945	1.7107105916	H	-2.0209857252	-0.6394338082	1.3816151612
H	-3.6406132764	-0.4347191137	0.7815819324	C	0.5682548176	-1.0594573238	-2.5807017850
H	-2.7024400092	-1.4791479973	1.8702698711	H	1.1377399934	-1.9877462045	-2.7165667780
H	-1.1652607425	1.9845923254	2.9312102890	H	0.8821288091	-0.3932059469	-3.3939710765
H	-0.8233624472	0.3166698040	3.4402020808	C	-1.7299241805	-0.2133094288	-2.0642021939
C	-3.1175832437	-1.8705141571	-5.1422817171	H	-2.7949907743	-0.3556624834	-2.2495472765
H	-2.2722789839	-1.1930926949	-5.3004550050	H	-1.4581663504	0.7502157005	-2.5144867196
H	-4.0002057287	-1.2789212332	-4.8776420124	C	-0.9275719338	-1.3362233445	-2.7247905860
H	-3.3182761276	-2.3961625479	-6.0731531417	H	-1.1936609190	-2.2841362891	-2.2447120829
C	-0.7457117444	-3.8271664084	-1.5342246608	H	-1.1836413135	-1.4314900622	-3.7842734693
H	-0.0479510872	-3.7100155228	-2.3671922176	H	-8.8601125116	-1.2298646051	1.2478749849
H	-0.5616602168	-4.8023835893	-1.0740223819	C	-8.1874562275	-1.4041660965	2.0798153031
H	-0.5251480280	-3.0569610952	-0.7915062296	C	-6.4689079897	-1.8675700564	4.2653949643
C	-3.1885677799	-3.9206828030	-0.8470924270	C	-6.8147712799	-1.2549007594	1.9693684536
H	-3.0267146114	-4.8898034801	-0.3666416814	C	-8.6919375792	-1.7948116864	3.3194661145
H	-4.2247234481	-3.8841885227	-1.1928878953	C	-7.8486346722	-2.0250609270	4.4013737003
H	-3.0522257030	-3.1424178121	-0.0923973930	C	-5.9584475874	-1.4813073094	3.0405052059
C	2.4666184450	1.7379409591	4.0965692310	H	-9.7631091190	-1.9204805225	3.4365383872
H	1.4803650673	1.3461463793	3.8379838774	H	-8.2656005876	-2.3285841472	5.3553696145
H	2.3343126284	2.7107832784	4.5767576597	H	-5.8122197509	-2.0482254971	5.1114428211
H	2.9177048182	1.0595719194	4.8263981706	C	-4.5283696000	-1.2285535756	2.6072794284
C	3.5619789022	0.4738453358	2.1857634710	C	-4.7194456261	-0.8474745692	1.1335076683
H	4.2183518854	0.5501356938	1.3152690746	C	-3.7783057430	-0.5193966017	0.1792784700
H	2.6095808086	0.0489161538	1.8600947501	H	-4.1516356701	-0.2844805431	-0.8090251908
H	4.0193445677	-0.2230073348	2.8942785740	N	-6.0469018271	-0.8751314570	0.8481113998
H	-2.4424303045	0.9966556558	3.6576259708	N	0.3684279600	0.0530629951	1.0458984945
H	-3.7499567241	-0.2164932098	2.5355081436	C	1.4689163581	-0.6451679652	1.6929493439
Cyanine-like Franck-Condon point				H	1.1008963868	-1.1106851585	2.6157992688
H	7.8399089996	1.0278848789	-4.4058463663	H	2.2812702991	0.0374820038	1.9703441738
C	7.6869688737	1.5416551392	-3.4637916045	C	-0.2558424258	1.0508357797	1.9008757159
C	7.3239505095	2.8913625955	-1.0157629315	H	-0.7126102020	0.6008008875	2.7905771657
C	6.5322419732	1.3904069421	-2.7142348293	H	-1.0140682186	1.6034137501	1.3496287685
C	8.6697853026	2.3929924040	-2.9609109413	H	1.8628751851	-1.4217816528	1.0406041243
C	8.4957938634	3.0617104887	-1.7536791329	H	0.5118777826	1.7543017555	2.2473177485
C	6.3423353640	2.0508671574	-1.5061946335	C	-6.6002442164	-0.5585262264	-0.4519335895
H	9.5854390807	2.5328272539	-3.5255669212	H	-6.2300143875	-1.2556281632	-1.2100101420
H	9.2754177071	3.7184468904	-1.3836024409	H	-6.3326128217	0.4609916853	-0.7450690605
H	7.1915032763	3.4138980614	-0.0729351548	H	-7.6846346704	-0.6334951240	-0.4120742630
N	5.3902017048	0.6049292118	-2.9847304591	C	4.1082913911	2.9237004799	-0.7744188655
C	4.4574066214	0.7232998580	-2.0087365980	H	3.1219281770	2.6799426858	-0.3738683611
C	4.9919631498	1.6739685957	-0.9306460581	H	3.9721058230	3.4315985504	-1.7325794895
H	6.1069609319	-0.1290505191	-4.7954123024	H	4.5879942388	3.6259038901	-0.0867804061
C	5.2252898101	-0.2185257542	-4.1648692185	C	5.1825520191	0.9482858585	0.4142327046
H	5.0995565331	-1.2691152322	-3.8865708182	H	5.8133578050	0.0635704285	0.2966484756
H	4.3515789202	0.1035736100	-4.7396118049	H	4.2302969227	0.6343664433	0.8474003026

C	-1.0132567106	5.8858109670	-1.8291055396	H	1.4227146705	2.7068226130	1.5146061526
H	-0.5838778020	5.2290312277	-2.5931694872	H	2.2794909495	4.0163679457	2.3395217453
H	-2.0870622010	5.6847455907	-1.7543157255	C	3.1921805171	-2.3761275035	1.8686470760
C	-0.9848247217	3.3774699128	-0.3892271325	H	3.9114511771	-2.1418171324	1.0797715912
H	-1.4877318775	3.4859248069	-1.3416263665	H	3.7218404486	-2.3505538542	2.8253803278
C	-1.0355557380	2.0949263387	0.2352831481	H	2.4338242322	-1.5894855693	1.8822323760
H	-0.5614260943	2.0199253799	1.2079656105	C	1.5674642229	-4.1126087557	2.7671598565
C	-1.5649690546	0.9500565922	-0.2797057048	H	2.0810155845	-4.1406750740	3.7323000551
C	-1.4222861005	-0.3184782174	0.4491315839	H	1.1149956442	-5.0931527017	2.5982431113
C	-0.8032913401	-1.4128052238	-0.2866409200	H	0.7649556790	-3.3742473126	2.8367870417
C	0.1623061583	-2.1898518900	0.3000501190	H	-2.7507044175	-1.7800264964	3.0287246837
H	0.4189523059	-1.9596491487	1.3268253035	C	-4.1307422769	0.4369705616	2.1288401351
C	-2.0684565200	0.8153041246	-1.6989021287	H	-4.3361219559	0.6199469743	1.0709200920
H	-2.0671574713	1.7855773368	-2.1962737617	H	-4.6913115553	1.1689925384	2.7161723427
H	-3.1095631009	0.4650383315	-1.7032350485	H	-4.5065656223	-0.5567573812	2.3873734796
C	-1.1670746961	-1.5247492977	-1.7564935110	Bis-dipole S₁ minimum			
H	-0.4656043595	-2.1861096166	-2.2665109806	H	-0.4532525559	8.5786797297	-1.0704564991
H	-2.1554587831	-1.9962220875	-1.8474842580	C	0.1180083780	8.1684684061	-0.2463105941
C	-1.1980219689	-0.1747848298	-2.4707864257	C	1.6424716894	7.1234910824	1.8904819167
H	-0.1812521655	0.2255960490	-2.5479315155	C	0.0668152499	6.8272897032	0.1050174762
H	-1.5772833236	-0.3041587699	-3.4894848526	C	0.9540494412	8.9882635779	0.5050680393
H	4.5248856260	-6.9748976954	-0.9022278732	C	1.7059506410	8.4770200108	1.5611087817
C	4.5352421802	-6.4741292991	0.0590587290	C	0.8165667852	6.2983085393	1.1499973505
C	4.5881680010	-5.1982374667	2.5704980977	H	1.0204303587	10.0423342155	0.2593245141
C	3.6478316715	-5.4586683970	0.3755761381	H	2.3485120888	9.1393467373	2.1307498809
C	5.4621720384	-6.8442380850	1.0328018063	H	2.2333970918	6.7335229580	2.7133880049
C	5.4934321507	-6.2181785362	2.2741011044	N	-0.6929361082	5.7885422128	-0.4724475533
C	3.6656331114	-4.8234285938	1.6122904688	C	-0.4527172852	4.6042674828	0.1276482441
H	6.1692136251	-7.6370551183	0.8124188778	C	0.5500170447	4.8133705716	1.2634035274
H	6.2240208206	-6.5238043793	3.0149930411	H	-1.7703470656	7.0511795549	-1.7279398917
H	4.6142772466	-4.7109995028	3.5409866031	C	-1.6116404624	5.9856554875	-1.5809381117
C	2.5758929042	-3.7697414351	1.6560954686	H	-1.2069375659	5.5539547096	-2.5003093511
C	1.9562358109	-3.9132178004	0.2581626089	H	-2.5747185682	5.5248989088	-1.3536450397
C	0.9158075403	-3.2240524850	-0.3160183330	C	-1.0635256978	3.4281088617	-0.3019269808
H	0.6452324610	-3.5046056936	-1.3251377958	H	-1.7410642502	3.5060109116	-1.1433015491
N	2.6229194471	-4.8958697551	-0.4107741150	C	-0.8717340758	2.1529661314	0.2575939215
N	-1.8475648574	-0.4467786493	1.7064891941	H	-0.2083210704	2.0576705694	1.1085215263
C	-2.6416000711	0.5856624595	2.4172196590	C	-1.4990762239	0.9939571199	-0.1566213093
H	-2.3111369530	1.5774463984	2.1390802721	C	-1.2210034282	-0.3011688339	0.5095357307
C	-1.8373720156	-1.7175076431	2.4359143398	C	-0.3666715342	-1.1664521797	-0.2166985757
H	-0.9850060261	-1.7732312925	3.1191486000	C	0.4107270457	-2.1279807851	0.4062686962
H	-1.8021102247	-2.5567937248	1.7450348019	H	0.4682457011	-2.0617397140	1.4873770941
H	-2.4304628951	0.4607675122	3.4818457389	C	-2.1753479186	0.8173246897	-1.4721063686
C	2.3133402620	-5.2984355792	-1.7649351601	H	-2.5275336826	1.7404204024	-1.9417964615
H	2.4135734389	-4.4512496674	-2.4508480279	H	-3.0241955577	0.1327989040	-1.3772334788
H	1.2929550383	-5.6894418080	-1.8309333906	C	-0.4612436932	-1.1103422935	-1.7400184374
H	3.0034335775	-6.0788990452	-2.0781490010	H	0.5238784542	-1.2728971369	-2.1892936565
C	-0.4533071459	4.4424489065	2.6579581046	H	-1.0775037898	-1.9638107782	-2.0563404667
H	-0.7585849409	3.3981579770	2.7643488327	C	-1.0627163765	0.1695143975	-2.3439881812
H	-1.3537394252	5.0606262457	2.6150754495	H	-0.2745249467	0.9177676140	-2.4799728684
H	0.1021843479	4.7189687059	3.5586334711	H	-1.4696156421	-0.0463369645	-3.3368654584
C	1.6801458991	3.7675661471	1.4590519373	H	4.5206067783	-7.1251273994	-0.8832533029
H	2.3023028173	3.9210655849	0.5736788076	C	4.4879734046	-6.6992332237	0.1132092196

C	4.4508219831	-5.5971330974	2.7039363311	H	-2.1512618813	-3.6641150189	-9.6070480070
C	3.6158175238	-5.6746018218	0.4503108907	H	-1.6775437117	-1.2528607769	-9.8355983383
C	5.3475780046	-7.1695128177	1.1056059002	H	-1.1415411654	0.1140687677	-7.8365363781
C	5.3355572456	-6.6299029874	2.3867671902	N	-1.4927143871	-3.2864422202	-5.0209809218
C	3.5944403075	-5.1232064061	1.7298439727	C	-1.1663449335	-2.2310423835	-4.2361346069
H	6.0418998756	-7.9683015674	0.8660605529	C	-1.0313359815	-0.9845679304	-5.1196438513
H	6.0177748155	-7.0070074676	3.1407203254	H	-1.9760894589	-5.2837226062	-5.3471667033
H	4.4434862345	-5.1741756045	3.7044999223	C	-1.7015509728	-4.6302398972	-4.5222140191
C	2.5503961411	-4.0247643797	1.7909539448	H	-0.7879868553	-5.0162567535	-4.0595579426
C	2.0300683031	-4.0172854837	0.3479986770	H	-2.5079084206	-4.6431797820	-3.7833049730
C	1.1264722528	-3.1713931290	-0.2400618506	C	-0.9885172228	-2.3634980052	-2.8716853373
H	0.9536010289	-3.3030973819	-1.3031846450	H	-1.1087442046	-3.3557035574	-2.4549430569
N	2.6613052045	-5.0254084999	-0.3442886575	C	-0.6529071314	-1.3278351999	-1.9800078063
N	-1.8489380832	-0.6413597270	1.6975658000	H	-0.5981058570	-0.3205734530	-2.3724701834
C	-2.4543068791	0.3626628885	2.5598116825	C	-0.3270607356	-1.4974951296	-0.6463692796
H	-1.7933054939	1.2324541548	2.6066552567	C	0.0187370023	-0.3587836033	0.1474907682
C	-2.3293460069	-1.9963348600	1.9382871043	C	0.8471979016	-0.5360398889	1.3037718195
H	-2.0111943273	-2.3480127021	2.9258606402	C	0.8274151905	0.3875079052	2.3291079663
H	-1.9311411289	-2.6748211506	1.1873285739	H	0.1480349166	1.2217337008	2.2055727973
H	-2.4841645401	-0.0585613726	3.5707978246	C	-0.1903543239	-2.9019266367	-0.0877179213
C	2.3968602266	-5.3366039608	-1.7273455211	H	0.4174582235	-3.4858099465	-0.7901701731
H	2.7800269086	-4.5572123249	-2.3971531045	H	-1.1713923640	-3.3935081163	-0.0606714930
H	1.3196949195	-5.4401416258	-1.8909869741	C	1.5315775139	-1.8760658079	1.4167527753
H	2.8725194173	-6.2818530779	-1.9845585781	H	2.2814444865	-2.0036333788	0.6255470444
C	-0.0727283832	4.4878544772	2.6355820375	H	2.0570542121	-1.9747032808	2.3670642510
H	-0.2875026236	3.4230716980	2.7439679572	C	0.4619648561	-2.9635415378	1.2936192334
H	-1.0002228132	5.0448476928	2.7906432370	H	0.8935728812	-3.9565318392	1.4514179590
H	0.6271127262	4.7729807525	3.4253543849	H	-0.2840314147	-2.8101531348	2.0808401879
C	1.8530936020	4.0233207546	1.0356750717	H	3.2219132597	1.6027463397	8.3341318739
H	2.2892079335	4.2538306188	0.0604349234	C	2.4337720742	2.2332131627	7.9388140414
H	1.6963818126	2.9447401322	1.0954218061	C	0.3775487044	3.8861507157	6.9467272032
H	2.5805588329	4.3016885068	1.8027959794	C	1.8927896380	2.0430568889	6.6779328395
C	3.2075462256	-2.6871013993	2.1726877206	C	1.9216646577	3.2795832700	8.7046593880
H	4.0167449179	-2.4411113960	1.4802499531	C	0.9073119997	4.0986629843	8.2201144143
H	3.6327205253	-2.7568656156	3.1785767615	C	0.8772408410	2.8509586445	6.1796518474
H	2.4892326358	-1.8646799306	2.1622691737	H	2.3248642773	3.4528156785	9.6968330645
C	1.4469322250	-4.4093089401	2.7940676086	H	0.5252517638	4.9056511779	8.8356787001
H	1.8813543015	-4.5362296972	3.7900350270	H	-0.4158572676	4.5264208367	6.5720674984
H	0.9763851692	-5.3545836482	2.5112563111	C	0.5056946470	2.3932461411	4.7829562335
H	0.6679365984	-3.6458512713	2.8593249000	C	1.4505889743	1.1995672511	4.5934654760
H	-3.4251631690	-2.0376251868	1.9008934514	C	1.5695284827	0.3327845348	3.5270960440
C	-3.8610105062	0.7985463781	2.1515380613	H	2.2980480167	-0.4614916209	3.6260540390
H	-3.8543824717	1.2837245372	1.1708956817	N	2.2200635114	1.0744053940	5.7058401301
H	-4.2665043269	1.5078836608	2.8794107771	N	-0.4357245103	0.8884999883	-0.2107539562
H	-4.5451399896	-0.0528919475	2.1034539423	C	0.3989497102	2.0918338845	-0.1582115458
Cyanine-like Franck-Condon point				H	-0.0551046996	2.8270635131	0.5199076602
H	-2.1005241148	-4.7622497151	-7.3991372083	C	-1.8078395211	1.1170270608	-0.6478456973
C	-1.8907795622	-3.7019818633	-7.4808085848	H	-2.2357284377	1.9317129005	-0.0503550591
C	-1.3488160721	-0.9468748815	-7.7319381318	H	-2.4005859698	0.2177948590	-0.4896161633
C	-1.5880776930	-2.9169382047	-6.3807155187	H	1.3671591172	1.8151492223	0.2560976690
C	-1.9176060082	-3.0757053449	-8.7261106551	H	-1.8850085714	1.4042077206	-1.7006666506
C	-1.6508486131	-1.7167005830	-8.8556635321	C	3.2365967768	0.0576351879	5.8751823804
C	-1.3183978156	-1.5582053445	-6.4926317738	H	3.9670742169	0.1086199845	5.0626365994

H	2.7897176437	-0.9415729631	5.8902115007	H	2.2195702968	-2.1066173754	0.9424059749
H	3.7573232526	0.2207202211	6.8162004744	H	1.7216487627	-2.1138315440	2.6305504833
C	-2.0859470243	0.0809929000	-4.7692871967	C	0.3113796434	-3.0570290884	1.2945119008
H	-1.9115796245	0.5214155691	-3.7851677950	H	0.7072536526	-4.0564652097	1.4980595685
H	-3.0937187106	-0.3419723010	-4.7824424673	H	-0.5505368086	-2.9115793574	1.9548381476
H	-2.0484857507	0.8858377074	-5.5085644724	H	3.2191652402	1.6463332489	8.3681307749
C	0.3918581898	-0.4022046741	-5.0686434205	C	2.4530719108	2.2960416596	7.9612410777
H	1.1364053041	-1.1597246487	-5.3264488151	C	0.4495655636	4.0011292695	6.9364482210
H	0.6350879035	-0.0073330767	-4.0795379694	C	1.8840835775	2.0827433485	6.7089344646
H	0.4797924548	0.4150587646	-5.7901357418	C	1.9980514273	3.3867322351	8.6934920089
C	0.8007629770	3.5153538382	3.7707151242	C	1.0089007887	4.2333414302	8.1938936532
H	1.8513944759	3.8141360559	3.8106060746	C	0.8915436710	2.9223335748	6.1963365643
H	0.1916321156	4.3919266691	4.0087637388	H	2.4227553339	3.5789992387	9.6731129031
H	0.5701771173	3.2130126951	2.7468030600	H	0.6720687963	5.0766563540	8.7869201306
C	-0.9723039258	1.9688819478	4.7337436276	H	-0.3226201108	4.6614518440	6.5526676619
H	-1.6055997601	2.8182999203	5.0048418029	C	0.4786076907	2.4366175388	4.8226235748
H	-1.1724178117	1.1597880819	5.4407100813	C	1.3693645444	1.2056824785	4.6597798875
H	-1.2686019070	1.6326064673	3.7372698977	C	1.4395991407	0.2965465000	3.6208297427
C	0.5979544677	2.7262383099	-1.5326762986	H	2.1373413430	-0.5226931435	3.7452241340
H	1.2747421460	3.5807697203	-1.4445949285	N	2.1523469083	1.0798884015	5.7771819520
H	-0.3375751835	3.0929698044	-1.9627704872	N	-0.4138307717	0.8451831142	-0.1570546973
H	1.0451576755	2.0110627188	-2.2299502246	C	0.5102319947	1.9736960081	-0.2104355894
Cyanine-like S₁ minimum				H	0.0476477606	2.8362976153	0.2892233062
H	-2.0970446081	-4.6902095948	-7.4782609148	C	-1.7733732207	1.1183231943	-0.5881005168
C	-1.9021996453	-3.6260813122	-7.5451102684	H	-2.1918711274	1.9329434053	0.0178917163
C	-1.3854720052	-0.8588300070	-7.7581772764	H	-2.3904697771	0.2312568883	-0.4468425432
C	-1.5956659749	-2.8533611329	-6.4298393378	H	1.4050127869	1.7146895604	0.3575460660
C	-1.9468348277	-2.9817905848	-8.7770282746	H	-1.8464600159	1.4225336965	-1.6394494152
C	-1.6932037751	-1.6156647824	-8.8895928124	C	3.1263227587	0.0264250502	5.9656844603
C	-1.3367970025	-1.4848865904	-6.5278708430	H	3.8498110905	0.0253302116	5.1446984555
H	-2.1825661647	-3.5581028278	-9.6654884833	H	2.6364397436	-0.9522878013	6.0082307258
H	-1.7349384697	-1.1382159683	-9.8625478033	H	3.6616911574	0.1897905190	6.8983055673
H	-1.1875515728	0.2048936526	-7.8502189386	C	-2.1045889667	0.1251303952	-4.7736480906
N	-1.4872054978	-3.2373196669	-5.0900133043	H	-1.9363710906	0.5322028158	-3.7742653267
C	-1.1493215210	-2.1834508791	-4.2888999153	H	-3.1101520559	-0.3017076038	-4.8059613981
C	-1.0419746810	-0.9267371683	-5.1516846738	H	-2.0658403312	0.9538259288	-5.4864862180
H	-2.0700901405	-5.2065655661	-5.4212701803	C	0.3733692790	-0.3198049775	-5.1049298558
C	-1.6914873016	-4.5879389045	-4.6104672367	H	1.1279974939	-1.0608875930	-5.3801300437
H	-0.7531453661	-5.0195167960	-4.2458605031	H	0.6152036552	0.0630123933	-4.1111612297
H	-2.4243132813	-4.5939809003	-3.7984661582	H	0.4410341779	0.5110386917	-5.8132312727
C	-0.9311178750	-2.3395435227	-2.9278107831	C	0.7870635377	3.5160863397	3.7651769199
H	-1.0067926177	-3.3484292438	-2.5383924732	H	1.8480259103	3.7783313334	3.7680968181
C	-0.6105318512	-1.3246390990	-2.0097442447	H	0.2142298338	4.4206335000	3.9889261626
H	-0.5847418988	-0.3012846746	-2.3594772977	H	0.5170013384	3.1872723276	2.7591877842
C	-0.2679060446	-1.5383001260	-0.6705250671	C	-1.0175227639	2.0666745421	4.8072486737
C	0.0068957715	-0.4364066360	0.1874452654	H	-1.6163980320	2.9518708180	5.0404420947
C	0.7173421418	-0.6352124580	1.4221007934	H	-1.2404706793	1.3009361502	5.5544094162
C	0.7061610458	0.3368879953	2.4140193668	H	-1.3313507283	1.6935775965	3.8296443867
H	0.0641848206	1.1903600922	2.2341339558	C	0.9113533541	2.3611882493	-1.6331406495
C	-0.1154677799	-2.9585779392	-0.1670631066	H	1.5981337313	3.2128570774	-1.6123407007
H	0.6343178343	-3.4628485860	-0.7918299216	H	0.0470026708	2.6504826645	-2.2379443620
H	-1.0508939863	-3.5115408531	-0.3188751446	H	1.4201589976	1.5296805650	-2.1305704993
C	1.3561731918	-1.9855660070	1.6106145897				

Dye II-12

Bis-dipole Franck-Condon point

H	-5.9127742892	-5.5544325253	-3.7623788414
C	-5.3216751816	-5.8525759240	-2.9040518722
C	-3.7981683100	-6.6634609513	-0.6749012102
C	-4.4814805952	-4.9749303783	-2.2391883162
C	-5.3877310236	-7.1608561557	-2.4270548777
C	-4.6385868000	-7.5660617912	-1.3272878752
C	-3.7243998087	-5.3641534627	-1.1403665206
H	-6.0374240386	-7.8720101129	-2.9260896434
H	-4.7086424163	-8.5892724504	-0.9748399247
H	-3.2149063761	-6.9833548169	0.1837474667
N	-4.2266031565	-3.6120317634	-2.5043682255
C	-3.3313803084	-3.0897192842	-1.6298359844
C	-2.9129466155	-4.1852487597	-0.6413875253
H	-5.4144087179	-2.0134122955	-3.1677006144
C	-4.8484603839	-2.8577819231	-3.5729873656
H	-4.0939393900	-2.4798225436	-4.2694395094
H	-5.5327410809	-3.5022112725	-4.1203484788
C	-2.9276423416	-1.7702968940	-1.6998983997
H	-3.3519820658	-1.1712343329	-2.4956820730
C	-2.0087285105	-1.1477251054	-0.8346736365
H	-1.5766405365	-1.7500997762	-0.0466273599
C	-1.5596276116	0.1552200347	-0.9430649063
C	-0.5594951395	0.6431071972	-0.0450186756
C	0.2089884200	1.8061173050	-0.3622671183
C	1.4046895046	2.0690708025	0.2826867827
H	1.7232529198	1.3740629888	1.0469957324
C	-2.0312972889	1.0400630257	-2.0749764256
H	-3.1098413095	0.9093309728	-2.2118349865
H	-1.5625887489	0.7283781504	-3.0192488028
C	-0.2500755328	2.6904155159	-1.5023076818
H	-0.0624859533	3.7373599268	-1.2438208229
H	0.3447187266	2.4846492828	-2.4036407209
C	-1.7279423490	2.5076809199	-1.8146015366
H	-2.3276447732	2.8615761918	-0.9671143437
H	-2.0089646731	3.1133735690	-2.6806694405
H	6.3713988573	6.3771234060	0.3446190681
C	6.3837929446	5.5442554071	1.0381633456
C	6.4442529977	3.3923458411	2.8588207985
C	5.3825578764	4.5876342441	1.0676521066
C	7.4297591100	5.4039317673	1.9489762096
C	7.4647724522	4.3438139795	2.8488316291
C	5.4012588499	3.5229785128	1.9611417553
H	8.2279648390	6.1385540190	1.9528320318
H	8.2894876516	4.2574716683	3.5476205962
H	6.4739586183	2.5670968492	3.5643164838
C	4.1691858826	2.6659687540	1.7516934233
C	3.4655037564	3.4177272757	0.6152945292
C	2.2694948320	3.1383184505	-0.0182895439
H	1.9723317730	3.8116901087	-0.8115010550
N	4.2190418870	4.4919270283	0.2738966074
N	-0.2790543391	-0.0923161706	1.0826490789

C	-0.0080782464	0.4022149355	2.4123710734
H	0.8693332215	-0.0086676145	2.9064810809
C	-1.1990167745	-0.4532513386	2.1570410006
H	-1.1275643701	-1.5003291939	2.4479559668
H	-0.1884454670	1.4599785263	2.5969187637
C	-2.5811753943	0.1415805080	2.2317068883
H	-2.5735930547	1.1957074929	1.9414995352
H	-2.9526780599	0.0697127157	3.2580402075
H	-3.2833605386	-0.3828365285	1.5783670803
C	3.8591394802	5.4351881388	-0.7645687959
H	2.9031140405	5.9154762267	-0.5343843414
H	3.7809661378	4.9308393666	-1.7322463090
H	4.6252011481	6.2039033248	-0.8356558788
C	3.3200289952	2.6444575060	3.0352656900
H	3.0233737202	3.6548112985	3.3284690017
H	3.9049060902	2.2144061895	3.8531430596
H	2.4172114376	2.0426988205	2.9147331624
C	4.5723330101	1.2434648750	1.3221826690
H	5.1751423409	0.7811234545	2.1089167541
H	5.1706967606	1.2646731649	0.4077681824
H	3.7017665157	0.6074515520	1.1456069685
C	-3.3270790223	-3.8369596036	0.8000112463
H	-4.3940857593	-3.6062857253	0.8575041455
H	-2.7697064867	-2.9825103890	1.1909731479
H	-3.1321406752	-4.6928739357	1.4520677234
C	-1.4088105469	-4.4996092767	-0.7332864025
H	-0.7912852399	-3.6619177656	-0.4016340132
H	-1.1231591944	-4.7498711442	-1.7581369521
H	-1.1791653124	-5.3608090683	-0.0995829748

Bis-dipole S₁ minimum

H	-5.9181845748	-5.5528385541	-3.7800354623
C	-5.3268808417	-5.8591882178	-2.9250003642
C	-3.7987232503	-6.6933966382	-0.7027083487
C	-4.4732708841	-4.9860690489	-2.2578474185
C	-5.4025259500	-7.1653815112	-2.4538572374
C	-4.6512760559	-7.5840637253	-1.3565509958
C	-3.7130143517	-5.3923742094	-1.1587665705
H	-6.0601329642	-7.8690475486	-2.9534502172
H	-4.7308173677	-8.6084597164	-1.0092287096
H	-3.2145532199	-7.0244365932	0.1508899382
N	-4.2121316466	-3.6381132196	-2.5125689198
C	-3.3037459743	-3.1234863012	-1.6284498516
C	-2.8888172512	-4.2261956574	-0.6549628000
H	-5.3588585413	-2.0066176140	-3.1618059171
C	-4.8285312267	-2.8710479869	-3.5736901258
H	-4.0742007263	-2.5181849601	-4.2845154704
H	-5.5443475686	-3.4939148340	-4.1053382042
C	-2.8938001660	-1.8031272995	-1.6915001610
H	-3.3260697432	-1.1992548407	-2.4808362924
C	-1.9700203685	-1.1756477489	-0.8309980957
H	-1.5157509773	-1.7694359716	-0.0490430468
C	-1.5532935886	0.1482250623	-0.9288948664
C	-0.5946077513	0.6700589736	-0.0019201607

C	0.1907818724	1.8186848181	-0.3283037812	C	-1.3848449884	-4.5508513040	-0.7550858929
C	1.4051921556	2.0653965685	0.3090518068	H	-0.7645625945	-3.7138982882	-0.4272239101
H	1.7310838254	1.3455924262	1.0466754289	H	-1.1059140739	-4.8035000120	-1.7810233968
C	-2.0305113510	1.0356082198	-2.0534235735	H	-1.1556645883	-5.4117065341	-0.1203755000
H	-3.1041073377	0.8860056391	-2.2102110519	Cyanine-like Franck-Condon Point			
H	-1.5410260565	0.7413240178	-2.9935116699	H	-6.3804304284	-5.3975243414	-3.6313602336
C	-0.2798759031	2.7104820454	-1.4551488142	C	-5.8736311388	-5.6590494492	-2.7096826333
H	-0.1063228748	3.7582872409	-1.1888249635	C	-4.5662620208	-6.3755234511	-0.3153489978
H	0.3208539944	2.5204366504	-2.3565936237	C	-4.9330553148	-4.8334362072	-2.1169016052
C	-1.7543444499	2.5061751543	-1.7742092461	C	-6.1535786137	-6.8669714637	-2.0728981621
H	-2.3619651497	2.8381879294	-0.9240788893	C	-5.5104141896	-7.2252474613	-0.8921056245
H	-2.0445163593	3.1177930255	-2.6333034634	C	-4.2819854114	-5.1747526613	-0.9381063878
H	6.3871432187	6.3798043692	0.3056955509	H	-6.8862527472	-7.5365266783	-2.5104512502
C	6.4039967853	5.5493225572	1.0018945988	H	-5.7440510441	-8.1719029775	-0.4174306991
C	6.4746261267	3.4023614711	2.8337090242	H	-4.0665173561	-6.6595523553	0.6060894203
C	5.3924984399	4.5951456940	1.0464888393	N	-4.4632233302	-3.5678295596	-2.5399823092
C	7.4573584342	5.4076521221	1.8984916928	C	-3.5317027098	-3.0741891028	-1.6985235327
C	7.4988441763	4.3501024556	2.8060416141	C	-3.3188092241	-4.0707198549	-0.5537243162
C	5.4203719231	3.5309084962	1.9505489839	H	-5.2886910550	-1.8802115991	-3.4693026427
H	8.2601052948	6.1374852473	1.8884706654	C	-4.9332985601	-2.8810339973	-3.7280090635
H	8.3316405961	4.2648718437	3.4954767937	H	-4.1336635899	-2.7977911376	-4.4697626499
H	6.5105087861	2.5796966275	3.5417063647	H	-5.7592375972	-3.4386503155	-4.1637122093
C	4.1885102722	2.6722830460	1.7577795823	C	-2.9057481131	-1.8540203354	-1.9273713703
C	3.4712207976	3.4232821955	0.6364912958	H	-3.1605707168	-1.3349274101	-2.8430687034
C	2.2582763978	3.1514771865	0.0268010660	C	-1.9807154078	-1.2686763113	-1.0626481871
H	1.9385294687	3.8452697779	-0.7413326239	H	-1.7143570081	-1.7910920536	-0.1561076218
N	4.2317298328	4.5010812552	0.2754237320	C	-1.3397004531	-0.0401809545	-1.2413779583
N	-0.3102601559	-0.0763480000	1.1342772925	C	-0.3673607146	0.3801937469	-0.3015608820
C	-0.1006135875	0.4805847623	2.4558188741	C	0.3322965485	1.6150610405	-0.4736088918
H	0.7566509660	0.0952899834	3.0028326837	C	1.4594182111	1.9679164402	0.2574055694
C	-1.2772283778	-0.3869828782	2.1895732283	H	1.7923483947	1.3214241750	1.0505006144
H	-1.2185666951	-1.4214055822	2.5255412397	C	-1.6724060689	0.8332675294	-2.4264952025
H	-0.2913222806	1.5445661567	2.5866241345	H	-2.6956038149	0.6396409523	-2.7589872094
C	-2.6633905926	0.2040172989	2.1914165125	H	-1.0179475260	0.5924723019	-3.2759900362
H	-2.6520418220	1.2439869300	1.8537813358	C	-0.1150947773	2.5698548042	-1.5671842868
H	-3.0692742369	0.1776721632	3.2070032816	H	-0.0560075071	3.5960820985	-1.1907418280
H	-3.3397552772	-0.3556535567	1.5397468392	H	0.5856153462	2.5125483320	-2.4125883450
C	3.8674500870	5.4336342204	-0.7695224813	C	-1.5248441677	2.3027561407	-2.0662715116
H	2.9436720521	5.9631896677	-0.5134829362	H	-2.2506127133	2.5578307162	-1.2854552216
H	3.7231795843	4.9068127694	-1.7177852135	H	-1.7428720819	2.9385461171	-2.9291960905
H	4.6630513811	6.1640966237	-0.8975252288	H	6.1410100400	6.5763982278	0.5231315403
C	3.3525606008	2.6375582111	3.0518623136	C	6.0978711949	5.8225686212	1.3007471974
H	3.0570947339	3.6448684199	3.3559059381	C	6.0078675542	3.8819987666	3.3435982141
H	3.9449890366	2.1991506259	3.8600663139	C	5.1433928742	4.8189380230	1.3096551997
H	2.4496567149	2.0361212199	2.9301199049	C	7.0200585501	5.8377987626	2.3460337043
C	4.5926696277	1.2478259420	1.3255328646	C	6.9798596463	4.8829533565	3.3568559470
H	5.2026675494	0.7880864812	2.1085560513	C	5.0886868782	3.8576168552	2.3116951310
H	5.1829751509	1.2697342677	0.4060629054	H	7.7798046275	6.6117422123	2.3677564119
H	3.7211464884	0.6109971865	1.1582050601	H	7.7072972973	4.9176188119	4.1604015928
C	-3.2817488233	-3.8864879493	0.7965452957	H	5.9778070562	3.1389778027	4.1350594899
H	-4.3465368331	-3.6511827810	0.8701221357	C	3.9356893930	2.9116583674	2.0425663689
H	-2.7137873668	-3.0361177799	1.1807821190	C	3.3588808584	3.4966390780	0.7470030200
H	-3.0792986266	-4.7467771680	1.4409232142	C	2.2565167598	3.1015143197	0.0101177437

H	1.9992858105	3.7202130314	-0.8384917437	H	-1.7023971008	-1.8062922989	-0.1694074396
N	4.1038005419	4.5705138754	0.3876678385	C	-1.3465253596	-0.0436771058	-1.2442239167
N	-0.1772398302	-0.5461844318	0.7608273237	C	-0.3650407355	0.3848742756	-0.3017917639
C	0.2644739794	-0.2576259934	2.1161842511	C	0.3420057883	1.6152116013	-0.4807767210
H	0.5735533827	0.7472268858	2.3804682178	C	1.4737173601	1.9744310101	0.2598168596
C	1.1010619457	-1.0925956449	1.2149835311	H	1.8010122581	1.3272270660	1.0540470146
H	1.9904928688	-0.6239339841	0.7986523582	C	-1.6724560160	0.8326905554	-2.4251389337
H	-0.3283007726	-0.7491760144	2.8847592588	H	-2.6891811465	0.6366656034	-2.7746600801
C	1.1976006141	-2.5875959400	1.3636488571	H	-1.0039803787	0.5980664844	-3.2665306353
H	0.2860061190	-2.9913945037	1.8123158778	C	-0.1131534507	2.5683545433	-1.5696160936
H	2.0432807282	-2.8543764677	2.0052664538	H	-0.0455489381	3.5964333144	-1.2003484901
H	1.3481264998	-3.0667251716	0.3912088799	H	0.5804726533	2.5016466265	-2.4211273938
C	3.8583571556	5.3673861086	-0.7971393038	C	-1.5272408235	2.3016082299	-2.0588705577
H	2.8990772451	5.8892172625	-0.7240741292	H	-2.2473977993	2.5523943150	-1.2717212115
H	3.8518806494	4.7315435290	-1.6868077937	H	-1.7520299853	2.9396129066	-2.9185533553
H	4.6497685531	6.1054323428	-0.9068524437	H	6.1592293109	6.5976031597	0.5264136847
C	2.9137716363	2.9815661855	3.1908412760	C	6.1156939310	5.8410936571	1.3014114477
H	2.5468368783	4.0013918572	3.3302528871	C	6.0216225112	3.8908391777	3.3416691838
H	3.3867543258	2.6619269952	4.1235545220	C	5.1535234240	4.8358646055	1.3064978413
H	2.0548666264	2.3320167465	3.0078935457	C	7.0359324011	5.8501331655	2.3436563097
C	4.4606576641	1.4773004579	1.8509298631	C	6.9954529861	4.8902643104	3.3544677665
H	5.0015486123	1.1663093419	2.7488724380	C	5.1003407295	3.8691745898	2.3127021581
H	5.1494731458	1.4173544255	1.0045721070	H	7.7979405237	6.6220208556	2.3678373918
H	3.6508982968	0.7627353053	1.6892181638	H	7.7249973174	4.9220283201	4.1563051351
C	-3.7122816064	-3.4772047460	0.8126547148	H	5.9914349836	3.1456540018	4.1309830529
H	-4.7288759474	-3.0759480021	0.7906135204	C	3.9492663520	2.9235311158	2.0452943652
H	-3.0346781170	-2.6801814070	1.1244437708	C	3.3735463992	3.5088467128	0.7551766354
H	-3.6790066281	-4.2649682160	1.5704871219	C	2.2701626836	3.1105658579	0.0149912684
C	-1.8755549256	-4.6069509645	-0.5389923015	H	2.0157105112	3.7270763031	-0.8378184464
H	-1.1546375649	-3.8269214768	-0.2866175188	N	4.1233021412	4.5932805478	0.3953102473
H	-1.6023781436	-5.0270068900	-1.5106371301	N	-0.1764659344	-0.5365047503	0.7638555796
H	-1.7910455766	-5.4023424142	0.2066640906	C	0.2530989957	-0.2510596302	2.1215747366
Cyanine-like S₁ minimum				H	0.5681664991	0.7522812074	2.3880035459
H	-6.3939553743	-5.4193757773	-3.6474783909	C	1.0950566653	-1.0876290159	1.2234171939
C	-5.8883785675	-5.6764070661	-2.7239847187	H	1.9907793623	-0.6192039254	0.8186079998
C	-4.5796812497	-6.3825681182	-0.3231329633	H	-0.3449436949	-0.7392321608	2.8885423685
C	-4.9472285384	-4.8397116569	-2.1318531594	C	1.1886431410	-2.5838842060	1.3649809825
C	-6.1649072499	-6.8798378422	-2.0846058552	H	0.2699017514	-2.9887057943	1.7983597503
C	-5.5227757830	-7.2347603468	-0.8988660770	H	2.0257786238	-2.8579975878	2.0148857760
C	-4.2950339781	-5.1831706689	-0.9459374282	H	1.3498451092	-3.0564260272	0.3906832879
H	-6.8948490682	-7.5535307203	-2.5211115146	C	3.8772495828	5.3923673265	-0.7870897944
H	-5.7574212194	-8.1800363442	-0.4217249239	H	2.9142141361	5.9082613567	-0.7141726685
H	-4.0807355741	-6.6633216402	0.5997025333	H	3.8744040537	4.7592275651	-1.6793265379
N	-4.4875966281	-3.5882758380	-2.5513659558	H	4.6647699639	6.1352221068	-0.8926025893
C	-3.5477860591	-3.0849328685	-1.6994762720	C	2.9285034610	2.9860082071	3.1990419258
C	-3.3328775176	-4.0806104105	-0.5599214059	H	2.5636263915	4.0054499603	3.3471836856
H	-5.3109706822	-1.9061185626	-3.4930054530	H	3.4033687850	2.6564538734	4.1276687659
C	-4.9505489451	-2.9080997167	-3.7432043287	H	2.0687896726	2.3390064283	3.0111008844
H	-4.1449491725	-2.8227071146	-4.4797149649	C	4.4782096351	1.4867720551	1.8578922349
H	-5.7712157410	-3.4694177906	-4.1846687971	H	5.0208236256	1.1803497755	2.7567230403
C	-2.9331610668	-1.8586937168	-1.9197876535	H	5.1655924011	1.4248895255	1.0104386863
H	-3.2121129808	-1.3256793832	-2.8218263912	H	3.6687115812	0.7710151627	1.7003803930
C	-1.9867710338	-1.2761999881	-1.0657131272	C	-3.7218697820	-3.4889232294	0.8110601509

H	-4.7410016045	-3.0940388760	0.7940849332	H	-3.0207137899	-8.1329361993	-4.0874038773
H	-3.0467907860	-2.6861294444	1.1136304913	H	-2.2861777181	-6.7698871166	-2.1488162565
H	-3.6766495492	-4.2747105858	1.5707672344	C	-2.3314132951	-3.8397973901	-2.1313251375
C	-1.8881605899	-4.6214489146	-0.5358672295	C	-2.6538782953	-2.5572751987	-2.9100272419
H	-1.1682015834	-3.8416971249	-0.2794294356	C	-2.5129347777	-1.2435813290	-2.5271783021
H	-1.6095005883	-5.0428932688	-1.5053427465	H	-2.7828021983	-0.4889335033	-3.2551142709
H	-1.8100554337	-5.4153779402	0.2126588858	N	-3.1302831111	-2.9041378109	-4.1369953372

Dye II-13

Bis-dipole Franck-Condon point

H	6.1765096223	5.6417629972	2.4354406411
C	6.0223527085	4.7077934497	2.9633603422
C	5.6580359158	2.2808998680	4.3473406960
C	4.9054658295	3.9150804237	2.7564344567
C	6.9651979145	4.2603496671	3.8877396320
C	6.7907022399	3.0638012347	4.5746034646
C	4.7175136570	2.7147616238	3.4326326520
H	7.8497715456	4.8612931486	4.0701807773
H	7.5384514712	2.7367016034	5.2885616548
H	5.5246155711	1.3459254103	4.8836596749
N	3.8108442449	4.1271773749	1.8943287667
C	2.9107451659	3.1085086002	1.9634042008
C	3.4129662636	2.0822927763	2.9882982618
H	4.4752629050	5.9741309190	1.2047140530
C	3.6604400525	5.2754862600	1.0277374133
H	3.6796305701	4.9742829249	-0.0247769991
H	2.7157703967	5.7886014159	1.2320510943
C	1.7703269003	3.0933428444	1.1942102165
H	1.6252766252	3.9247953096	0.5164774572
C	0.7827995734	2.0777424265	1.1888858528
H	0.9377403308	1.2385742938	1.8534934149
C	-0.2988557390	2.0374726975	0.3431085840
C	-1.1711108945	0.8854354614	0.3003748476
C	-1.7931371441	0.5264419762	-0.9550047468
C	-2.0288374380	-0.7880114435	-1.2758863388
H	-1.7620252321	-1.5418280269	-0.5470947604
C	-0.5052256403	3.1222707847	-0.6941442645
H	0.2921535199	3.0802045885	-1.4495573826
H	-0.4162762495	4.1008669507	-0.2096835517
C	-2.0196044046	1.6198371402	-1.9787077314
H	-1.3217102200	1.4992100135	-2.8194748003
H	-3.0256450928	1.5115621590	-2.3993036099
C	-1.8591712644	3.0087984384	-1.3788788447
H	-1.9565315989	3.7716986569	-2.1560870317
H	-2.6581649985	3.1915251651	-0.6495906231
H	-3.9426685462	-4.5786549132	-6.3117737457
C	-3.5822534200	-5.0424342804	-5.4008302113
C	-2.6457601567	-6.2847161641	-3.0516324929
C	-3.1679179665	-4.3033494082	-4.3048900381
C	-3.5202020018	-6.4317144099	-5.2993068281
C	-3.0594196635	-7.0506221550	-4.1423555783
C	-2.7025408963	-4.9070742956	-3.1421600582
H	-3.8385304173	-7.0362370930	-6.1421108777

H	-3.0207137899	-8.1329361993	-4.0874038773
H	-2.2861777181	-6.7698871166	-2.1488162565
C	-2.3314132951	-3.8397973901	-2.1313251375
C	-2.6538782953	-2.5572751987	-2.9100272419
C	-2.5129347777	-1.2435813290	-2.5271783021
H	-2.7828021983	-0.4889335033	-3.2551142709
N	-3.1302831111	-2.9041378109	-4.1369953372
N	-1.3857055309	0.1494961309	1.3981180839
C	-1.1862991786	0.4841954189	2.8213891733
C	-2.4671659454	-0.8076591376	1.7024729009
C	-2.4329654193	-0.3504492343	3.1738386649
H	-2.2839966519	-1.1383443293	3.9117338504
H	-3.2928002885	0.2568585105	3.4580391615
H	-3.3781710233	-0.6143039125	1.1300916527
H	-2.1667415361	-1.8494392877	1.5585144081
H	-1.2234436522	1.5599936857	3.0135486626
H	-0.2552092497	0.0781808650	3.2270815301
C	-3.5428948065	-1.9465954704	-5.1396283091
H	-2.7004816071	-1.3193512124	-5.4486639117
H	-4.3393422838	-1.3036691517	-4.7521504561
H	-3.9199810810	-2.4747587259	-6.0128371201
C	-0.8358327175	-3.9337676521	-1.7819555448
H	-0.2172680160	-3.8154338786	-2.6751990136
H	-0.6202157743	-4.9154008352	-1.3506821631
H	-0.5346647454	-3.1731183067	-1.0575697403
C	-3.2131930678	-3.9819746731	-0.8780373320
H	-3.0398136732	-4.9581747682	-0.4164010346
H	-4.2733774640	-3.9141729280	-1.1350296187
H	-2.9938048159	-3.2133189831	-0.1333928049
C	2.4542728507	1.9587828867	4.1858137900
H	1.4936708217	1.5254889901	3.8971373160
H	2.2646446643	2.9345675972	4.6402991062
H	2.9002609272	1.3135544592	4.9479699119
C	3.6829841680	0.7119012966	2.3418837282
H	4.3586604454	0.8083959862	1.4884449750
H	2.7643976529	0.2319194491	1.9960149569
H	4.1556941476	0.0491573204	3.0722220151

Bis-dipole S₁ minimum

H	6.1661378899	5.6801872758	2.4689353625
C	6.0265241248	4.7375994479	2.9853103022
C	5.6953565425	2.2869692527	4.3448295152
C	4.9170520322	3.9276310040	2.7660526103
C	6.9713343844	4.2955889680	3.9055661113
C	6.8146887421	3.0864814808	4.5809632811
C	4.7480071495	2.7135954688	3.4350170590
H	7.8457165571	4.9080325007	4.0992428270
H	7.5661355545	2.7659623995	5.2942629103
H	5.5760526342	1.3451688953	4.8723879533
N	3.8287693194	4.1289284328	1.9136885959
C	2.9354659833	3.0923540491	1.9811622333
C	3.4524111338	2.0677085088	2.9909282314
H	4.4962359337	5.9657531653	1.1970397146
C	3.6604119082	5.2835270647	1.0585883631

H	3.6253524052	4.9823206192	0.0063654375	C	-3.1983462167	-4.0181808284	-0.8840676007
H	2.7348829655	5.8140344215	1.3050666327	H	-3.0202188785	-4.9925250489	-0.4200742756
C	1.7865232002	3.0687159742	1.2150703815	H	-4.2602517096	-3.9507225664	-1.1335174212
H	1.6220985340	3.9183236616	0.5627569969	H	-2.9706768969	-3.2447734446	-0.1472996110
C	0.8197618810	2.0361069019	1.1773101276	C	2.4951629151	1.9216732192	4.1896889241
H	0.9747897828	1.1744153856	1.8121639420	H	1.5334478327	1.5007714271	3.8884209977
C	-0.2796581530	2.0149791110	0.3314056833	H	2.3109107398	2.8884292802	4.6650340980
C	-1.1892094381	0.8995676081	0.3096400692	H	2.9386579577	1.2564348091	4.9360800328
C	-1.7630127705	0.5166550235	-0.9558489393	C	3.7335760439	0.6994404562	2.3389016856
C	-1.9744028350	-0.8163129582	-1.2752354379	H	4.4095258688	0.8025120599	1.4864073318
H	-1.6693106723	-1.5558535713	-0.5467484403	H	2.8171707803	0.2170757923	1.9922538815
C	-0.4847512644	3.1057642358	-0.6973126018	H	4.2080981061	0.0378291190	3.0693820416
H	0.3137627022	3.0647770213	-1.4521651721	Cyanine-like Franck-Condon point			
H	-0.3932584619	4.0836425649	-0.2109114810	H	4.2935582544	6.8462183223	4.0198453120
C	-2.0050807066	1.6050613179	-1.9782455380	C	4.7274082498	5.8569649855	4.1097249385
H	-1.3146995530	1.4823395402	-2.8252070682	C	5.8885686757	3.3007466074	4.3570307407
H	-3.0145493982	1.4951913670	-2.3916437903	C	4.1416275334	4.7350710410	3.5471646590
C	-1.8398413048	2.9957379665	-1.3818262510	C	5.9199619098	5.6749317492	4.8087478338
H	-1.9352113939	3.7566713988	-2.1615006112	C	6.4968492700	4.4156145784	4.9348226996
H	-2.6361778984	3.1808272749	-0.6513205468	C	4.7066676414	3.4703968331	3.6609017860
H	-3.9743489690	-4.5607247313	-6.3275605270	H	6.4033220913	6.5351639595	5.2596626417
C	-3.6082432210	-5.0358954412	-5.4248688504	H	7.4246008202	4.2994089105	5.4842196933
C	-2.6563646594	-6.3058999770	-3.0913048037	H	6.3418477436	2.3187721962	4.4564733173
C	-3.1792151172	-4.3052614272	-4.3216588481	N	2.9496206384	4.6325314995	2.7984212555
C	-3.5538754293	-6.4229911451	-5.3357314474	C	2.7107232265	3.3552574853	2.4063396007
C	-3.0847732681	-7.0572787129	-4.1866314674	C	3.8366056160	2.4597459995	2.9402756408
C	-2.7067231582	-4.9277137828	-3.1644251555	H	2.4766942464	6.6538668667	2.9385793361
H	-3.8849883894	-7.0192768397	-6.1795426331	C	2.0921183690	5.7515068874	2.4684415262
H	-3.0535481621	-8.1405507984	-4.1435363403	H	2.0583324786	5.9074164899	1.3854549673
H	-2.2912529703	-6.8030334481	-2.1973701151	H	1.0765252948	5.5756449571	2.8345187677
C	-2.3236517255	-3.8756150018	-2.1449677462	C	1.6175381353	3.0221743470	1.6329317229
C	-2.6429819269	-2.5885823776	-2.9055909799	H	0.9631991602	3.8313105196	1.3330617897
C	-2.4949295985	-1.2737475808	-2.5091435028	C	1.2788926750	1.7261051563	1.1908552469
H	-2.7925769478	-0.5164355484	-3.2251446431	H	1.8725147882	0.8977527513	1.5557487191
N	-3.1329110271	-2.9207804715	-4.1410061960	C	0.2915877030	1.4292687669	0.2746943956
N	-1.3770093378	0.1227897525	1.4176353597	C	0.0492434394	0.0622335386	-0.0901029237
C	-1.2761552793	0.5754027474	2.8212682070	C	-0.4395947408	-0.2317277972	-1.4061837453
C	-2.5731708833	-0.6999952872	1.6987573220	C	-1.1457152043	-1.3875519173	-1.6593815781
C	-2.4880997688	-0.3031987071	3.1849621711	H	-1.3289528157	-2.0324481578	-0.8106598605
H	-2.2657769150	-1.1269263412	3.8636872360	C	-0.4088932688	2.5504460116	-0.4710052674
H	-3.3521872828	0.2459467225	3.5594736275	H	0.3469381196	3.3004556813	-0.7311441365
H	-3.4610976007	-0.3499902687	1.1628522105	H	-1.1237812971	3.0592195159	0.1883289163
H	-2.4342882304	-1.7651849678	1.4962810495	C	-0.3652385430	0.9171118499	-2.3820462920
H	-1.4207953547	1.6551816589	2.9278616688	H	0.6750005697	1.1990595529	-2.5868525307
H	-0.3393139195	0.2930040488	3.3090183792	H	-0.8155917712	0.6548783396	-3.3399207561
C	-3.5489054434	-1.9508236513	-5.1303878950	C	-1.1121707335	2.0986048360	-1.7559864683
H	-2.7083969754	-1.3129962429	-5.4232867861	H	-1.1723885846	2.9391008406	-2.4539727620
H	-4.3514974237	-1.3192752743	-4.7359189722	H	-2.1395483712	1.7841881428	-1.5444865010
H	-3.9182766898	-2.4665443793	-6.0140116396	H	-4.5486311052	-4.4909732514	-6.3610992038
C	-0.8272560498	-3.9882179830	-1.7937160110	C	-4.6256175589	-4.8336030141	-5.3356616805
H	-0.2043233071	-3.8743144005	-2.6844427395	C	-4.8506501255	-5.7519943521	-2.6805849256
H	-0.6260652266	-4.9735734483	-1.3634369828	C	-3.9260746107	-4.2378758243	-4.2991067180
H	-0.5223657975	-3.2339157707	-1.0651174442	C	-5.4519200860	-5.9101294640	-5.0161213904

C	-5.5676461965	-6.3670544272	-3.7075472382	C	3.8668425640	2.4525767230	2.9518749103
C	-4.0294310905	-4.6833672957	-2.9863929060	H	2.5100516580	6.6505206291	3.0092681003
H	-6.0123889568	-6.3968803213	-5.8072127987	C	2.1709232028	5.7709042087	2.4664367652
H	-6.2188374531	-7.2049440365	-3.4841415526	H	2.2136533095	5.9816376799	1.3924532475
H	-4.9427250810	-6.1104478332	-1.6594379158	H	1.1333964862	5.5687056676	2.7475152219
C	-3.1427572090	-3.8381004875	-2.0937974008	C	1.7010097469	3.0474429809	1.5691352482
C	-2.5531648340	-2.8443003795	-3.1037199250	H	1.0881874584	3.8775870143	1.2366861787
C	-1.6994017466	-1.7818075617	-2.8972954166	C	1.3357325654	1.7673657729	1.1119138349
H	-1.4423131126	-1.1901502979	-3.7663342610	H	1.8799121222	0.9097515777	1.4851607501
N	-3.0341381390	-3.1459976698	-4.3385454397	C	0.3513929862	1.5164435517	0.1558531272
N	0.3097371830	-0.9227460345	0.8021386041	C	0.0118947858	0.1750296261	-0.1926424590
C	0.1791893763	-1.0014655507	2.2709121661	C	-0.6171584447	-0.1111656686	-1.4515903022
C	0.7896849533	-2.3128692354	0.6753698622	C	-1.2715414786	-1.3165630001	-1.6616270841
C	0.7350703217	-2.4407291696	2.2128284934	H	-1.3607368558	-1.9614768966	-0.7971718911
H	1.7084904857	-2.5638952497	2.6877601872	C	-0.2867840428	2.6755825994	-0.5806873215
H	0.0573830275	-3.2094158073	2.5839515220	H	0.5176611208	3.3018054033	-0.9883139250
H	0.1340965167	-2.9990044194	0.1396544816	H	-0.8340646308	3.3151763306	0.1240154789
H	1.7861737625	-2.3635316101	0.2252087644	C	-0.6460712821	1.0243173667	-2.4402181460
H	-0.8665009997	-0.9197755692	2.5855197082	H	0.3617286171	1.2469554006	-2.8152035015
H	0.7700482756	-0.2897886792	2.8462300741	H	-1.2643800680	0.7846451010	-3.3066787258
C	-2.6900742759	-2.4138263335	-5.5387804222	C	-1.2111666615	2.2532848541	-1.7221023414
H	-1.6111446414	-2.4519108823	-5.7167251479	H	-1.3363665057	3.0863073201	-2.4203857363
H	-2.9997444627	-1.3673576048	-5.4557201917	H	-2.2065901884	2.0052802318	-1.3377831765
H	-3.1980388584	-2.8573429967	-6.3922520956	H	-4.5977281326	-4.6594736653	-6.2721762877
C	-2.0513697691	-4.7199894767	-1.4604519603	C	-4.6366045746	-4.9928749147	-5.2415781397
H	-1.4449535989	-5.2085716265	-2.2272884956	C	-4.7746025209	-5.8759994228	-2.5630879763
H	-2.5170830483	-5.4991004088	-0.8503104308	C	-3.9445114991	-4.3441130080	-4.2230053163
H	-1.3867991897	-4.1418933762	-0.8150631179	C	-5.4018083046	-6.0996067525	-4.8910143536
C	-3.9826243984	-3.1287098855	-1.0178652751	C	-5.4743734263	-6.5417401560	-3.5706009573
H	-4.4875982634	-3.8736876014	-0.3965042446	C	-4.0109257100	-4.7743694414	-2.8952819897
H	-4.7482439063	-2.4947143358	-1.4723220931	H	-5.9537441358	-6.6252986302	-5.6631305179
H	-3.3668200137	-2.5049639984	-0.3656467676	H	-6.0800347373	-7.4072838886	-3.3251496894
C	3.3183556615	1.4098922926	3.9397984112	H	-4.8355595894	-6.2226702750	-1.5357352914
H	2.7183435247	0.6393109909	3.4498135586	C	-3.1596918747	-3.8714893581	-2.0280974422
H	2.7134428284	1.8735468786	4.7232157305	C	-2.6371795478	-2.8705230680	-3.0589289240
H	4.1667944928	0.9135820095	4.4189048637	C	-1.8480828550	-1.7503425817	-2.8772271521
C	4.6217910713	1.7965035874	1.7948554972	H	-1.6545538126	-1.1480174795	-3.7570126089
H	4.9851224093	2.5423276106	1.0835117473	N	-3.1130902963	-3.2262916469	-4.2939665955
H	4.0097764286	1.0746887499	1.2488569788	N	0.3013294619	-0.8532044855	0.6736717343
H	5.4881610935	1.2683326012	2.2029156808	C	0.1383431060	-1.0073013814	2.1243519975
Cyanine-like S₁ minimum				C	0.9600358436	-2.1532077254	0.4945038295
H	4.3429114639	6.8394811607	4.0577100929	C	0.7741274966	-2.4122487501	2.0073879997
C	4.7621348699	5.8449623382	4.1569352952	H	1.7005161278	-2.5476440619	2.5661121116
C	5.8898318570	3.2705183953	4.4207065624	H	0.0954222684	-3.2322166431	2.2442651977
C	4.1739526687	4.7276662303	3.5728768178	H	0.4569926735	-2.8564432277	-0.1753398304
C	5.9317580934	5.6465176901	4.8828310935	H	2.0024631221	-2.0587963593	0.1664156208
C	6.4936826824	4.3779169799	5.0180851947	H	-0.9118382660	-0.9897546161	2.4383985365
C	4.7274122894	3.4516840583	3.6967249780	H	0.6904243127	-0.2956364765	2.7450840564
H	6.4142299755	6.4989300627	5.3495627647	C	-2.8062951756	-2.5154760757	-5.5165671294
H	7.4061025723	4.2512840820	5.5906346464	H	-1.7242328904	-2.3957456021	-5.6208850150
H	6.3329793764	2.2846954056	4.5262706530	H	-3.2758644543	-1.5255730009	-5.5257760074
N	3.0107632986	4.6413732546	2.8041096743	H	-3.1720943152	-3.0852314414	-6.3682707289
C	2.7707740383	3.3596750257	2.3926606426	C	-2.0201774072	-4.6841493125	-1.3811802105

H	-1.3909611349	-5.1555401418	-2.1403893598	H	4.3637997674	-7.0105924973	-0.8615873391
H	-2.4445510853	-5.4736713098	-0.7541458259	C	4.4813908585	-6.3953269660	0.0231765766
H	-1.3872806177	-4.0591909623	-0.7475515903	C	4.8176755520	-4.8160890768	2.3302406177
C	-4.0213605393	-3.1849911445	-0.9501626177	C	3.6096313845	-5.3618799535	0.3261112871
H	-4.4545494334	-3.9418094481	-0.2897265863	C	5.5368639699	-6.6279369225	0.9044543132
H	-4.8406358956	-2.6208963400	-1.4028725826	C	5.7089585867	-5.8519609056	2.0451407832
H	-3.4292423492	-2.4997145605	-0.3398583418	C	3.7682611366	-4.5769091934	1.4638697668
C	3.3145858844	1.3978524678	3.9317233332	H	6.2338685867	-7.4314827464	0.6904945142
H	2.7086802020	0.6458186079	3.4209138761	H	6.5376853664	-6.0520919327	2.7154283270
H	2.7054210217	1.8617733575	4.7116590017	H	4.9530429819	-4.2104719489	3.2219621449
H	4.1481696146	0.8811861981	4.4160372924	C	2.6623178888	-3.5396674291	1.5226246765
C	4.6740832097	1.7800073308	1.8238572122	C	1.8721441327	-3.8622718383	0.2443783523
H	5.0757165123	2.5241122067	1.1315132825	C	0.7566210504	-3.2619515734	-0.2700917476
H	4.0596221077	1.0787583009	1.2548013499	H	0.3771803165	-3.6554006835	-1.2042869445
H	5.5146219425	1.2269197538	2.2530259592	N	2.4780475459	-4.9193808694	-0.3811327649

Dye II-14

Bis-dipole Franck-Condon point

H	0.6349376915	8.2892412142	-1.0881209221
C	0.8789553559	7.8614932833	-0.1224432698
C	1.5287573768	6.7839474921	2.3979682200
C	0.5510003985	6.5586853649	0.2154564513
C	1.5465749165	8.6254137538	0.8342830234
C	1.8704565662	8.0993219342	2.0799823804
C	0.8669294961	6.0181532314	1.4572328156
H	1.8159019870	9.6491800057	0.5965310134
H	2.3901457468	8.7133067675	2.8073439819
H	1.7825135858	6.3747950606	3.3717179713
N	-0.1134695840	5.5817836974	-0.5510622012
C	-0.2493271751	4.4097348641	0.1341235636
C	0.3758491373	4.5846308689	1.5263748223
H	-0.3589664778	6.7942519011	-2.2213757415
C	-0.5907099929	5.7807799542	-1.9010985550
H	-0.1079329920	5.0799359098	-2.5899626290
H	-1.6749017797	5.6388577967	-1.9531656509
C	-0.8577940448	3.3117128975	-0.4193658530
H	-1.2275147063	3.4137224977	-1.4312158533
C	-1.0524915729	2.0590881191	0.2265268587
H	-0.7272413969	1.9993495665	1.2591693647
C	-1.5524330606	0.9128520615	-0.3286030884
C	-1.5813106525	-0.3218787389	0.4504898406
C	-1.0075833460	-1.4986310846	-0.2256223632
C	0.0428195271	-2.1711159728	0.3163040976
H	0.4073976422	-1.8265213465	1.2773865471
C	-1.9136045988	0.7828042446	-1.7960302057
H	-1.6324393393	1.6899779819	-2.3325559456
H	-3.0047391962	0.6949306987	-1.8936432327
C	-1.5047847372	-1.6923997234	-1.6418172306
H	-1.0080099747	-2.5450278868	-2.1057175498
H	-2.5793872102	-1.9217701077	-1.6404119448
C	-1.2576492517	-0.4266189370	-2.4628908774
H	-0.1782408261	-0.2594780252	-2.5457883288
H	-1.6494567350	-0.5469899241	-3.4779953228

Bis-dipole S₁ minimum

H	0.2860838718	8.4573592234	-1.3483677394
C	0.3785756838	8.1904280933	-0.3017331995

C	0.6236791619	7.5335170424	2.4248502099	H	-0.6149162792	-1.4648278603	2.9945802167
C	0.2025782892	6.8901608443	0.1469112506	H	-3.3209839846	0.7118080464	3.1077515769
C	0.6821992334	9.1663018634	0.6468943473	C	1.1400623534	-6.1261535344	-1.1980250776
C	0.8045424105	8.8497434605	1.9950838515	H	1.1823324434	-5.6393140316	-2.1764242627
C	0.3218118203	6.5578742818	1.4947111357	H	0.1136481741	-6.1138667502	-0.8276811826
H	0.8263454524	10.1910805163	0.3209411342	H	1.4522487860	-7.1627342527	-1.3026095550
H	1.0408143417	9.6264998334	2.7139556758	C	-1.1334018173	4.8380916828	2.5944989824
H	0.7217996318	7.2861742446	3.4780178697	H	-1.3373107481	3.7741324434	2.7355970561
N	-0.1038267286	5.7335369017	-0.5840764312	H	-2.0315505769	5.3077952192	2.1853684922
C	-0.1997610055	4.6308700213	0.2323539366	H	-0.9410431221	5.2769902778	3.5780516075
C	0.0783306803	5.0709913381	1.6747492280	C	1.3378640970	4.3909583631	2.2411517935
H	-0.1147072094	6.6741347171	-2.4366250402	H	2.2016430810	4.5705982532	1.5957386420
C	-0.2834728156	5.6855187205	-2.0140004614	H	1.2046242082	3.3110762263	2.3382240547
H	0.4288197219	4.9890157734	-2.4702985543	H	1.5662712709	4.7973672042	3.2311002564
H	-1.2992864971	5.3653181776	-2.2715399760	C	3.6326592910	-2.6263714953	0.8957105604
C	-0.4861875731	3.3812438366	-0.2554598732	H	3.9754583378	-2.6614538258	-0.1414804837
H	-0.6439480729	3.3040024249	-1.3258409024	H	4.5085548070	-2.4965416201	1.5365064666
C	-0.5851264947	2.1822974927	0.4933801176	H	2.9954539343	-1.7484350374	1.0168024821
H	-0.4817188418	2.2357755348	1.5709452146	C	2.4132347255	-3.8719081228	2.7498028862
C	-0.7832076128	0.9129024200	-0.0320141178	H	3.2709384332	-3.7518671522	3.4165888426
C	-1.0765740890	-0.1949114568	0.7894255738	H	1.8949449626	-4.7927770119	3.0291275271
C	-0.8072800179	-1.5227141501	0.1821379081	H	1.7373446011	-3.0306832493	2.9177151749
C	0.2942489546	-2.2721587570	0.5485682227	C	-2.6237230660	-2.2591586516	3.0070685887
H	0.9210006823	-1.8559677336	1.3275372196	C	-4.1027745546	0.4505229346	1.1140153637
C	-0.8600462785	0.7094379199	-1.5445043186	H	-2.4163776007	-2.9520509843	3.8288545088
H	-0.0327850502	1.2248185814	-2.0435552959	H	-2.5502922542	-2.8125155791	2.0658574350
H	-1.7717730152	1.2177794234	-1.8878320238	H	-3.7817544963	0.5746238869	0.0757171106
C	-1.5903842024	-1.7374456270	-1.0651824660	H	-4.9449238421	1.1285482814	1.2829836538
H	-1.5570492662	-2.7509289779	-1.4746902665	H	-4.4600762977	-0.5748984183	1.2452414575
H	-2.6380650131	-1.4597544478	-0.9160923489	H	-3.6556909293	-1.9140436613	3.1161878478
C	-0.9033895355	-0.7454841950	-2.0479720826	Cyanine-like Franck-Condon point			
H	0.1155927349	-1.1084248466	-2.2195743712	H	-2.3741513178	7.3412183402	-4.8119609291
H	-1.4171902299	-0.7872758483	-3.0132311173	C	-2.0416422170	7.4397967681	-3.7850189082
H	3.4524088129	-7.8244417990	-0.9805234658	C	-1.1749442069	7.7337156438	-1.1195130824
C	3.8853060320	-7.1559397293	-0.2455368583	C	-1.6814306125	6.3473044259	-3.0133771531
C	5.0533562070	-5.4133635058	1.6471117825	C	-1.9596258981	8.6988231457	-3.1917891425
C	3.2597964911	-5.9873591852	0.1625602966	C	-1.5320663865	8.8499068945	-1.8769555090
C	5.1234028189	-7.4415142207	0.3212816804	C	-1.2519730311	6.4810373400	-1.6980951713
C	5.7016301135	-6.5848362373	1.2563983436	H	-2.2340124652	9.5736181093	-3.7717918512
C	3.8243656489	-5.1163119763	1.0879933963	H	-1.4757008727	9.8401092576	-1.4383036374
H	5.6457763505	-8.3443353158	0.0249552925	H	-0.8414520605	7.8544445378	-0.0929641817
H	6.6684774985	-6.8303287340	1.6812116687	N	-1.6690611268	4.9793715762	-3.3574802034
H	5.5143132198	-4.7497358266	2.3716432812	C	-1.2335445707	4.2061530755	-2.3287026367
C	2.9079404107	-3.9285653971	1.2902491150	C	-0.9406663539	5.1123214899	-1.1255789334
C	1.7684552247	-4.2683607800	0.3292017881	H	-1.1953316249	3.9992034986	-5.1565298976
C	0.6341004096	-3.5231506204	0.0097555980	C	-2.0514758884	4.4596861901	-4.6533843754
H	-0.0296406869	-3.9390422756	-0.7381678966	H	-2.8449811725	3.7142648795	-4.5471768745
N	2.0178766160	-5.4593710558	-0.2502350815	H	-2.4237540414	5.2723382949	-5.2733483898
N	-1.8035776423	-0.1096753613	1.9709082746	C	-1.0938743823	2.8398682499	-2.4529885010
C	-2.9657702903	0.7813086248	2.0763208708	H	-1.3332456404	2.4113859622	-3.4178229712
H	-2.6626826914	1.8195592869	1.9212321622	C	-0.6600457063	1.9598003393	-1.4390921958
C	-1.6409441472	-1.0905791028	3.0352995503	H	-0.5015132923	2.3802322423	-0.4536506316
H	-1.7335979790	-0.5648650214	3.9931751250	C	-0.3770913799	0.6166135509	-1.5755576017

C	0.0753892204	-0.1462578026	-0.4485732035	H	0.6071733074	-3.9337381833	4.3830809285
C	0.8125997341	-1.3516255105	-0.6719051374	H	0.8630507264	-2.7055361834	3.1374183992
C	0.8268844843	-2.3386164366	0.2979845137	C	0.5335280672	5.0350683387	-0.6932832991
H	0.2399148118	-2.1568000239	1.1893707343	H	1.2000300784	5.2451951742	-1.5335255780
C	-0.2902779267	-0.0735097298	-2.9141727975	H	0.7903540597	4.0514497818	-0.2929289442
H	-0.5514716112	0.6030629322	-3.7286262146	H	0.7273667448	5.7781207969	0.0854527736
H	-0.9879065579	-0.9190821837	-2.9678114487	C	-1.8881923943	4.8159457458	0.0512003204
C	1.4536846660	-1.6285477314	-2.0200581248	H	-1.7020146242	3.8333306910	0.4907319565
H	2.5400062202	-1.7370389245	-1.9064724151	H	-2.9332663476	4.8563012280	-0.2664935789
H	1.0898086420	-2.6026344607	-2.3704961828	H	-1.7449526131	5.5669517510	0.8331980492
C	1.1438517411	-0.5782454849	-3.0858181090	Cyanine-like S₁ minimum			
H	1.8259907561	0.2741243977	-2.9969733179	H	-2.4484752646	7.4003298605	-4.7331659734
H	1.2956638311	-1.0076172985	-4.0806821032	C	-2.1293321189	7.4961712208	-3.7018912937
H	3.0845058427	-8.4281320943	1.3319510706	C	-1.2889619137	7.7796976982	-1.0213244276
C	2.3990888396	-7.9896803260	2.0480891289	C	-1.7365951501	6.3995248964	-2.9406497613
C	0.6204121573	-6.8782889783	3.9318550727	C	-2.0931003598	8.7447460964	-3.0914193347
C	1.8844844472	-6.7127415001	1.8977703260	C	-1.6788564273	8.8924441142	-1.7682624496
C	2.0021307136	-8.7113355241	3.1727626694	C	-1.3176902700	6.5325973161	-1.6143366888
C	1.1240690992	-8.1679700780	4.1049002583	H	-2.3913689260	9.6191350056	-3.6601248982
C	1.0073290794	-6.1541445680	2.8199848081	H	-1.6583428622	9.8789565693	-1.3180795934
H	2.3878805701	-9.7147312276	3.3184980069	H	-0.9666183841	7.8999447906	0.0087199016
H	0.8299604131	-8.7500898007	4.9713478132	N	-1.6769962572	5.0527846975	-3.2999487650
H	-0.0648914831	-6.4572951118	4.6617705237	C	-1.2102346672	4.2763061515	-2.2730033953
C	0.6358991343	-4.7524707727	2.3788748982	C	-0.9604231850	5.1700835217	-1.0585373223
C	1.4292129195	-4.6249084337	1.0732594884	H	-1.1617916145	4.1647500364	-5.1365313202
C	1.4975934691	-3.5699543543	0.1828022024	C	-2.0421787265	4.5387237832	-4.6025042114
H	2.1250634774	-3.7090486227	-0.6882119366	H	-2.7670222745	3.7257802009	-4.4996404304
N	2.1134268733	-5.7764467592	0.8661335883	H	-2.4975058770	5.3322732324	-5.1911827931
N	-0.2113399781	0.2668292723	0.8328254653	C	-1.0072535055	2.9170841909	-2.4224931242
C	0.7922926290	0.2317575172	1.9047404390	H	-1.2146702351	2.5026209697	-3.4019451466
H	1.7178597836	-0.1484334402	1.4741769918	C	-0.5608567067	2.0228464188	-1.4243343511
H	0.4935288408	-0.4677011859	2.6933311880	H	-0.4407918250	2.4018758845	-0.4165256751
C	-1.5451908507	0.7562299079	1.2067892088	C	-0.2380655341	0.6849310697	-1.6106512190
H	-2.1710105679	0.7128664723	0.3164594336	C	0.1128071452	-0.1479206706	-0.4922488272
H	-1.5017004093	1.8059414649	1.5179077940	C	0.7553686906	-1.4009098379	-0.7036162291
C	1.0428084997	1.6076682352	2.5156873536	C	0.7728384623	-2.3704701673	0.3051775545
H	1.3285100847	2.3329244994	1.7475662607	H	0.2192902862	-2.1435900079	1.2074716713
H	1.8617511101	1.5403739204	3.2375236241	C	-0.1221792797	0.0577318874	-2.9744774493
H	0.1703085085	1.9939743470	3.0494245636	H	-0.2332120029	0.8014480177	-3.7652195462
C	-2.1829049817	-0.0738438017	2.3179539513	H	-0.9101935693	-0.6924126571	-3.1268347566
H	-1.6510962974	0.0197219872	3.2685950591	C	1.3685393215	-1.7301035787	-2.0487015363
H	-2.2209954404	-1.1327634611	2.0441206309	H	2.4232735757	-2.0052867225	-1.9220713816
H	-3.2082239789	0.2689347590	2.4833265570	H	0.8711853677	-2.6288581683	-2.4381423128
C	2.9727943826	-6.0118809786	-0.2761575147	C	1.2483509656	-0.6115978766	-3.0795657388
H	3.8018357153	-5.2980687745	-0.2876459092	H	2.0222239776	0.1463006173	-2.9143688961
H	2.4069462126	-5.9160573850	-1.2075484152	H	1.4066576990	-1.0166422025	-4.0835206393
H	3.3802667518	-7.0187797127	-0.2209019785	H	3.0422589304	-8.4580622038	1.3978786751
C	-0.8799787884	-4.6497806488	2.1344742848	C	2.3847971866	-8.0006919811	2.1282345327
H	-1.4160568992	-4.8678738836	3.0624935416	C	0.6663059958	-6.8412394864	4.0450103576
H	-1.2065527532	-5.3698443386	1.3798913762	C	1.8731554685	-6.7174043250	1.9681379512
H	-1.1717354387	-3.6506107359	1.8019804868	C	2.0175603427	-8.6967136243	3.2748334657
C	1.1035262085	-3.7299207154	3.4301701312	C	1.1698473687	-8.1302931860	4.2256014074
H	2.1825653360	-3.7959448649	3.5914921148	C	1.0207763306	-6.1376847259	2.9101664447

H	2.3997295185	-9.7004593130	3.4278036308	H	1.0256538771	10.0475232758	0.5989792850
H	0.9004388445	-8.6964532392	5.1106583880	H	1.8217472689	9.1135705973	2.7409036312
H	0.0054636003	-6.4049596802	4.7882625473	H	1.5198840178	6.7014463230	3.2420653256
C	0.6389789552	-4.7448187506	2.4546515481	N	-0.4809563032	5.8219020719	-0.6085960561
C	1.3878369432	-4.6472829259	1.1274210419	C	-0.4390952078	4.6175537813	0.0349517111
C	1.4174136680	-3.6147161844	0.2017141768	C	0.2347372230	4.8212467379	1.4002714828
H	1.9977505854	-3.7931504137	-0.6957367416	H	-0.9766252048	7.0555999917	-2.2071297147
N	2.0783294885	-5.8085906971	0.9263165300	C	-1.0513425080	6.0079101161	-1.9234548329
N	-0.1955658834	0.2791492509	0.7980014734	H	-0.5173762765	5.4075348515	-2.6675647527
C	0.8084714758	0.3236229487	1.8587661223	H	-2.1079644053	5.7217327238	-1.9305069806
H	1.6597558336	-0.2902798822	1.5604349751	C	-0.9307764317	3.4730203131	-0.5376141713
H	0.3995473684	-0.1269679576	2.7722595759	H	-1.3542978980	3.5687082617	-1.5285252467
C	-1.5691280815	0.6063890934	1.1767470621	C	-0.9382237968	2.1782516964	0.0566426106
H	-2.1076920855	0.9398696465	0.2876898841	H	-0.5826885111	2.1248177836	1.0768748289
H	-1.5546360587	1.4533805147	1.8727452134	C	-1.2848470556	1.0001348440	-0.5450775956
C	1.2885030360	1.7436959042	2.1528290255	C	-1.1767954100	-0.2791695116	0.1558689888
H	1.7655385972	2.1769823221	1.2684787681	C	-0.5752033325	-1.3922813490	-0.5641059433
H	2.0208439361	1.7385667377	2.9662791489	C	0.2781078020	-2.2430255499	0.0927334597
H	0.4646135602	2.3982683032	2.4538663051	H	0.4600725466	-2.0375307980	1.1406440131
C	-2.3119537915	-0.5700126205	1.8072440529	C	-1.6239987459	0.9007375204	-2.0178237262
H	-1.8073119895	-0.9308646908	2.7094694601	H	-1.5413898044	1.8785842222	-2.4923980300
H	-2.3888712306	-1.4011989086	1.0994991676	H	-2.6684455087	0.5836719593	-2.1424203137
H	-3.3261017296	-0.2730235837	2.0923465066	C	-0.8000040966	-1.4634182552	-2.0603682554
C	2.9166347541	-6.0631966800	-0.2263761090	H	-0.0706691776	-2.1340310946	-2.5168973263
H	3.6844026197	-5.2890203866	-0.3163043020	H	-1.7889449691	-1.8975328330	-2.2633651418
H	2.3202913282	-6.0810429472	-1.1444053478	C	-0.7103314979	-0.0940909985	-2.7268649122
H	3.4084238497	-7.0264626275	-0.1115814835	H	0.3226488323	0.2688879153	-2.6845584377
C	-0.8861176191	-4.6376401720	2.2590998652	H	-0.9845642650	-0.1744060641	-3.7834520382
H	-1.3920444686	-4.8339230323	3.2089001644	H	4.3944203142	-7.3039890220	-0.8184518946
H	-1.2414566471	-5.3692187698	1.5289975457	C	4.3764661314	-6.7980145992	0.1400092908
H	-1.1793133895	-3.6421960035	1.9182207758	C	4.3562531388	-5.5076892436	2.6445464235
C	1.1369138831	-3.6976839414	3.4711022634	C	3.5327604301	-5.7304099647	0.3990643861
H	2.2175111234	-3.7729857680	3.6165959511	C	5.2214122340	-7.2136135309	1.1685188392
H	0.6526324390	-3.8678549595	4.4369966711	C	5.2161857428	-6.5807555422	2.4067523350
H	0.9037894241	-2.6799792343	3.1499670180	C	3.5151019808	-5.0874580308	1.6318894318
C	0.5139475252	5.1372325827	-0.6126105718	H	5.8933372678	-8.0472676841	0.9935938065
H	1.1799928148	5.3923565307	-1.4405808353	H	5.8832020683	-6.9221958909	3.1907352721
H	0.7994330770	4.1532794092	-0.2344249376	H	4.3538455724	-5.0145955742	3.6124249217
H	0.6724896533	5.8664111777	0.1871260485	C	2.4910784698	-3.9695945662	1.6052801717
C	-1.8991515368	4.8194804617	0.1143015804	C	1.9518152369	-4.0834593804	0.1718733662
H	-1.6855533728	3.8302998566	0.5261890056	C	0.9982981390	-3.3298726023	-0.4695217076
H	-2.9457034647	4.8422132106	-0.2000229282	H	0.7760891165	-3.5971074081	-1.4941609526
H	-1.7715927379	5.5535736252	0.9151483346	N	2.5920273290	-5.1136678781	-0.4495969767

Dye II-15

Bis-dipole Franck-Condon point

H	-0.0788502215	8.6143485034	-1.0769606899	H	-2.8948579530	1.2399472146	1.5204223390
C	0.2641587630	8.1868941755	-0.1417019097	C	-1.8879861814	-1.7396450634	2.0507193367
C	1.1685372162	7.1107609009	2.2991468835	H	-1.1117109271	-1.9548326109	2.7937865041
C	0.1069894603	6.8438753881	0.1602564042	H	-1.8786356045	-2.5299820944	1.3032723670
C	0.8893403968	8.9920092272	0.8099558164	H	-1.5535222849	1.2769899907	2.6666121771
C	1.3380726772	8.4671001532	2.0168638923	C	2.3374542048	-5.5095833754	-1.8170481004
C	0.5510807867	6.3040131680	1.3626629008	H	2.5411533978	-4.6811011251	-2.5029864603
				H	1.2970474310	-5.8259977684	-1.9420657712

H	2.9860084737	-6.3424162606	-2.0801424426	C	-0.5737746348	-1.3223411481	-2.0597610682
C	-0.7282770000	4.5254290430	2.5635101758	H	0.2920812654	-1.8259824813	-2.4966107806
H	-0.9856172891	3.4652128528	2.6226965642	H	-1.4524283401	-1.9299318766	-2.3200066892
H	-1.6546855988	5.0963284804	2.4616661389	C	-0.7193368013	0.0529825595	-2.7141865130
H	-0.2595549361	4.8094243883	3.5100360540	H	0.2473562604	0.5689897485	-2.7028938534
C	1.5313927381	4.0031970224	1.5260159605	H	-1.0123148848	-0.0624980703	-3.7626103553
H	2.2123477456	4.2207153662	0.6993318450	H	4.3205625126	-7.3647480864	-0.8171040539
H	1.3388308357	2.9274739899	1.5333420433	C	4.3225506870	-6.8636253193	0.1441242981
H	2.0408062084	4.2614482074	2.4589431917	C	4.3597486959	-5.5798421751	2.6538010942
C	3.1758660773	-2.6145679329	1.8540319320	C	3.5034721986	-5.7750332726	0.4148335203
H	3.9556709316	-2.4277237108	1.1113631399	C	5.1673513855	-7.3017374345	1.1610260328
H	3.6455482111	-2.6161357192	2.8419388042	C	5.1914655947	-6.6725773326	2.4026201954
H	2.4667087180	-1.7839274134	1.8194074118	C	3.5170532342	-5.1348560966	1.6538525416
C	1.3929831319	-4.2415131016	2.6492507171	H	5.8178430488	-8.1505177308	0.9766740756
H	1.8382077645	-4.2901043571	3.6469851339	H	5.8603481818	-7.0318243862	3.1771633161
H	0.8941311116	-5.1946064428	2.4559591379	H	4.3812533442	-5.0899955875	3.6231396916
H	0.6365032288	-3.4538379430	2.6570687723	C	2.5233378649	-3.9907069450	1.6427668526
C	-3.2366787213	-1.5340600593	2.7252180591	C	1.9718081833	-4.0808445312	0.2172521785
C	-3.1299137247	-0.1059334919	3.2543745843	C	1.0528959757	-3.2749389484	-0.4192809235
H	-3.4218177379	-2.2712320841	3.5089430979	H	0.8260638391	-3.5207810880	-1.4500208350
H	-4.0372237626	-1.6171846242	1.9835435677	N	2.5731369276	-5.1377650515	-0.4154634841
H	-4.1002693498	0.3717983362	3.4006447143	N	-1.7281023511	-0.4474426614	1.3942099958
H	-2.6105869825	-0.0979207203	4.2171673422	C	-2.5802570982	0.5712328772	2.0314409837
Bis-dipole S₁ minimum				H	-3.3190389839	0.9422377542	1.3106951780
H	-0.1939757702	8.6536866392	-1.0157902563	C	-2.0106699461	-1.7777959792	1.9615718983
C	0.1956146783	8.2244210241	-0.1000405494	H	-1.2236156929	-2.0742088565	2.6651562497
C	1.2241767923	7.1390600281	2.2938122459	H	-2.0433462330	-2.5232375503	1.1650672073
C	0.0905421767	6.8693244724	0.1906468647	H	-1.9953043156	1.4283633147	2.3720322339
C	0.8286928206	9.0327883490	0.8389577016	C	2.2837054687	-5.5299199059	-1.7758825852
C	1.3367917276	8.5034676215	2.0237745945	H	2.5346630687	-4.7245264589	-2.4745672656
C	0.5993607007	6.3245622540	1.3694881030	H	1.2226469126	-5.7759653584	-1.8875938067
H	0.9263736911	10.0948775614	0.6408070219	H	2.8721802489	-6.4077515790	-2.0343667596
H	1.8233294661	9.1566105098	2.7399137389	C	-0.5139665965	4.4492992369	2.6059983471
H	1.6236251210	6.7300859781	3.2171488560	H	-0.7101579731	3.3755202339	2.6433901676
N	-0.4963077111	5.8451856252	-0.5625224169	H	-1.4717629511	4.9756439243	2.5940337931
C	-0.3969001073	4.6354994200	0.0655133125	H	0.0115521813	4.7242623203	3.5248583439
C	0.3468709294	4.8315645666	1.3882931411	C	1.6890094638	4.0719055563	1.3996914549
H	-1.0605533546	7.0853807001	-2.1357309784	H	2.3007191035	4.3449535800	0.5362205514
C	-1.1218891407	6.0367289977	-1.8541948962	H	1.5441189069	2.9892846742	1.3896040832
H	-0.6134146245	5.4403375198	-2.6180109768	H	2.2464066004	4.3313322086	2.3041247117
H	-2.1763525477	5.7457835341	-1.8185577385	C	3.2449379965	-2.6541175680	1.8959460022
C	-0.8984081644	3.4817389761	-0.5008756986	H	4.0283604391	-2.4858776141	1.1525746812
H	-1.3988015985	3.5884497015	-1.4556114125	H	3.7147875519	-2.6713208671	2.8838127114
C	-0.8206182701	2.1716675077	0.0422626149	H	2.5551625758	-1.8077133151	1.8629953933
H	-0.3545602069	2.0580496152	1.0139343169	C	1.4249659711	-4.2321763810	2.6958696264
C	-1.3048120479	1.0255370580	-0.5433766101	H	1.8731291218	-4.2750963054	3.6928397228
C	-1.2113102803	-0.2787364121	0.1401266357	H	0.9103967882	-5.1792891517	2.5151472360
C	-0.4448678082	-1.2770408709	-0.5457182243	H	0.6825739369	-3.4311834570	2.6931283111
C	0.3811590008	-2.1586286354	0.1370155352	C	-3.3389622378	-1.6004239274	2.6911573500
H	0.5225522541	-1.9633933124	1.1932596433	C	-3.2534009115	-0.1610017896	3.1919956094
C	-1.7463507156	0.9252511066	-1.9744260769	H	-3.4734756126	-2.3310567709	3.4918045862
H	-1.8210807046	1.9015876937	-2.4575319817	H	-4.1721381841	-1.7108588380	1.9892514547
H	-2.7348785127	0.4519057445	-2.0326132856	H	-4.2240731213	0.2737157445	3.4392222825

H	-2.6269665268	-0.1083348086	4.0883417298	C	-0.1972780781	1.2004597392	-1.2525756911
Cyanine-like Franck-Condon point				H	-1.0996154180	1.7835980372	-1.0689923211
H	8.8108258670	-0.5040163616	2.8121686602	C	0.4521745979	-1.0907467634	-0.7500848092
C	8.5154400847	-0.2616323177	1.7978357994	H	-0.3832855562	-1.7942224016	-0.6269585790
C	7.7838552654	0.3709967033	-0.8503648442	H	1.3180713452	-1.5278919779	-0.2526669309
C	7.1896795799	-0.1199099218	1.4232201651	H	0.6404869898	1.9098627279	-1.3150958870
C	9.4823782828	-0.0785518090	0.8104247837	C	-5.9512051919	2.8889115178	2.4615865944
C	9.1268062121	0.2337646443	-0.4976134201	H	-6.9582978877	3.2856876671	2.5692147027
C	6.8170221233	0.1925706939	0.1211518169	H	-5.2625751340	3.7268500038	2.3207021501
H	10.5298889565	-0.1825548077	1.0725995495	H	-5.6837992298	2.3579484089	3.3805848413
H	9.8979865086	0.3717614945	-1.2474952914	C	4.7810055134	-0.8040611060	-0.9356986563
H	7.5100674908	0.6146971238	-1.8727347522	H	3.6907951226	-0.7962851743	-1.0023795917
N	6.0228379914	-0.2477667979	2.2088207806	H	5.0979740747	-1.8026857547	-0.6243844834
C	4.9021163174	-0.0270127765	1.4813177913	H	5.1818117597	-0.6204239198	-1.9365759266
C	5.3063476698	0.2717613986	0.0325712315	C	4.8677248937	1.6811374431	-0.4022018059
H	5.5683148485	0.2523554090	4.1976722265	H	5.2336723460	2.4392074536	0.2949096506
C	6.0194916388	-0.5623244830	3.6232682754	H	3.7807023279	1.7694154059	-0.4625299011
H	5.4589511936	-1.4829649252	3.8093345489	H	5.2806367664	1.9051292798	-1.3899095767
H	7.0422978232	-0.7034666513	3.9652014282	C	-4.4287121946	1.0688555713	-1.6289742019
C	3.6412771374	-0.0731129033	2.0488206860	H	-4.6366138701	2.1307065257	-1.7839553378
H	3.5887148347	-0.2853629416	3.1095693865	H	-4.8076762158	0.5225024221	-2.4972939102
C	2.4285596037	0.1487833109	1.3751302798	H	-3.3455035700	0.9327235399	-1.5932540558
H	2.4566870345	0.3043735058	0.3035444166	C	-4.8117929897	-0.9408781074	-0.1200966765
C	1.1846357399	0.2434960376	1.9757198198	H	-5.1861106891	-1.5282599535	-0.9633461578
C	0.0432642575	0.5096590008	1.1630708804	H	-5.3006272287	-1.3048082295	0.7871694140
C	-1.1154297610	1.1108434449	1.7399578716	H	-3.7392697412	-1.1269491997	-0.0282909936
C	-2.3280501886	1.0301815823	1.0824390679	C	0.6936243091	-0.7951891322	-2.2286951923
H	-2.3236265731	0.4530183502	0.1655006409	H	0.5317654669	-1.6727183001	-2.8581453372
C	1.0737383681	0.2248477069	3.4871058342	H	1.7238618800	-0.4557936006	-2.3852208133
H	1.7868935278	0.9555339140	3.8902269865	C	-0.2821575152	0.3480312765	-2.5160712078
H	1.3927957315	-0.7507777514	3.8756079890	H	-1.2968134314	-0.0480342678	-2.6363414637
C	-0.9653849778	1.6466827759	3.1420191840	H	-0.0356028100	0.9148614133	-3.4163173344
H	-0.3353688219	2.5457609077	3.1541923329	Cyanine-like S₁ minimum			
H	-1.9313455025	1.9340054168	3.5606381552	H	8.8374019483	-0.5097944766	2.8248571490
C	-0.3244182447	0.5582544411	4.0065667918	C	8.5482131574	-0.2702379337	1.8080813653
H	-0.2623936972	0.8760678802	5.0516933642	C	7.8297944575	0.3647040051	-0.8476738840
H	-0.9646199935	-0.3303448906	3.9804998455	C	7.2182491157	-0.1289990760	1.4261845268
H	-8.6791181929	2.6819038475	1.4860400590	C	9.5179620708	-0.0863110235	0.8280735732
C	-8.3516146477	2.0123563839	0.6990459466	C	9.1704544243	0.2269151713	-0.4852725226
C	-7.5367873295	0.2624108402	-1.3549531629	C	6.8553635169	0.1868104907	0.1150418108
C	-7.0282668488	1.6311450463	0.5508370833	H	10.5644217741	-0.1881056638	1.0957779978
C	-9.2725745901	1.4965964074	-0.2117319120	H	9.9472108627	0.3652763862	-1.2295788674
C	-8.8759065369	0.6329033716	-1.2273382102	H	7.5634023623	0.6097922272	-1.8716355648
C	-6.6156648301	0.7672852547	-0.4567717608	N	6.0582602125	-0.2551308154	2.1962240555
H	-10.3167860995	1.7764336579	-0.1212653766	C	4.9347825438	-0.0204013581	1.4567377230
H	-9.6115597428	0.2446399383	-1.9231746339	C	5.3471919244	0.2716196938	0.0150155688
H	-7.2303221951	-0.4125583758	-2.1487369243	H	5.6360019579	0.2535925846	4.1916252625
C	-5.1193350114	0.5481882443	-0.3547361344	C	6.0424290292	-0.5787882323	3.6075686177
C	-4.7707065815	1.4032886879	0.8704091823	H	5.4316562893	-1.4689892059	3.7862844586
C	-3.5519531126	1.5896893321	1.4933416771	H	7.0562245789	-0.7798585412	3.9464233217
H	-3.5432856008	2.2252537711	2.3699528999	C	3.6696098614	-0.0357648344	2.0249063777
N	-5.9036871536	1.9985581255	1.3203807460	H	3.6206158832	-0.2179988699	3.0924834124
N	0.0734315032	0.2179585186	-0.1870422720	C	2.4534833850	0.1831121343	1.3571681459

C	5.2987435605	-6.2884156978	2.4269305630	C	0.8185171206	6.4853979918	1.0067785182
C	3.5397923427	-4.8748378349	1.6315425630	H	0.9571693255	10.2097939194	0.0271346556
H	6.0776392817	-7.7033156369	1.0137199815	H	2.3587557714	9.3592458871	1.8695896739
H	5.9661133325	-6.6043979044	3.2212149414	H	2.2816237790	6.9654296607	2.5111229201
H	4.3336970828	-4.7807210204	3.6294024003	N	-0.7246685433	5.9214590908	-0.5652963301
C	2.4620652055	-3.8086800017	1.5950498948	C	-0.4511111196	4.7538809418	0.0538679253
C	1.9515245023	-3.9391216930	0.1520553150	C	0.5705767394	5.0015481001	1.1631054155
C	0.9671006526	-3.2369851330	-0.4974412711	H	-1.8039212184	7.1299554577	-1.8734137145
H	0.7759142944	-3.5086018005	-1.5269904022	C	-1.6602319330	6.0722752491	-1.6668916955
N	2.6597340211	-4.9269336906	-0.4680391605	H	-1.2764433308	5.5836216011	-2.5667705038
N	-1.9940329615	-0.4496993363	1.2985198744	H	-2.6263965092	5.6380918762	-1.4012044137
C	-2.9083473324	0.5658890463	1.8848611378	C	-1.0352909922	3.5569120599	-0.3511111815
H	-3.9287159449	0.2726582133	1.6133339659	H	-1.7155940913	3.6024713388	-1.1928212444
C	-1.9630300827	-1.7142792297	2.0709126691	C	-0.8012048349	2.2943464033	0.2219587245
H	-1.0449431149	-1.7409227707	2.6680984001	H	-0.1671419948	2.2311825983	1.0978023806
H	-1.9198189651	-2.5424884661	1.3625263522	C	-1.3476893649	1.1079272046	-0.2189010566
H	-2.7247675456	1.5315469351	1.4359426541	C	-1.0317778898	-0.1804774460	0.4468258354
C	2.4504604853	-5.3215922561	-1.8430772055	C	-0.1371548067	-1.0139082649	-0.2511210985
H	2.6236109502	-4.4772592977	-2.5181327958	C	0.5689207226	-2.0315291156	0.3800806042
H	1.4298981360	-5.6894252807	-1.9902611166	H	0.5197950198	-2.0419044224	1.4622480997
H	3.1448800521	-6.1180759845	-2.1019000580	C	-1.9665929300	0.9041386466	-1.5574100308
C	-0.7959514742	4.3522334423	2.5115520214	H	-2.3677478368	1.8043705920	-2.0318505323
H	-1.1030775452	3.3036559595	2.5481071990	H	-2.7644708149	0.1571430863	-1.4997177203
H	-1.6865545469	4.9665935389	2.3567996155	C	-0.0836600264	-0.8772173717	-1.7715594921
H	-0.3748953428	4.6093425339	3.4877696680	H	0.9532549413	-0.9039019440	-2.1231623370
C	1.4867520080	3.7148457895	1.5972842346	H	-0.5554691922	-1.7788682186	-2.1849323642
H	2.2247263493	3.8998611168	0.8126117281	C	-0.7739755387	0.3537701975	-2.3899328192
H	1.2289175926	2.6529817999	1.5773485626	H	-0.0511743841	1.1693135212	-2.4975436832
H	1.9581331861	3.9300393527	2.5607423296	H	-1.1256660179	0.1113038804	-3.3974017625
C	3.0770221170	-2.4232188873	1.8593952319	H	4.6484109593	-7.0583814975	-0.9039017168
H	3.8544446939	-2.1944089247	1.1260900555	C	4.4404944450	-6.7854177742	0.1245237163
H	3.5354360775	-2.4075551248	2.8524786303	C	3.9199811534	-6.1101067473	2.8075764498
H	2.3284764194	-1.6277973618	1.8209853601	C	3.5839241559	-5.7454103239	0.4543288418
C	1.3651192721	-4.1387387950	2.6229164554	C	5.0384305533	-7.4877812278	1.1702924691
H	1.7999694439	-4.1758626912	3.6257867457	C	4.7860151746	-7.1606875223	2.4978116625
H	0.9118261322	-5.1117000786	2.4163354168	C	3.3226137940	-5.4060377464	1.7806009013
H	0.5727279131	-3.3868372952	2.6290415442	H	5.7128798604	-8.3054138726	0.9373331353
C	-3.1575635454	-1.8465548983	3.0074092901	H	5.2617735172	-7.7226795297	3.2941251683
H	-3.0896740673	-2.8227721143	3.4957508703	H	3.7222464074	-5.8539466512	3.8447705876
H	-4.0836567465	-1.8634711040	2.4236874025	C	2.3548272156	-4.2390216461	1.8249082852
C	-2.7631618621	0.6166158125	3.4002888035	C	2.1216869122	-3.9791521310	0.3328594427
H	-3.3714911296	1.4437276017	3.7762602141	C	1.3439626820	-3.0231302995	-0.2695665365
H	-1.7234303814	0.8606377438	3.6460548226	H	1.3343225146	-3.0186082374	-1.3539875332
C	-3.1823978929	-0.7194021124	4.0463885487	N	2.8610456890	-4.8895345220	-0.3877538853
H	-4.1844743212	-0.6418232555	4.4768213969	N	-1.7424440935	-0.5682741396	1.5697082281
H	-2.5078936546	-0.9599384283	4.8736388024	C	-2.3482657838	0.4300501314	2.4497031151
Bis-dipole S₁ minimum				H	-3.1859068637	0.9482077010	1.9573339992
H	-0.5463447582	8.7038273515	-1.2206936985	C	-2.2433091712	-1.9437735716	1.7100822429
C	0.0577703054	8.3167858327	-0.4086459438	H	-1.6706219134	-2.4941311195	2.4684389546
C	1.6599761808	7.3339431429	1.7010782268	H	-2.0825764754	-2.4563778433	0.7609965198
C	0.0330631774	6.9829753280	-0.0281780977	H	-1.5980954286	1.1913670507	2.6871927576
C	0.9096306849	9.1606198422	0.2970834640	C	2.8901432982	-4.9302881359	-1.8288059052
C	1.7015109936	8.6798011645	1.3384196805	H	3.2473772910	-3.9784320489	-2.2375022134

H	1.8923765822	-5.1312147688	-2.2346698500	C	-1.8561680318	6.3658064970	-1.8200605123
H	3.5624142765	-5.7201062707	-2.1585391420	H	-1.7639456209	9.7216158501	-3.7060834135
C	-0.0228934501	4.7041691663	2.5549229835	H	-3.3515509800	9.3924917726	-1.8444408427
H	-0.2343689558	3.6415883961	2.6895287268	H	-3.4177919338	7.2363760618	-0.6212742150
H	-0.9475275148	5.2638327679	2.7171382285	N	-0.2161222636	5.3866151358	-3.0582006437
H	0.6925646899	5.0052135697	3.3246360599	C	-0.5650515535	4.4221456418	-2.1709074249
C	1.8750036644	4.2161367901	0.9278769231	C	-1.6723043698	4.9688836073	-1.2617047735
H	2.2878782855	4.4228808447	-0.0629166019	H	0.8675723477	6.1241793357	-4.6747482342
H	1.7264454558	3.1389429280	1.0197493593	C	0.7972353410	5.2168007238	-4.0790796111
H	2.6171599084	4.5184558649	1.6712775911	H	1.7730715182	5.0196535897	-3.6252868209
C	3.0066822190	-3.0319062880	2.5220883236	H	0.5373621617	4.3852122241	-4.7407914769
H	3.9258880641	-2.7355175027	2.0100169343	C	0.0367174903	3.1785079557	-2.1770853604
H	3.2632433475	-3.2937754134	3.5529581450	H	0.8003564854	3.0130872745	-2.9262566945
H	2.3377818852	-2.1686867874	2.5475593380	C	-0.2434912258	2.1098847285	-1.3040614710
C	1.0580719035	-4.6542314940	2.5433573522	H	-0.9591831552	2.2759027419	-0.5099735809
H	1.2812393432	-4.9368104845	3.5764414243	C	0.2825537390	0.8361190249	-1.4165213533
H	0.5970037945	-5.5131228158	2.0492725950	C	-0.0730668551	-0.1756706385	-0.4677423779
H	0.3304306552	-3.8398436480	2.5640328583	C	0.0078984991	-1.5532589242	-0.8680119966
C	-3.7209912600	-1.9387759346	2.0898100957	C	0.2991850550	-2.5250171018	0.0631569421
H	-4.0970316015	-2.9663963571	2.0998146359	H	0.4329473533	-2.1835901631	1.0809661275
H	-4.2764598054	-1.4109925410	1.3060495119	C	1.1108968536	0.4840920428	-2.6416178959
C	-2.8448933560	-0.2234910057	3.7351036953	H	2.0844744723	0.9891071521	-2.5984172942
H	-3.2071272478	0.5525128540	4.4157530735	H	0.5986456617	0.8984437916	-3.5181954362
H	-1.9915001441	-0.6997479065	4.2298340844	C	0.0915236639	-1.7898992693	-2.3546735764
C	-3.9442231284	-1.2605890689	3.4532768604	H	0.1864265491	-2.8509559423	-2.5873468806
H	-4.9286037564	-0.7824873832	3.4698232136	H	-0.8123524576	-1.4330919123	-2.8635128178
H	-3.9494267672	-2.0065310035	4.2537779902	C	1.3119649366	-1.0181603477	-2.8633834715
Cyanine-like Franck-Condon Point				H	2.1957674703	-1.3761155330	-2.3248834369
H	-0.2234359147	7.9225059394	-4.3912593911	H	1.4866657319	-1.2105391948	-3.9264127561
C	-0.9130857608	7.7603076986	-3.5708820058	H	1.8770626329	-8.8769496660	0.7280175574
C	-2.7185097432	7.3767786772	-1.4402897117	C	2.0124987742	-8.2028988916	1.5661223364
C	-0.9717935218	6.5649240167	-2.8735969833	C	2.3809464988	-6.4796418549	3.7650586885
C	-1.7866237334	8.7736817190	-3.1789375489				
C	-2.6804391639	8.5895560946	-2.1292052161	C	0.8364786646	-6.6883959355	-0.8774518885
C	1.6849643704	-6.8587235007	1.4981662374	H	1.4644452940	-6.2427764254	-1.6557622246
C	2.5353753405	-8.6759510415	2.7688937752	H	-0.2146141904	-6.5151244223	-1.1263417512
C	2.7187671963	-7.8303411852	3.8577100832	H	1.0143847613	-7.7614528301	-0.8599728305
C	1.8639555829	-5.9998914882	2.5765278222	C	-2.9745323169	4.1611015624	-1.4000255216
H	2.8034173066	-9.7240789529	2.8506619657	H	-2.8647790144	3.1426130502	-1.0199205217
H	3.1273910529	-8.2219359676	4.7828027270	H	-3.2919231101	4.1033870395	-2.4442627885
H	2.5271879139	-5.8212873935	4.6164754620	H	-3.7709309554	4.6505744386	-0.8322892869
C	1.4177977867	-4.6030647764	2.1918487470	C	-1.2171998475	5.0466072202	0.2068327887
C	0.9793278764	-4.8147344361	0.7358601625	H	-0.2701743149	5.5841588920	0.2999196947
C	0.5072585820	-3.9008104142	-0.1807183351	H	-1.0938939414	4.0543229215	0.6459569514
H	0.2954342934	-4.2709067249	-1.1756068079	H	-1.9682615717	5.5822705847	0.7940975242
N	1.1489595689	-6.1262167117	0.4190817497	C	2.5966921021	-3.6198835739	2.2991839855
N	-0.4868052983	0.1546882191	0.7934999943	H	3.4305556613	-3.9351661949	1.6666523454
C	0.1358909131	1.2405255724	1.5748666065	H	2.9520882958	-3.5862436792	3.3331256823
H	-0.3937330207	2.1914709595	1.4557404825	H	2.3108183296	-2.6066475554	2.0065205315
C	-1.5754809092	-0.5753235430	1.4768319573	C	0.2442408690	-4.1650369903	3.0869098241
H	-1.2073039469	-1.4428138992	2.0338911473	H	0.5578315056	-4.1851078715	4.1343715695
H	-2.2592816301	-0.9512712771	0.7132077837	H	-0.6089770234	-4.8390949699	2.9764998348
H	1.1499161017	1.3861675771	1.1984854649				

H	-0.0881302441	-3.1496790626	2.8581460458	C	-1.0864761558	6.6007738491	-2.8438983473
C	-2.2814011767	0.3555016427	2.4563553902	C	-1.9273816778	8.8117549104	-3.0730976159
H	-3.1530226766	-0.1599856352	2.8695975855	C	-2.7456892274	8.6156288598	-1.9614177099
H	-2.6657590663	1.2254128376	1.9119105338	C	-1.8996143789	6.3899590702	-1.7282055286
C	0.1249296028	0.8723732759	3.0543586456	H	-1.9465407007	9.7649049975	-3.5904514812
H	0.7028267743	1.6143864622	3.6126874792	H	-3.3934559127	9.4166429227	-1.6227917231
H	0.6384067787	-0.0866070664	3.1874202690	H	-3.3750282819	7.2475690893	-0.4181769107
C	-1.3213357743	0.7944828568	3.5766658617	N	-0.3480432475	5.4392678253	-3.0880180775
H	-1.6355290388	1.7675211643	3.9662502655	C	-0.6366953434	4.4581751154	-2.1829797967
H	-1.3731294378	0.0940934430	4.4158605683	C	-1.6767936222	4.9890492954	-1.1983491148
Cyanine-like S₁ minimum				H	0.6574346424	6.2112052452	-4.7392176233
H	-0.4568018528	7.9781395612	-4.4031659099	C	0.5933543802	5.2824987539	-4.1767803597
C	-1.0832605870	7.8074433570	-3.5351533245	H	1.5880168508	5.0387386258	-3.7910126013
C	-2.7345797306	7.3963131153	-1.2824803274	H	0.2697962090	4.4845932893	-4.8530558689
C	-0.0388628104	3.2077244838	-2.2508311870	H	1.3486431884	1.1578171535	1.1664018639
H	0.6575316326	3.0543414014	-3.0671871144	C	0.9122773029	-6.7158282114	-0.7933179012
C	-0.2485273271	2.1226078715	-1.3848567924	H	1.6027778231	-6.3199892485	-1.5456988581
H	-0.8994768444	2.2507350979	-0.5300735415	H	-0.1136312883	-6.4920988164	-1.1015440284
C	0.2818184531	0.8409291602	-1.5735486265	H	1.0315996096	-7.7958552702	-0.7458839200
C	0.0457508095	-0.1811563794	-0.6153946646	C	-2.9863453036	4.1772693873	-1.2582639226
C	0.2583233102	-1.5618502115	-0.9613365791	H	-2.8423847202	3.1531952768	-0.9062473771
C	0.4667892902	-2.5068468190	0.0316394406	H	-3.3779544419	4.1379079025	-2.2780682600
H	0.5186767121	-2.1196920018	1.0413117079	H	-3.7411501263	4.6514213941	-0.6245302348
C	1.0347555217	0.5349320806	-2.8525488401	C	-1.1285317277	5.0422969668	0.2416315505
H	1.9065305439	1.1956750929	-2.9413356127	H	-0.2019781873	5.6203096647	0.2903693217
H	0.3818582285	0.7888981830	-3.6983208576	H	-0.9292033318	4.0420641102	0.6318453619
C	0.4079203615	-1.8596903918	-2.4289465894	H	-1.8625447796	5.5209516495	0.8962853223
H	0.6923569342	-2.8983851389	-2.6047289239	C	2.5751471719	-3.6296614341	2.4467777494
H	-0.5403211337	-1.6922195492	-2.9568895283	H	3.4434970724	-3.9696802580	1.8769076623
C	1.4790392254	-0.9208030280	-2.9896901586	H	2.8583048813	-3.5863868099	3.5025064004
H	2.4118456879	-1.0865932641	-2.4396616280	H	2.3271751181	-2.6169839000	2.1206638485
H	1.6816943272	-1.1469498612	-4.0411268287	C	0.1682126404	-4.1040769881	3.0872125763
H	1.8114210408	-8.9023419689	0.8806787081	H	0.4237650067	-4.0942057820	4.1507805313
C	1.9120921823	-8.2229357561	1.7190085293	H	-0.6907415533	-4.7658681004	2.9510175136
C	2.1940790290	-6.4763809620	3.9191604618	H	-0.1274228645	-3.0915267636	2.8030756437
C	1.6269809658	-6.8647475811	1.6132613318	C	-2.2044368927	0.4211513708	2.2924104470
C	2.3430012315	-8.6924533693	2.9545440749	H	-3.1414114707	-0.0168362055	2.6493137721
C	2.4842404077	-7.8358605495	4.0459449308	H	-2.4653873502	1.3826759469	1.8346768057
C	1.7667257178	-5.9941075372	2.6976003247	C	0.2364261497	0.6578667946	2.9653871888
H	2.5732172552	-9.7464125356	3.0679085501	H	0.8452278852	1.3234405515	3.5845962759
H	2.8222313371	-8.2295860213	4.9981511177	H	0.6853025297	-0.3394726617	3.0452678695
H	2.3070386564	-5.8134208011	4.7719106800	C	-1.2243941288	0.6313611274	3.4592065158
C	1.3834038627	-4.5919449638	2.2722864772	H	-1.4679354388	1.5655445551	3.9744286030
C	1.0338667077	-4.8105156438	0.7998970300	H	-1.3457656076	-0.1674545465	4.1980670217
C	0.6552718423	-3.8940912034	-0.1619639464				
H	0.4967265483	-4.2791982405	-1.1624471658				
N	1.1816195971	-6.1411601256	0.5074561695				
N	-0.3971804501	0.1413510146	0.6626083539				
C	0.3121889783	1.1057639938	1.5086524411				
H	-0.0979229783	2.1225928138	1.4315281842				
C	-1.6014573647	-0.4858588444	1.2250308420				
H	-1.3976368993	-1.4679508276	1.6736759654				
H	-2.3129881353	-0.6544083471	0.4116102886				

REFERENCES

- (1) Rathore, N.; Panwar, N. L.; Yettou, F.; Gama, A. A comprehensive review of different types of solar photovoltaic cells and their applications. *International Journal of Ambient Energy* **2021**, *42* (10), 1200-1217. DOI: 10.1080/01430750.2019.1592774.
- (2) Husain, A. A. F.; Hasan, W. Z. W.; Shafie, S.; Hamidon, M. N.; Pandey, S. S. A review of transparent solar photovoltaic technologies. *Renew Sust Energ Rev* **2018**, *94*, 779-791. DOI: 10.1016/j.rser.2018.06.031.
- (3) Traverse, C. J.; Pandey, R.; Barr, M. C.; Lunt, R. R. Emergence of highly transparent photovoltaics for distributed applications. *Nat Energy* **2017**, *2* (11). DOI: 10.1038/s41560-017-0016-9.
- (4) Yang, C. C.; Lunt, R. R. Limits of Visibly Transparent Luminescent Solar Concentrators. *Adv Opt Mater* **2017**, *5* (8). DOI: ARTN 160085110.1002/adom.201600851.
- (5) Sharma, M.; Gungor, K.; Yeltik, A.; Olutas, M.; Guzelturk, B.; Kelestemur, Y.; Erdem, T.; Delikanli, S.; McBride, J. R.; Demir, H. V. Near-Unity Emitting Copper-Doped Colloidal Semiconductor Quantum Wells for Luminescent Solar Concentrators. *Adv Mater* **2017**, *29* (30). DOI: ARTN 170082110.1002/adma.201700821.
- (6) Ooyama, Y.; Harima, Y. Photophysical and Electrochemical Properties, and Molecular Structures of Organic Dyes for Dye-Sensitized Solar Cells. *Chemphyschem* **2012**, *13* (18), 4032-4080. DOI: 10.1002/cphc.201200218.
- (7) Yang, C. In PhD Thesis "HIGH-PERFORMANCE VISIBLY TRANSPARENT LUMINESCENT SOLAR CONCENTRATORS". *Michigan State University* **2022**.
- (8) Zhao, Y.; Lunt, R. R. Transparent Luminescent Solar Concentrators for Large-Area Solar Windows Enabled by Massive Stokes-Shift Nanocluster Phosphors. *Adv Energy Mater* **2013**, *3* (9), 1143-1148. DOI: 10.1002/aenm.201300173.
- (9) Kuttipillai, P. S.; Yang, C. C.; Chen, P.; Wang, L. L.; Bates, M.; Lunt, S. Y.; Lunt, R. R. Enhanced Electroluminescence Efficiency in Metal Halide Nanocluster Based Light Emitting Diodes through Apical Halide Exchange. *Acs Appl Energ Mater* **2018**, *1* (8), 3587-3592. DOI: 10.1021/acsaem.8b00837.
- (10) Sun, W.; Guo, S. G.; Hu, C.; Fan, J. L.; Peng, X. J. Recent Development of Chemosensors Based on Cyanine Platforms. *Chem Rev* **2016**, *116* (14), 7768-7817. DOI: 10.1021/acs.chemrev.6b00001.

- (11) Samanta, A.; Vendrell, M.; Das, R.; Chang, Y. T. Development of photostable near-infrared cyanine dyes. *Chem Commun* **2010**, *46* (39), 7406-7408. DOI: 10.1039/c0cc02366c.
- (12) Davydenko, I.; Barlow, S.; Sharma, R.; Benis, S.; Simon, J.; Allen, T. G.; Cooper, M. W.; Khrustalev, V.; Jucov, E. V.; Castaneda, R.; et al. Facile Incorporation of Pd(PPh₃)₂Hal Substituents into Polymethines, Merocyanines, and Perylene Diimides as a Means of Suppressing Intermolecular Interactions. *J Am Chem Soc* **2016**, *138* (32), 10112-10115. DOI: 10.1021/jacs.6b06361.
- (13) Zhao, Y. M.; Meek, G. A.; Levine, B. G.; Lunt, R. R. Near-Infrared Harvesting Transparent Luminescent Solar Concentrators. *Adv Opt Mater* **2014**, *2* (7), 606-611. DOI: 10.1002/adom.201400103.
- (14) Yang, C. C.; Zhang, J.; Peng, W. T.; Sheng, W.; Liu, D. Y.; Kuttipillai, P. S.; Young, M.; Donahue, M. R.; Levine, B. G.; Borhan, B.; et al. Impact of Stokes Shift on the Performance of Near-Infrared Harvesting Transparent Luminescent Solar Concentrators. *Sci Rep-Uk* **2018**, *8*. DOI: ARTN 1635910.1038/s41598-018-34442-3.
- (15) Peng, X. J.; Song, F. L.; Lu, E.; Wang, Y. N.; Zhou, W.; Fan, J. L.; Gao, Y. L. Heptamethine cyanine dyes with a large stokes shift and strong fluorescence: A paradigm for excited-state intramolecular charge transfer. *J Am Chem Soc* **2005**, *127* (12), 4170-4171. DOI: 10.1021/ja043413z.
- (16) Pascal, S.; Haefele, A.; Monnereau, C.; Charaf-Eddin, A.; Jacquemin, D.; Le Guennic, B.; Andraud, C.; Maury, O. Expanding the Polymethine Paradigm: Evidence for the Contribution of a Bis-Dipolar Electronic Structure. *J Phys Chem A* **2014**, *118* (23), 4038-4047. DOI: 10.1021/jp501358q.
- (17) Das, R. K.; Samanta, A.; Ha, H. H.; Chang, Y. T. Solid phase synthesis of ultra-photostable cyanine NIR dye library. *Rsc Adv* **2011**, *1* (4), 573-575. DOI: 10.1039/c1ra00498k.
- (18) Le Guennic, B.; Jacquemin, D. Taking Up the Cyanine Challenge with Quantum Tools. *Accounts Chem Res* **2015**, *48* (3), 530-537. DOI: 10.1021/ar500447q.
- (19) Bassal, F.; Laurent, A. D.; Le Guennic, B.; Jacquemin, D. Exploring the excited-states of squaraine dyes with TD-DFT, SOS-CIS(D) and ADC(2). *Dyes Pigments* **2017**, *138*, 169-175. DOI: 10.1016/j.dyepig.2016.11.046.
- (20) Yanai, T.; Tew, D. P.; Handy, N. C. A new hybrid exchange-correlation functional using the Coulomb-attenuating method (CAM-B3LYP). *Chem Phys Lett* **2004**, *393* (1-3), 51-57. DOI: 10.1016/j.cplett.2004.06.011.

- (21) Ufimtsev, I. S.; Martinez, T. J. Quantum Chemistry on Graphical Processing Units. 3. Analytical Energy Gradients, Geometry Optimization, and First Principles Molecular Dynamics. *J Chem Theory Comput* **2009**, *5* (10), 2619-2628. DOI: 10.1021/ct9003004.
- (22) Isborn, C. M.; Luehr, N.; Ufimtsev, I. S.; Martinez, T. J. Excited-State Electronic Structure with Configuration Interaction Singles and Tamm-Dancoff Time-Dependent Density Functional Theory on Graphical Processing Units. *J Chem Theory Comput* **2011**, *7* (6), 1814-1823. DOI: 10.1021/ct200030k.
- (23) Liu, X. G.; Xu, Z. C.; Cole, J. M. Molecular Design of UV-vis Absorption and Emission Properties in Organic Fluorophores: Toward Larger Bathochromic Shifts, Enhanced Molar Extinction Coefficients, and Greater Stokes Shifts. *J Phys Chem C* **2013**, *117* (32), 16584-16595. DOI: 10.1021/jp404170w.
- (24) Siebert, M. R.; Tantillo, D. J. Fundamental properties of N-alkenylaziridines-implications for the design of new reactions and organocatalysts. *J Phys Org Chem* **2011**, *24* (6), 445-449. DOI: 10.1002/poc.1776.
- (25) Dong, V. M.; Fiedler, D.; Carl, B.; Bergman, R. G.; Raymond, K. N. Molecular recognition and stabilization of iminium ions in water. *J Am Chem Soc* **2006**, *128* (45), 14464-14465. DOI: 10.1021/ja0657915.
- (26) Zhang, J.; Moemeni, M.; Yang, C. C.; Liang, F. C.; Peng, W. T.; Levine, B. G.; Lunt, R. R.; Borhan, B. General strategy for tuning the Stokes shifts of near infrared cyanine dyes. *J Mater Chem C* **2020**, *8* (47), 16769-16773. DOI: 10.1039/d0tc03615c.
- (27) Zhang, Q.; Kan, B.; Liu, F.; Long, G. K.; Wan, X. J.; Chen, X. Q.; Zuo, Y.; Ni, W.; Zhang, H. J.; Li, M. M.; et al. Small-molecule solar cells with efficiency over 9%. *Nat Photonics* **2015**, *9* (1), 35-41. DOI: 10.1038/Nphoton.2014.269.
- (28) Xiao, Z.; Jia, X.; Ding, L. M. Ternary organic solar cells offer 14% power conversion efficiency. *Sci Bull* **2017**, *62* (23), 1562-1564. DOI: 10.1016/j.scib.2017.11.003.
- (29) Meng, L. X.; Zhang, Y. M.; Wan, X. J.; Li, C. X.; Zhang, X.; Wang, Y. B.; Ke, X.; Xiao, Z.; Ding, L. M.; Xia, R. X.; et al. Organic and solution-processed tandem solar cells with 17.3% efficiency. *Science* **2018**, *361* (6407), 1094-+. DOI: 10.1126/science.aat2612.
- (30) Xiao, Z.; Jia, X.; Li, D.; Wang, S. Z.; Geng, X. J.; Liu, F.; Chen, J. W.; Yang, S. F.; Russell, T. P.; Ding, L. M. 26 mA cm⁻² J(sc) from organic solar cells with a low-bandgap nonfullerene acceptor. *Sci Bull* **2017**, *62* (22), 1494-1496. DOI: 10.1016/j.scib.2017.10.017.

- (31) Wang, J. Y.; Zhang, J. X.; Xiao, Y. Q.; Xiao, T.; Zhu, R. Y.; Yan, C. Q.; Fu, Y. Q.; Lu, G. H.; Lu, X. H.; Marder, S. R.; et al. Effect of Isomerization on High-Performance Nonfullerene Electron Acceptors. *J Am Chem Soc* **2018**, *140* (29), 9140-9147. DOI: 10.1021/jacs.8b04027.
- (32) Yang, C. H.; Moemeni, M.; Bates, M.; Sheng, W.; Borhan, B.; Lunt, R. R. High-Performance Near-Infrared Harvesting Transparent Luminescent Solar Concentrators. *Adv Opt Mater* **2020**, *8* (8). DOI: ARTN 190153610.1002/adom.201901536.
- (33) Liu, G. J.; Zhao, H. G.; Diao, F. Y.; Ling, Z. B.; Wang, Y. Q. Stable tandem luminescent solar concentrators based on CdSe/CdS quantum dots and carbon dots. *J Mater Chem C* **2018**, *6* (37), 10059-10066. DOI: 10.1039/c8tc02532k.
- (34) Mateen, F.; Ali, M.; Lee, S. Y.; Jeong, S. H.; Ko, M. J.; Hong, S. K. Tandem structured luminescent solar concentrator based on inorganic carbon quantum dots and organic dyes. *Sol Energy* **2019**, *190*, 488-494. DOI: 10.1016/j.solener.2019.08.045.
- (35) Liu, C.; Li, B. Multiple dyes containing luminescent solar concentrators with enhanced absorption and efficiency. *J Optics-Uk* **2015**, *17* (2). DOI: Artn 02590110.1088/2040-8978/17/2/025901.
- (36) Banal, J. L.; Zhang, B. L.; Jones, D. J.; Ghiggino, K. P.; Wong, W. W. H. Emissive Molecular Aggregates and Energy Migration in Luminescent Solar Concentrators. *Accounts Chem Res* **2017**, *50* (1), 49-57. DOI: 10.1021/acs.accounts.6b00432.
- (37) Zhang, B. L.; Banal, J. L.; Jones, D. J.; Tang, B. Z.; Ghiggino, K. P.; Wong, W. W. H. Aggregation-induced emission-mediated spectral downconversion in luminescent solar concentrators. *Mater Chem Front* **2018**, *2* (3), 615-619. DOI: 10.1039/c7qm00598a.
- (38) Goetzberger, A.; Greubel, W. Solar-Energy Conversion with Fluorescent Collectors. *Appl Phys* **1977**, *14* (2), 123-139. DOI: Doi 10.1007/Bf00883080.
- (39) Kirakci, K.; Kubat, P.; Dusek, M.; Fejfarova, K.; Sicha, V.; Mosinger, J.; Lang, K. A Highly Luminescent Hexanuclear Molybdenum Cluster - A Promising Candidate toward Photoactive Materials. *Eur J Inorg Chem* **2012**, (19), 3107-3111. DOI: 10.1002/ejic.201200402.
- (40) Sarma, T.; Panda, P. K.; Setsune, J. Bis-naphthobipyrrolylmethene derived BODIPY complex: an intense near-infrared fluorescent dye. *Chem Commun* **2013**, *49* (84), 9806-9808. DOI: 10.1039/c3cc44834g.
- (41) Yang, C. C.; Sheng, W.; Moemeni, M.; Bates, M.; Herrera, C. K.; Borhan, B.; Lunt, R. R. Ultraviolet and Near-Infrared Dual-Band Selective-Harvesting Transparent

Luminescent Solar Concentrators. *Adv Energy Mater* **2021**, *11* (12). DOI: ARTN 200358110.1002/aenm.202003581.

- (42) Michie, M. S.; Gotz, R.; Franke, C.; Bowler, M.; Kumari, N.; Magidson, V.; Levitus, M.; Loncarek, J.; Sauer, M.; Schnermann, M. J. Cyanine Conformational Restraint in the Far-Red Range. *J Am Chem Soc* **2017**, *139* (36), 12406-12409. DOI: 10.1021/jacs.7b07272.
- (43) Matikonda, S. S.; Hammersley, G.; Kumari, N.; Grabenhorst, L.; Glembockyte, V.; Tinnefeld, P.; Ivanic, J.; Levitus, M.; Schnermann, M. J. Impact of Cyanine Conformational Restraint in the Near-Infrared Range. *J Org Chem* **2020**, *85* (9), 5907-5915. DOI: 10.1021/acs.joc.0c00236.
- (44) Yang, Q. L.; Ma, Z. R.; Wang, H. S.; Zhou, B.; Zhu, S. J.; Zhong, Y. T.; Wang, J. Y.; Wan, H.; Antaris, A.; Ma, R.; et al. Rational Design of Molecular Fluorophores for Biological Imaging in the NIR-II Window. *Adv Mater* **2017**, *29* (12). DOI: ARTN 160549710.1002/adma.201605497.

Chapter III: Discovery of a Novel Cyanine Degradation Pathway

III-1 Introduction to cyanine fluorescent dyes

Organic fluorescent dyes have grown to be instrumental in applications including but not limited to: cellular biology, biomedical drug design, advanced materials engineering, as well as energy capture/conversion.¹⁻⁸ The ability to synthetically tune structure and in turn, photophysical properties of a chromophore to suit a particular application, are crucial to the continuation of the growth of the field. Among one of the most widely utilized chromophores, cyanine dyes, have caught the attention of many different disciplines, due to their unique structural characteristics.⁹⁻¹² Cyanines in particular boast a high relative brightness, and have significant advantages as a result of their ease of synthetic tunability, as well as an electronic push-pull structure that gives them the absorption and emission wavelength ranging from ultraviolet (UV) to deep far-red. Cyanine dyes are typically classed based on the number of methine carbons between the two indolinium based heterocyclic units connecting the methine chain (Figure III-1).

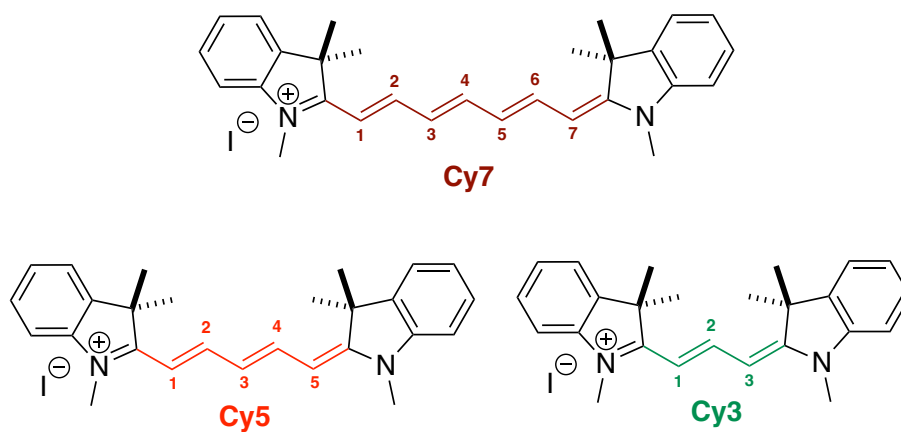


Figure III-1. Structure of famous cyanine dyes

In general, the monomethine (Cy1) and trimethine (Cy3) cyanines absorb and emit light in the UV to visible range of the spectrum, while pentamethine (Cy5) and heptamethine (Cy7) cyanines absorb and emit in the near infrared region (NIR). More specifically, pentamethine and heptamethine cyanines find a diverse range of applications both for in vivo imaging and photodynamic therapy owing to their NIR spectrum profile displaying deep tissue penetration with minimal autofluorescence.^{4, 13-17} Additionally, the NIR cyanines (Cy5 & Cy7) have become a focus for solar energy harvesting, as a result of a high flux of solar radiation in this region of the spectrum.^{2, 7, 18-21}

III-2 Photo-degradation pathways of cyanine dyes

The stability of the cyanine fluorophores however, tends to suffer as a result of the reactivity of their methine backbone with other reactive species. In particular, the oxidative degradation of cyanines involving singlet oxygen has been of intense interest in the last decades and different studies have reported the oxidative cleavage of the methine chain to yield carbonyl containing fragments (Figure III-2).²²⁻²⁴

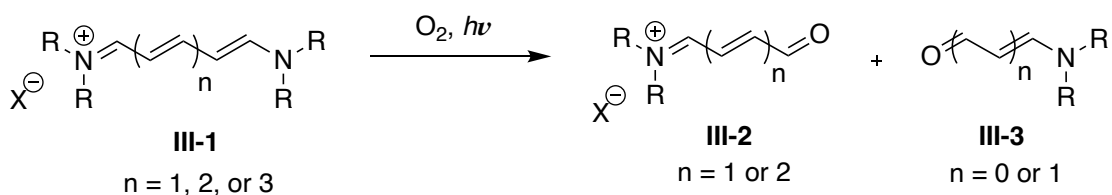


Figure III-2. Cyanine photolysis products

As shown in Figure III-3, in 2015, Schnermann and co-workers²⁵ reported an experimental and theoretical study on the photooxidative cleavage of heptamethine cyanines. The degraded fragments of this reaction were identified via mass spectroscopy,

demonstrating that the photolysis products were obtained only in the presence of a source of singlet oxygen (generated chemically or via photosensitization).

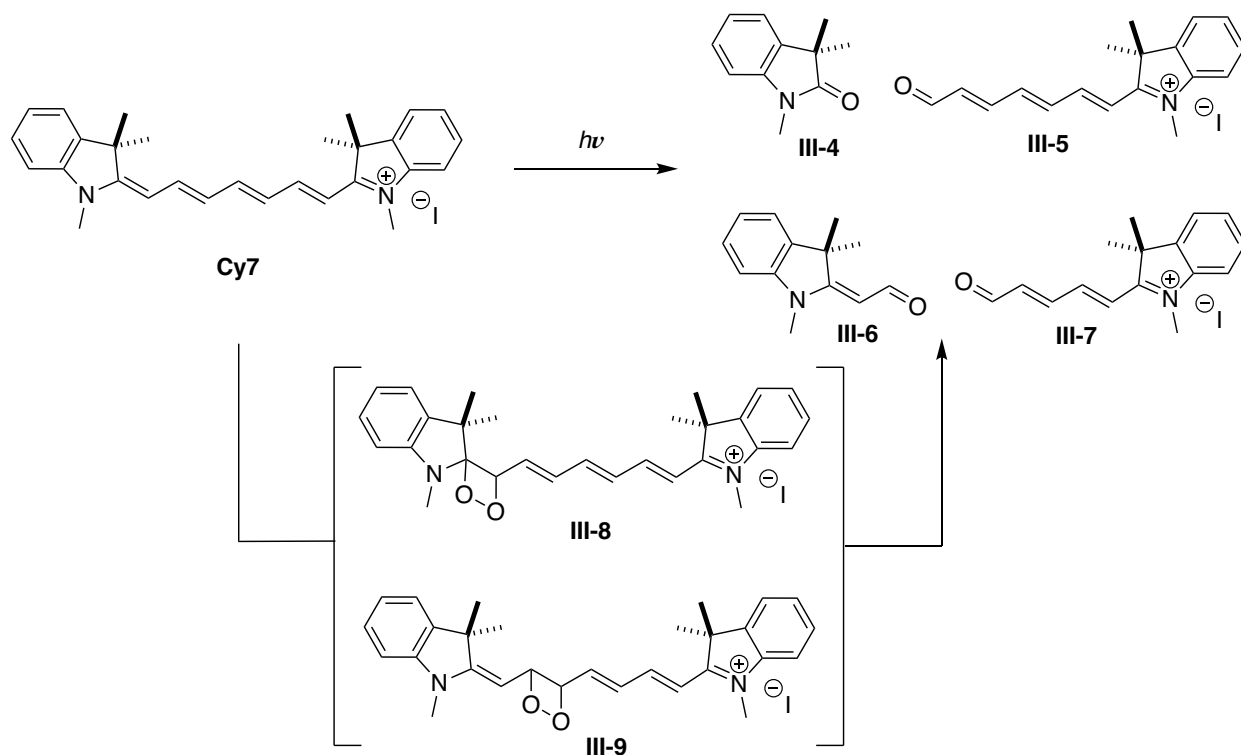


Figure III-3. Mechanism and degradation products of cyanine photooxidation

Understanding the basis of cyanines degradation through photooxidation has opened development of novel methods. Recent literature reports highlight the photooxidative degradation process of heptamethine cyanines as the critical step for a NIR uncaging strategy relevant for biological studies.²⁶ Alternatively, the oxidative cleavage of cyanines with respect to a reactive singlet oxygen (RSO) species, has led to the development of NIR fluorescent probes.^{27, 28} In more recent advancements, a phenomenon defined as “photoblueing” takes place through selective photodegradation using various wavelengths of light, cleaving away smaller cyanine fragments, demonstrating potential applications in super-resolution imaging and single-particle

tracking.²⁹⁻³¹ This blue shifting effect is the result of phototruncation of two methine carbons from the cyanine's unsaturated backbone, initiated by a singlet oxygen species (Figure III-4).

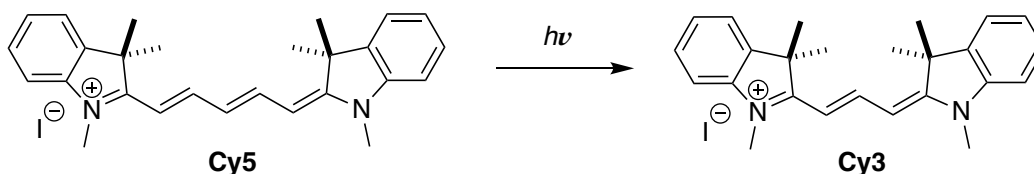


Figure III-4. Photoblueing results from two carbon truncation

In 2021, Schnermann and co-workers proposed a detailed mechanism for this transformation.³² As shown in Figure III-5, This mechanism initiates with attack by singlet oxygen to the C1 position of Cy5 to generate a peroxy intermediate **III-10** which as described before, could generate fragments **III-4** and **III-7** (path A) or carry out a hydration to yield the hydroperoxyethanol **III-11** (path B). Attack from the uncharged nitrogen to the iminium side, led to the formation of a four member intermediate in **III-12**. Elimination of hydroperoxyethanol in the final step resulted in a truncated trimethine cyanine as the final product. Initially, the isolated yield of the photo-truncated cyanine (Cy3) in this reaction was less than 2%, however, in this recently published report, investigators optimized the reaction increasing the pH to 9.5 and improving the yield to 17.2%.

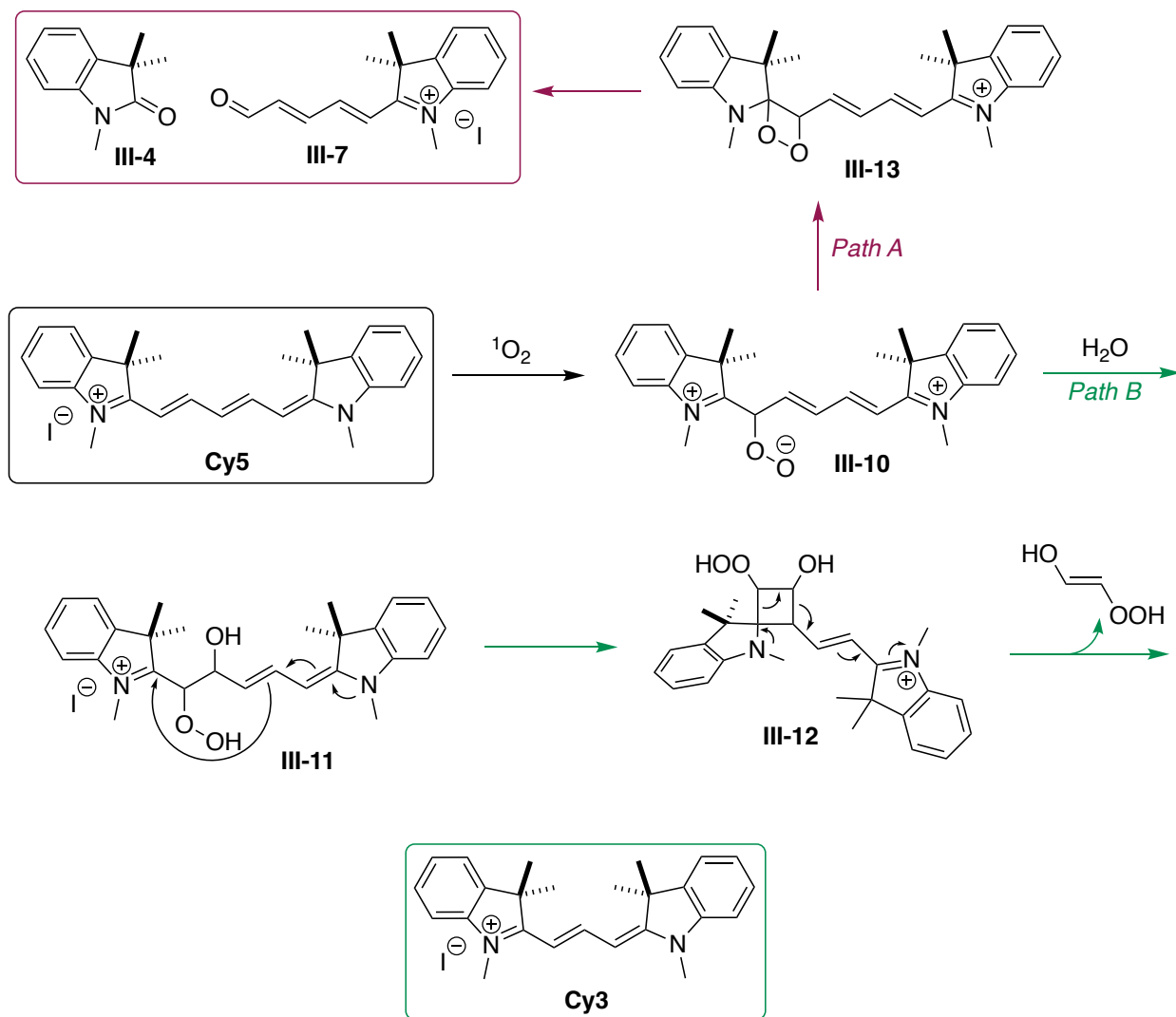


Figure III-5. Photodegradation mechanism (by Schnermann and co-workers)

A separate published work by Lee and co-workers in the same year, applied the cyanine photoconversion for single-particle tracking in a living cell.³³ In this study, they showed another mechanistic approach to cyanine phototruncation. As shown in Figure III-6, the carbonyl products **III-14** and **III-15** were formed through the previously described mechanism. The conversion of these aldehydes to their respective Fischer base **III-16** is not clear, however they hypothesized a retro-aldol-type carbon-carbon bond cleavage or

a ROS-mediated decarbonylation. The subsequent condensation of the Fisher base **III-16** with another aldehyde **III-15** provides the Cy3 product.

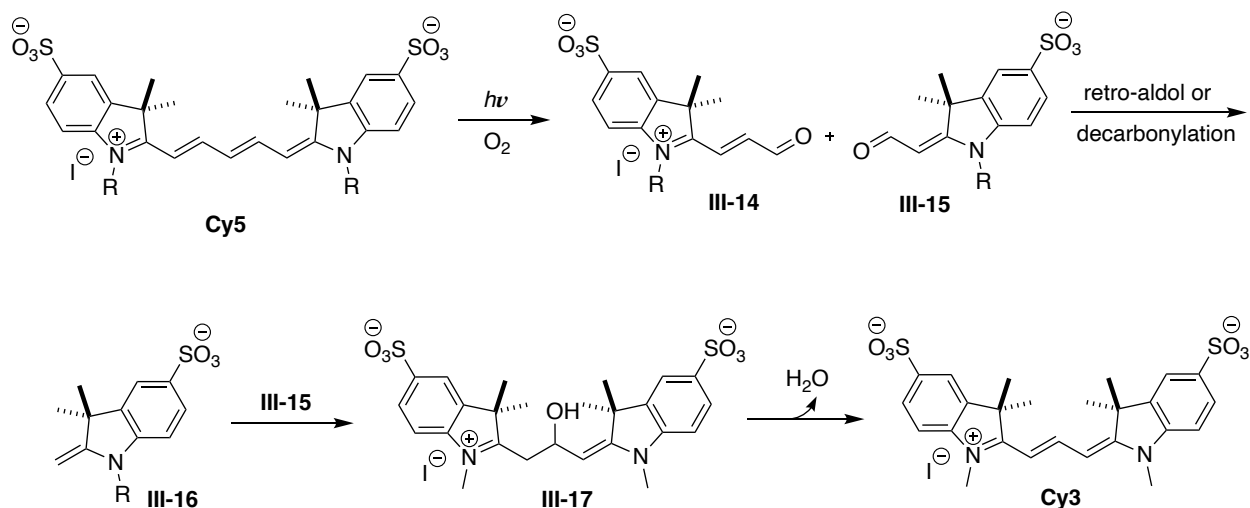


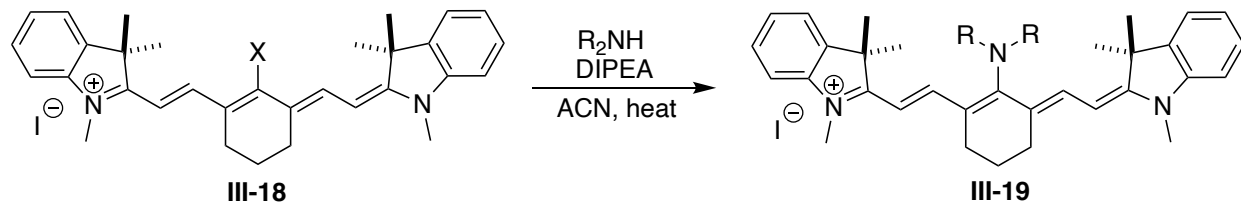
Figure III-6. Photodegradation mechanism (by Lee and co-workers)

III-3 Discovery and development of a non-photoactivated, oxygen-free degradation of cyanine dyes

III-3-1 An observation leads to novel cyanine degradation pathway

As described in Chapter II, we previously reported a general strategy to tune heptamethine cyanine's photophysical properties (Stokes shift) through the C4'-substitution of an existing halogen with a variety of structurally diverse amines³⁴ (Figure III-7a). In subsequent studies used to supplement the initial findings, we attempted to synthetically access the C3' (asymmetric) position, but to our surprise, instead of the expected aminated cyanine product, we observed truncation of the parent Cy7 heptamethine cyanine, to yield Cy5 and AsCy5 as the primary species (Figure III-7b).

A. Reaction for amination at C4' position



B. Reaction for amination at C3' position

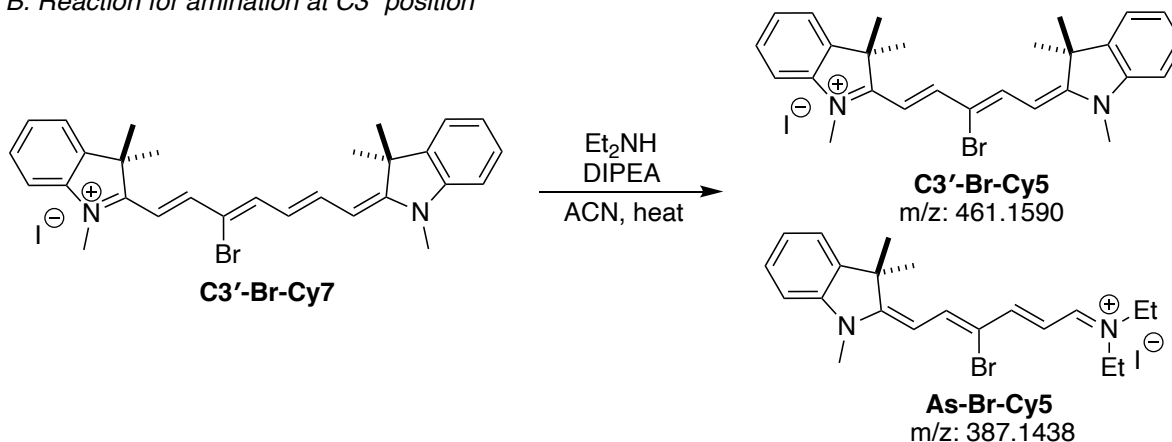


Figure III-7. A. Amination at C4' for tuning the Stokes shift, B. Amination at C3' resulted in corresponding Cy5 and As-Cy5 derivatives

These findings inspired us to investigate the working mechanism of this two-carbon truncation that converts the parent Cy7 to symmetrical Cy5 and smaller products. As outlined below, the heterocyclic indolinium “head groups”, can be exchanged between dyes in the truncation process. Via separation and spectroscopic identification of key degradation products as well as synthesis of cyanines labeled with deuterium atoms we developed insight into the nature of the degradation pathways. This work is the first study of non-photoactivated, anaerobic, thermally driven degradation of a commonly utilized class of cyanines. The truncation reaction is also a practical and novel method for the conversion of heptamethine cyanine dyes to their corresponding symmetric and asymmetric pentamethine cyanine derivatives with high efficiency.

III-3-2 Identification and optimization of degradation products

The heptamethine cyanines Cy7 and C3'-bromo substituted Cy7 (C3'-Br-Cy7) were synthesized according to the procedure reported by Klan and co-workers³⁵ (Figure III-8). The Zincke salts were generated from substituted pyridine and react with heterocycle head groups to make the cyanines.

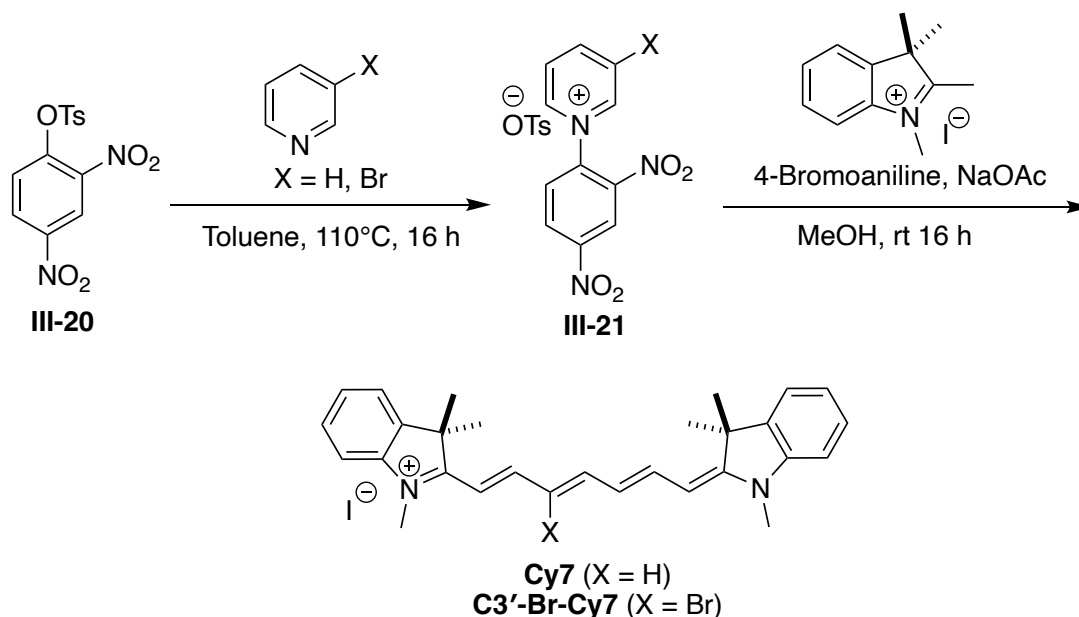


Figure III-8. General synthesis of heptamethine cyanines

As shown in Figure III-7B, we initially observed this two carbon truncation while attempting the amination of the asymmetrically halogenated heptamethane cyanines (C3'-Br-Cy7), by subjecting them to previously employed methods: nucleophilic addition of an amine under basic conditions, (NHET₂ – 10 equiv, DIPEA – 2 equiv, at 70 °C for 24 h). Upon the reaction of the C3'-Br-Cy7 under these conditions, we observed two compounds with the mass of *m/z*: 461.1590 and *m/z*: 387.1438 corresponding to C3'-Br-Cy5 and As-Br-Cy5, respectively (Figure III-7B). These fragments were subsequently isolated as the main products and their structures were assigned based on NMR and

Mass spectroscopies. Notably, apparent dehalogenation of C3'-Br-Cy7 to Cy7 was also observed under these conditions. For further studies, we chose heptamethine (Cy7) in order to establish a generalized approach for our degradation studies. Degradation of Cy7 under the abovementioned conditions led to fragments with observed masses of m/z : 383.2477 for Cy5 and m/z : 309.2327 for AsCy5. These were obtained as primary degradation products (Figure III-9).

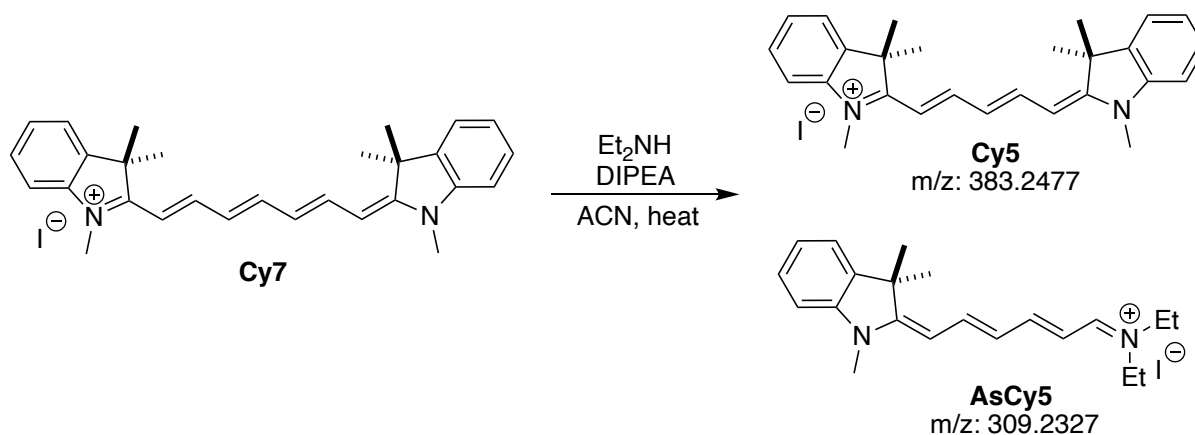
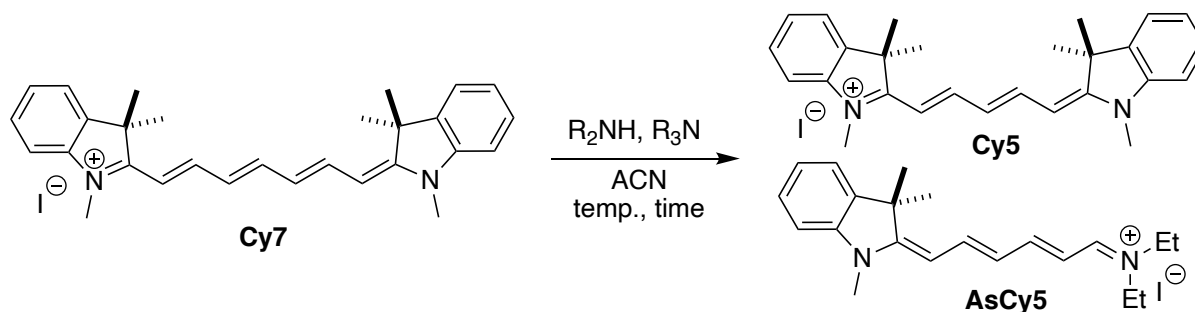


Figure III-9. Study the conversions on Cy7 to investigate the generality of this reaction

These findings led us to investigate a series of reaction conditions using Cy7 to better comprehend the role of each of the reaction parameters in this unique transformation. All reactions were degassed and run in the dark under Argon atmosphere. First, we omitted the tertiary amine (DIPEA) and ran the reaction using only 10 equivalents of diethylamine. These results are summarized in Table III-1. Interestingly, not only we saw a change in the ratio of AsCy5/ Cy5 (2.75:1) but also an improvement in the yield of the previously isolated AsCy5 (Table III-1, entry 2). Next, we lowered the temperature from 70 °C to room temperature. The same products were formed but more

slowly and in a ratio of AsCy5/ Cy5 (3.3:1). Extending the reaction time we were able to achieve a yield of 41% for AsCy5 (Table III-1, entry 3).

Table III-1. Reaction optimization with secondary amine



Entry ^a	Secondary Amine	Tertiary Amine	Temp.	Time	Product (yield %)
1	Et ₂ N (10 equiv.)	DIPEA (2 equiv.)	70 °C	60 h	Cy5 (11), AsCy5 (24)
2	Et ₂ N (10 equiv.)	-	70 °C	60 h	Cy5 (12), AsCy5 (33)
3	Et ₂ N (10 equiv.)	-	r.t.	160 h	Cy5 (17), AsCy5 (41)
4	Morpholine (10 equiv.)	-	r.t.	20 h	Cy5 (11), M-As-Cy5 (40)

[a] The reactions was done in sealed tube, under argon, and followed by LC-MS.

Increasing the reaction time also led interestingly to the conversion of AsCy5 to AsCy3 and subsequently to AsCy1 (Figure III-10). The degradation products AsCy5, AsCy3 and AsCy1 were isolated and characterized by NMR and mass spectroscopy. As discussed above, the conversion of Cy7 to AsCy5 is higher yielding at room temperature. At higher temperatures, AsCy5 converts to smaller fragments AsCy3 and AsCy1 faster, reducing the isolated yield of AsCy5. As shown in Figure III-10 (dashed box), there were two hypothesized key fragments **III-22** and **III-23** that were present in the crude reaction mass, but were not isolable presumably due to their limited formation, and/or instability

during purification. The structures were hypothesized according to the mass of the compounds.

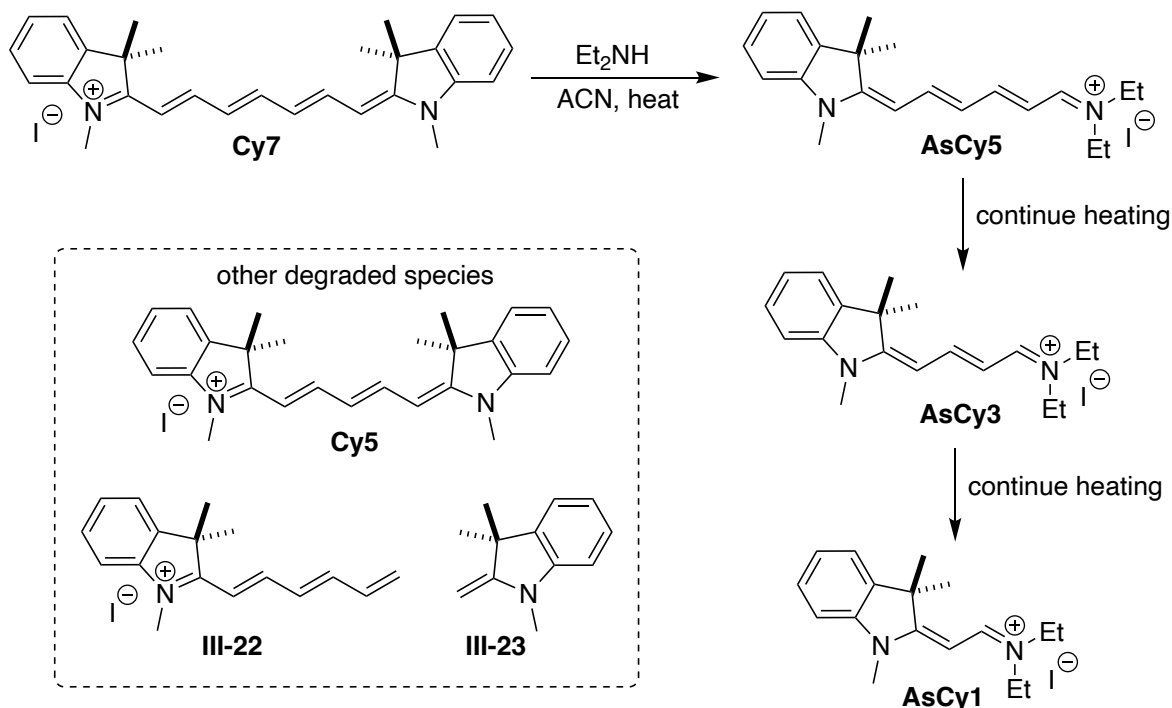


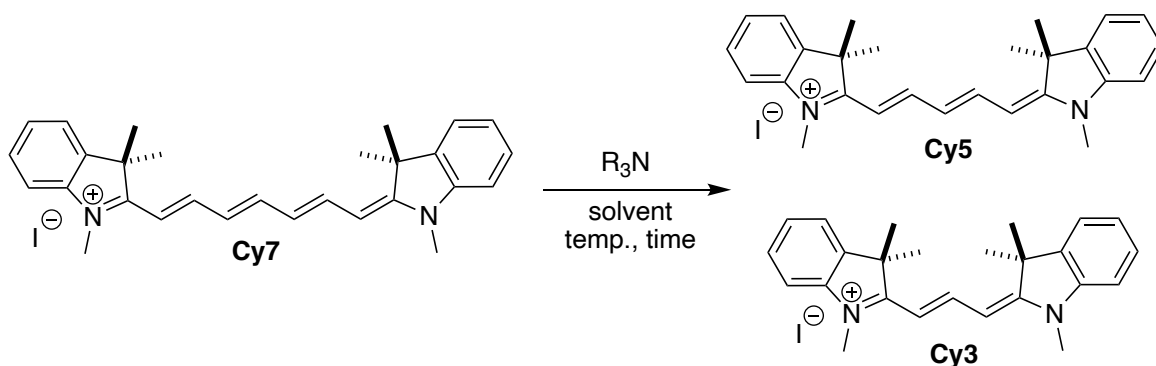
Figure III-10. Identified compounds from cyanine truncation with secondary amine

To extend the generality of our method, we additionally studied a variety of secondary amines. For instance, as listed in Table III-1 (entry 4), when the amine was changed to morpholine we successfully isolated and characterized the corresponding M-As-Cy5 and M-As-Cy3 (Reaction details in the experimental section).

In summary, use of a 2° amine instead of a 3° amine, along with decreasing the temperature to room temperature with longer reaction time, improved the yield of AsCy5. On the other hand, under identical conditions at higher temperature, AsCy5 converts to the smaller fragments AsCy3 and AsCy1 with a higher rate. Optimization studies have enabled us to selectively favor the formation of the asymmetric-aminated hemi-cyanines. We next examined the role of a tertiary amine to optimize conversion to symmetrically

substituted truncated structures. Reacting heptamethine Cy7 with 10 equivalents of DIPEA disabled the formation of AsCy5, but improved the yield of Cy5. As listed in Table III-2, in our initial attempt, after 60 hours, we isolated 18% of Cy5. This represented a 7% improvement relative to using the secondary and tertiary amine together (entry 1). There were other compounds in this reaction, including but not limited to Cy3 which were isolated and characterized, in addition to masses suggesting **III-22** and **III-23** species.

Table III-2. Reaction optimization with tertiary amine



Entry ^a	Tertiary Amine	Solvent	Temp.	Time	Product (yield %)
1	DIPEA	ACN	70 °C	60 h	Cy5 (18), Cy3 ^b
2	DIPEA	ACN	100 °C	30 h	Cy5 (44), Cy3 ^b
3	DIPEA	ACN	180 °C	1 h	Cy5 (38), Cy3 (8)
4	DIPEA	EtOH	70 °C	60 h	Cy5 ^b
5	DIPEA	DCM	70 °C	60 h	Cy5 (26), Cy3 ^b
6	Quinuclidine	ACN	70 °C	60 h	Cy5 (5), Cy3 (15)
7	Quinuclidine	ACN	100 °C	36 h	Cy5 (10), Cy3 (21)

[a] The reaction was done in sealed tube, under argon, and followed by LC-MS. [b] trace amount.

Increasing the temperature to 100 °C, led to the full conversion of Cy7 in 30 hours with substantial improvement in the yield for Cy5 (44%). Increasing the temperature to 180 °C led to complete degradation of Cy7 in 1 hour with 38% yield of Cy5. As listed in Table III-2, using 10 equivalents of DIPEA, we observed the partial formation of Cy3 in the reaction (up to 8% at 180 °C). We also screened various solvents to observe any influence on the reaction. Switching acetonitrile to a protic solvent such as ethanol decreased the yield of Cy5 dramatically. For instance, at 70 °C using 10 equivalents DIPEA in ethanol provided a trace amount of Cy5. While the reaction in dichloromethane had improved the yield of Cy5 to 26% (Table III-2, entry 5). Having changed the solvent and temperature, the next parameter was varying the nature of the tertiary amine. The reaction with quinuclidine finished in 36 hours at 100°C and both Cy5 (10%) and Cy3 (21%) were observed as the products. Interestingly, the major product was to Cy3, not Cy5. To summarize the effect of tertiary amines, we saw that different tertiary amines could convert Cy7 to Cy5 (DIPEA); similarly, we can also choose to convert Cy7 to Cy3 as the favored product in the presence of quinuclidine. On the other hand, we studied the generality of this conversion by testing cyanines with different backbones (Cy7.5) in the presence of DIPEA and we observed the same pattern of the reaction with Cy5.5 being the major product (Figure III-11).

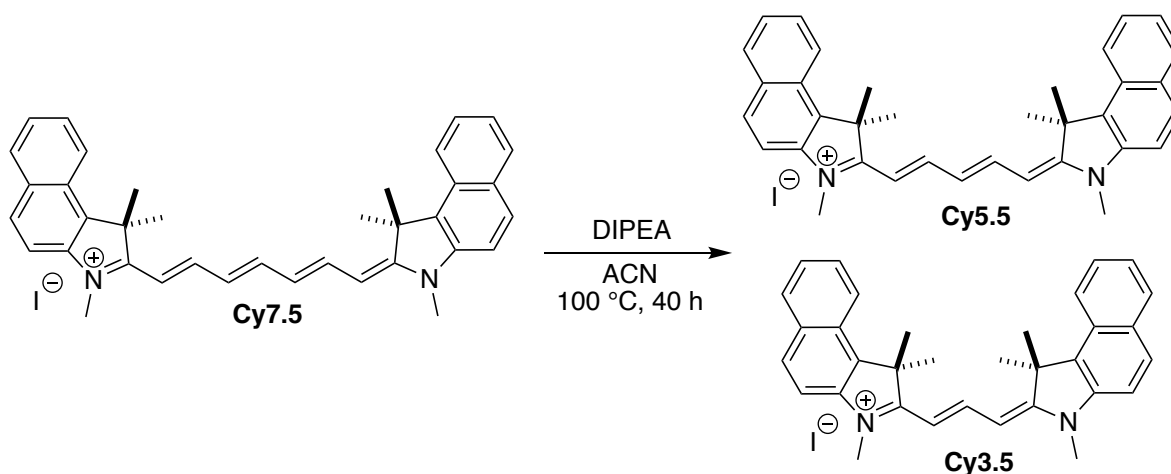


Figure III-11. Conversion of Cy7.5 in the presence of tertiary amine (DIPEA)

The degradation pattern of di-substituted cyanine **III-24** was also studied. As shown in Figure III-12, the mass of the methylated Cy5 **III-25** was observed while the bromo substituted Cy5 was not observed. Compound **III-25** could not be isolated as it was produced in low amounts, but as shown previously, the asymmetric brominated Cy7 (C3'-Br-Cy7) converts to the symmetric C3'-Br-Cy5 (Figure III-7B), therefore the methyl substitution would present at C3' position. In this reaction after 16 hours, Cy3 was the dominant signal in mass analysis. Noteworthy, there were other masses that we could not identify.

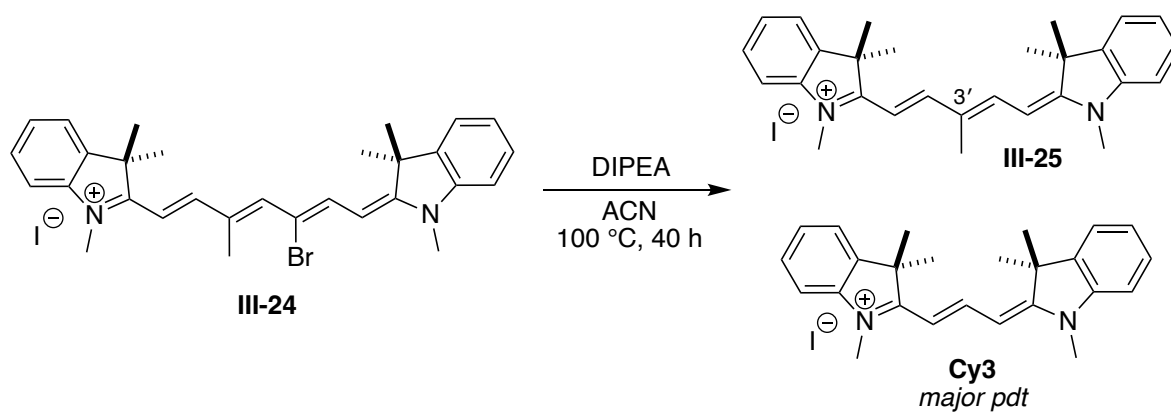


Figure III-12. Conversion of di-substituted cyanine

These optimizations take advantage of the unique cyanine degradation pathways, and can easily serve as a synthetic handle to transform traditional heptamethine cyanines into a wide series of cyanines and hemi-cyanines with varying degrees of conjugation, and maximum absorption/emission that can extend the wavelength range from UV to NIR. The absorption/emission of all convertible cyanines from the blue shifted AsCy1 to the red shifted Cy7 is shown in Figure III-13.

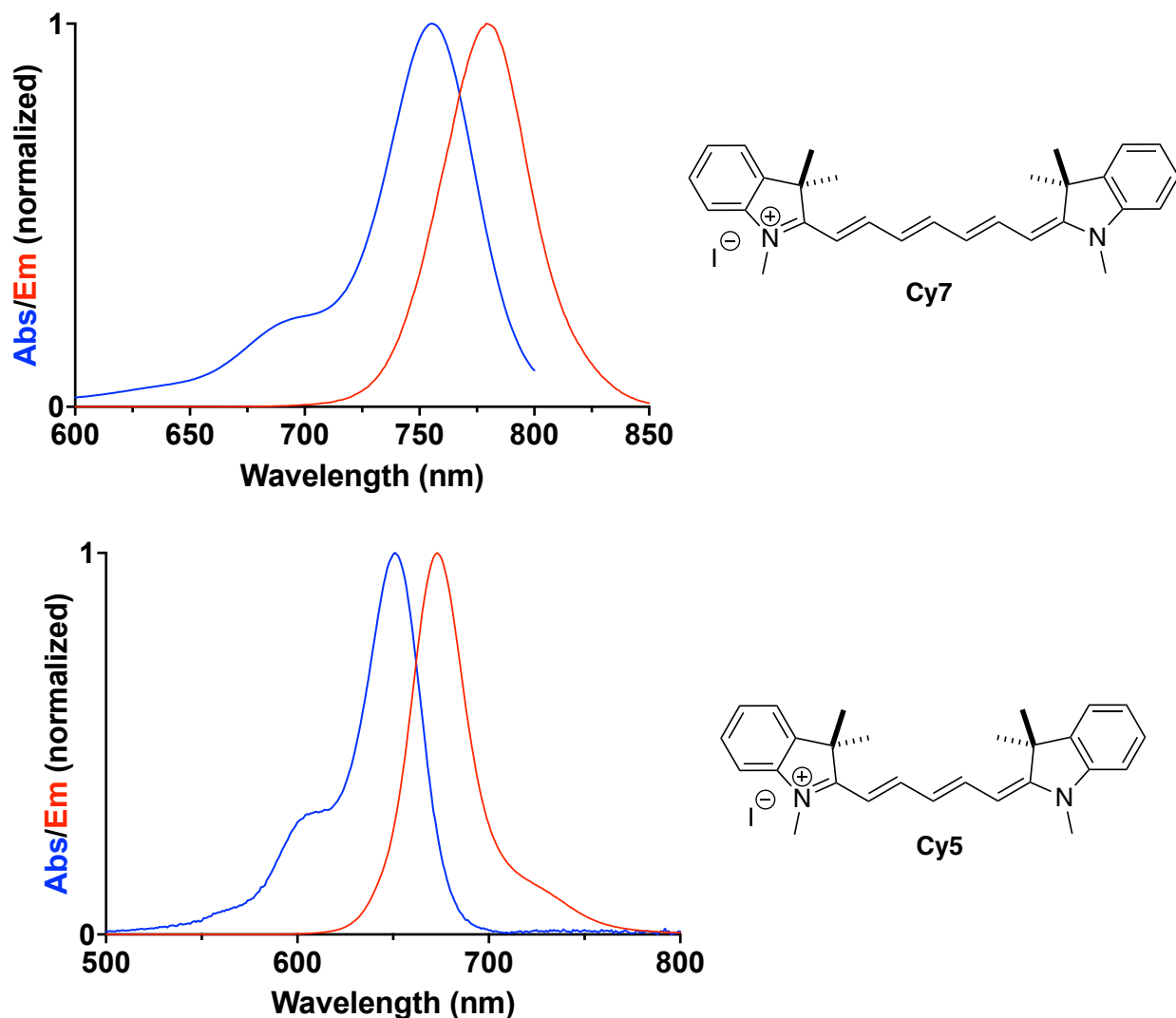


Figure III-13. Normalized absorption and emission of all cyanine's degradation fragments

Figure III-13 (cont'd)

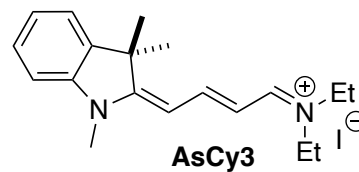
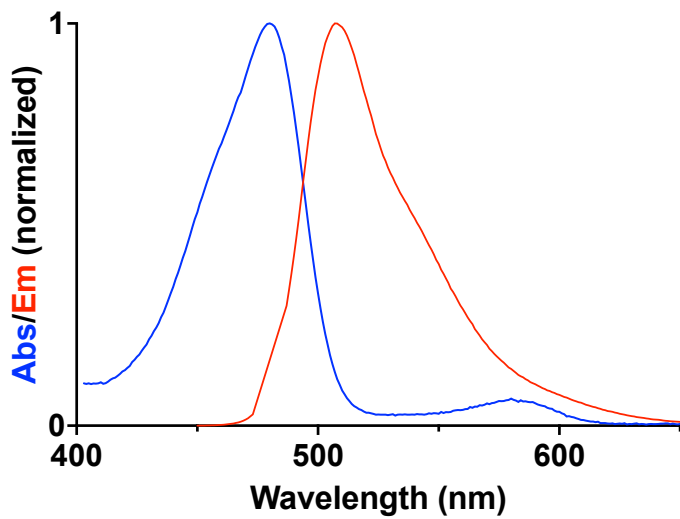
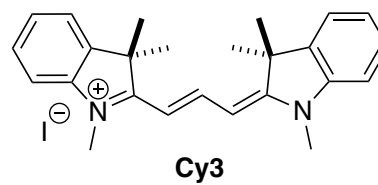
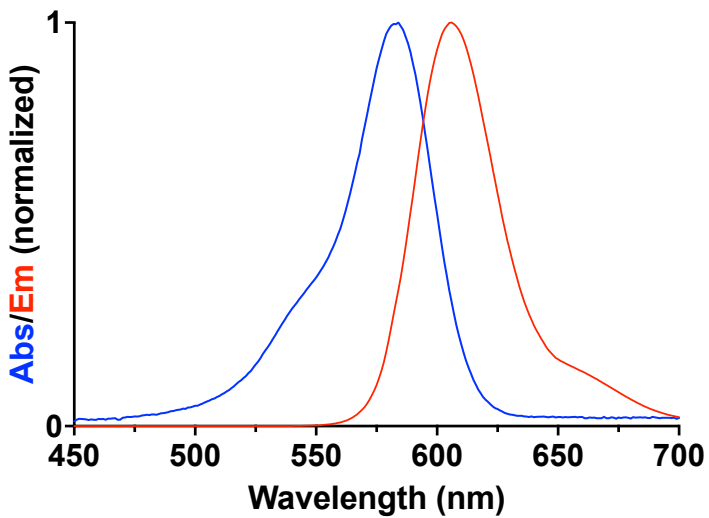
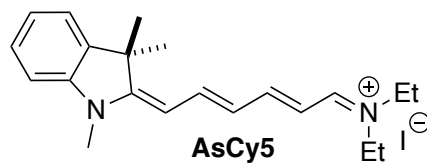
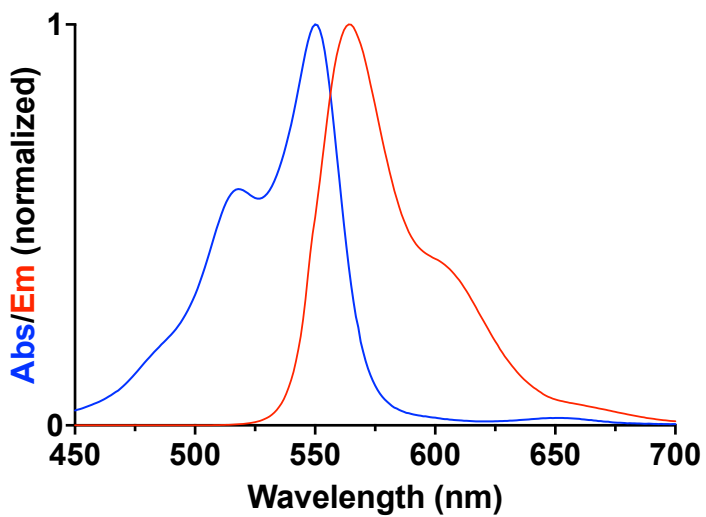
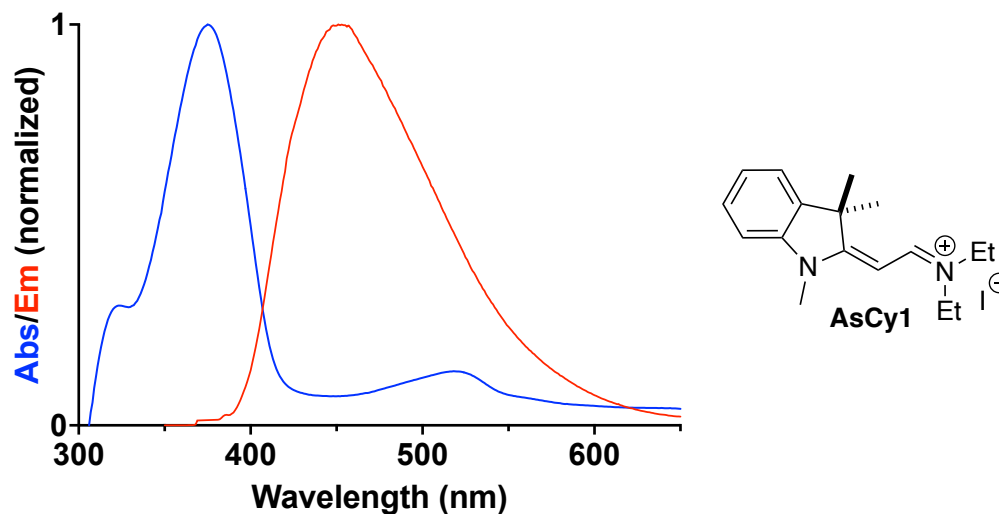


Figure III-13 (cont'd)

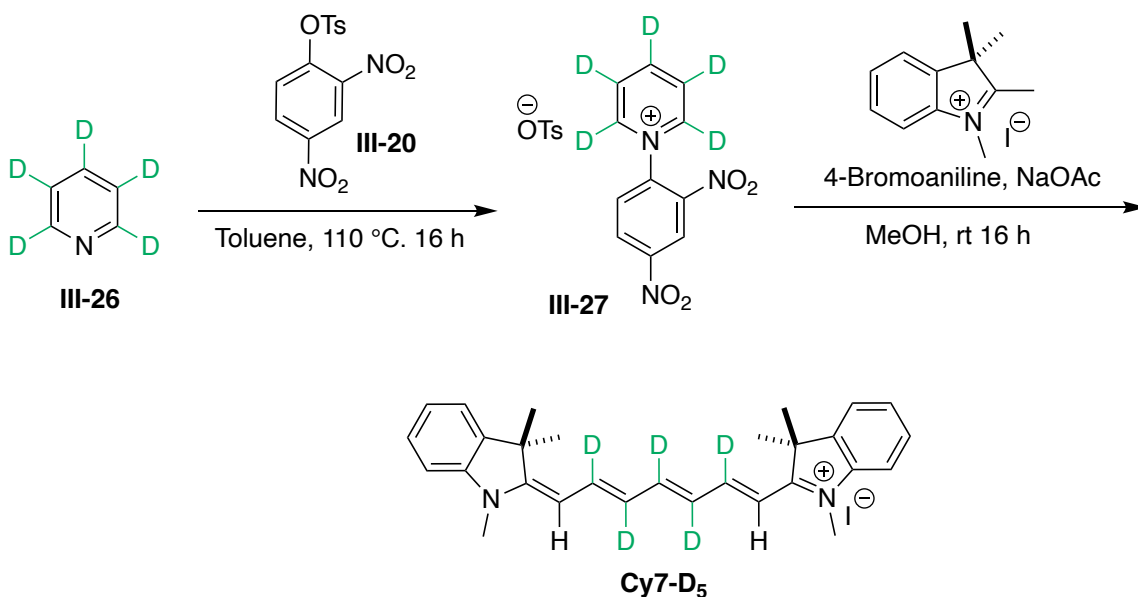


III-3-3 Investigation into the mechanism of cyanine degradation

The non-oxidative degradation of cyanines has not been reported and thus its mechanism would be of particular interest and significance. Initially we studied the mechanism for the conversion of Cy7 to the series of aminated hemi-cyanines. A series of studies were conducted to deduce whether Cy7 directly converts to AsCy3 and AsCy1, or alternatively, via a domino reaction, it first generates AsCy5 and subsequently AsCy5 converts to AsCy3, and further degradation leads to AsCy1. There are two main pieces of evidence in support of the former mechanistic hypothesis; 1) based on mass spectral data, AsCy5 is first formed from Cy7, and further less conjugated asymmetric Cy derivatives are generated more slowly (Figure III-10). 2) Continuation of the reaction after full conversion of Cy7, results in the yield and ratio between AsCy5, AsCy3 and AsCy1 to swing in favor of the less conjugated derivatives, pointing in the direction that AsCy5 is converting to AsCy3, which would then further convert to AsCy1.

To interrogate the site at which amine reacts and carbons that are lost, we resorted to deuterium labeling studies. For the synthesis of the deuterated heptamethine cyanine, a fully deuterated pyridine **III-26** was converted to its Zinke Salt precursor **III-27**, followed by nucleophilic ring opening to yield Cy7-D₅ (Figure III-14a). The deuterated cyanine was subsequently heated in the presence of diethylamine in acetonitrile as before. The asymmetric hemi-cyanine (AsCy5-D₅) was isolated and identified by mass spectroetry and NMR (Figure III-14b). Retention of all five deuterium atoms is evidence for C1'- C2' methine cleavage, following C2' attack by the amine. In isotopic studies, the AsCy3-D₃ was isolated and characterized, suggesting that the secondary amine would have attacked the C3' methine position of AsCy5 derivative to neutralize the charge, and later, the amine's nitrogen atom would donate its lone pair of electrons to cleave the C2'- C3' bond. Perhaps the same steps would happen to convert the AsCy3-D₃ to AsCy1-D₁, since we isolated and characterized the AsCy1-D₁ (Figure III-14b).

A. Synthesis of deuterated Cy7



B. Deuterium isotopic tracing studies

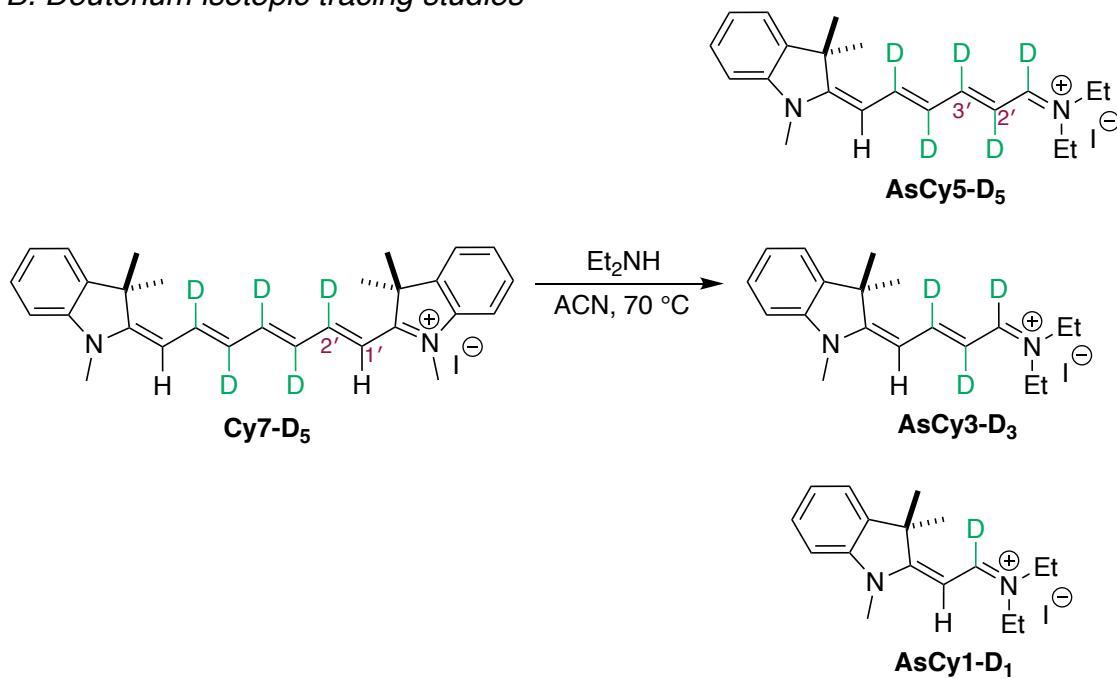


Figure III-14. A. Synthesis of **Cy7-D₅**, B. Conversion of deuterated Cy7 with secondary amine

Deuterium isotopic labeling studies, suggest that the amine attacks the C2' position, which upon the engagement of the nitrogen atom leads to the cleavage of the C1'-C2'. This cleavage requires a proton exchange to release the Fisher base head group. To discover the most electron dense carbon capable of the required proton exchange, we conducted a deuterium exchange study to identify the most acidic protons. Subsequently, we heated Cy7 in acetonitrile in presence of 20 equivalents of D₂O and isolated and characterized (NMR and ESI-MS) the C1'-deuterated-Cy7 (**III-28**) as the proton exchanged cyanine product (Figure III-15A).

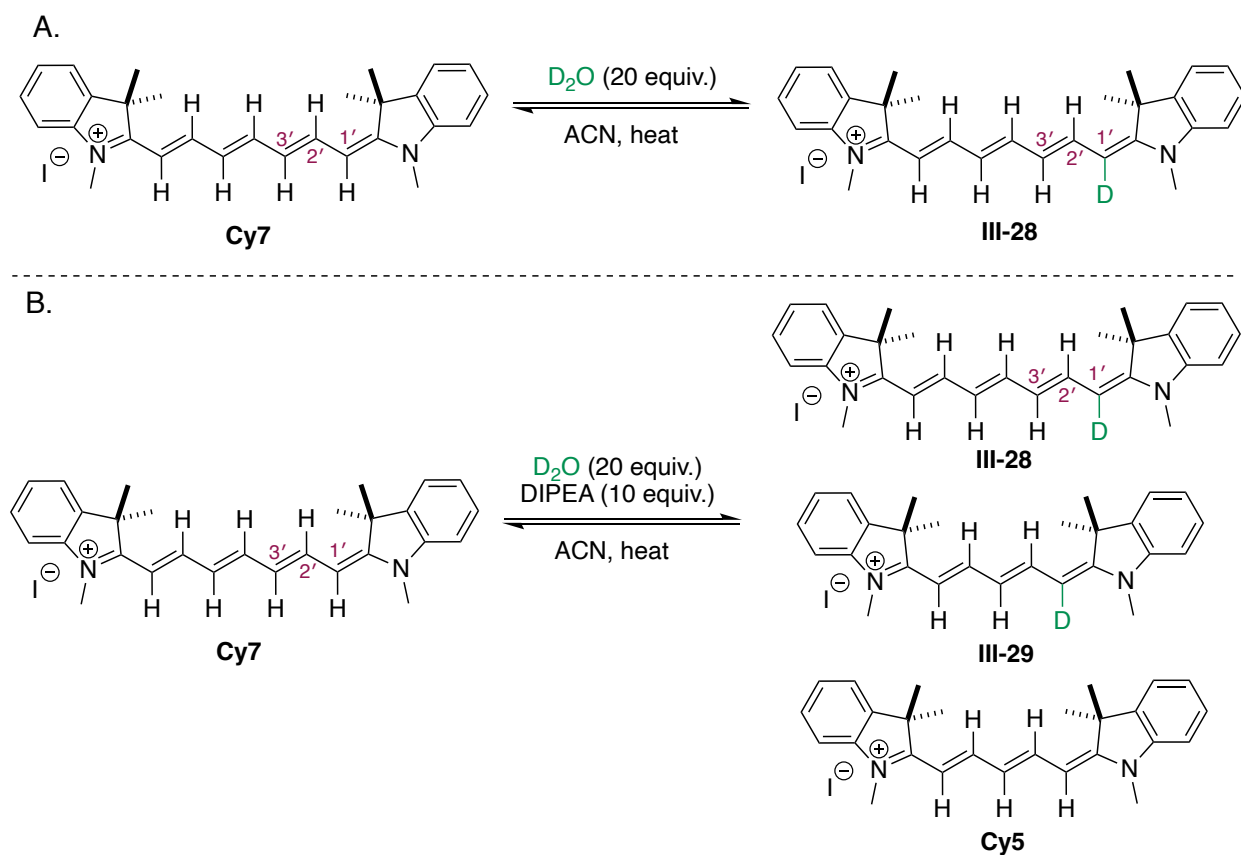


Figure III-15. A. Deuterium exchange in D₂O, B. Deuterium exchange in D₂O and DIPEA

The same study performed in the presence of the 10 equivalents of DIPEA, showed the mass of the C1'-deuterated-Cy7 (**III-28**) and C1'-deuterated-Cy5 (**III-29**) in addition to Cy5 (Figure III-15B). Extended heating shows a small amount of exchange in other sites, but the C1'-exchange occurred at a faster rate.

These experimental results helped us to propose a mechanism for the conversion of Cy7 to the series of aminated hemi-cyanines (Figure III-16). Based on deuterium isotope labeling and species isolated during purification, it is likely that a secondary amine would attack the C2' position of the methine backbone, and push the pi electrons towards the indolinium end, neutralizing the charge on the nitrogen atom (also, DFT computational modeling (EDF2/6-31G*/SM8 CH₃CN) finds a free energy preference of 5.8 kcal/mol for C2' vs C4' attack on Cy7) (insert the computational). Following that, the proton transfer likely happens at C1' position, according to our deuterium exchange study, to yield **III-31**. Subsequently, the lone pair of the amine would regenerate the conjugated cyanine by breaking the C1'-C2' bond, yielding AsCy5 and the Fischer base **III-23** (Figure III-16). AsCy5 could convert to the AsCy3 in a similar fashion. The secondary amine would attack the C3' position (shown on the structure) of the methine backbone, and push pi electrons towards the diethyliminium end, neutralizing the charge on the nitrogen atom. Upon proton transfer, the lone pair of the amine would reestablish the conjugated cyanine that leads to formation of AsCy3. The same scenario is possible for truncation of AsCy3 to AsCy1.

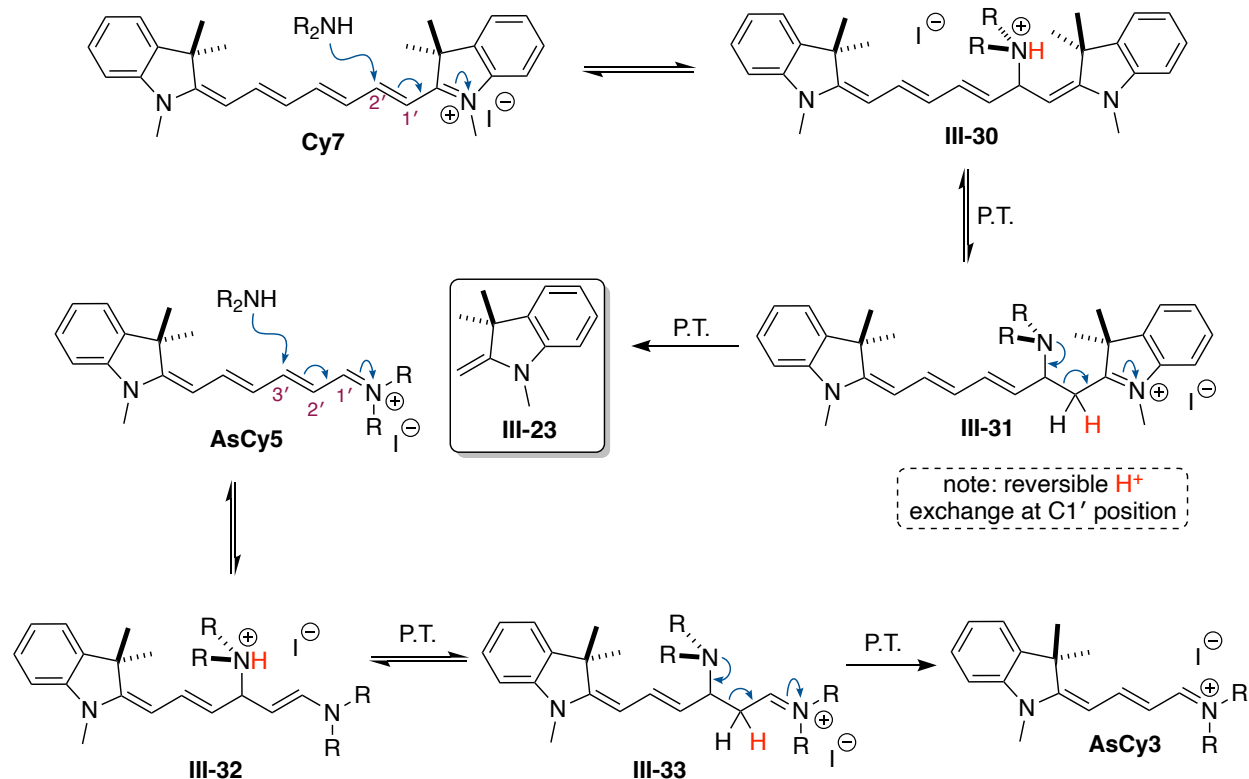


Figure III-16. Proposed mechanism of cyanine conversion with secondary amines

Next, we probed the mechanism for the conversion of Cy7 to symmetric Cy5. The net change in this transformation is the loss of ethyne, which from a thermodynamic perspective cannot be supported. We first subjected, a Cy7-D₅ with DIPEA under the same conditions as previously employed. We successfully isolated and characterized the centrally deuterated pentamethine Cy5-D₃ which presumably is derived from the cleavage of the C2' and C3' carbons from the backbone chain (Figure III-17).

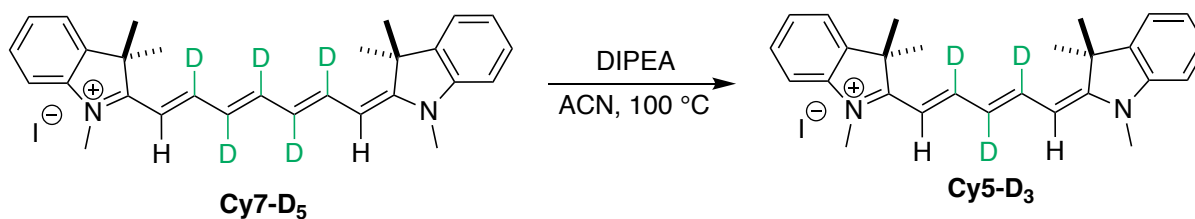
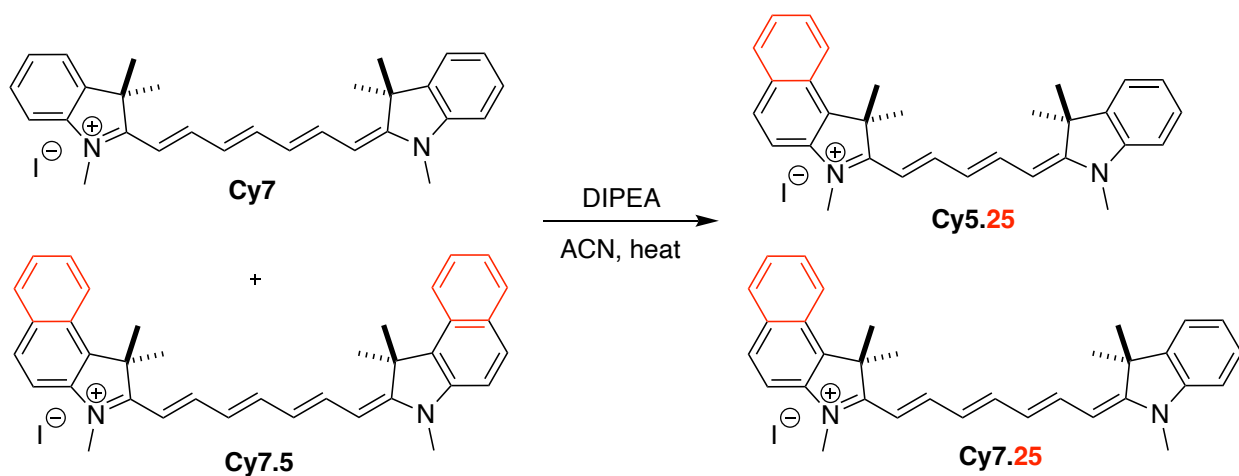


Figure III-17. Conversion of deuterated Cy7 with tertiary amine (DIPEA)

In our previous attempts to understand the mechanism of cyanine's degradation in the presence of secondary amines, we observed cleavage at C1'-C2' along with the formation of Fisher base **III-23**. A potential process for the conversion of Cy7 to Cy5 could be the generation of Fisher base **III-23** through the aforementioned nucleophilic attack, and subsequent attack of the Fisher base to form the shortened cyanine. To support the idea of the heterocyclic indole (**III-23**) breaking off from the methine chain and re-attacking, we reacted a 1:1 mixture of symmetric cyanines; Cy7 and Cy7.5 with DIPEA and we were pleased to observe the mass of the scrambled heptamethine cyanine with mixed head groups, (i.e. mismatched indole cyanines), showing a clear m/z corresponding to Cy7.25 and also, recombination chain shortening which led to formation of Cy 5.25 (Figure III-18). This observation pointed us in the direction of the indole unit playing a role in displacement and re-appendage to the cyanine chain to facilitate formation of scrambled cyanines.



(Note: Mass signals for Cy5, Cy5.5, Head group and starting materials were observed as well)

Figure III-18. Recombinative chain shortening

Our initial hypothesis involved attack of the amine to the methine chain of the cyanine, followed by formation of a cyclobutane intermediate which would undergo the elimination of acetylene, leading to the formation of a symmetric Cy5. This proposed mechanism has two primary issues, 1) From an energetic standpoint, thermochemistry (and calculations) predict the actual loss of acetylene gas would be uphill in energy by 30-40 kcal/mol, and 2) detection and confirmation of the presence of acetylene via NMR and HRMS was unsuccessful. An alternate hypothesis is supported by two facts: first of which being the observation of the indolinium head group cleavage, originating from the parent heptamethine chain between C1'- C2' and, second, the observation of a small amount of acetaldehyde by NMR study, during the course of the reaction. In this instance, a water molecule (water was not intentionally added to the reaction directly, however a trace amount of water could have been introduced via solvent, amine or other reagents) would attack the C2' methine carbon generating the **III-34**, after a proton transfer (Figure III-19). Subsequently, the lone pair of oxygen would donate its electrons, facilitating the formation of the conjugated cyanine that leads to the cleavage of the C1'- C2' bond. This then generates aldehyde **III-35**, and Fischer base **III-23**. At this step, the Fischer base could act as a nucleophile, attacking the β -position of the carbonyl generating Cy5 via elimination of acetaldehyde. Hydration of acetylene could effectively pay for the release of $(\text{CH})_2$ as its exothermicity (33 kcal/mol) compensates for what would be a high energy reaction.

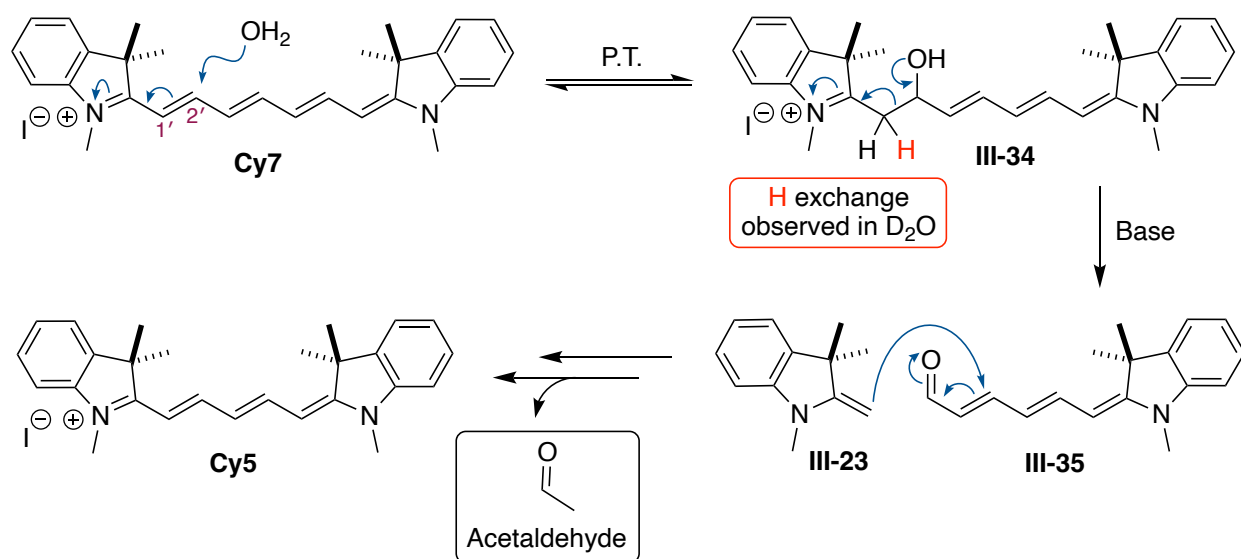


Figure III-19. Proposed mechanism of cyanine conversion with tertiary amines

Lastly, we proposed a mechanism for the truncation of the heptamethine Cy7 to a symmetric trimethine Cy3. The first part of the mechanism is analogous to that described for the truncation of Cy7 to AsCy5 (Figure III-16) and Cy7 to Cy5 (Figure III-19) in which the nucleophilic attack, (amine or water) would lead to generation of Fischer's base **III-23**. With the exception of generating the free indole unit, (Fisher's base) it could undergo an attack to a different Cy7 backbone to form **III-36** (Figure III-20). Presumably of the indole attacking the C2' carbon would generate an intermediate with three indolinium head groups (the relative *m/z* for this compound was observed in the reaction mass spectroscopy analysis) that upon proton transfer, converts to the observed trimethine Cy3 by donation of the nitrogen atom lone pair from one of the nearby head groups, thereby cleaving the C2'- C3' bond (Figure III-20). Our mechanism is supported by observing the *m/z* of the Fisher base **III-23** and the degraded fragment **III-38** in the reaction mixture.

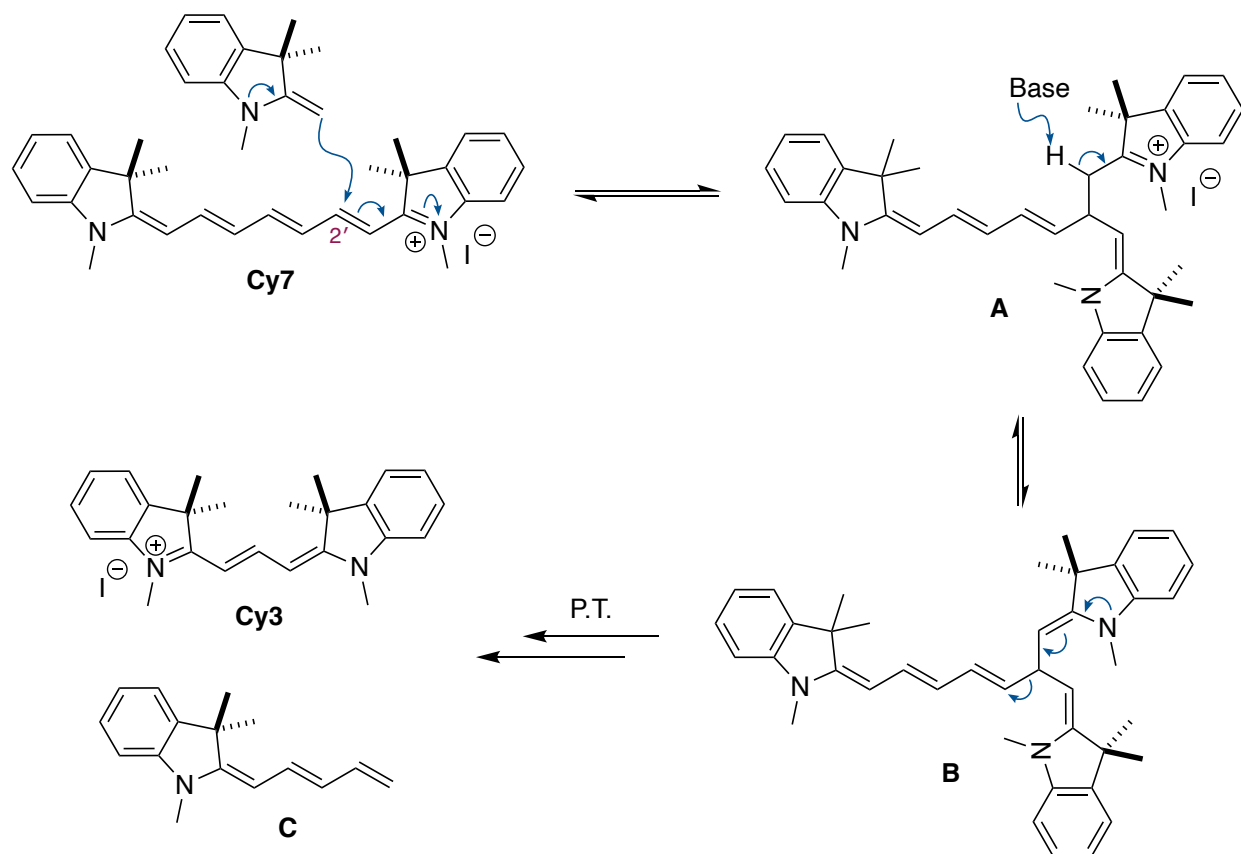


Figure III-20. Proposed mechanism of Cy7 conversion to Cy3

In a supplementary experiment conducted to further support our mechanistic proposal, Cy7 was heated with a neutral indole containing an exocyclic methylene group (vs methyl) in acetonitrile in the absence of any amine. Interestingly, the trimethine cyanine Cy3 was observed as the main product (Figure III-21).

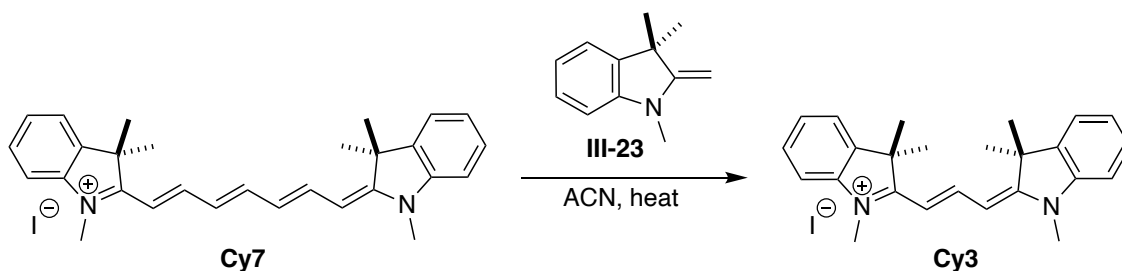


Figure III-21. Cy7 reaction with; A. neutralized head group, B. charged head group

In addition, to prove that a pentamethine Cy5 is not an intermediate structure facilitating conversion of Cy7 to Cy3, we subjected a pentamethine Cy5 cyanine under the same reaction conditions using tertiary amines, and did not observe formation of any trimethine cyanine in the reaction mixture (Figure III-22, Path A). To complement the prior experiment, Cy5 was heated with the neutral indole in acetonitrile in absence of the tertiary amine, and as expected, Cy3 was not observed (Figure III-22, Path B).

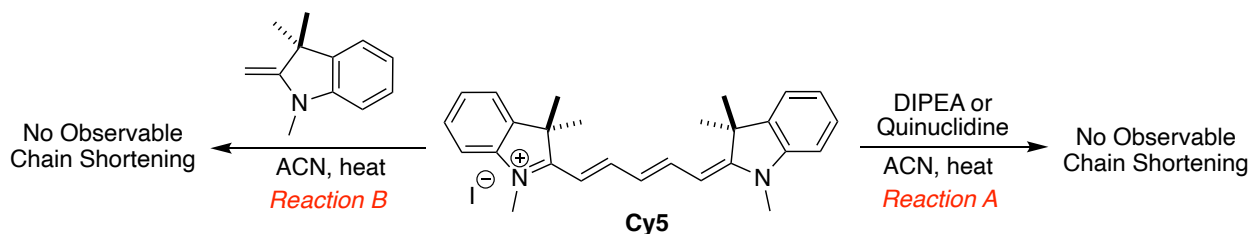


Figure III-22. Cy5 conversion reactions failed in different conditions

In summary, we have discovered a non-photoactivated, oxygen-free, degradative pathway for cyanine dyes that could have important ramifications for this family of molecules. During the reaction of heptamethine cyanines (Cy7) with amine, we obtained the two-carbon truncated Cy5 and AsCy5 as major products. We optimized the reaction and were able to develop a practical and novel method for conversion of heptamethine cyanine dyes to corresponding pentamethane and trimethine cyanine derivatives with high efficiency (Figure III-23).

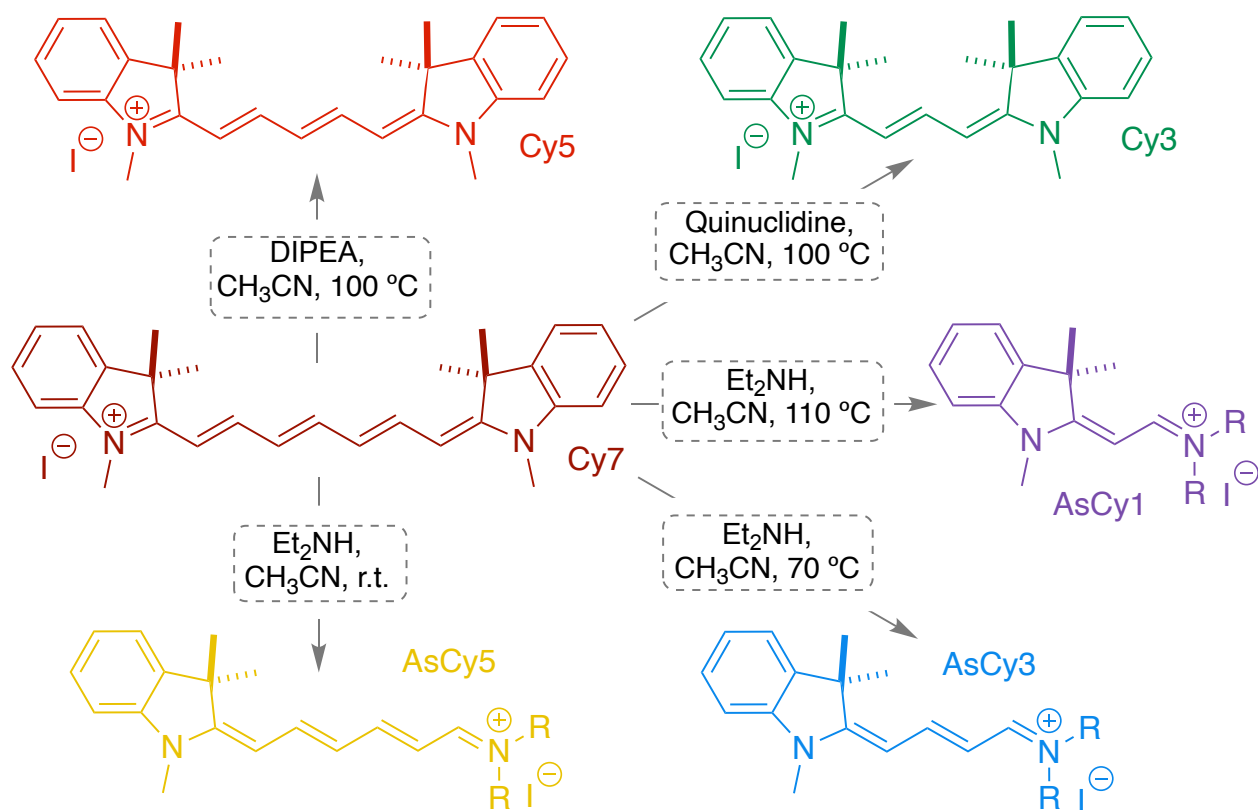


Figure III-23. Optimized cyanine conversion reactions

This is the first known transformation that provides products in good yields and can be tailored to produce a wide novel series of cyanines and hemi-cyanines with varying degrees of conjugation, with maximum absorption/emission that can extend the wavelength range from ultraviolet to near infrared (Figure III-24). We separated and identified all degraded species and have used deuterium label tracing studies and deuterium exchange studies in addition to other supporting experiment reactions to propose a multi-step mechanisms for the degradation to different fragments.

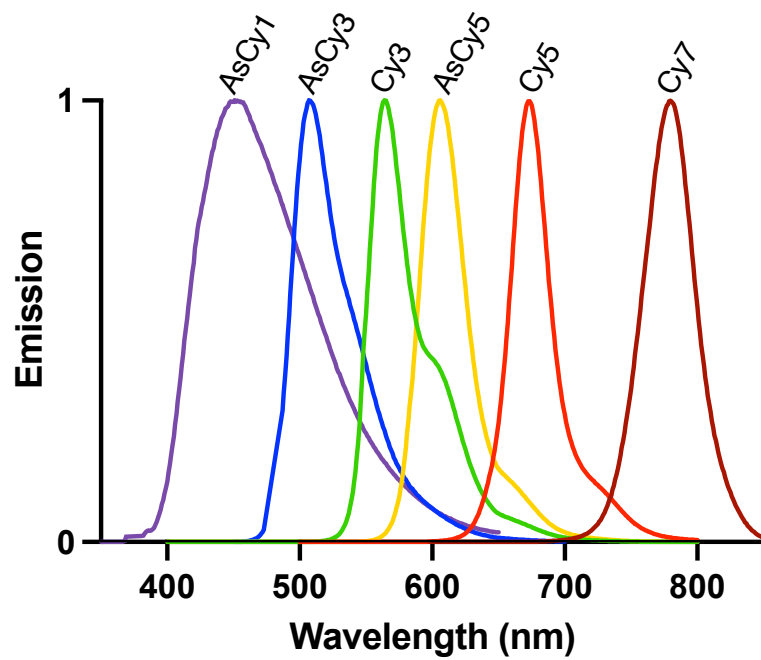
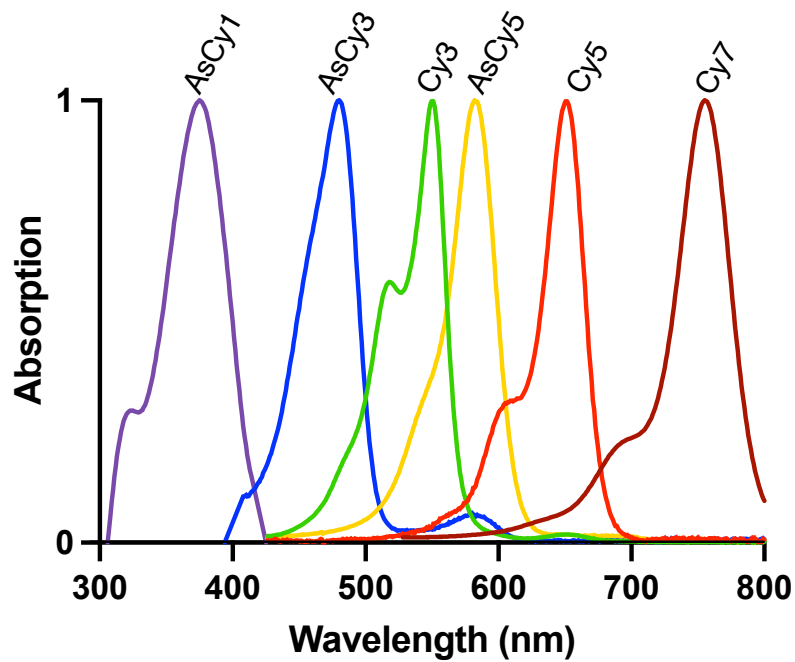


Figure III-24. *top:* Normalized absorptions (in DCM), *bottom:* Normalized emissions (in DCM)

III-3-4 Future work

While the factors governing cyanine degradation pathways is critical for further developments within this chromophore family, it is of equal importance to understand the mitigation of these pathways, in an effort to bolster stability when employed in various applications. As such, our group is actively seeking to design and synthesize various substituted cyanines which, based on our understanding, would potentially hinder the previously observed conversion. The basis for appropriate structural modifications, is our prior mechanistic studies where we observed nucleophilic attack at the C2', initiating truncation. Therefore, we aim to synthesize C2'-substituted cyanines to study the stability and propensity to degrade relative to the parent Cy7 (Figure III-25A). We also showed that the exchangeable proton at C1' is essential for expelling Fisher base **III-23**, from which we hypothesize there may be valuable potential for studying C1'-substituted cyanines (Figure III-25B).

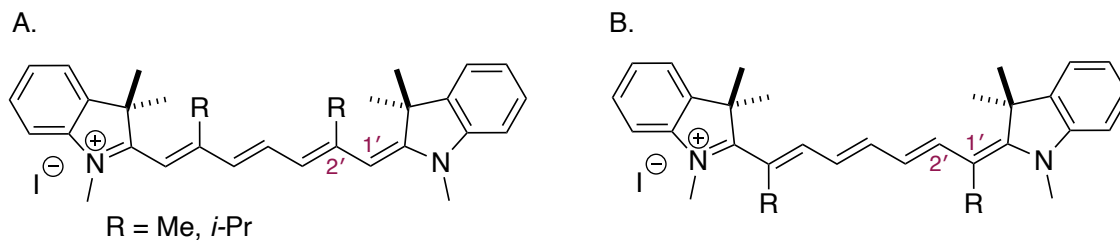


Figure III-25. Cyanine structures for stability study

As previously mentioned, NIR cyanines have been applied widely as fluorescent probes in biological cell imaging.^{4, 16, 17} The discovery of non-photoactivated cyanine degradation has inspired us to further probe this conversion in a cellular environment, in the hopes of developing a novel fluorescent probe with completely distinct fluorescent

emissions upon degradation. To mimic the cellular environment, we are actively studying cyanine truncation in the presence of various amino acids under different conditions.

III-4 Experimental section

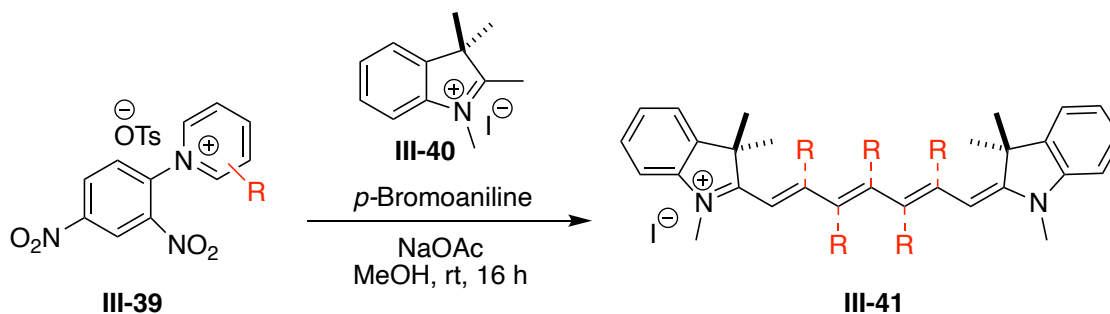
III-4-1 General remarks

Molecular sieves (4Å) were dried at 160 °C under 0.25 mtorr vacuum prior to use. Unless otherwise mentioned, solvents were purified as follows. CHCl₃ (amylene stabilized) was purchased from Sigma Aldrich and incubated over 4Å MS for 48 h prior to use. Toluene and CH₂Cl₂ were dried over CaH₂ whereas Et₂O were dried over sodium (dryness was monitored by colorization of benzophenone ketyl radical); they were freshly distilled prior to use. Acetonitrile (ACN) and dimethylformamide (DMF) for reactions was HPLC grade from Sigma-Aldrich.

NMR spectra were obtained using a 500 MHz or 600 MHz Varian NMR spectrometer and referenced using the residual ¹H peak from the deuterated solvent. Waters 2795 (Alliance HT) instrument was used for HRMS (ESI) analysis with polyethylene glycol (PEG-400-600) as a reference. UV-Vis was performed on Agilent Cary 100 series machine and PL was recorded on Fluorolog by ISA instrument. Quantum yield measurement was performed on absolute PL quantum yield spectrometer C11347 by Hamamatsu.

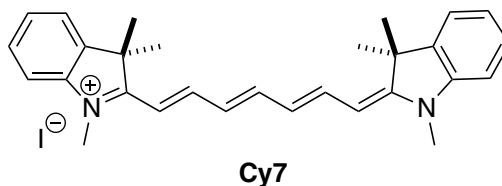
Column chromatography was performed using Silicycle 60Å, 35-75 μm silica gel. Pre-coated 0.25 mm thick silica gel 60 F254 plates were used for analytical TLC and visualized using UV light.

III-4-2 General synthesis of substituted cyanines



Substituted cyanines **III-40** were synthesized according to the previous reported procedures³⁵. To a solution of corresponding Zincke salt (1 equiv.) in methanol (7 mL/mmol of Zincke salt), was added the and 4-bromoaniline (1.2 equiv.). The mixture was stirred at room temperature for 30 minutes. Then, 1,2,3,3-tetramethyl-3H-indolium iodide (3 equiv.) and NaOAc (6 equiv.) were added at once, at which point the mixture was stirred at this temperature for 16 hours. Then, diethyl ether (21 mL/mmol Zincke salt) was added, and the mixture was cooled at -15 °C for 3 hours. The resulting solid was collected by vacuum filtration, rinsed with water (2 x 10 mL/mmol Zincke salt) followed by diethyl ether (10 mL/mmol Zincke salt). The crude solid was then purified using column chromatography (100% DCM gradually to 15% MeOH/DCM).

III-4-2-1 Analytical Data

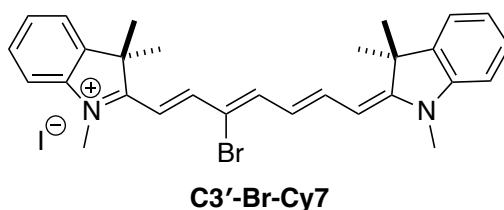


1,3,3-trimethyl-2-((1E,3E,5E)-7-((E)-1,3,3-trimethylindolin-2-ylidene)hepta-1,3,5-trien-1-yl)-3H-indol-1-ium iodide

The title compound was prepared according to the general procedure at 1 mmol scale. Product was isolated as a green solid (455 mg, 85%).

^1H NMR (500 MHz, Methanol- d_4) δ 7.65 (t, $J = 13.1$ Hz, 2H), 7.33 (t, $J = 12.4$ Hz, 1H), 7.18 (dd, $J = 7.5, 1.2$ Hz, 2H), 7.11 (td, $J = 7.7, 1.2$ Hz, 2H), 7.00 – 6.91 (m, 4H), 6.27 (t, $J = 12.6$ Hz, 2H), 5.98 (d, $J = 13.6$ Hz, 2H), 3.31 (s, 6H), 1.41 (s, 12H).

^{13}C NMR (126 MHz, Methanol- d_4) δ 173.79, 157.83, 153.00, 144.41, 142.34, 129.72, 126.94, 125.98, 123.26, 111.61, 104.79, 50.24, 31.45, 27.89.

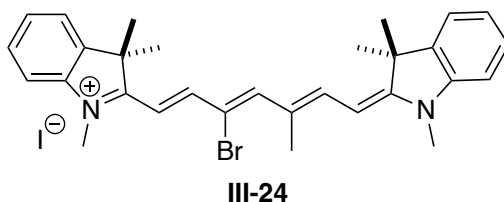


2-(((1E,3Z,5E)-3-bromo-7-((E)-1,3,3-trimethylindolin-2-ylidene)hepta-1,3,5-trien-1-yl)-1,3,3-trimethyl-3H-indol-1-ium

The title compound was prepared according to the general procedure at 1 mmol scale. Product was isolated as a green solid (577 mg, 94%).

^1H -NMR (500 MHz, Methanol- d_4): δ 8.16 (dd, $J = 14.2, 12.1$ Hz, 1H), 7.95 (d, $J = 13.10$ Hz, 1H), 7.85 (d, $J = 12.6$ Hz, 1H), 7.56 (dt, $J = 7.4, 1.0$ Hz, 1H), 7.50-7.43 (m, 3H), 7.41-7.34 (m, 2H), 7.27-7.20 (m, 2H), 6.85 (t, $J = 12.3$ Hz, 1H), 6.60 (d, $J = 14.2$ Hz, 1H), 6.23 (d, $J = 13.0$ Hz, 1H), 3.75 (s, 3H), 3.59 (s, 3H), 1.74 (s, 6H), 1.72 (s, 6H).

^{13}C -NMR (126 MHz, Methanol- d_4): δ 177.33, 173.28, 155.16, 153.74, 146.93, 144.46, 143.94, 143.13, 142.03, 129.96, 129.68, 127.59, 125.73, 123.47, 123.26, 116.34, 112.98, 111.34, 108.08, 101.56, 51.31, 50.06, 32.30, 31.30, 27.88, 27.54.

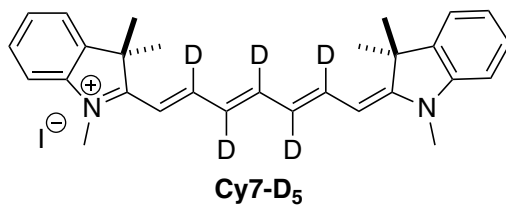


2-((1E,3Z,5E)-3-bromo-5-methyl-7-((E)-1,3,3-trimethylindolin-2-ylidene)hepta-1,3,5-trien-1-yl)-1,3,3-trimethyl-3H-indol-1-ium iodide

The title compound was prepared according to the general procedure at 1 mmol scale. Product was isolated as a green solid (314 mg, 50%).

^1H -NMR (500 MHz, DMSO- d_6): δ 8.07 (d, $J = 14.7$ Hz, 1H), 7.97 – 7.90 (m, 2H), 7.70 (d, $J = 7.4$ Hz, 1H), 7.59 – 7.55 (m, 2H), 7.51 – 7.46 (tm, 1H), 7.40 – 7.33 (m, 3H), 7.22 – 7.17 (m, 1H), 6.44 (d, $J = 14.7$ Hz, 1H), 6.09 (d, $J = 12.9$ Hz, 1H), 3.79 (s, 3H), 3.55 (s, 3H), 2.38 (s, 3H), 1.71 (s, 6H), 1.65 (s, 6H).

^{13}C NMR (126 MHz, DMSO- d_6): δ 175.54, 172.04, 170.81, 156.09, 152.32, 145.95, 143.03, 142.46, 141.75, 140.45, 128.60, 128.36, 126.24, 124.08, 122.51, 122.29, 112.41, 111.07, 110.47, 103.65, 99.71, 49.79, 48.34, 32.10, 30.82, 27.15, 26.58, 13.65.



1,3,3-trimethyl-2-((1E,3E,5E)-7-((E)-1,3,3-trimethylindolin-2-ylidene)hepta-1,3,5-trien-1-yl-2,3,4,5,6-d₅)-3H-indol-1-ium iodide

The title compound was prepared according to the general procedure at 0.1 mmol scale. Product was isolated as a dark green solid (24 mg, 60%)

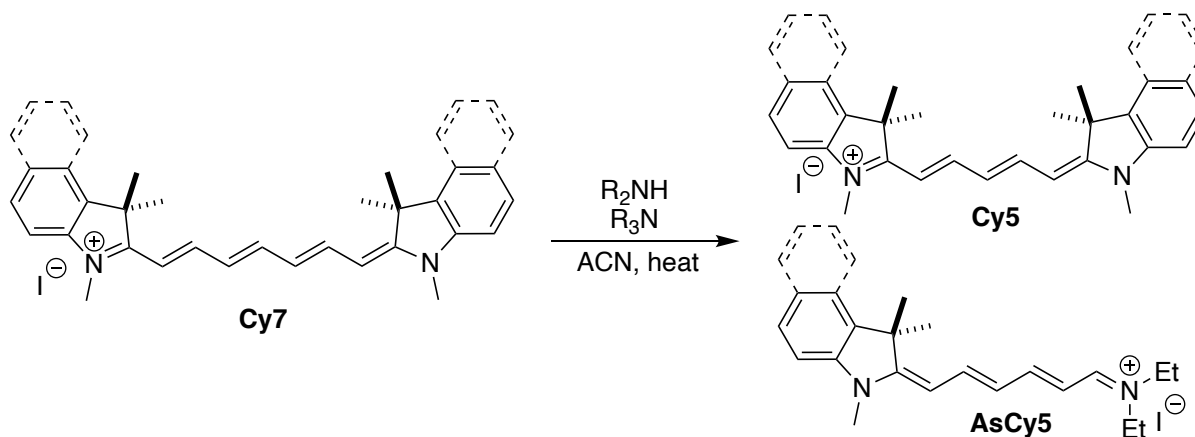
¹H-NMR (500 MHz, Methanol-*d*₄): δ 7.47 (d, *J* = 7.5 Hz, 2H), 7.42 – 7.38 (m, 2H), 7.28 – 7.22 (m, 4H), 6.26 (bs, 2H), 3.59 (s, 6H), 1.69 (s, 12H).

¹³C NMR (151 MHz, Methanol-*d*₄) δ 172.34, 155.69, 151.11, 143.01, 140.95, 128.31, 125.15, 124.55, 121.87, 110.23, 103.32, 48.83, 30.25, 26.57.

HRMS (ESI⁺): calcd. for C₂₉H₂₈ D₅N₂⁺ [M-I⁻]: 414.2952; found 414.2950

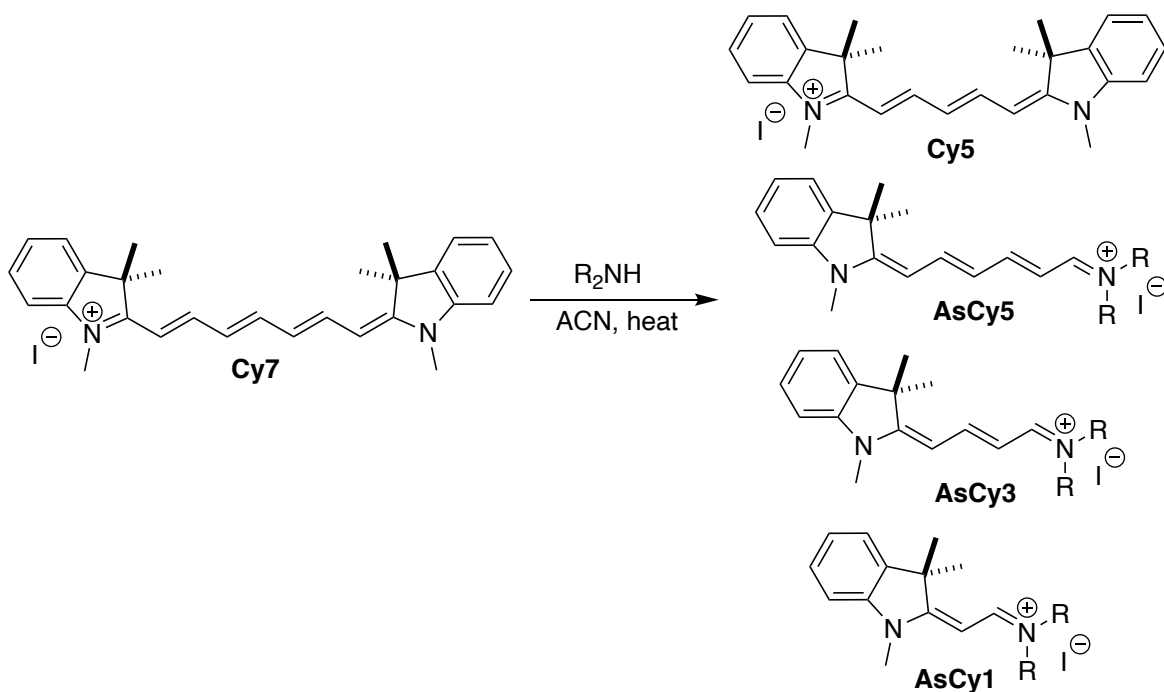
III-4-3 General Procedure for cyanine degradation

III-4-3-1 General Procedure: Cyanine degradation with amine and base



In a 15 mL sealed tube, was added dry acetonitrile (0.03 mM) and degassed under an atmosphere of argon for a period of 15 minutes. Then, the cyanine derivative (1 equiv.) was added, followed by the secondary amine (10 equiv.), base (2 equiv.) followed placing it in a pre-heated oil bath in the dark. The reaction mixture was stirred at the desired temperature for the designated time and monitored by LC-MS, before cooling to room temperature. The solvent was removed under reduced pressure, and the residue purified via column chromatography (100% DCM gradually to 10% MeOH/DCM).

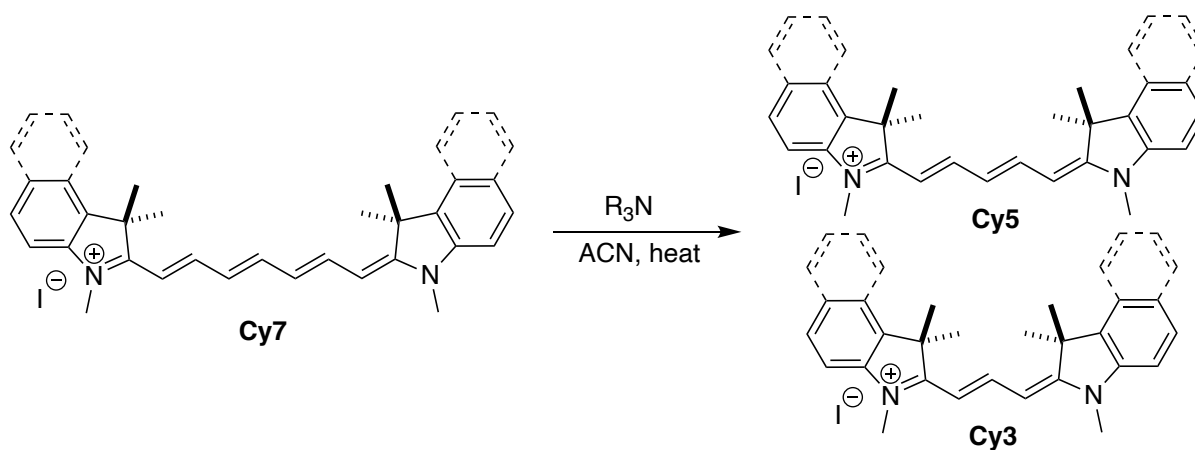
III-4-3-2 General Procedure: Cyanine degradation with amine only



In a 15 mL sealed tube, was added dry acetonitrile (0.03 mM) and degassed under an atmosphere of argon for a period of 15 minutes. Then, the cyanine derivative (1 equiv.) was added, followed by the secondary amine (10 equiv.) followed by capping the mixture prior to placing it in a pre-heated oil bath in the dark. The mixture was stirred at the desired

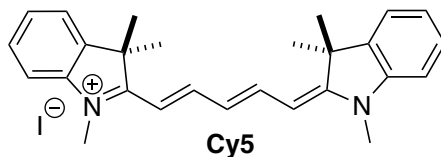
temperature for the designated time and monitored by LC-MS, before removing and cooling to room temperature. The solvent was removed under reduced pressure, and the residue directly purified via column chromatography (100% DCM gradually to 10% MeOH/DCM).

III-4-3-3 General Procedure: Cyanine degradation with base only



In a 15 mL sealed tube, was added dry acetonitrile (0.03 mM) and degassed under an atmosphere of argon for a period of 15 minutes. Then, the cyanine derivative (1 equiv.) was added, followed by the base (10 equiv.) followed by capping the mixture prior to placing it in a pre-heated oil bath in the dark. The mixture was stirred at the desired temperature for the designated time and monitored by LC-MS, before removing and cooling to room temperature. The solvent was removed under reduced pressure, and the residue directly purified via column chromatography (100% DCM gradually to 10% MeOH/DCM).

III-4-3-4 Analytical Data



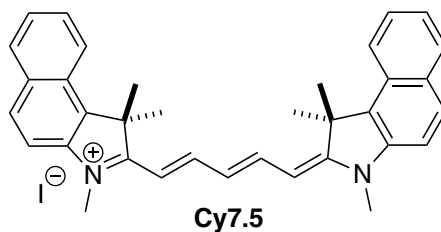
1,3,3-trimethyl-2-((1E,3E)-5-((E)-1,3,3-trimethylindolin-2-ylidene)penta-1,3-dien-1-yl)-3H-indol-1-ium iodide

The title compound was isolated according to the general procedure III-4-3-3 with DIPEA as the base at 0.05 mmol scale, 100°C and 30 h. The product was isolated as dark blue solid (11.8 mg, 44%).

¹H-NMR (500 MHz, Methanol-*d*₄): δ 8.23 (t, *J* = 13.1 Hz, 2H), 7.46 (d, *J* = 7.4 Hz, 2H), 7.37 (t, *J* = 7.7 Hz, 2H), 7.29 (d, *J* = 7.9 Hz, 2H), 7.22 (t, *J* = 7.5 Hz, 2H), 6.67 (t, *J* = 12.4 Hz, 1H), 6.28 (d, *J* = 13.7 Hz, 2H), 3.64 (s, 6H), 1.68 (s, 12H).

¹³C-NMR (126 MHz, Methanol-*d*₄): δ 175.19, 155.44, 144.23, 142.52, 129.66, 126.68, 126.15, 123.27, 111.79, 104.41, 50.45, 31.71, 27.86.

HRMS (ESI⁺): calcd. for C₂₇H₃₁N₂⁺ [M-I⁻]: 383.2482; found 383.2477

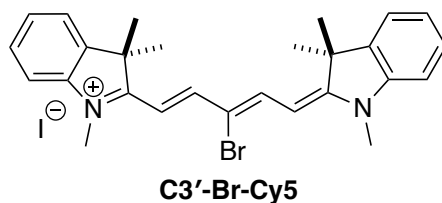


1,1,3-trimethyl-2-((1E,3E,5E)-5-(1,1,3-trimethyl-1,3-dihydro-2H-benzo[e]indol-2-ylidene)penta-1,3-dien-1-yl)-1H-benzo[e]indol-3-ium iodide

The title compound was isolated according to the general procedure III-4-3-3 with DIPEA as the base at 0.05 mmol scale, 100°C and 40 h. The product was isolated as dark blue solid (7.3 mg, 24%).

¹H-NMR (500 MHz, Methanol-*d*₄): δ 8.37 (t, *J* = 12.4 Hz, 2H), 8.25 (d, *J* = 8.6 Hz, 2H), 8.04 – 7.98 (m, 4H), 7.67 – 7.60 (m, 4H), 7.50 – 7.46 (m 2H), 6.68 (t, *J* = 12.4 Hz, 1H), 6.33 (d, *J* = 13.8 Hz, 2H), 3.76 (s, 6H), 2.02 (s, 12H).

¹³C-NMR (126 MHz, Methanol-*d*₄): δ 176.44, 154.42, 141.68, 134.86, 133.40, 131.66, 131.12, 129.42, 128.72, 126.04, 123.34, 111.92, 103.99, 52.35, 31.83, 27.49.



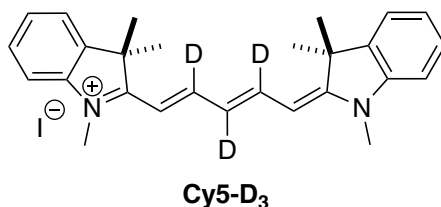
2-((1E,3Z)-3-bromo-5-((E)-1,3,3-trimethylindolin-2-ylidene)penta-1,3-dien-1-yl)-1,3,3-trimethyl-3H-indol-1-ium iodide

The title compound was isolated according to the general procedure III-4-3-3 with DIPEA as the base at 0.05 mmol scale, 70°C and 60 h. The product was isolated as a purple solid.

$^1\text{H-NMR}$ (500 MHz, Methanol- d_4): δ (ppm) 8.54 (d, $J = 14.1$ Hz, 2H), 7.53 (d, $J = 7.8$ Hz, 2H), 7.44 – 7.36 (m, 2H) 7.31 – 7.24 (m, 4H), 5.88 (d, $J = 14.1$ Hz, 2H), 3.47 (s, 6H), 1.83 (s, 12H).

$^{13}\text{C-NMR}$ (126 MHz, Methanol- d_4): δ (ppm): 174.7, 152.3, 142.7, 141.1, 128.4, 125.3, 121.9, 110.8, 100.8, 49.5, 30.3, 26.2.

HRMS (ESI+): calcd. for $\text{C}_{27}\text{H}_{30}\text{BrN}_2^+$ [M-I]: 461.1587; found 461.1590



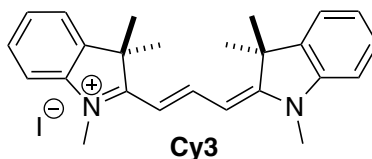
1,3,3-trimethyl-2-((1E,3E)-5-((E)-1,3,3-trimethylindolin-2-ylidene)penta-1,3-dien-1-yl-2,3,4-d₃)-3H-indol-1-ium iodide

The title compound was isolated according to the general procedure III-4-3-3 with DIPEA as the base at 0.05 mmol scale, 100°C and 30 h. The product was isolated as a dark blue solid.

$^1\text{H-NMR}$ (500 MHz, Methanol- d_4): δ 7.49 (dd, $J = 7.5, 1.2$ Hz, 2H), 7.41 (td, $J = 7.7, 1.2$ Hz, 2H), 7.32 – 7.24 (m, 4H), 6.26 (s, 2H), 3.62 (s, 6H), 1.73 (s, 12H).

$^{13}\text{C-NMR}$ (126 MHz, Methanol- d_4): 173.95, 144.3, 142.5, 129.7, 126.2, 123.3, 111.8, 104.1, 50.5, 31.5, 27.8.

HRMS (ESI+): calcd. for $C_{27}H_{28}D_3N_2^+$ [M-I]: 386.2670; found 386.2679



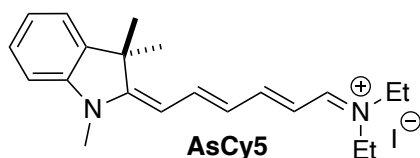
1,3,3-trimethyl-2-((E)-3-((E)-1,3,3-trimethylindolin-2-ylidene)prop-1-en-1-yl)-3H-indol-1-ium iodide

The title compound was isolated according to the general procedure III-4-3-3 with quinuclidine as the base at 0.05 mmol scale, 100°C and 36 h. The product was isolated as pink-red solid (5.6 mg, 21%).

1H -NMR (500 MHz, Methanol- d_4): δ 8.56 (t, $J = 13.5$ Hz, 1H), 7.54 (dt, $J = 7.3, 1.0$ Hz, 2H), 7.45 (td, $J = 7.4, 1.0$ Hz, 2H), 7.36 (d, $J = 7.9$ Hz, 2H), 7.32 (td, $J = 7.5, 1.0$ Hz, 2H), 6.41 (d, $J = 13.5$ Hz, 2H), 3.68 (s, 6H), 1.78 (s, 12H).

^{13}C -NMR (126 MHz, Methanol- d_4): δ 176.66, 152.15, 144.09, 142.06, 129.96, 126.75, 123.39, 112.24, 103.65, 49.00, 31.70, 28.15.

HRMS (ESI+): calcd. for $C_{25}H_{29}N_2^+$ [M-I]: 357.2325; found 357.2326



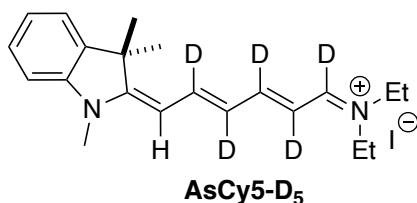
*2-((1E,3E,5E)-6-(diethylamino)hexa-1,3,5-trien-1-yl)-1,3,3-trimethyl-3H-indol-1-ium
iodide*

The title compound was isolated according to the general procedure III-4-3-2 with diethylamine at 0.05 mmol scale, r.t. and 160 h. The product was isolated as pink-red solid (8.9 mg, 41%).

¹H-NMR (500 MHz, Methanol-*d*₄): δ 7.91 (t, *J* = 13.1 Hz, 1H), 7.83 (d, *J* = 11.7 Hz, 1H), 7.64 (t, *J* = 12.7 Hz, 1H), 7.43 – 7.39 (m, 1H), 7.37 – 7.32 (m, 1H), 7.16 – 7.14 (m, 2H), 6.48 (t, *J* = 12.6 Hz, 1H), 6.19 (t, *J* = 13.1 Hz, 1H), 6.02 (d, *J* = 13.1 Hz, 1H), 3.65 (q, *J* = 7.3 Hz, 4H), 3.48 (s, 3H), 1.65 (s, 6H), 1.36 (t, *J* = 7.2 Hz, 3H), 1.31 (t, *J* = 7.3 Hz, 3H).

¹³C NMR (126 MHz, Methanol-*d*₄) δ 171.23, 161.58, 161.46, 152.54, 143.20, 140.25, 131.60, 128.12, 121.97, 121.68, 109.29, 107.98, 99.80, 51.99, 44.20, 29.36, 26.77, 13.11, 11.45.

HRMS (ESI+): calcd. for C₂₁H₂₉N₂⁺ [M-I⁻]: 309.2325; found 309.2327

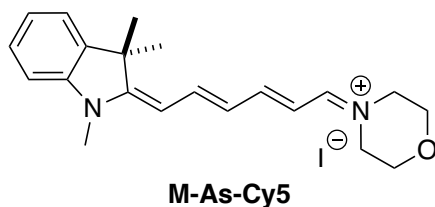


N-ethyl-*N*-((2*E*,4*E*)-6-((*E*)-1,3,3-trimethylindolin-2-ylidene)hexa-2,4-dien-1-ylidene-1,2,3,4,5-*d*₅)ethanaminium iodide

The title compound was isolated according to the general procedure III-4-3-2 with diethylamine at 0.05 mmol scale, 70°C and 40 h. The product was isolated as red solid.

¹H NMR (500 MHz, Methanol-*d*₄) δ 7.42 – 7.33 (m, 2H), 7.16 (t, *J* = 7.5 Hz, 2H), 6.01 (s, 1H), 3.65 (q, *J* = 7.2 Hz, 4H), 3.48 (s, 3H), 1.65 (s, 6H), 1.34 – 1.29 (m, 6H).

HRMS (ESI⁺): calcd. for C₂₁H₂₄D₅N₂⁺ [M-I⁻]: 314.2639; found 314.2638

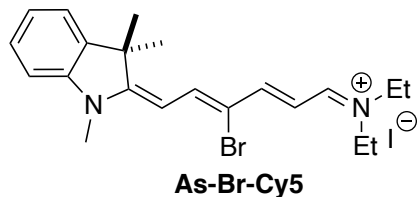


4-((2E,4E)-6-((E)-1,3,3-trimethylindolin-2-ylidene)hexa-2,4-dien-1-ylidene)morpholin-4-ium iodide

The title compound was isolated according to the general procedure III-4-3-2 with morpholine at 0.05 mmol scale, r.t. and 20 h. The product was isolated as purple-red solid (9 mg, 40%).

¹H NMR (500 MHz, Methanol-*d*₄): δ 7.96 (t, *J* = 13.1 Hz, 1H), 7.77 (d, *J* = 11.7 Hz, 1H), 7.65 (t, *J* = 12.7 Hz, 1H), 7.45 – 7.42 (m, 1H), 7.37 (t, *J* = 7.6 Hz, 1H), 7.22 – 7.18 (m, 2H), 6.48 (t, *J* = 12.7 Hz, 1H), 6.21 (t, *J* = 11.7 Hz, 1H), 6.08 (d, *J* = 13.5 Hz, 1H), 3.85 – 3.80 (m, 4H), 3.75 – 3.72 (m, 4H), 3.52 (s, 3H), 1.66 (s, 6H).

HRMS (ESI⁺): calcd. for C₂₁H₂₇N₂O⁺ [M-I⁻]: 323.2118; found 323.2124

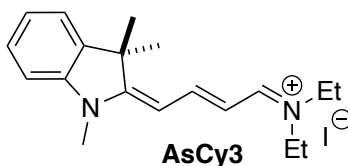


N-((2Z,4E)-3-bromo-6-((E)-1,3,3-trimethylindolin-2-ylidene)hexa-2,4-dien-1-ylidene)-N-ethylethanaminium

The title compound was isolated according to the general procedure III-4-3-2 with diethylamine at 0.05 mmol scale, 70°C and 40 h. The product was isolated as a purple solid.

¹H NMR (500 MHz, Methanol-*d*₄): δ (ppm) 8.04 (d, *J* = 13.1 Hz, 1H), 7.97 (d, *J* = 11.6 Hz, 1H), 7.82 (d, *J* = 12.5 Hz, 1H), 7.47 (d, *J* = 7.6 Hz, 1H), 7.43 – 7.39 (m, 1H), 7.29 – 7.24 (m, 2H), 6.28 (t, *J* = 12.1 Hz, 1H), 6.20 (d, *J* = 13.1 Hz, 1H), 3.72 (m, 4H), 3.60 (s, 3H), 1.68 (s, 6H), 1.39 (m, 6H).

HRMS (ESI⁺): calcd. for C₂₁H₂₈BrN₂⁺ [M-I⁻]: 387.1430; found 387.1438



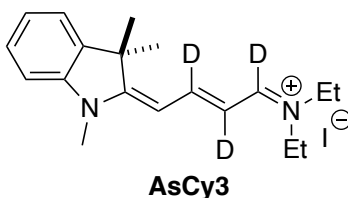
2-((1E,3E)-4-(diethylamino)buta-1,3-dien-1-yl)-1,3,3-trimethyl-3H-indol-1-ium iodide

The title compound was isolated according to the general procedure III-4-3-2 with diethylamine at 0.05 mmol scale, 70°C and 40 h. The product was isolated as an orange solid.

^1H NMR (500 MHz, Methanol- d_4) δ 8.24 – 8.15 (t, J = 12.7 Hz, 1H), 8.02 (d, J = 11.7 Hz, 1H), 7.48 – 7.43 (m, 1H), 7.39 (ddd, J = 8.5, 7.5, 1.2 Hz, 1H), 7.29 – 7.16 (m, 2H), 6.24 – 6.11 (m, 2H), 3.68 – 3.61 (m, 4H), 3.54 (s, 3H), 1.68 (s, 6H), 1.40 – 1.32 (m, 6H).

^{13}C NMR (126 MHz, Methanol- d_4) δ 175.72, 162.97, 159.11, 130.87, 129.65, 125.75, 123.19, 117.18, 111.34, 108.26, 100.51, 53.24, 45.43, 30.78, 28.08, 14.55, 12.80.

HRMS (ESI+): calcd. for $\text{C}_{19}\text{H}_{27}\text{N}_2^+$ [M-I⁻]: 283.2174; found 283.2179



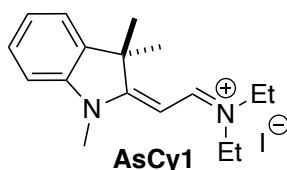
N-ethyl-*N*-((*E*)-4-((*E*)-1,3,3-trimethylindolin-2-ylidene)but-2-en-1-ylidene-1,2,3- d_3)ethanaminium iodide

The title compound was isolated according to the general procedure III-4-3-2 with diethylamine at 0.05 mmol scale, 70°C and 40 h. The product was isolated as an orange solid.

^1H NMR (500 MHz, Methanol- d_4) δ 7.45 (d, J = 7.4 Hz, 1H), 7.39 (d, J = 7.9 Hz, 1H), 7.25 – 7.21 (m, 2H), 6.15 (s, 1H), 3.64 (q, J = 7.3 Hz, 4H), 3.54 (s, 3H), 1.68 (s, 6H), 1.37 (t, J = 7.3 Hz, 3H), 1.33 (t, J = 7.3 Hz, 3H).

^{13}C NMR (201 MHz, Methanol- d_4) δ 174.24, 172.03, 161.67 (t, J = 31.4 Hz), 161.14 (t, J = 24.9 Hz), 157.24 (t, J = 22.8 Hz), 129.47, 128.24, 124.31, 121.79, 109.92, 98.92, 51.76, 43.96, 31.69, 26.67, 13.15, 11.39.

HRMS (ESI+): calcd. for $\text{C}_{19}\text{H}_{24}\text{D}_3\text{N}_2^+$ [$\text{M}-\text{I}^-$]: 286.2357; found 286.2353

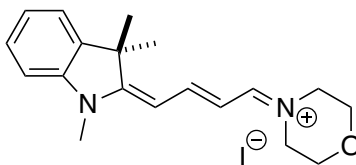


(E)-2-(2-(diethylamino)vinyl)-1,3,3-trimethyl-3H-indol-1-ium iodide

The title compound was isolated according to the general procedure III-4-3-2 with diethylamine at 0.05 mmol scale, 110°C and 30 h. The product was isolated as a yellow solid.

^1H -NMR (500 MHz, Methanol- d_4): δ 8.27 (d, J = 12.8 Hz, 1H), 7.50 (d, J = 7.4, 1H), 7.43 (td, J = 7.7, 1.2 Hz, 1H), 7.34 – 7.27 (m, 2H), 5.67 (d, J = 12.9 Hz, 1H), 3.80 – 3.70 (m, 4H), 3.62 (s, 3H), 1.68 (s, 6H), 1.41-1.35 (m, 6H).

HRMS (ESI+): calcd. for $\text{C}_{17}\text{H}_{25}\text{N}_2^+$ [$\text{M}-\text{I}^-$]: 257.2018; found 257.2126



M-As-Cy3

4-((E)-4-((E)-1,3,3-trimethylindolin-2-ylidene)but-2-en-1-ylidene)morpholin-4-ium iodide

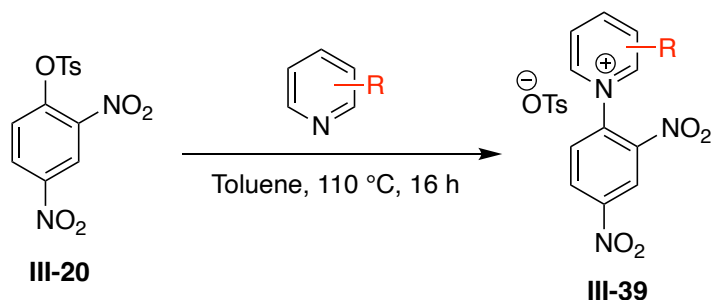
The title compound was isolated according to the general procedure III-4-3-2 with morpholine at 0.05 mmol scale, 70°C and 24 h. The product was isolated as an orange solid.

¹H-NMR (500 MHz, Methanol-*d*₄): δ 8.21 (t, *J* = 12.9 Hz, 1H), 7.98 (d, *J* = 11.7 Hz, 1H), 7.47 (d, *J* = 7.4 Hz, 1H), 7.40 (t, *J* = 7.7 Hz, 1H), 7.28-7.23 (m, 2H), 6.24 (t, *J* = 12.7 Hz, 1H), 6.18 (d, *J* = 13.7 Hz, 1H), 3.86 – 3.81 (m, 4H), 3.76 – 3.71 (m, 4H), 3.57, (s, 3H), 1.68 (s, 6H).

¹³C NMR (126 MHz, Methanol-*d*₄): δ 176.27, 162.49, 159.48, 144.15, 142.01, 129.69, 126.03, 123.24, 111.61, 107.27, 101.04, 68.08, 67.11, 56.17, 30.77, 28.04.

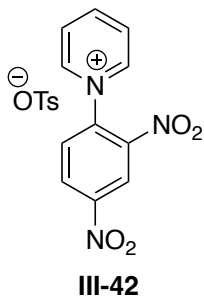
HRMS (ESI⁺): calcd. for C₁₉H₂₅N₂O⁺ [M-I⁻]: 297.1961; found 297.1976

III-4-4 General Procedure for synthesis of Zincke salts



Substituted Zincke salts **III-39** were synthesized according to the previous reported procedures.³⁵ To a mixture 2,4-dinitrophenyl p-toluenesulfonate **III-20** (1.1 equiv.) in toluene (7 mL/mmol) was added the corresponding pyridine derivative (1 equiv.) The reaction mixture was refluxed for 16 h and then cooled to rt. Vacuum filtration was used to isolate the suspended solids, which were then washed with toluene (2 × 5 mL/mmol) and Et₂O (2×5 mL/mmol), and dried under vacuum to give the Zincke salt products.

III-4-4-1 Analytical Data

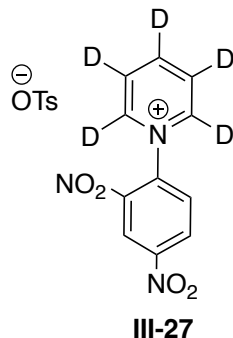


1-(2,4-dinitrophenyl)pyridin-1-ium 4-methylbenzenesulfonate

The title compound was isolated according to the general procedure at 3 mmol scale,. The product was isolated as a white solid (1 g, 80%).

¹H-NMR (500 MHz, DMSO-*d*₆): δ (ppm) 9.42-9.35 (m, 2H), 9.12 (d, *J* = 2.5 Hz, 1H), 9.00-9.81 (m, 2H), 8.48-8.37 (m, 3H), 7.46 (d, *J* = 8.1 Hz, 2H), 7.10 (d, *J* = 7.8 Hz, 2H), 2.28 (s, 3H).

¹³C NMR (126 MHz, DMSO-*d*₆): δ (ppm) 149.1, 148.8, 146.1, 145.8, 143.0, 138.7, 137.5, 131.9, 130.2, 128.0, 125.5, 121.4, 20.8.



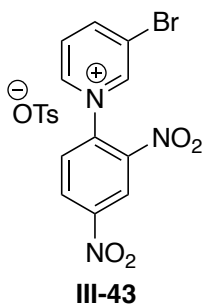
1-(2,4-dinitrophenyl)pyridin-1-ium-2,3,4,5,6-d₅ 4-methylbenzenesulfonate

The title compound was isolated according to the general procedure at 3 mmol scale,. The product was isolated as a white solid (760 mg, 60%).

¹H-NMR (500 MHz, DMSO-*d*₆): δ (ppm) 9.12 (d, *J* = 2.4 Hz, 1H), 8.97 (dd, *J* = 8.7, 2.4 Hz, 1H) 8.42 (d, *J* = 8.7 Hz, 1H), 7.45 (d, *J* = 8.1 Hz, 2H), 7.10 (d, *J* = 7.5 Hz, 2H), 2.28 (s, 3H).

¹³C NMR (126 MHz, DMSO-*d*₆): 149.18, 145.84, 144.64, 143.08, 138.68, 137.54, 136.36, 131.88, 130.23, 128.05, 125.50, 121.46, 20.80.

HRMS (ESI+): calcd. for C₁₁H₃ D₅N₃O₄ [M-TsO⁻]: 251.0823; found 251.0850

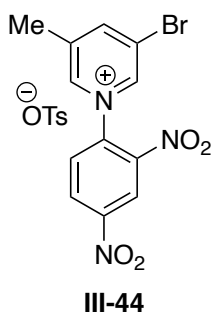


3-bromo-1-(2,4-dinitrophenyl)pyridin-1-ium 4-methylbenzenesulfonate

The title compound was isolated according to the general procedure at 3 mmol scale,. The product was isolated as a white solid (1.38 g, 93%).

$^1\text{H-NMR}$ (500 MHz, $\text{DMSO-}d_6$): δ (ppm) 9.85 (d, $J = 1.7$ Hz, 1H), 9.44 (dt, $J = 6.1, 1.2$ Hz, 1H), 9.30-9.19 (m, 1H), 9.10 (d, $J = 2.5$ Hz, 1H), 8.97 (dd, $J = 8.7, 2.5$ Hz, 1H), 8.43 – 8.37 (m, 2H), 7.43 (d, $J = 8.1$ Hz, 2H), 7.10 (d, $J = 7.8$ Hz, 2H), 2.28 (3H).

$^{13}\text{C NMR}$ (126 MHz, $\text{DMSO-}d_6$): δ 151.10, 149.26, 147.27, 145.71, 145.35, 142.80, 137.98, 137.61, 132.03, 130.24, 128.65, 128.06, 125.47, 121.84, 121.36, 20.80.



3-bromo-1-(2,4-dinitrophenyl)-5-methylpyridin-1-ium 4-methylbenzenesulfonate

The title compound was isolated according to the general procedure at 1 mmol scale,. The product was isolated as a white solid (270 mg, 53%).

$^1\text{H-NMR}$ (500 MHz, $\text{DMSO-}d_6$): δ (ppm) 9.70 – 9.67 (m, 1H), 9.36 – 9.34 (m, 1H), 9.16 – 9.13 (m, 1H), 9.12 (d, $J = 2.4$ Hz, 1H), 8.99 (dd, $J = 8.7, 2.6$ Hz, 1H), 8.37 (d, $J = 8.7$ Hz, 1H), 7.46 (d, $J = 8.1$ Hz, 2H), 7.11 (m, 2H), 2.59 (s, 3H), 2.28 (s, 3H).

$^{13}\text{C NMR}$ (126 MHz, $\text{DMSO-}d_6$): δ (ppm) 151.2, 149.3, 145.8, 144.8, 144.3, 142.7, 139.8, 137.9, 137.6, 131.9, 130.3, 128.0, 125.4, 121.4, 120.9, 20.8, 17.7.

REFERENCES

- (1) Lou, Z. R.; Li, P.; Song, P.; Han, K. L. Ratiometric fluorescence imaging of cellular hypochlorous acid based on heptamethine cyanine dyes. *Analyst* **2013**, *138* (21), 6291-6295. DOI: 10.1039/c3an00198a.
- (2) Geiger, T.; Schoger, I.; Rentsch, D.; Veron, A. C.; Oswald, F.; Meyer, T.; Nuesch, F. Unsymmetrical Heptamethine Dyes for NIR Dye-Sensitized Solar Cells. *Int J Photoenergy* **2014**, *2014*. DOI: Artn 25898410.1155/2014/258984.
- (3) Ooyama, Y.; Harima, Y. Photophysical and Electrochemical Properties, and Molecular Structures of Organic Dyes for Dye-Sensitized Solar Cells. *Chemphyschem* **2012**, *13* (18), 4032-4080. DOI: 10.1002/cphc.201200218.
- (4) Shi, C. H.; Wu, J. B.; Pan, D. F. Review on near-infrared heptamethine cyanine dyes as theranostic agents for tumor imaging, targeting, and photodynamic therapy. *J Biomed Opt* **2016**, *21* (5). DOI: Artn 05090110.1117/1.Jbo.21.5.050901.
- (5) Sun, W.; Guo, S. G.; Hu, C.; Fan, J. L.; Peng, X. J. Recent Development of Chemosensors Based on Cyanine Platforms. *Chem Rev* **2016**, *116* (14), 7768-7817. DOI: 10.1021/acs.chemrev.6b00001.
- (6) Hong, G. S.; Antaris, A. L.; Dai, H. J. Near-infrared fluorophores for biomedical imaging. *Nat Biomed Eng* **2017**, *1* (1). DOI: ARTN 001010.1038/s41551-016-0010.
- (7) Traverse, C. J.; Pandey, R.; Barr, M. C.; Lunt, R. R. Emergence of highly transparent photovoltaics for distributed applications. *Nat Energy* **2017**, *2* (11). DOI: 10.1038/s41560-017-0016-9.
- (8) Kiyose, K.; Aizawa, S.; Sasaki, E.; Kojima, H.; Hanaoka, K.; Terai, T.; Urano, Y.; Nagano, T. Molecular Design Strategies for Near-Infrared Ratiometric Fluorescent Probes Based on the Unique Spectral Properties of Aminocyanines. *Chem-Eur J* **2009**, *15* (36), 9191-9200. DOI: 10.1002/chem.200900035.
- (9) Samanta, A.; Vendrell, M.; Das, R.; Chang, Y. T. Development of photostable near-infrared cyanine dyes. *Chem Commun* **2010**, *46* (39), 7406-7408. DOI: 10.1039/c0cc02366c.
- (10) Arjona-Esteban, A.; Stolte, M.; Wurthner, F. Conformational Switching of pi-Conjugated Junctions from Merocyanine to Cyanine States by Solvent Polarity. *Angew Chem Int Edit* **2016**, *55* (7), 2470-2473. DOI: 10.1002/anie.201510620.
- (11) Davydenko, I.; Barlow, S.; Sharma, R.; Benis, S.; Simon, J.; Allen, T. G.; Cooper, M. W.; Khrustalev, V.; Jucov, E. V.; Castaneda, R.; et al. Facile Incorporation of Pd(PPh₃)₂Hal Substituents into Polymethines, Merocyanines, and Perylene

Diimides as a Means of Suppressing Intermolecular Interactions. *J Am Chem Soc* **2016**, *138* (32), 10112-10115. DOI: 10.1021/jacs.6b06361.

- (12) Gopika, G. S.; Prasad, P. M. H.; Lekshmi, A. G.; Lekshmypriya, S.; Sreesaila, S.; Arunima, C.; Kumar, M. S.; Anil, A.; Sreekumar, A.; Pillai, Z. S. Chemistry of cyanine dyes-A review. *Mater Today-Proc* **2021**, *46*, 3102-3108. DOI: 10.1016/j.matpr.2021.02.622.
- (13) Bilici, K.; Cetin, S.; Aydindogan, E.; Acar, H. Y.; Kolemen, S. Recent Advances in Cyanine-Based Phototherapy Agents. *Front Chem* **2021**, *9*. DOI: ARTN 70787610.3389/fchem.2021.707876.
- (14) Usama, S. M.; Thavornpradit, S.; Burgess, K. Optimized Heptamethine Cyanines for Photodynamic Therapy. *Acs Appl Bio Mater* **2018**, *1* (4), 1195-1205. DOI: 10.1021/acsubm.8b00414.
- (15) Lange, N.; Szlasa, W.; Saczko, J.; Chwilkowska, A. Potential of Cyanine Derived Dyes in Photodynamic Therapy. *Pharmaceutics* **2021**, *13* (6). DOI: ARTN 81810.3390/pharmaceutics13060818.
- (16) Li, Y.; Zhou, Y. M.; Yue, X. L.; Dai, Z. F. Cyanine Conjugate-Based Biomedical Imaging Probes. *Adv Healthc Mater* **2020**, *9* (22). DOI: ARTN 200132710.1002/adhm.202001327.
- (17) Onoe, S.; Temma, T.; Shimizu, Y.; Ono, M.; Saji, H. Investigation of cyanine dyes for in vivo optical imaging of altered mitochondrial membrane potential in tumors. *Cancer Med-Us* **2014**, *3* (4), 775-786. DOI: 10.1002/cam4.252.
- (18) Malinkiewicz, O.; Grancha, T.; Molina-Ontoria, A.; Soriano, A.; Brine, H.; Bolink, H. J. Efficient, Cyanine Dye Based Bilayer Solar Cells. *Adv Energy Mater* **2013**, *3* (4), 472-477. DOI: 10.1002/aenm.201200764.
- (19) Yang, C. C.; Liu, D. Y.; Renny, A.; Kuttipillai, P. S.; Lunt, R. R. Integration of near-infrared harvesting transparent luminescent solar concentrators onto arbitrary surfaces. *J Lumin* **2019**, *210*, 239-246. DOI: 10.1016/j.jlumin.2019.02.042.
- (20) Zhao, Y. M.; Meek, G. A.; Levine, B. G.; Lunt, R. R. Near-Infrared Harvesting Transparent Luminescent Solar Concentrators. *Adv Opt Mater* **2014**, *2* (7), 606-611. DOI: 10.1002/adom.201400103.
- (21) Yang, C. C.; Zhang, J.; Peng, W. T.; Sheng, W.; Liu, D. Y.; Kuttipillai, P. S.; Young, M.; Donahue, M. R.; Levine, B. G.; Borhan, B.; et al. Impact of Stokes Shift on the Performance of Near-Infrared Harvesting Transparent Luminescent Solar Concentrators. *Sci Rep-Uk* **2018**, *8*. DOI: ARTN 1635910.1038/s41598-018-34442-3.

- (22) Byers, G. W.; Gross, S.; Henrichs, P. M. Direct and Sensitized Photooxidation of Cyanine Dyes. *Photochem Photobiol* **1976**, *23* (1), 37-43. DOI: DOI 10.1111/j.1751-1097.1976.tb06768.x.
- (23) Patel, N. J.; Manivannan, E.; Joshi, P.; Ohulchanskyy, T. J.; Nani, R. R.; Schnermann, M. J.; Pandey, R. K. Impact of Substituents in Tumor Uptake and Fluorescence Imaging Ability of Near-Infrared Cyanine-like Dyes. *Photochem Photobiol* **2015**, *91* (5), 1219-1230. DOI: 10.1111/php.12482.
- (24) Toutchkine, A.; Nguyen, D. V.; Hahn, K. M. Merocyanine dyes with improved photostability. *Org Lett* **2007**, *9* (15), 2775-2777. DOI: 10.1021/ol070780h.
- (25) Nani, R. R.; Kelley, J. A.; Ivanic, J.; Schnermann, M. J. Reactive species involved in the regioselective photooxidation of heptamethine cyanines. *Chem Sci* **2015**, *6* (11), 6556-6563. DOI: 10.1039/c5sc02396c.
- (26) Gorke, A. P.; Nani, R. R.; Zhu, J. J.; Mackem, S.; Schnermann, M. J. A Near-IR Uncaging Strategy Based on Cyanine Photochemistry. *J Am Chem Soc* **2014**, *136* (40), 14153-14159. DOI: 10.1021/ja5065203.
- (27) Oshiki, D.; Kojima, H.; Terai, T.; Arita, M.; Hanaoka, K.; Urano, Y.; Nagano, T. Development and Application of a Near-Infrared Fluorescence Probe for Oxidative Stress Based on Differential Reactivity of Linked Cyanine Dyes. *J Am Chem Soc* **2010**, *132* (8), 2795-2801. DOI: 10.1021/ja910090v.
- (28) Sun, M. T.; Yu, H.; Zhu, H. J.; Ma, F.; Zhang, S.; Huang, D. J.; Wang, S. H. Oxidative Cleavage-Based Near-Infrared Fluorescent Probe for Hypochlorous Acid Detection and Myeloperoxidase Activity Evaluation. *Anal Chem* **2014**, *86* (1), 671-677. DOI: 10.1021/ac403603r.
- (29) Dirix, L.; Kennes, K.; Fron, E.; Debyser, Z.; van der Auweraer, M.; Hofkens, J.; Rocha, S. Photoconversion of Far-Red Organic Dyes: Implications for Multicolor Super-Resolution Imaging. *Chemphotochem* **2018**, *2* (5), 433-441. DOI: 10.1002/cptc.201700216.
- (30) Stone, M. B.; Veatch, S. L. Far-Red Organic Fluorophores Contain a Fluorescent Impurity. *Chemphyschem* **2014**, *15* (11), 2240-2246. DOI: 10.1002/cphc.201402002.
- (31) Helmerich, D. A.; Beliu, G.; Matikonda, S. S.; Schnermann, M. J.; Sauer, M. Photobleaching of organic dyes can cause artifacts in super-resolution microscopy. *Nat Methods* **2021**, *18* (3), 253-+. DOI: 10.1038/s41592-021-01061-2.
- (32) Matikonda, S. S.; Helmerich, D. A.; Meub, M.; Beliu, G.; Kollmannsberger, P.; Greer, A.; Sauer, M.; Schnermann, M. J. Defining the Basis of Cyanine Phototruncation Enables a New Approach to Single-Molecule Localization

- Microscopy. *Acs Central Sci* **2021**, *7* (7), 1144-1155. DOI: 10.1021/acscentsci.1c00483.
- (33) Cho, Y.; An, H. J.; Kim, T.; Lee, C.; Lee, N. K. Mechanism of Cyanine5 to Cyanine3 Photoconversion and Its Application for High-Density Single-Particle Tracking in a Living Cell. *J Am Chem Soc* **2021**, *143* (35), 14125-14135. DOI: 10.1021/jacs.1c04178.
- (34) Zhang, J.; Moemeni, M.; Yang, C. C.; Liang, F. C.; Peng, W. T.; Levine, B. G.; Lunt, R. R.; Borhan, B. General strategy for tuning the Stokes shifts of near infrared cyanine dyes. *J Mater Chem C* **2020**, *8* (47), 16769-16773. DOI: 10.1039/d0tc03615c.
- (35) Stackova, L.; Stacko, P.; Klan, P. Approach to a Substituted Heptamethine Cyanine Chain by the Ring Opening of Zincke Salts. *J Am Chem Soc* **2019**, *141* (17), 7155-7162. DOI: 10.1021/jacs.9b02537.